

AD-A080 133

DYNAMIC CONTROLS INC DAYTON OHIO
RESEARCH AND DEVELOPMENT OF CONTROL ACTUATION SYSTEMS FOR AIRCR--ETC(U)
AUG 79 © D JENNEY

F/6 1/3

F33615-77-C-3077

UNCLASSIFIED

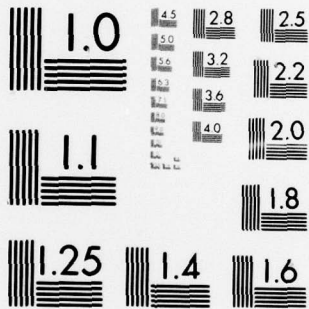
AFFDL-TR-79-3117-VOL-1

NL

1 of 3

AD
A080133





MICROCOPY RESOLUTION TEST CHART
NATIONAL BUREAU OF STANDARDS-1963-A

ADA080133

② LEVEL II

AFFDL-TR-79-3117
VOLUME I

RESEARCH AND DEVELOPMENT OF CONTROL ACTUATION
SYSTEMS FOR AIRCRAFT - VOLUME I

The Development and Wind Tunnel Test of a Flutter Suppression Technique,
The Flightworthiness Testing of a Direct Drive Fly-By-Wire System, The
Evaluation of Three Different Fly-By-Wire Actuation Systems and the
Evaluation of an Angular Rate Sensing Augmentation Actuator.

DYNAMIC CONTROLS, INC.
DAYTON, OHIO 45424

August 1979

DDC
RECEIVED
JAN 30 1980
B

DDC FILE COPY

TECHNICAL REPORT AFFDL-TR-79
Final Report for Period July 1977 - February 1979

Approved for public release; distribution unlimited.

AIR FORCE FLIGHT DYNAMICS LABORATORY
AIR FORCE WRIGHT AERONAUTICAL LABORATORIES
AIR FORCE SYSTEMS COMMAND
WRIGHT-PATTERSON AIR FORCE BASE, OHIO 45433

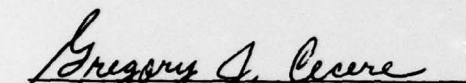
80 1 28 080

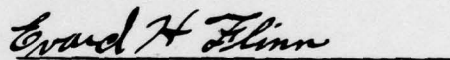
NOTICE

When Government drawings, specifications, or other data are used for any purpose other than in connection with a definitely related Government procurement operation, the United States Government thereby incurs no responsibility nor any obligation whatsoever; and the fact that the government may have formulated, furnished, or in any way supplied the said drawings, specifications, or other data, is not to be regarded by implication or otherwise as in any manner licensing the holder or any other person or corporation, or conveying any rights or permission to manufacture, use or sell any patented invention that may in any way be related thereto.

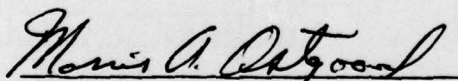
This report has been reviewed by the Information Office (ASD/PAM) and is releaseable to the National Technical Information Service (NTIS). At NTIS, it will be available to the general public, including foreign nations.

This technical report has been reviewed and is approved for publication.


GREGORY J. CERE
Project Engineer


EVARD H. FLINN, Chief
Control Systems Development
Branch
Flight Control Division

FOR THE COMMANDER


MORRIS A. OSTGAARD
Acting Chief
Flight Control Division

Copies of this report should not be returned unless return is required by security considerations, contractual obligations, or notice on a specific document.

SECURITY CLASSIFICATION OF THIS PAGE (When Data Entered)

19 REPORT DOCUMENTATION PAGE		READ INSTRUCTIONS BEFORE COMPLETING FORM
1. REPORT NUMBER	2. GOVT ACCESSION NO.	3. RECIPIENT'S CATALOG NUMBER
18 AFFDL-TR-79-3117-VOLUME 1	NA	9 NA
4. TITLE (and Subtitle)	5. TYPE OF REPORT & PERIOD COVERED	
6 Research and Development of Control Actuation Systems for Aircraft, Volume I	Final rept. Jun 1977 - Feb 1979	
7. AUTHOR(s)	6. PERFORMING ORG. REPORT NUMBER	
10 Gavin D./Jenney	NA	
9. PERFORMING ORGANIZATION NAME AND ADDRESS	8. CONTRACT OR GRANT NUMBER(s)	
Dynamic Controls, Inc. 7060 Cliffwood Place Dayton, Ohio 45424	15 F33615-77-C-3077/pw	
11. CONTROLLING OFFICE NAME AND ADDRESS	10. PROGRAM ELEMENT, PROJECT, TASK AREA & WORK UNIT NUMBERS	
Air Force Flight Dynamics Laboratory AFFDL/FGL, Flight Controls Division Wright-Patterson AFB, Ohio 45433	Project 24030212 17/72	
14. MONITORING AGENCY NAME & ADDRESS (if different from Controlling Office)	12. REPORT DATE	13. NUMBER OF PAGES
	11 Aug 1979	210 12 211
	15. SECURITY CLASS. (of this report)	15a. DECLASSIFICATION/DOWNGRADING SCHEDULE
16. DISTRIBUTION STATEMENT (of this Report)		
Approved for Public Release; Distribution Unlimited		
17. DISTRIBUTION STATEMENT (of the abstract entered in Block 20, if different from Report)		
18. SUPPLEMENTARY NOTES		
None		
19. KEY WORDS (Continue on reverse side if necessary and identify by block number)		
Flutter Suppression Fly-By-Wire Direct Drive Stability Augmentation		
20. ABSTRACT (Continue on reverse side if necessary and identify by block number)		
This report describes the development of a flutter suppression actuator technique and the wind tunnel evaluation of that technique. The report also describes the flightworthiness testing of a direct drive Fly-By-Wire flight control system applied to the aileron axis of an F-4 aircraft. Also included in the report is an evaluation of an angular rate sensing augmentation actuator supplied to the Air Force for evaluation. Presented →		

DD FORM 1 JAN 73 1473

EDITION OF 1 NOV 65 IS OBSOLETE

SECURITY CLASSIFICATION OF THIS PAGE (When Data Entered)

391 199

JOB

in the material are the test results of all three experimental evaluations.

Further testing of the flutter suppression is recommended to clarify an anomaly in the results of the testing. The direct drive control system passed its environmental testing used to establish flight worthiness. The rate sensing actuator operated as designed.

FOREWARD

The effort described in this document was performed by Dynamic Controls, Inc., of Dayton, Ohio, under Air Force Contract F33615-77-C-3077. The contract was performed under Project Number 24030212 entitled "Flight Control Actuation Systems Development". Work under the contract was carried out in the Air Force Flight Dynamics Laboratory (AFFDL), Flight Control Division of Wright-Patterson Air Force Base utilizing United States Air Force facilities. The work was administered by Greg Cecere, AFFDL/FGL Project Engineer.

This report covers work performed between June 1977 and February 1979. The technical report was submitted by the author in August 1979.

The author wishes to express his appreciation to the Dynamic Controls, Inc. personnel Carl N. Albright, Harry W. Schreadley, William G. Talley, and Heinrich J. Wieg for their contributions in the areas of analysis, design, fabrication and testing associated with the effort.

ACCESSION for	
NTIS	White Section <input checked="" type="checkbox"/>
DDC	Buff Section <input type="checkbox"/>
UNANNOUNCED	<input type="checkbox"/>
JUSTIFICATION _____	
BY _____	
DISTRIBUTION/AVAILABILITY CODES	
Dist.	AVAIL. and/or SPECIAL
A	

TABLE OF CONTENTS

	PAGE
SECTION I INTRODUCTION	1
SECTION II FLUTTER SUPPRESSION ACTUATOR EVALUATION	3
1. INTRODUCTION	3
2. DAMPING MODULE AND ACTUATOR DESIGN	4
2.1 Damping Module Design Description	4
2.2 Actuator Design Description	10
3. DAMPING MODULE LABORATORY TESTING	10
3.1 General	10
3.2 Damping Flow Gain Test	12
3.3 Damping Module Washout Break Frequency	16
3.4 Damping Module Dynamic Load Response	20
4. WIND TUNNEL TEST RIG DESIGN	24
4.1 General	24
4.2 Detail Design Description	25
4.2.1 <u>Support Structure</u>	25
4.2.2 <u>Safety Provisions</u>	27
4.2.3 <u>Flutter Interface Unit</u>	31
4.4.4 <u>Instrumentation</u>	34
5. TEST RIG LABORATORY EVALUATION	36
5.1 General	36
5.2 Specific Evaluation	38
5.2.1 <u>Control and Instrumentation Operation</u>	38
5.2.2 <u>Resonant Frequency Response Measurements</u>	39

TABLE OF CONTENTS (cont'd)

	PAGE
6. WIND TUNNEL EVALUATION	51
6.1 General	51
6.2 Test Section Installation	53
6.3 Wind Tunnel Test Installation	59
6.4 Test Procedure	63
6.5 Test Results	66
6.5.1 <u>Mach .6 Test Condition Results</u>	66
6.5.2 <u>Mach .8 Test Condition Results</u>	79
6.5.3 <u>Mach 0.95 Test Condition Results</u>	89
6.5.4 <u>Mach 0.95 Damping Tube Results</u>	101
7. CONCLUSIONS AND RECOMMENDATIONS	114
SECTION III FLIGHTWORTHINESS TESTING DIRECT-DRIVE ACTUATOR	
1. INTRODUCTION	116
2. FLIGHTWORTHINESS TEST PROCEDURE	121
3. TEST RESULTS SUMMARY	123
4. CONCLUSIONS AND RECOMMENDATIONS	124
SECTION IV ANGULAR RATE SENSING ACTUATOR EVALUATION	125
1. INTRODUCTION	125
2. EVALUATION TESTS	131
2.1 General	131
2.2 Specific	131
2.2.1 <u>Rate Coupler Torque and Linearity</u>	131
2.2.2 <u>Actuator Frequency Response</u>	134

TABLE OF CONTENTS (cont'd)

	PAGE
2.2.3 <u>Actuator Static Gain</u>	135
2.2.4 <u>Threshold Measurements</u>	138
2.2.5 <u>Actuator Seal Friction</u>	142
2.2.6 <u>Bandpass Response</u>	142
2.2.7 <u>Bandpass Gain</u>	145
2.2.8 <u>Cold Temperature Operation</u>	145
2.2.9 <u>Dynamic Range</u>	149
3. CONCLUSIONS AND RECOMMENDATIONS	149
APPENDIX A Flight Worthiness Tests Direct Drive FBW	156
APPENDIX B Test Report MIL-STD-810C Shock Test For Direct Drive FBW Actuator	179
BIBLIOGRAPHY	196

LIST OF ILLUSTRATIONS

FIGURE NO.	TITLE	PAGE
1		5
2	Damping Module Components	7
3	Damping Spool Sleeve	9
4	Flutter Suppression Actuator	11
5	Flow Gain Test Instrumentation Setup	13
6	Flow vs. Damping ΔP	15
7	Isolation Piston and Damping Spool Response @ 600 Psi Peak Driving Pressure	17
8	Isolation Piston and Damping Spool Response @ 1100 Psi Peak Driving Pressure	18
9	Isolation Piston and Damping Spool Response @ 1600 Psi Peak Driving Pressure	19
10	Isolation Piston and Damping Spool Pressure Response - Loaded Actuator	22
11	Damping Flow Gain Response	23
12	Wind Tunnel Test Item - Front View	26
13	Flutter Suppression Actuator Laboratory Installation	28
14	Safety Actuator Solenoid Mounting	30
15		32
16	Bending and Rotational Accelerometer Filter Response - Constant Amplitude Motion Input	35
17	Instrumentation & Control Schematic F-4 Flutter Test	37
18	Frequency Response - Actuator Position vs. SAS Command	40

LIST OF ILLUSTRATIONS (cont'd)

FIGURE NO.	TITLE	PAGE
19	Rotational Accelerometer/SAS Output Response - Magnitude Curve	44
20	Rotational Accelerometer/SAS Output Response - Phase Curve	45
21	Rotational Accelerometer/SAS Output Response - Real Part Curve	46
22	Rotational Accelerometer/SAS Output Response - Imaginary Part Curve	47
23	Rotational Accelerometer Response - Power Spectral Density	49
24	Rotational Accelerometer Response - Peak Hold Spectrum	50
25	Test Section Installation - Oblique View	54
26	Test Section Installation - Front View	55
27	Test Section Installation - Bottom View	56
28	Test Section Testing - Rotational Accelerometer/SAS Input Response	57
29	Test Section Testing - Bending Accelerometer/SAS Input Response	58
30	Response Analyzer Setup Tests - Flutter Tests	61
31	Wind Tunnel Testing Control & Measurement Setup	62
32	Bending Acceleration Amplitude Response - Mach .6 and $q = 300$ lb/sq ft	69
33	Expanded Acceleration Amplitude Response - First Bending Peak - Mach .6 and $q = 300$ lb/sq ft	70

LIST OF ILLUSTRATIONS (cont'd)

FIGURE NO.	TITLE	PAGE
34	Rotational Acceleration Amplitude Response - Mach .6 and q = 350 lb/sq ft with Damper On	73
35	Expanded Acceleration Amplitude Response - First Rotation Peak - Mach .6 and q = 350 lb/sq ft with Damper On	74
36	Rotational Acceleration Amplitude Response - Mach .6 and q = 350 lb/sq ft with Damper Off	75
37	Expanded Acceleration Amplitude Response - First Rotation Peak - Mach .6 and q = 350 lb/sq ft with Damper Off	
38	Rotational Acceleration Amplitude Response - Mach .6 and q = 500 lb/sq ft with Damper Off	77
39	Rotational Acceleration Amplitude Response - Mach .6 and q = 500 lb/sq ft with Damper On	78
40	Bending Acceleration Amplitude Response - Mach .8 and q = 500 lb/sq ft with Damper Off	81
41	Bending Acceleration Amplitude Response - Mach .8 and q = 500 lb/sq ft with Damper Off	82
42	Rotational Acceleration Amplitude Response - Mach .8 and q = 500 lb/sq ft with Damper Off	85
43	Expanded Acceleration Amplitude Response - First Rotation Peak - Mach .8 and q = 500 lb/sq ft with Damper Off	86
44	Rotational Acceleration Amplitude Response - Mach .8 and q = 500 lb/sq ft with Damper On	87
45	Expanded Acceleration Amplitude Response - First Rotation Peak - Mach .8 and q = 500 lb/sq ft with Damper On	88
46	Bending Acceleration Amplitude Response - Mach 0.95 and q = 500 lb/sq ft With Damper On	91
47	Expanded Acceleration Amplitude Response - First Bending Peak - Mach 0.95 and q = 500 lb/sq ft With Damper On	92

LIST OF ILLUSTRATIONS (cont'd)

FIGURE NO.	TITLE	PAGE
48	Bending Acceleration Amplitude Response - Mach 0.95 and $q = 500$ lb/sq ft with Damper Off	94
49	Expanded Acceleration Amplitude Response - First Bending Peak - Mach 0.95 and $q =$ 500 lb/sq ft with Damper Off	95
50	Rotational Acceleration Amplitude Response - Mach 0.95 and $q = 650$ lb/sq ft with Damper Off	96
51	Expanded Acceleration Amplitude Response - First Rotation Peak - Mach 0.95 and $q =$ 650 lb/sq ft with Damper Off	97
52	Rotational Acceleration Amplitude Response - Mach 0.95 and $q = 650$ lb/sq ft with Damper On	98
53	Expanded Acceleration Amplitude Response - First Rotation Peak - Mach 0.95 and $q =$ 650 lb/sq ft with Damper On	99
54	Bending Accelerometer Amplitude Response - Mach 0.95 and $q = 550$ lb/sq ft with Large Damping Tube	103
55	Expanded Acceleration Amplitude Response, Full Bending Peak - Mach 0.95 and $q =$ 550 lb/sq ft with Large Damping Tube	104
56	Bending Acceleration Amplitude Response - Mach 0.95 and $q = 550$ lb/sq ft with Small Damping Tube	107
57	Expanded Acceleration Amplitude Response, Full Bending Peak - Mach 0.95 and $q =$ 550 lb/sq ft with Small Damping Tube	108
58	Rotational Accelerometer Amplitude Response - Mach 0.95 and $q = 550$ lb/sq ft with Small Damping Tube	109
59	Expanded Acceleration Amplitude Response, Full Rotational Peak - Mach 0.95 and $q =$ 550 lb/sq ft with Small Damping Tube	110

LIST OF ILLUSTRATIONS (cont'd)

FIGURE NO.	TITLE	PAGE
60	Rotational Acceleration Amplitude Response - Mach 0.95 and $q = 550$ lb/sq ft with Large Damping Tube	111
61	Expanded Acceleration Amplitude Response, Full Rotational Peak - Mach 0.95 and $q = 550$ lb/sq ft with Large Damping Tube	112
62	Direct Drive "Fail-Operate" Control System	118
63	Direct Drive Aileron Flight Test Actuator	120
64	Direct Drive Aileron Flight Test Electronics	122
65	Rate Sensing Actuator Top View	128
66	Rate Sensing Actuator Rear View	129
67	Rate Sensor Actuator Front View	130
68	Section C Rate Sensing Actuator	132
69	Section D Rate Sensing Actuator	133
70	Eddy Current Coupler Torque Characteristics	135
71	Actuator Response Test Setup	137
72	Actuator Frequency Response	138
73	Rate Sensing Actuator on Test Rate Table	140
74	Threshold Data Strip	142
75	.3 Hz Frequency Response Data Strip	144
76	Frequency Response - Rate Sensing Actuator 80°F	145
77	Frequency Response - Rate Sensing Actuator -40°F	147
78	Cold Temperature Test	148

LIST OF ILLUSTRATIONS (cont'd)

FIGURE NO.	TITLE	PAGE
79	Frequency Response Data Strip -40°F	150
80	.1 Hz Amplitude Response Data Strip	151
81	.3 Hz Amplitude Response Data Strip	152
82	1 Hz Amplitude Response Data Strip	153
A-1	Direct Drive Performance Test Setup	159
A-2	Low Temperature Test Profile	164
A-3	High Temperature Test	166
A-4	Command Amplifier Thermocouple Location	168
A-5	Thermocouple Locations for Power Amp Module	169
A-6	Terminal Peak Sawtooth Shock Pulse	173
A-7	Vibration Test Curve	175
B-1	Positive and Negative Shock Pulse References and Tolerances	182
B-2	Electronic Module - A	183
B-3	Electronic Module - B	184
B-4	Electronic Module - C	185
B-5	Electronic Module - D	186
B-6	Control Panel X Axis	187
B-7	Control Panel Z Axis	188
B-8	Control Panel Y Axis	189
B-9	Control Valve X Axis First Test	190
B-10	Control Valve Y Axis First Test	191
B-11	Control Valve Z Axis First Test	192
B-12	Control Valve Z Axis Second Test	193
B-13	Control Valve X Axis Second Test	194
B-14	Control Valve Y Axis Second Test	195

LIST OF TABLES

TABLE	DESCRIPTION	PAGE
1	Mach .6 Wind Tunnel Test Results Bending Mode	68
2	Mach .6 Wind Tunnel Test Results Rotation Mode	72
3	Mach .8 Wind Tunnel Test Results Bending Mode	80
4	Mach .8 Wind Tunnel Test Results Rotation Mode	84
5	Mach 0.95 Wind Tunnel Test Results Bending Mode	90
6	Mach 0.95 Wind Tunnel Test Results Rotation Mode	93
7	Mach 0.95 Wind Tunnel Test Results Bending Mode	102
8	Mach 0.95 Wind Tunnel Test Results Rotation Mode	106
9	Measured Threshold	139 & 140

SECTION I
INTRODUCTION

This document describes the results of some of the specific technical efforts conducted under Air Force Contract F33615-77-C-3077 by Dynamic Controls, Inc. The efforts and the results presented in this technical report are:

1. The development of a flutter suppression actuator technique and the wind tunnel evaluation of that technique.
2. The development and flightworthiness testing of a direct drive Fly-By-Wire flight control system applied to the aileron axis of an F-4 aircraft.
3. The evaluation of an angular rate sensing augmentation actuator supplied to the Air Force by Dynamic Controls, Inc.

The first two efforts above are based on work previously conducted by Dynamic Controls, Inc. for the Air Force Flight Dynamics Laboratory. The theory of the flutter suppression actuator technique is described in technical report AFFDL-TR-75-29. The direct drive prototype hardware upon which the flight worthiness test hardware is based is described in technical report AFFDL-TR-77-91.

The angular rate sensing actuator evaluation is a performance evaluation of an angular rate sensor integrated with a hydro-mechanical actuator. The mechanization uses no electronics for its operation.

All the research and development activity described in this report (with the exception of the wind tunnel testing) was conducted at Wright-Patterson Air Force Base, Ohio, by Dynamic Controls, Inc. using the Actuation Laboratory in Bldg. 145, Area B. The

wind tunnel testing for the flutter suppression actuator was conducted at Arnold Engineering Development Center in Tennessee.

The three efforts are presented as separate sections of this report in the order listed on the previous page. The conclusions and recommendations for each technical effort are included in its corresponding section.

SECTION II

FLUTTER SUPPRESSION ACTUATOR EVALUATION

1. INTRODUCTION

The flutter suppression actuator investigation consisted of both laboratory and wind tunnel testing of a unique F-4 stabilator actuator. The actuator incorporated a reduced drive area and a damping module to increase the damping of the actuator over a specific frequency range. The theory for the technique and the sizing calculations used in the construction of the test hardware are presented in AFFDL TR-75-29 and are therefore not repeated in detail in this report.

Classical flutter is due to an exchange of energy extracted from the airstream and stored in the bending and torsional motions of an airfoil. At the flutter frequency, the motions of the airfoil in bending and torsion are in a phased relationship where the potential energy from bending is transferred to the torsional twisting of the airfoil. The flutter frequency lies between the individual resonant frequencies of the bending and torsional vibration modes. The conventional method of increasing the flutter speed of an airfoil is to increase the stiffness of the airfoil. For slab type surfaces (like the F-4 and F-111 horizontal tails) the torsional stiffness is primarily determined by the control actuator. Therefore, increasing the torsional stiffness of the slab type control surface is accomplished by increasing the actuator stiffness. This is done by increasing the actuator size, particularly the drive area since the oil column stiffness generally dominates the actuator stiffness value. This stiffness increase by increasing the size of the actuator carries with it a weight and hydraulic power consumption penalty.

The technique used for flutter suppression with the modified F-4 actuator is based upon using negative pressure feedback to cause the stabilator actuator to act as a damper and absorb energy in the torsional mode over the flutter frequency range. Suppression of the torsional mode should eliminate classical flutter since the transfer of energy between the torsion and bending modes is eliminated. The capability of adding torsional damping with little added weight allows sizing the control actuator for the force required to maneuver the aircraft, rather than oversizing the actuator to increase the torsional resonance frequency. For the F-4 stabilator application, the drive area required for maneuvering is 3.44 in^2 . The drive area of the normal F-4 stabilator is 6.0 in^2 as sized for the flutter requirements.

The following subsections describe the design of the damping modules and actuator, the laboratory tests of the damping modules, the design of the test rig for the wind tunnel, the laboratory evaluation of the test rig operation and the wind tunnel evaluation of the test rig.

2. DAMPING MODULE AND ACTUATOR DESIGN

2.1 Damping Module Design Description

Figure 1 shows the hydromechanical circuit used in the test hardware for the damping module. The operation of the damping circuit is designed to be effective over a limited frequency range. The isolation piston eliminates steady differential load pressures from being applied to the damping spool. As the load pressure varies with increasing frequency, the isolation piston movement creates a flow. At low frequencies, the flow generated by the isolation piston passes primarily through the washout orifice R_2 .

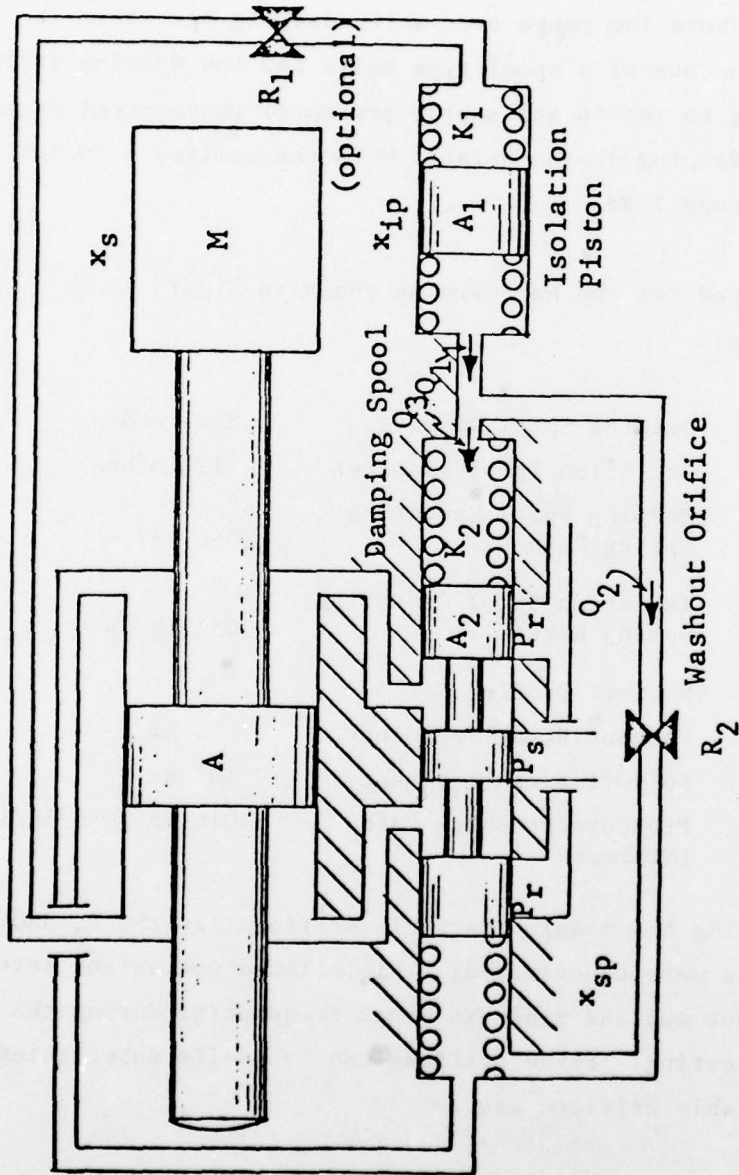


FIGURE 1 - Hydromechanical Damping Circuit Schematic

As the frequency of the load pressure variation increases, the damping spool moves, creating a damping orifice across the actuator piston. The orifice R_1 is used to attenuate the response of the isolation piston to load pressure variations at frequencies above the range over which damping operation is required. The use of a spool type valve for the damping orifice (with porting to return and supply pressure) is required to generate the correct damping characteristic with the control actuator holding a steady load.

The values used for the hardware as shown in Figure 1 are the following:

Damping Spool Diameter	.312 inches
Isolation Spool Diameter	.312 inches
Damping Spool Centering Spring Rate K_2	1050 lb/in
Isolation Spool Centering Spring Rate K_1	1050 lb/in
Nominal Damping Ratio	1
Washout Break Frequency	5 Hz
Rolloff Break Frequency	100 Hz
Pressure Feedback Gain (Minimum)	.016 in ³ /sec/lb/in ²

In constructing the module, variable orifices for the R_2 and R_1 components were constructed. This allowed convenient setting of the washout and the response break frequencies during the evaluation testing. Fixed orifices can be easily substituted for the variable orifices used.

Figure 2 shows the components of the damping module. Note that in Figure 2, the damping spool centering springs are positioned

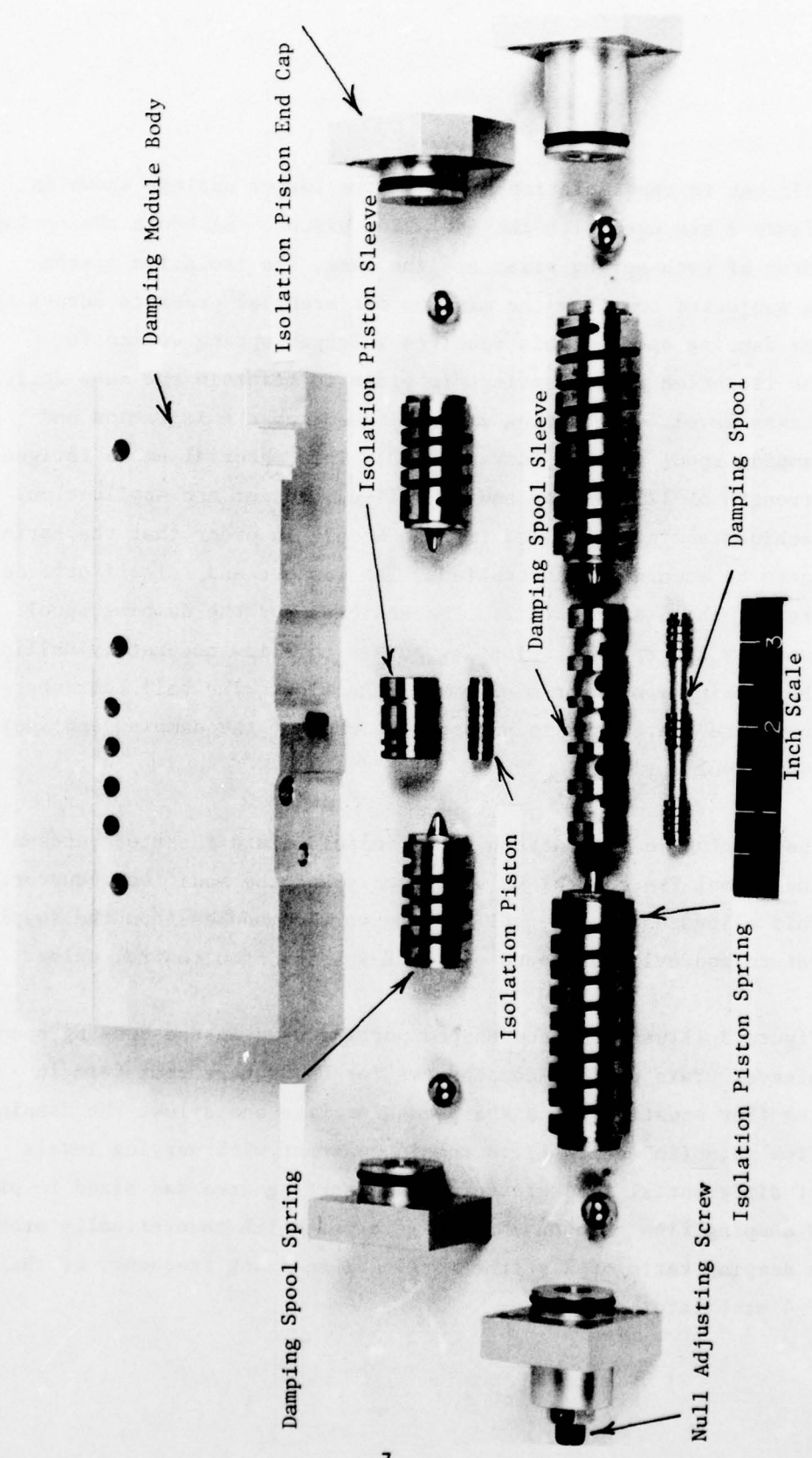


FIGURE 2 Damping Module Components

adjacent to the isolation piston. The larger springs shown in Figure 2 are used with the isolation piston. Although the spring rates of both spring sizes are the same, the isolation piston is subjected to twice the maximum differential pressure across the damping spool. This requires a larger spring volume for the isolation piston springs in order to maintain the same design stress level. The spring material used for the isolation and damping spool springs is Vasco 300. This material has a fatigue strength of 125,000 psi and is well suited for the application. Machined springs are used for the module in order that the spring rates be accurately controlled. The washout and rolloff orifices are not shown in Figure 2. The end caps for the damping spool assembly incorporate adjusting screws to allow accurately nulling the damping spool for minimum leakage flow. The ball bearings shown in Figure 2 are used to support the ends of the damping and isolation spool springs.

The damping modules attach to a manifold plate inserted between the normal F-4 control valve assembly and the modified actuator. This allows using internal porting to the modules from the supply, return and cylinder ports of the F-4 stabilator control valve.

Figure 3 illustrates the shaped porting used in the damping spool sleeve. This porting compensates for the square root term in the flow equation for a sharp edge orifice and allows the damping flow gain ($\text{in}^3/\text{sec}/\text{psi}$) to remain constant with varying levels of differential load pressure. The porting area was sized to provide a damping flow gain of $.032 \text{ in}^3/\text{sec}/\text{psi}$ which theoretically provides a damping ratio of 2 at the torsional resonant frequency of the F-4 stabilator surface.

Shaped Porting

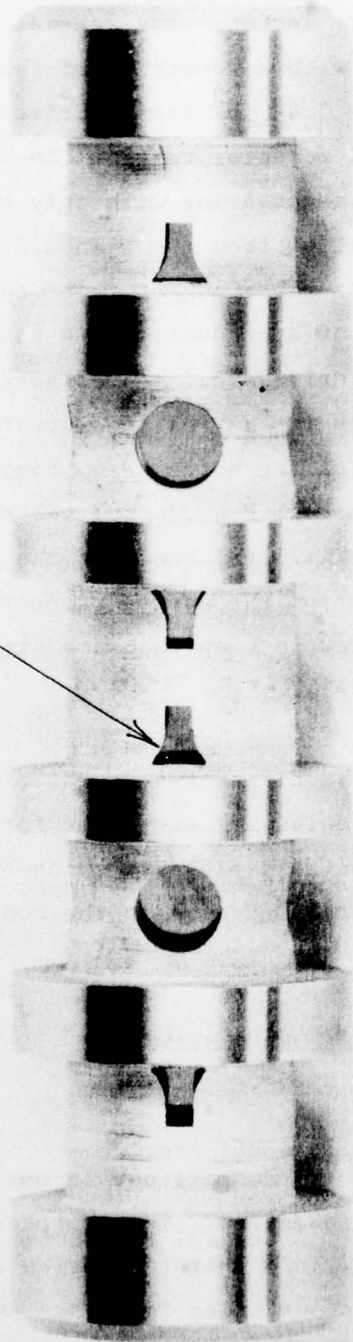


FIGURE 3 Damping Spool Sleeve

2.2 Actuator Design Description

The actuator used with the damping modules is designed with a drive area of 3.44 square inches. The general design is that of the normal F-4 actuator with a reduction of the piston diameter necessary to produce the 3.44 in² design drive area. This drive area allows the modified actuator to meet the hinge moment requirements for aircraft maneuvering with only one hydraulic system operating and is a reduction from the standard actuator's 6.0 in² drive area. To construct the actuator, a piston and rod assembly and the barrel end caps of a production F-4 actuator were modified to produce the required drive area. A new actuator barrel was fabricated. The new actuator barrel incorporated the same porting and mounting provisions as the normal F-4 stabilator actuator. This allowed using the normal F-4 control valve assembly with the modified actuator. The wall thickness of the actuator barrel was kept the same as that of the normal production actuator (although it could have been reduced to keep the same stress level as in the normal F-4 actuator barrel).

Figure 4 illustrates the modified F-4 actuator with the damping modules mounted. Two modules are used, one for each half of the tandem actuator. The manifold plate to which the manifolds are attached is mounted directly underneath the control valve assembly.

3. DAMPING MODULE LABORATORY TESTING

3.1 General

The correct operation of the damping module was evaluated with several different test procedures. These procedures were used to establish the static flow gain characteristics of the damping spool and sleeve, the washout break frequency and its amplitude dependence, and the frequency response characteristics of the damping module.

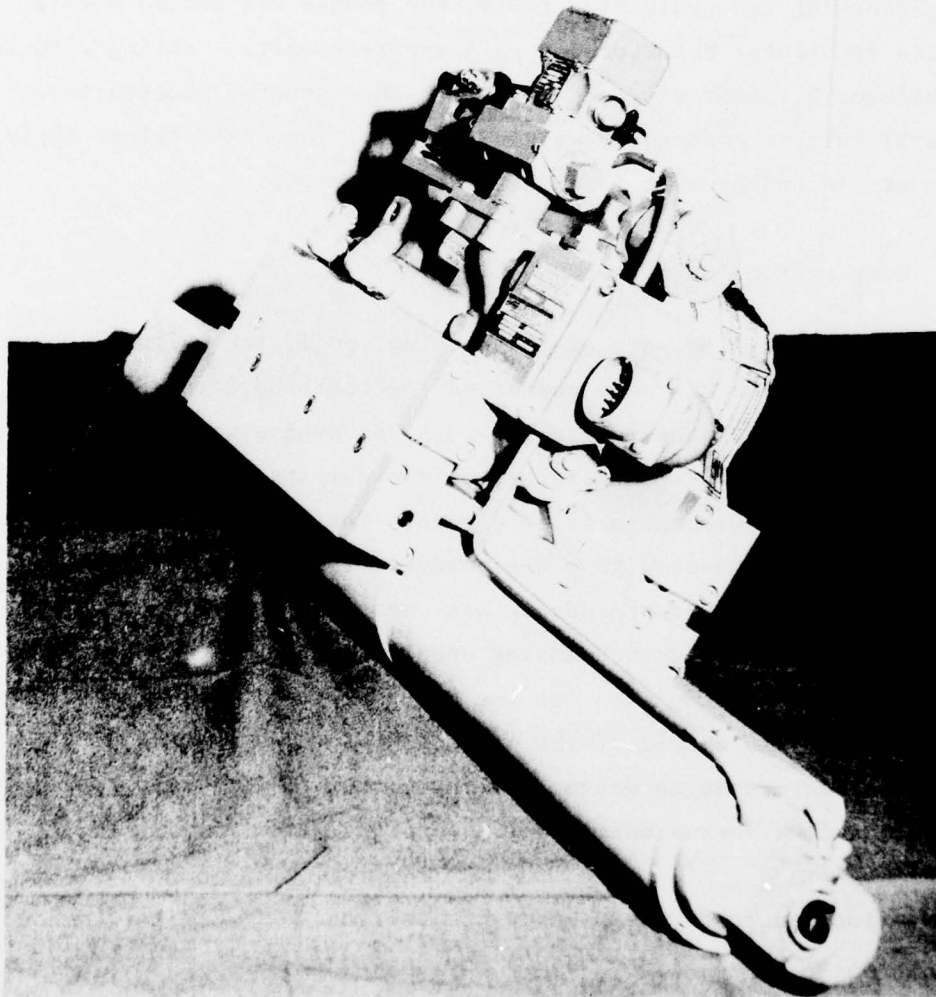


FIGURE 4 Flutter Suppression Actuator

To evaluate the performance parameters of the damping module, ports were added to the module body to allow external connection of supply and return pressure lines and the monitoring of pressures at the ends of the isolation and damping spools of the module. In addition, an adapter block was fabricated which allowed operation of the module separated from the stabilator actuator.

In performing the evaluation tests, the module was tested mounted on the stabilator actuator and as a separate unit. Testing with the stabilator actuator was conducted with the actuator mounted in a General Purpose Actuator Test Rig (GPATR). The GPATR allows applying both static and dynamic loads to a test actuator.

3.2 Damping Flow Gain Test

To evaluate the flow gain of the damping spool, the cylinder ports of the damping module were connected together and a turbine flow meter installed in the return line. A servovalve was used to apply a differential pressure across the damping and isolation spools with the washout orifice closed. The output of the turbine flowmeter was connected to a frequency-to-voltage converter. A differential pressure transducer was used to measure the pressure signal applied across the damping spool. Figure 5 shows the instrumentation setup used for the damping spool flow gain evaluation. The output of the pressure transducers and the flowmeter were used to drive an x-y recorder in order to create a plot of flow versus applied differential pressure.

A function generator was used to command the variation of the differential pressure applied to the damping module. In order to improve the controllability of the differential pressure generated

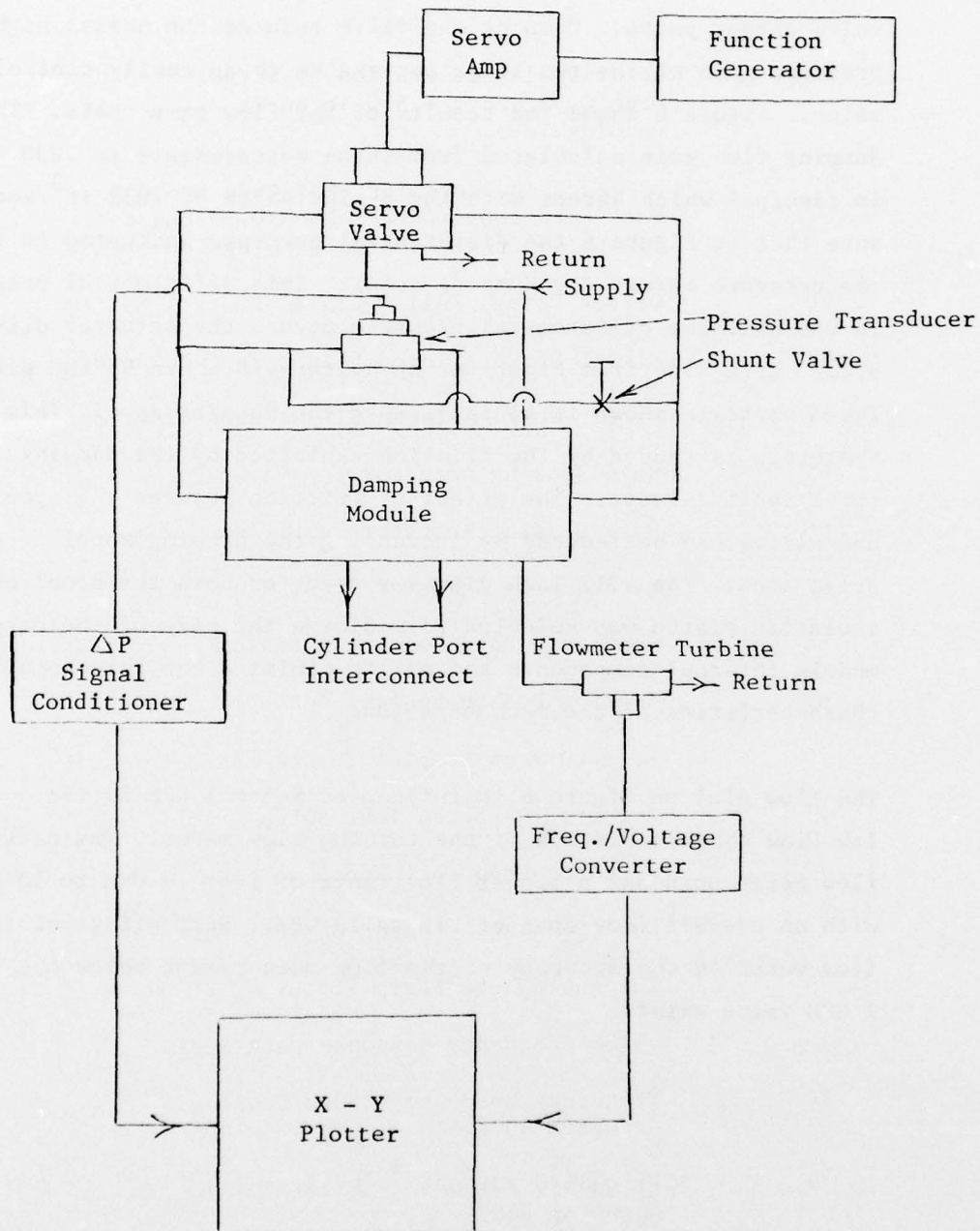


FIGURE 5 Flow Gain Test Instrumentation Setup

by the servovalve, a needle valve was installed across the servovalve output ports. Opening the valve reduced the normal high pressure gain of the two stage servovalve to an easily controlled value. Figure 6 shows the results of the flow gain tests. The damping flow gain calculated from these measurements is $.030 \text{ in}^3/\text{sec}/\text{psi}$ which agrees with the design value of $.032 \text{ in}^3/\text{sec}/\text{psi}$. Note that on Figure 6 the differential pressure indicated is for the pressure across the damping spool. This differential pressure is one half the differential pressure across the actuator drive area. Note also from Figure 6 the hysteresis shown by the plot. The hysteresis shown is 40 psi across the damping spool. This hysteresis is caused by the friction exhibited by the damping spool in its sleeve. The effect of friction between the spool and sleeve can be reduced by increasing the damping spool drive area. The .312 inch diameter used for both the spool and isolation piston was selected to minimize the size of the damping module internal components and not to minimize the threshold characteristics of the mechanization.

The flow plot on Figure 6 is influenced below 1 GPM by the low flow characteristics of the turbine flow meter. The particular flow meter used has a linear flow range of from .7 GPM to 10 GPM, with an overall flow span of .10 to 10 GPM. Some effect of the flow meter on the accuracy of the flow measurement below the 1 GPM value exists.

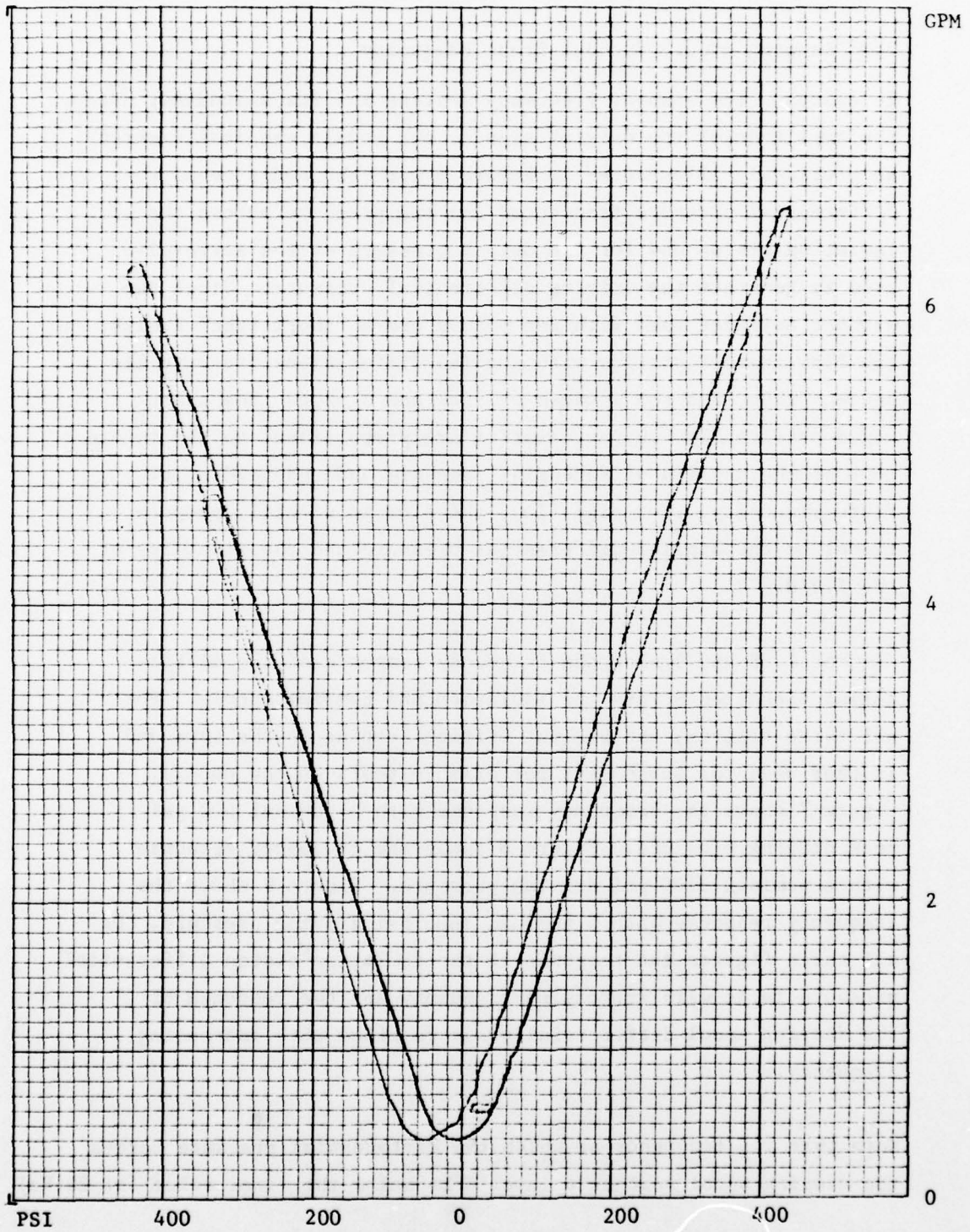


FIGURE 6 Flow vs. Damping Δp

3.3 Damping Module Washout Break Frequency

To evaluate the washout frequency setting and its dependency upon the amplitude of the driving signal, the module was instrumented as previously illustrated in Figure 5 with the addition of a differential pressure transducer for the pressure across the isolation piston and for the output pressure of the servovalve used to generate the driving differential pressure. Since the washout orifices used with the module are a "short tube" design, the flow characteristics with applied differential pressure lie between that of a sharp edged orifice and a pipe. The sharp edged orifice flow characteristics are proportional to the square root of the applied differential pressure and independent of fluid viscosity. For pipe flow, the flow is directly proportional to the applied differential pressure and the viscosity of the fluid.

Figures 7, 8 and 9 show the frequency response of the differential pressures across the isolation and damping spools. For all three figures, the washout orifice setting is the same and is that used for subsequent performance tests on the module. Figure 7 shows the frequency response with a nominal 600 psi peak driving pressure. Figure 8 shows the frequency response with a nominal 1100 psi driving pressure. Figure 9 shows the frequency response with a nominal 1600 psi driving pressure. On all three figures the response of the isolation piston differential pressure falls with increasing frequency and the response of the damping spool differential pressure rises with increasing frequency.

Note that the frequency at which the differential pressure across the damping spool reaches a level 3 Db below the final value (at 20 Hz)

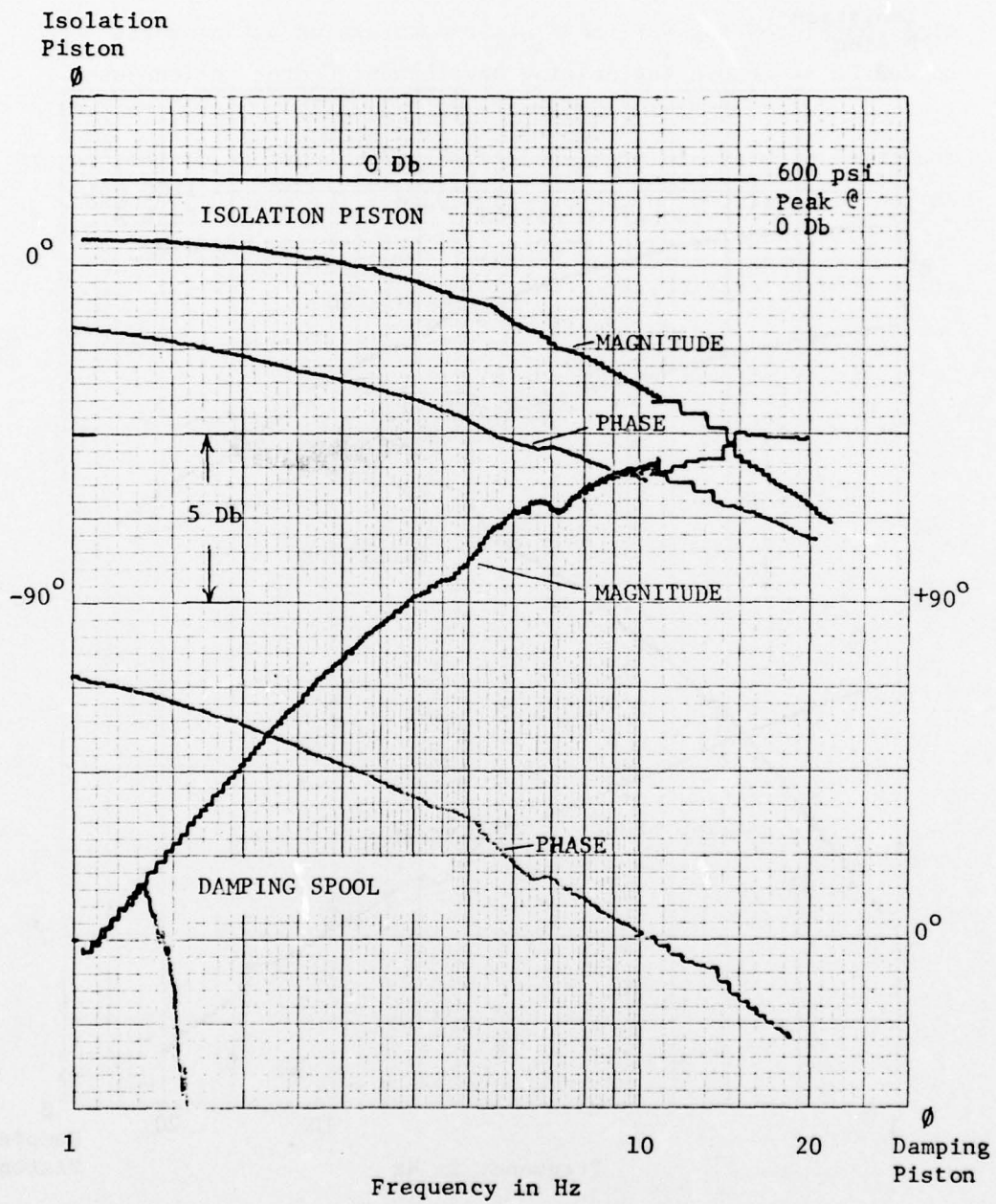


FIGURE 7 Isolation Piston and Damping Spool Response @ 600 Psi Peak Driving Pressure

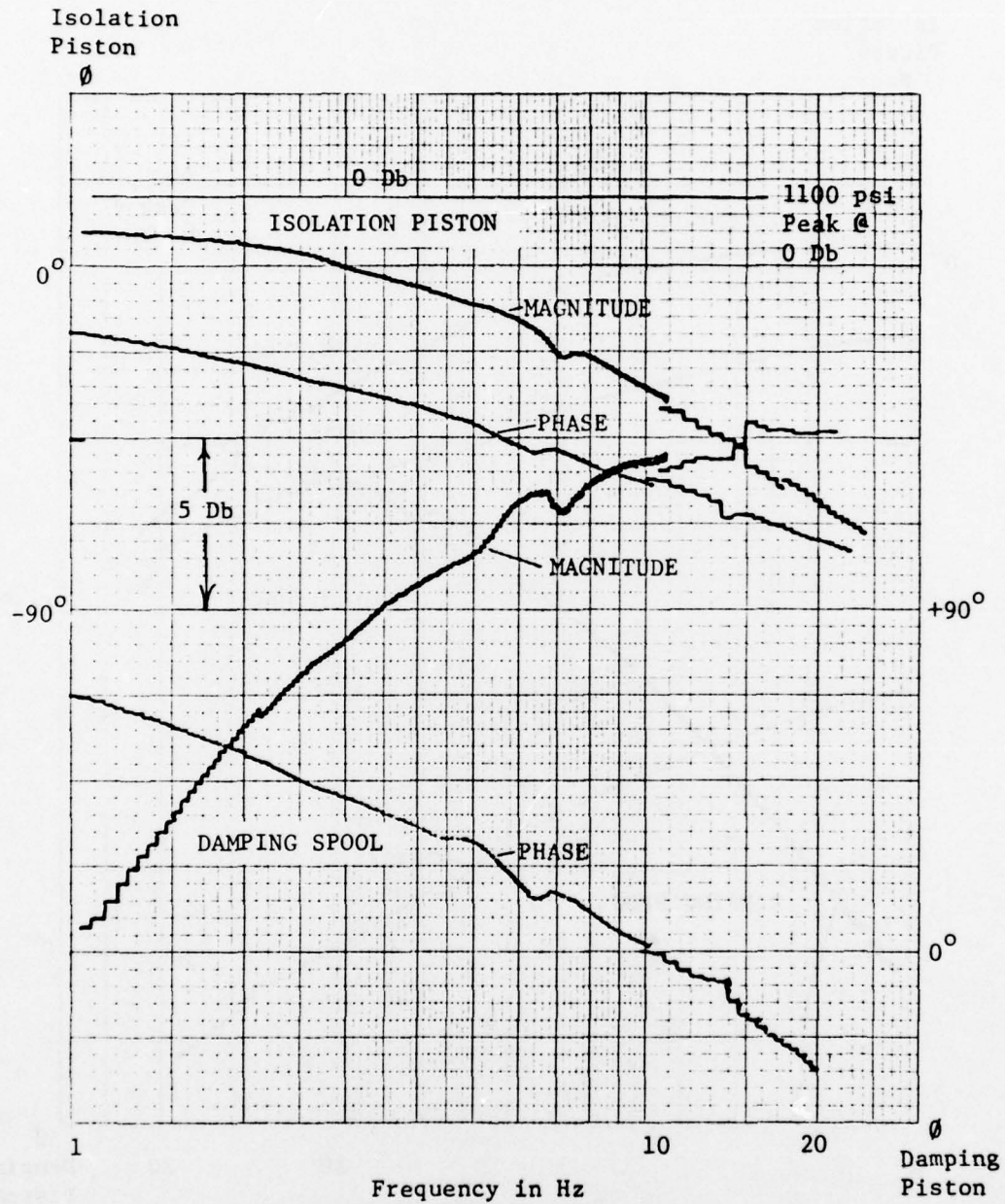


FIGURE 8 Isolation Piston and Damping Spool Response @ 1100 Psi Peak Driving Pressure

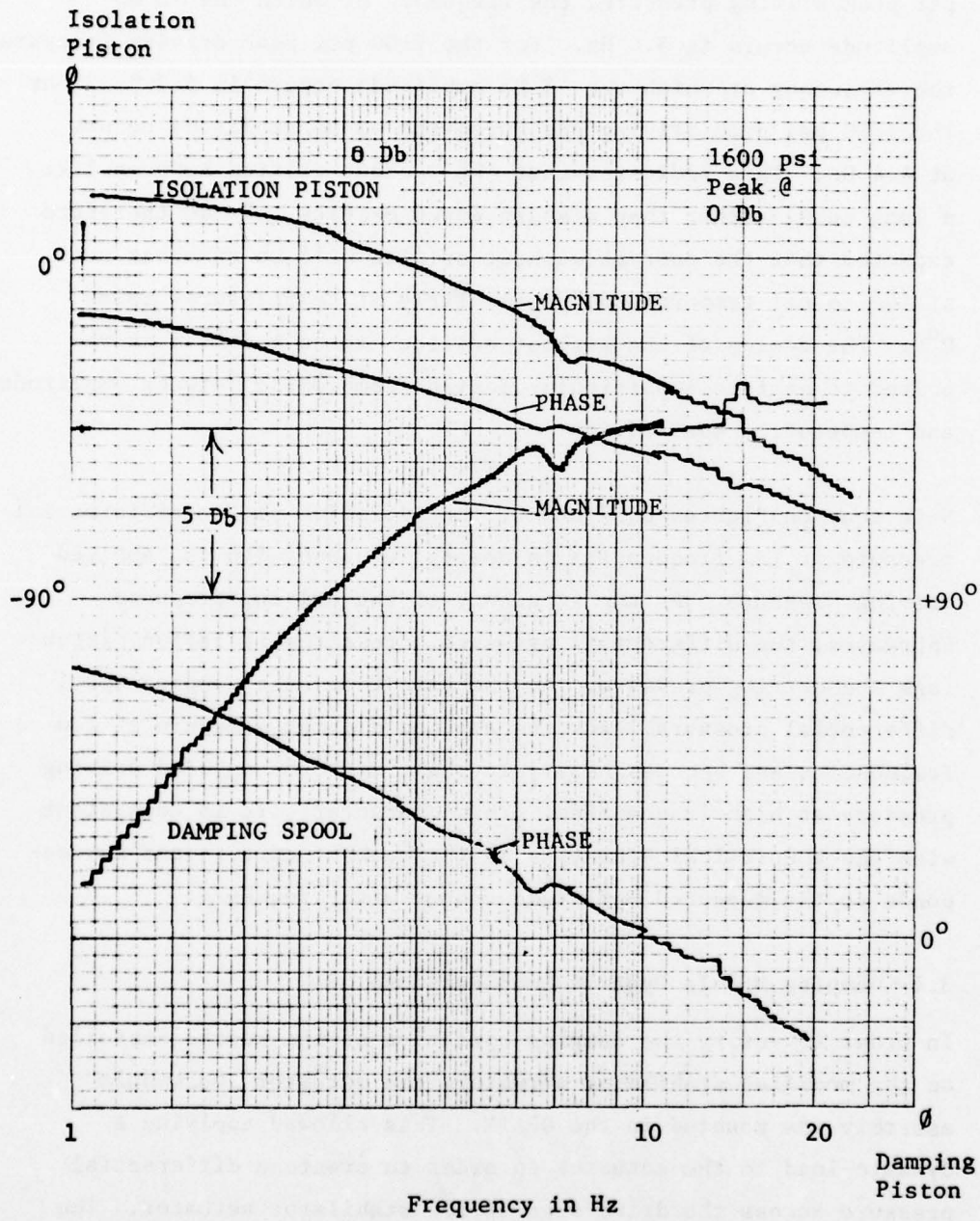


FIGURE 9 Isolation Piston and Damping Spool Response @ 1600 Psi Peak Driving Pressure

varies only slightly with driving pressure changes. For the 600 psi peak driving pressure, the frequency at which the -3 Db amplitude occurs is 5.4 Hz. For the 1100 psi peak driving pressure, the frequency at which the -3 Db amplitude occurs is 5.2 Hz. For the 1600 psi peak driving pressure, the -3 Db amplitude occurs at 4.4 Hz. This indicates that the washout orifice behaves like a long tube, rather than a sharp edged orifice. It is therefore expected that the current washout orifice will be somewhat sensitive to oil temperature, particularly at temperatures below 0°F. The design of the washout orifice can be modified as required to achieve a particular desired compromise between amplitude and temperature sensitivity.

Note that on Figures 6, 7 and 8, the isolation piston differential pressure at low frequencies is nearly in phase with the applied driving pressure. As the frequency of the driving pressure increases, the differential pressure across the isolation piston lags the driving pressure. At the same time, the damping spool differential pressure leads the applied driving pressure at low frequencies and becomes nearly in phase with the applied driving pressure at high frequencies. This characteristic is consistent with the theoretical operation of the washout circuit and corresponds to the measured amplitude change with frequency.

3.4 Damping Module Dynamic Load Response

In order to verify the damping operation of the module installed on the modified stabilator actuator, the actuator and module assembly was mounted in the GPATR. This allowed applying a dynamic load to the actuator in order to create a differential pressure across the drive area of the stabilator actuator. The module was instrumented to measure the flow passing through the damping spool by connecting the return line flow from the damping

module through a turbine flow meter. The module was also instrumented to allow recording of the differential pressures across the isolation piston and damping spool. For the load tests, the mechanical input to the control valve of the stabilator actuator was attached to the framework of the GPATR. This established a grounded input for the mechanical spool valve of the actuator.

Two performance tests were run with the stabilator actuator and module mounted in the GPATR. For these tests, only one half of the actuator and one module were operated (the other half of the actuator being bypassed and the module unpressurized). This allowed evaluating the performance characteristics of a single unit, without the interaction possible with two modules operating at the same time. Figure 10 is a response plot of the differential pressures across the isolation and damping spool with a constant 2000 lb peak load applied to the stabilator actuator. This plot is taken from chart recorder data of the applied load and the corresponding differential pressures. Only the amplitude response is presented. Note that the -3 Db amplitude for the damping spool differential pressure occurs at 4.3 Hz. This frequency agrees with that measured for the module separated from the stabilator actuator. The test results verify the correct operation of the washout circuit for the driving pressures for the damping module with the module mounted on the stabilator actuator.

Figure 11 shows the frequency response of the damping flow gain of the damping spool with the actuator subjected to a 2000 lb. peak load force. This figure was plotted from chart recorder data of the load force and the flow through the turbine flow meter. The response has been corrected for the measured response characteristics of the flow meter. For proper operation of the damping module, the damping flow gain should remain above .016 cis/psi from 10 to 20 Hz and the flow and the applied load should be nearly in phase with each other. Figure 11 shows

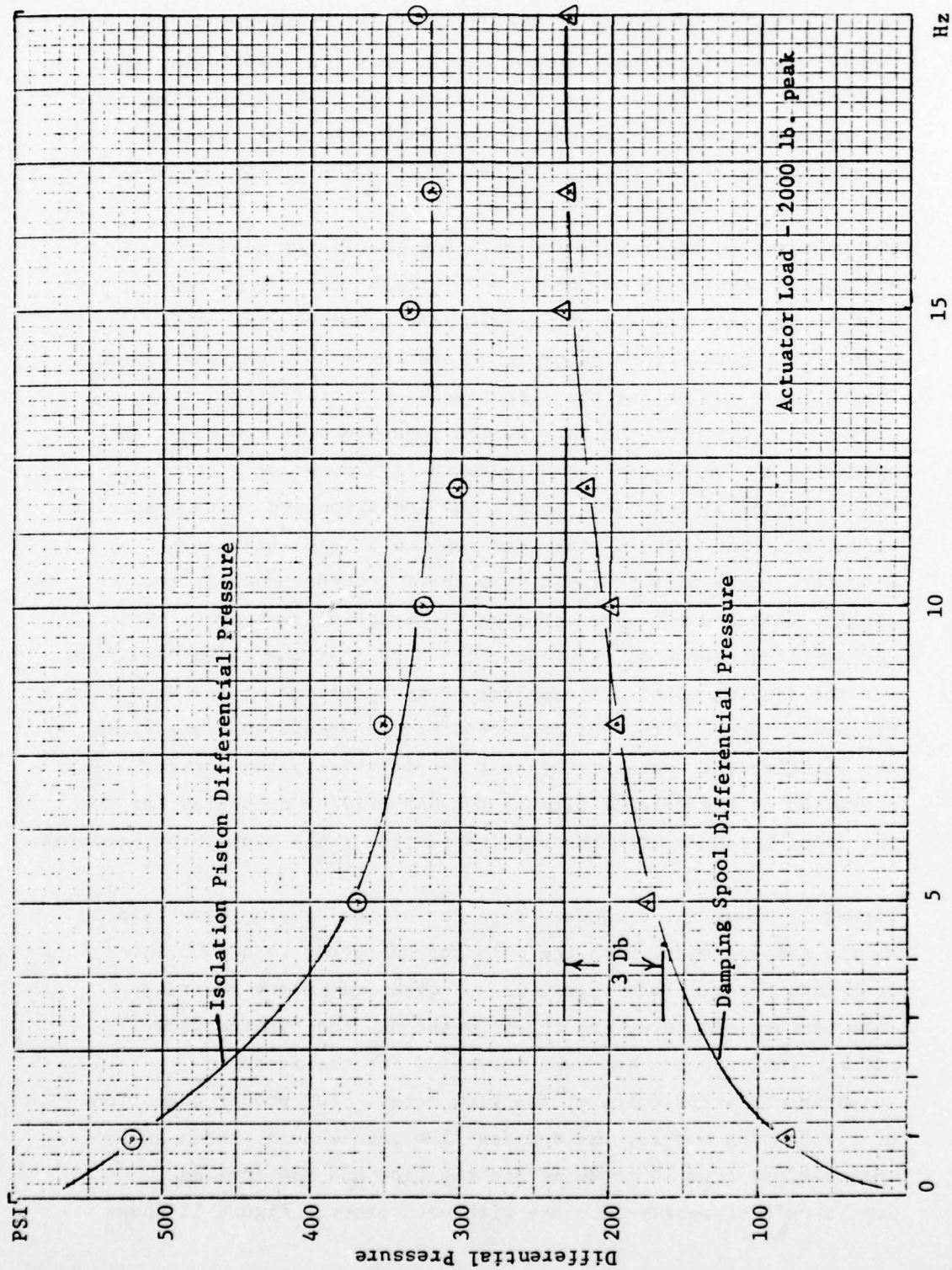


FIGURE 10 Isolation Piston and Damping Spool Pressure Response - Loaded Actuator

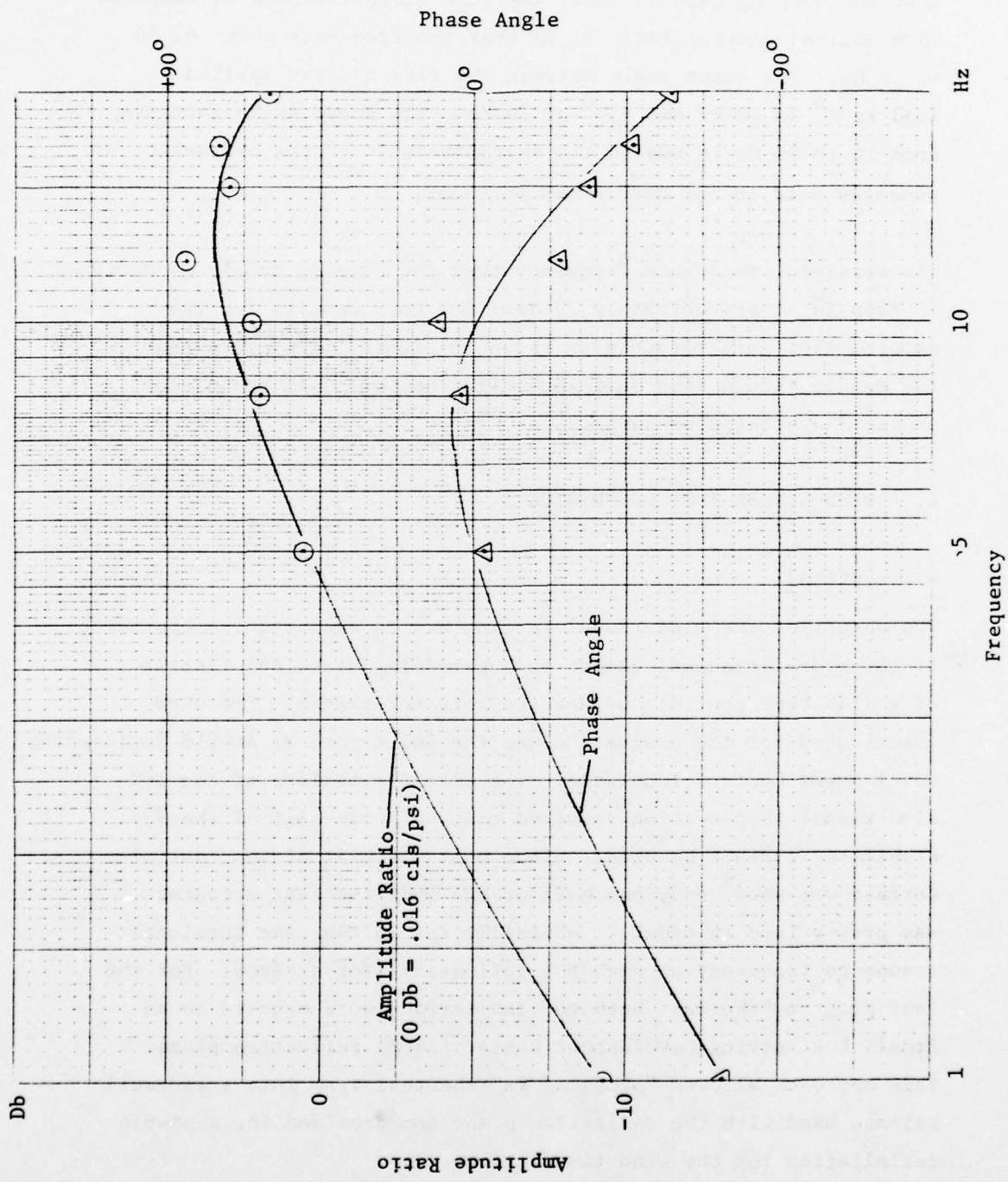


FIGURE 11 Damping Flow Gain Response

that the damping gain is above the .016 cis/psi (which corresponds to a nominal damping ratio of 1) over the frequency range of 10 to 20 Hz. The phase angle between the flow and the applied load is 0° at 10 Hz and -54° at 20 Hz. The phase angle increase from 10 to 20 Hz is due to the characteristic of the hydraulic passages used in the module and actuator.

The torsional resonance frequency that the damping module is designed to damp is at approximately 20 Hz. The test results for the damping flow gain response as shown in Figure 11 indicate that the module should damp satisfactorily the torsional resonance of the F-4 stabilator surface.

4. WIND TUNNEL TEST RIG DESIGN

4.1 General

The object of the wind tunnel testing was to evaluate the operation of the hydromechanical damper on suppressing classical flutter of a slab type control surface and actuator system. The wind tunnel used for the evaluation was the 16T tunnel at Arnold Engineering Development Center, Tennessee. The size limitations of the 16T wind tunnel test section required that only one half of the F-4 stabilator surface be used. Since only one half of the control surface was used, only one half of the modified test actuator was pressurized in order to nominally retain the same torsional resonance frequency as with the full stabilator surface. For the test program, the test actuator and surface were mounted to an Arnold Engineering Development Center (AEDC) reflection plane. This approach allowed "plugging in" the test item into a sidewall balance used with the reflection plane and provided for a simple installation for the wind tunnel tests.

To prevent damage to the test item and wind tunnel during the testing, several safety provisions, including a safety actuator and mechanical surface deflection limits, were incorporated in the wind tunnel test item design.

To monitor operation of the test item, the bending and torsional motions of the stabilator surface and the output motion of the stabilator actuator were instrumented.

The test item was designed to mate with existing structure of an AEDC reflection plane as defined by drawings provided by the test facility operators, ARO Inc.

4.2 Detail Design Description

4.2.1 Support Structure

Figure 12 is a photograph of the one half stabilator surface and support structure mounted in a laboratory framework prior to shipment to AEDC. The black framework in this photograph was constructed to hold the test item for shipment to AEDC and preliminary laboratory evaluation prior to shipment. Notice in Figure 12 that a fairing is part of the test item. This was required to replace that portion of the aircraft fuselage between the stabilator control actuator and the inboard edge of the stabilator surface.

The support structure incorporated the pivots for the surface and the stabilator mounting points. As mounted in the reflection plane, the control actuator and its support inboard of the fairing were not in the airstream of the wind tunnel, but were enclosed in a portion of the reflection plane support structure.

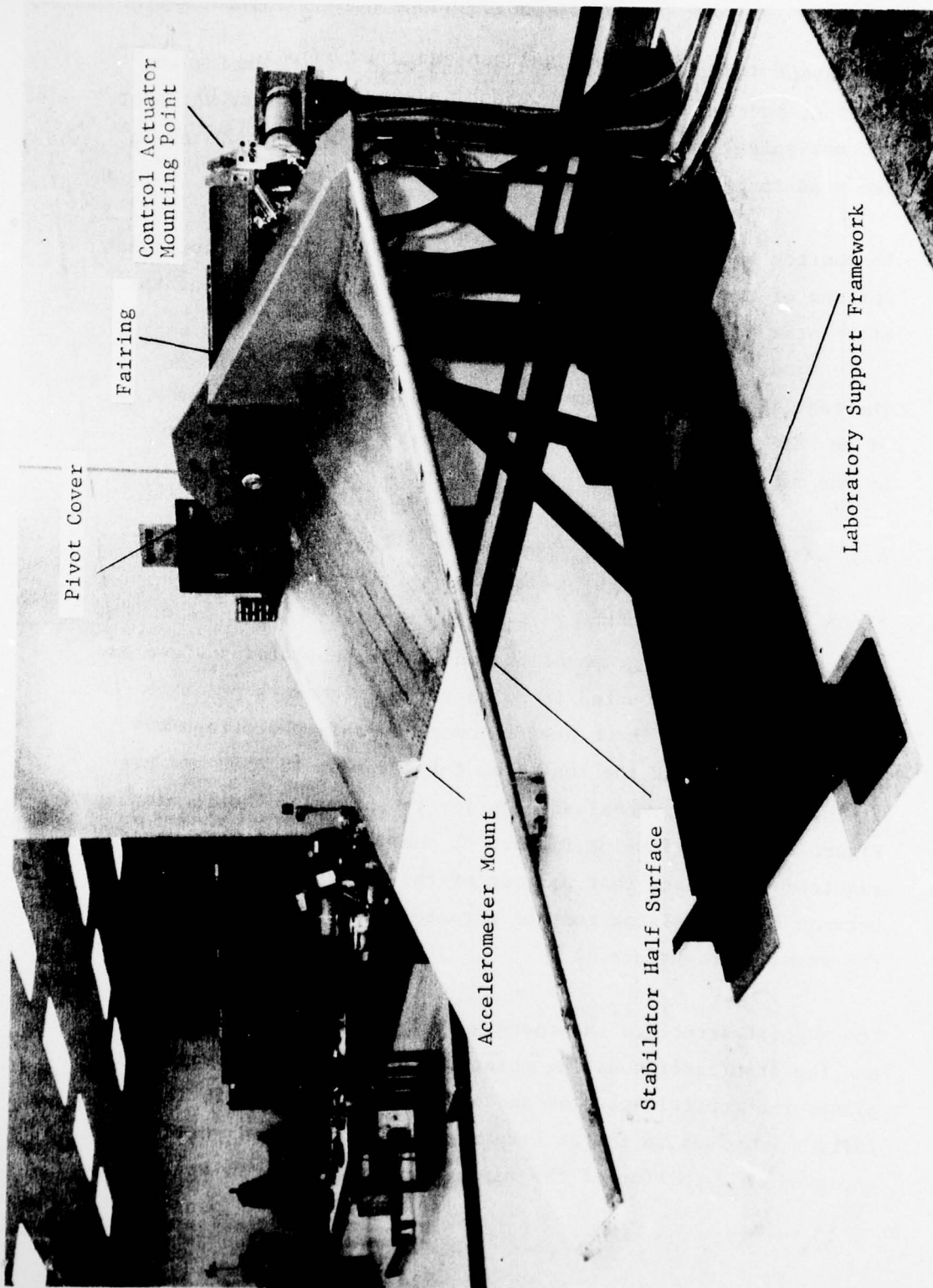


FIGURE 12 Wind Tunnel Test Item - Front View

The fairing filled in the space between the reflection plane face and the inboard edge of the stabilator surface.

The fairing was constructed of aluminum plate. The remainder of the support structure was constructed of structural steel. The structure was designed to accept an aerodynamic surface load of 5000 lbs and an aerodynamic hinge moment of 2500 foot lbs.

The support structure incorporated mounting provisions for a safety actuator. This actuator was mounted to operate in parallel with the modified stabilator control actuator.

4.2.2 Safety Provisions

To prevent catastrophic loss of the stabilator surface during the wind tunnel testing, the commanded angle of attack for the surface was limited to $\pm 1.5^\circ$. This was accomplished by adding mechanical stops to the control actuator to limit the control actuator stroke. One stop was incorporated externally around the actuator piston rod. The other was incorporated inside the actuator barrel in the section of the actuator which was not pressurized. Figure 13 is a view of the control actuator as mounted in the support structure. Note that the mechanical input for the control actuator is attached with a rod to the support structure. This photograph also shows the hydraulic hose connections and hydraulic filter used with the test item. Also shown is an accelerometer used to measure the rotational acceleration of the stabilator surface. The safety actuator was not mounted in the support structure at the time the photograph was taken. The actuator mounted between the arm that the rotational motion sensing accelerometer was attached to and the end of the beam to which the input link for the control actuator was attached.

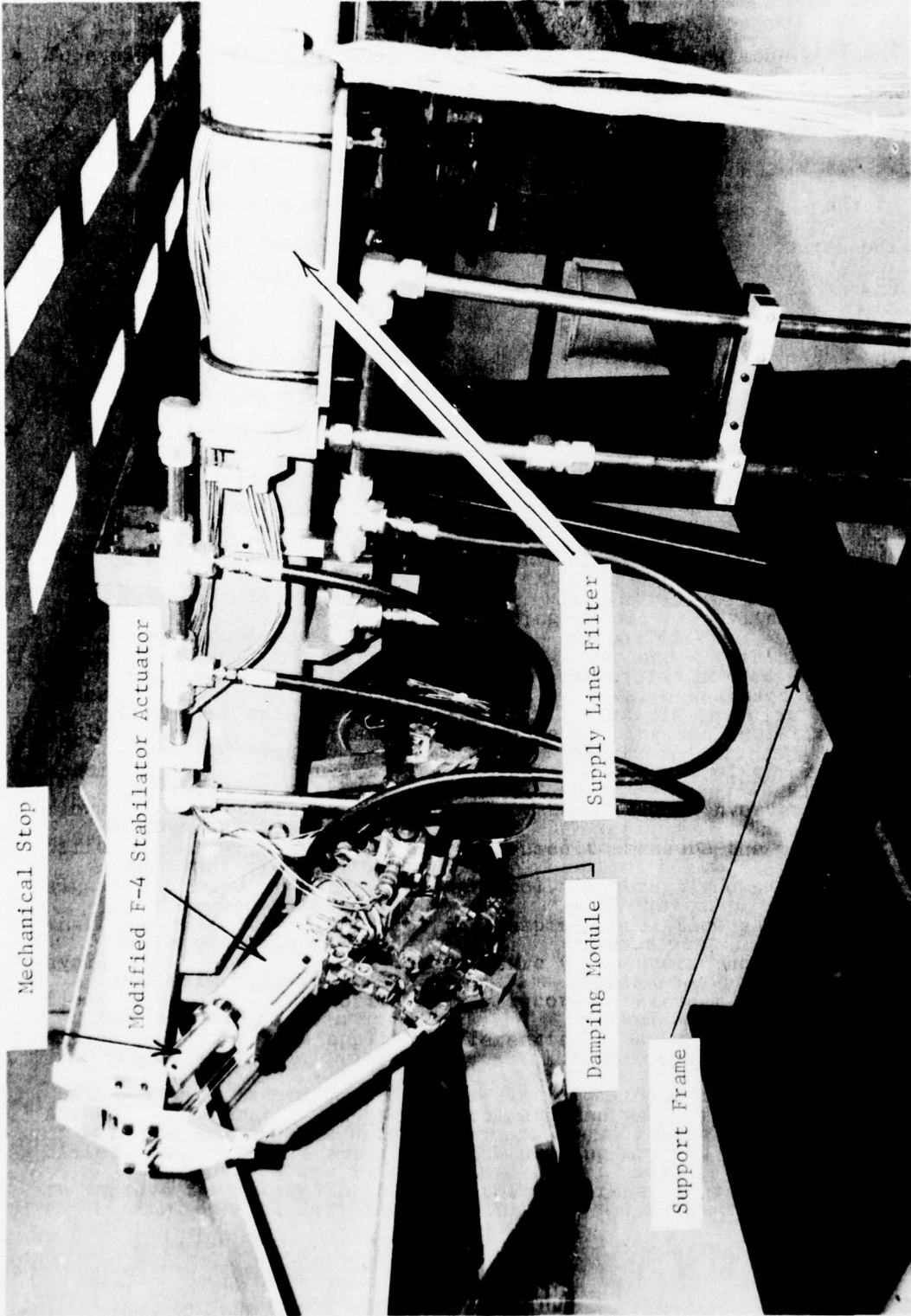


FIGURE 13 Flutter Suppression Actuator Laboratory Installation

The angle of attack limitations were incorporated to prevent the possibility of commanding angular surface deflections which could at the maximum dynamic pressure test conditions exceed the steady state stress limitations on the support structure and stabilator.

To limit flutter induced stress levels in the surface, accelerometers were mounted on the input arm to the surface and on the surface itself.

The accelerometer mounted on the surface was positioned to measure the first bending mode motion of the half stabilator (Reference Figure 12). The output of the accelerometers used to measure the rotational and bending motions of the surface were bandpass filtered and used to provide automatic shutdown capability when excessive acceleration levels at the expected rotational or bending natural frequencies were experienced. The automatic shutdown system was used to take the safety actuator out of bypass. This theoretically would increase the torsional resonance frequency by providing additional actuator (and hence rotational) stiffness. The safety actuator used had a drive area approximately equal to that of the modified stabilator control actuator and a stroke approximately 20% as long. The actuator stiffness theoretically added to that of the stabilator actuator when the safety actuator was taken out of bypass was therefore 5 times that of the stabilator actuator itself. This action would then increase the rotational resonance frequency and increase the dynamic pressure required for flutter.

The safety actuator was bypassed using two high flow pilot operated solenoid valves. Figure 14 shows the solenoid valves mounted on a manifold block attached to the support structure. Flexible hose (which detracted slightly from the stiffness increase with the safety actuator out of bypass) was used to couple the solenoid manifold to the safety actuator. Use of the

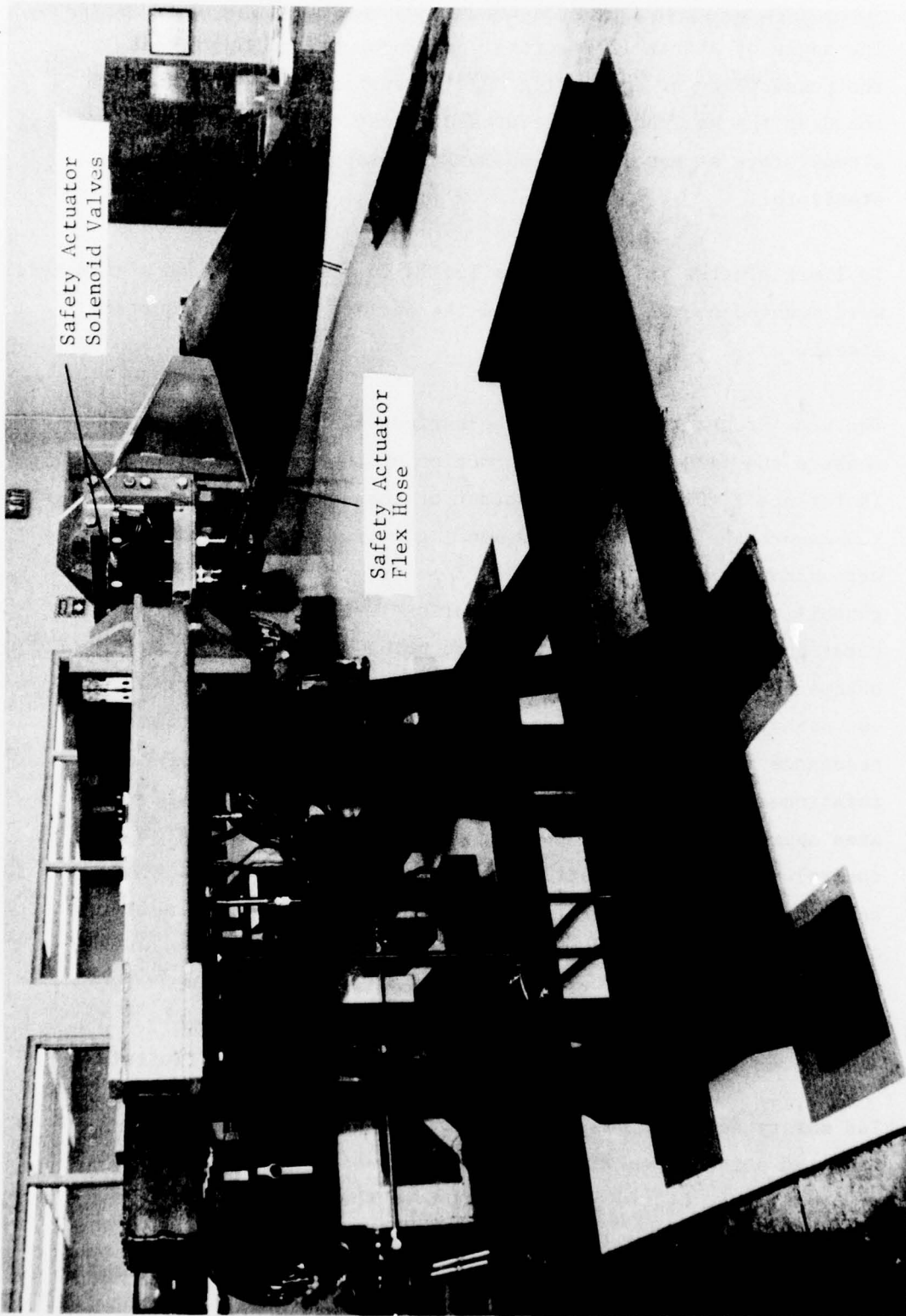


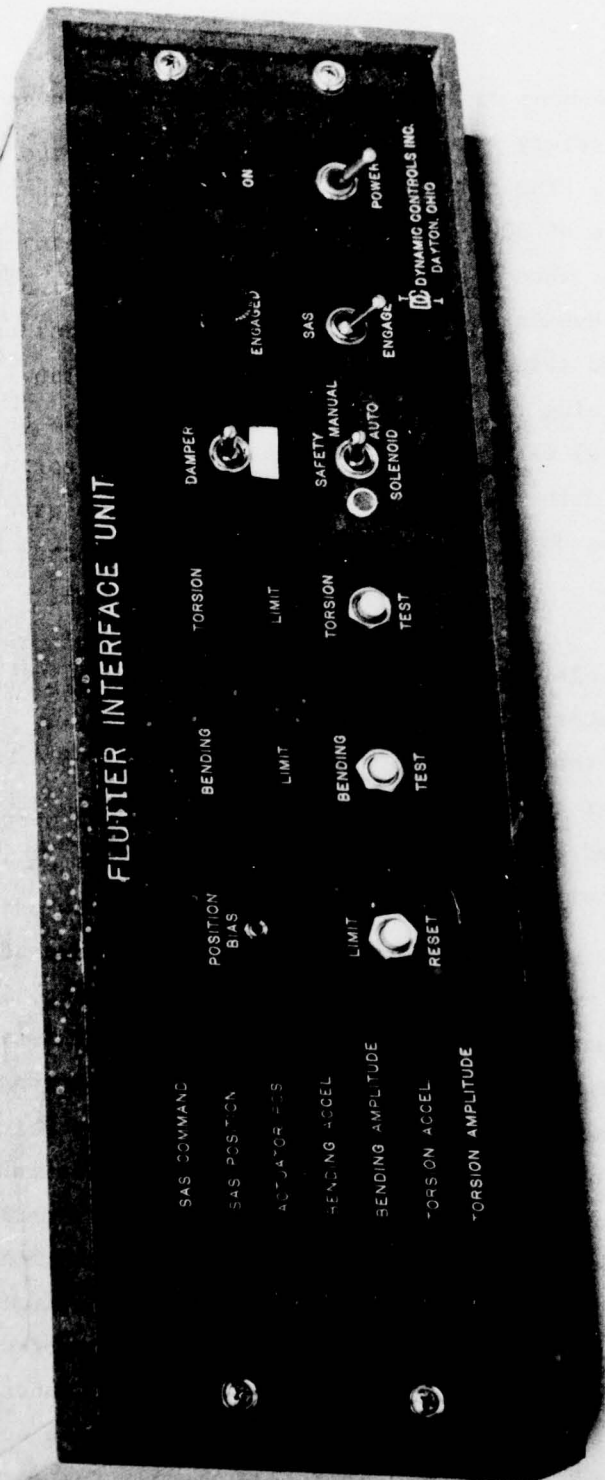
FIGURE 14 Safety Actuator Solenoid Mounting

flexible hose was required to accommodate the movement of the safety actuator body with deflection of the stabilator surface. The solenoid valves were connected so that system pressure of 3000 psi was maintained in both sides of the safety actuator when the actuator was bypassed. Taking the actuator out of bypass blocked the cylinder ports. The solenoids, flexible hose and safety actuator were rated for 5000 psi working pressure. Maintaining the cylinder ports at 3000 psi (rather than return pressure) when bypassed insured that the safety actuator was filled with oil and that the maximum stiffness increase available was obtained when the safety actuator was taken out of bypass.

Two accelerometers were mounted on the input arm of the half stabilator surface and on the surface itself. At each location, one of the accelerometers was used as a spare for the one being used for the safety system and performance monitoring. This provided a backup transducer in the event that a transducer failed during wind tunnel testing.

4.2.3 Flutter Interface Unit

In order to control the test item and provide automatic safety shutoff, a single electronics unit was constructed. Figure 15 is a photograph of the Flutter Interface Unit. This unit incorporated the bandpass filter networks and solenoid driver electronics to monitor the rotational and bending accelerations and take the safety actuator out of bypass if excessive torsional or bending motion of the control surface occurred. The unit also incorporated a servoamplifier and demodulator section for commanding the SAS portion of the flutter control actuator. This allowed commanding the output motion of test actuator in order to excite the control surface. The Flutter Interface Unit contained a position bias control to trim the control surface and



FLUTTER INTERFACE UNIT

SAS COMMAND
 SAS POSITION
 ACTUATOR PPS
 BENDING ACCEL
 BENDING AMPLITUDE
 TORSION ACCEL
 TORSION AMPLITUDE

POSITION BIAS
 LIMIT
 RESET

BENDING LIMIT
 TEST

TORSION LIMIT
 TEST

DAMPER
 SAFETY MANUAL
 SOLENOID

ENGAGED
 SAS
 ENGAGED

ON
 POWER

DYNAMIC CONTROLS INC.
 DAYTON OHIO

FIGURE 15 Flutter Interface Unit

a damper disable switch to turn the damper module on and off. The damper disable switch controlled a solenoid valve added to the damper module for the wind tunnel tests. The solenoid valve (Ref. Figure 13) was connected across the washout orifice of the damping module. When the solenoid valve was energized, the washout orifice was bypassed and the damping spool prevented from responding to differential pressure across the stabilator actuator drive area. Incorporation of this solenoid valve into the damping module allowed comparison testing of the rotational mode resonant frequency damping with and without the damping module operational.

For operation of the safety actuator, the flutter interface unit incorporated shutdown warning lights for the bending and rotational motion sensing circuits and test input switches for testing the operation of the two motion sensing circuits. The interface unit also included an over-ride switch to allow manually taking the safety actuator out of bypass. Used with the automatic operational circuitry for the safety actuator shut down was a reset switch. This switch reset the failure logic after the logic was tripped.

The Flutter Interface Unit incorporated test jacks on the front panel in order to allow monitoring of the test actuator position, SAS output position, bending and rotational accelerometer outputs and the bandpass filter outputs for the accelerometers. Included with the front panel test jacks was the SAS command input jack.

The bandpass filters used with the Flutter Interface Unit were used to convert the bending and rotational acceleration signals into an equivalent position amplitude signal. Since the intent of the failure detection circuits was to detect excessive motion amplitude of the stabilator surface at the first bending

and rotational resonant frequencies, conversion of the acceleration signals to an equivalent amplitude signal was required. The filters were designed to provide an equivalent amplitude response which was nominally flat over a frequency range of ± 5 Hz either side of the rotational and bending resonant frequencies. Figure 16 shows the measured response of the filter circuits with an input increasing 12 DB/octave (which is the characteristic of an accelerometer output with a constant amplitude motion input). The rotational filter response peak is centered at 20 Hz. The bending filter response peak is centered at 11 Hz. These frequencies correspond to the resonant frequencies for the stabilator surface and actuator. Note that the filters attenuate either side of the resonant peak in order to prevent nuisance shutdown from non-critical surface motions. The vertical cursors shown on the two response plots are separated by 10 Hz.

An engage switch and mode light were provided on the front panel of the interface unit for the control of the SAS engagement of the stabilator control actuator. Also included in the Flutter Interface Unit was a signal conditioning section for use with a differential pressure transducer. A pressure transducer was mounted on the test actuator to measure the actuator differential pressure. This was incorporated into the test item design to allow trimming the surface for minimum hinge moment and hence aerodynamic load at each wind tunnel test condition. The transducer also allowed monitoring the amplitude of the differential pressures due to the excitation of the surface by the SAS command inputs, both during the laboratory evaluation and the wind tunnel testing.

4.2.4 Instrumentation

Figure 17 is an instrumentation and control schematic for the testing performed on the wind tunnel test rig. This basic

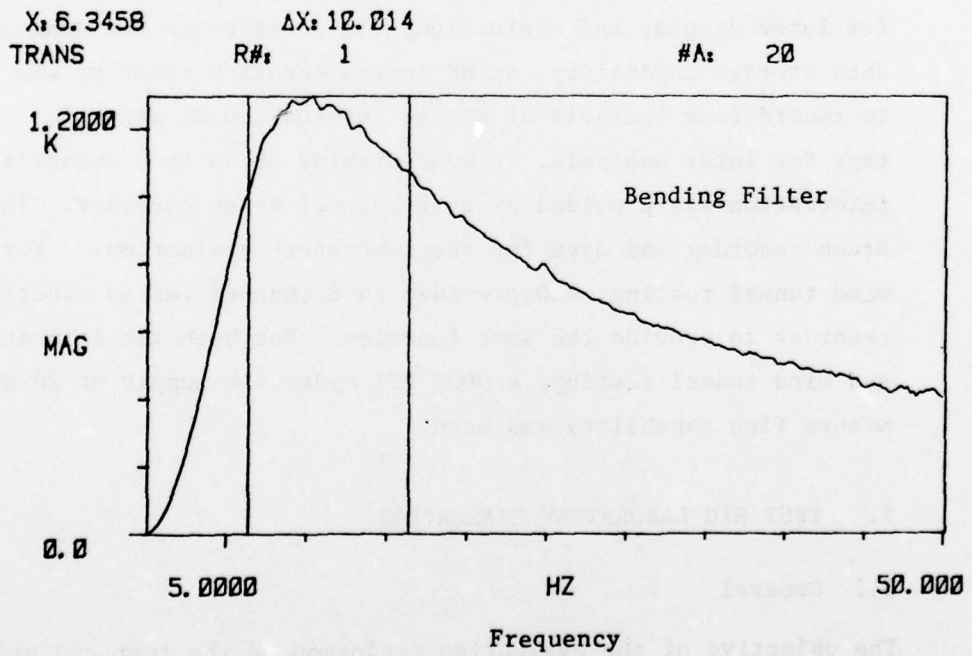
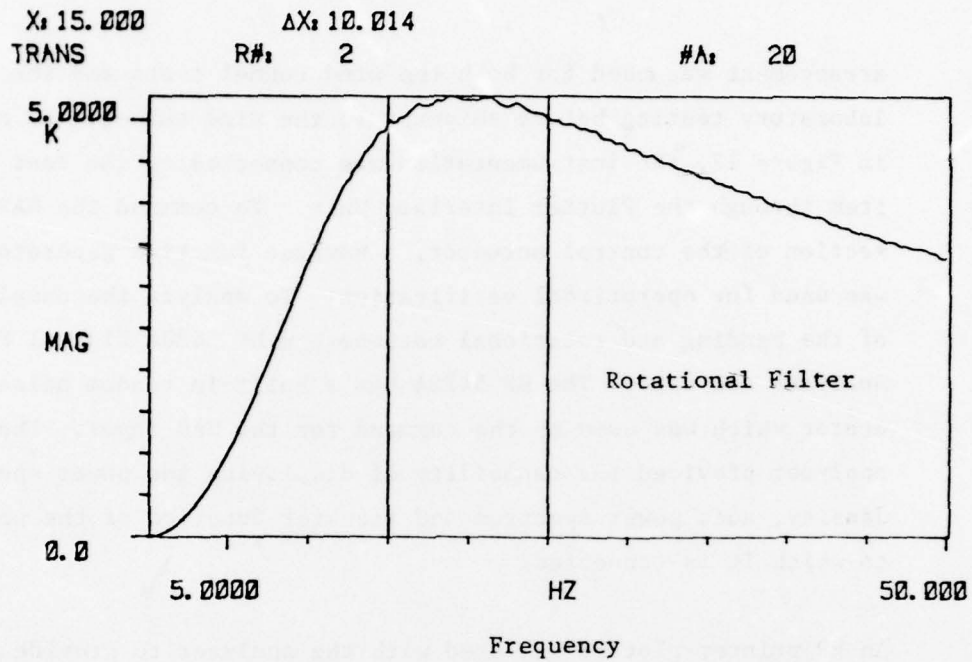


FIGURE 16 Bending and Rotational Accelerometer Filter Response - Constant Amplitude Motion Input

arrangement was used for both the wind tunnel tests and the laboratory testing before shipment to the wind tunnel. As shown in Figure 17, the instrumentation was connected to the test item through the Flutter Interface Unit. To command the SAS section of the control actuator, a Wavetec function generator was used for operational verification. To analyze the damping of the bending and rotational motions, an HP 5420A Digital Signal Analyzer was used. The HP 5420A has a built-in random noise generator which was used as the command for the SAS input. The signal analyzer provided the capability of displaying the power spectral density, auto power spectrum and transfer function of the signals to which it is connected.

An HP printer-plotter was used with the analyzer to provide hard copy of the analyzed data. The HP 5420A analyzer provides cassette tape storage of the analyzed data and the test setups. This allowed recording the analyzed data and recalling the data for later display and evaluation. In addition to the analyzed data storage capability, an HP instrumentation recorder was used to record four channels of signal information on magnetic tape for later analysis. Visual display of up to 8 channels of information was provided by an 8 channel Brush recorder. The Brush recorder was used for the laboratory evaluation. For the wind tunnel testing, ARO provided an 8 channel Varian electrostatic recorder to provide the same function. For both the laboratory and wind tunnel testing, a 3000 PSI hydraulic supply of 20 gallon/minute flow capability was used.

5. TEST RIG LABORATORY EVALUATION

5.1 General

The objective of the evaluation performed on the test rig prior to shipment to the wind tunnel was to verify operation of the

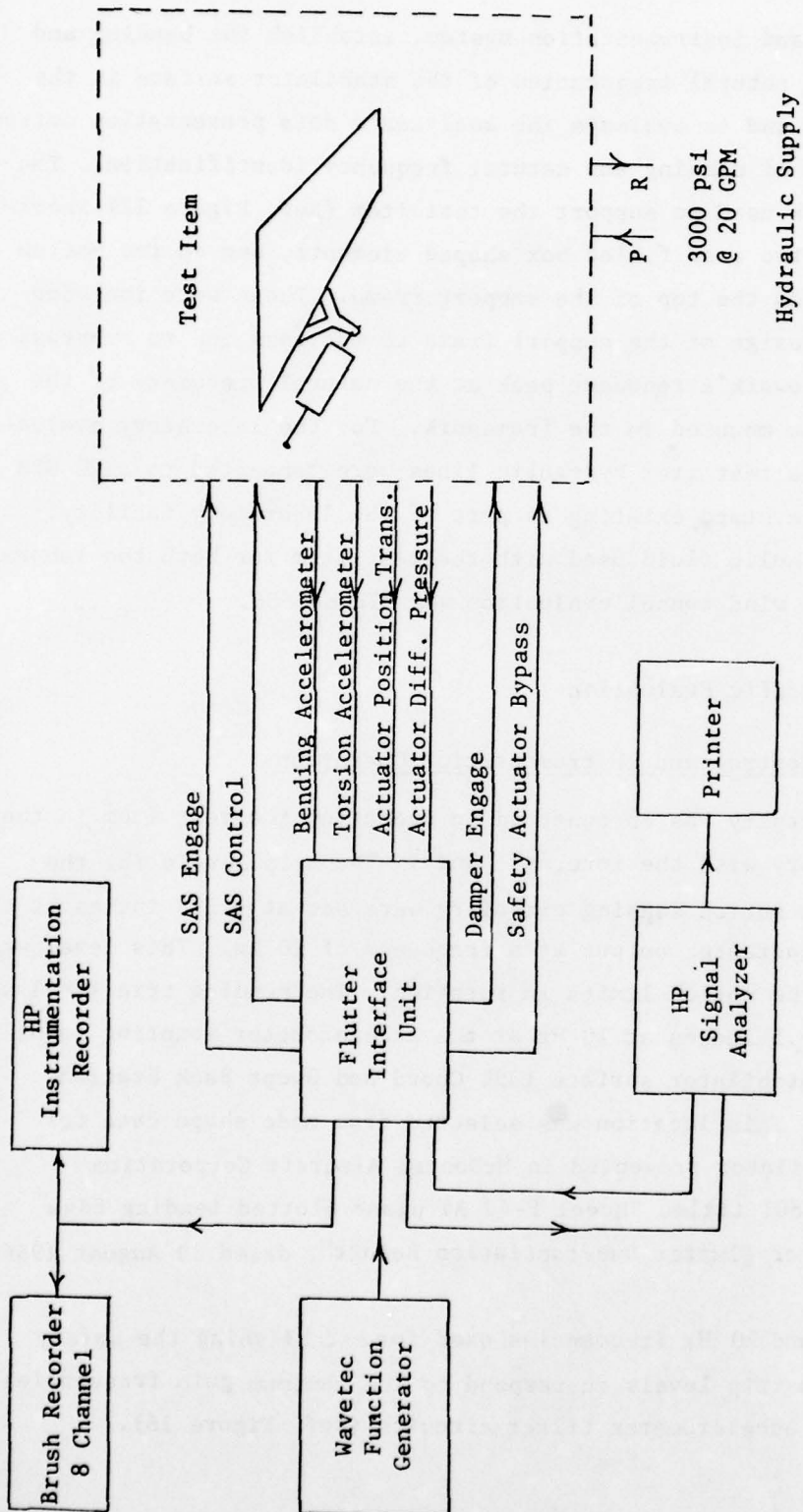


FIGURE 17 Instrumentation & Control Schematic
F-4 Flutter Test

control and instrumentation system, establish the bending and rotation natural frequencies of the stabilator surface in the test rig and to evaluate the analyzer's data presentation options in terms of damping and natural frequency identification. The framework used to support the test item (Ref. Figure 12) incorporated two sand filled box shaped elements, one on the bottom and one on the top of the support frame. These were included in the design of the support frame to add mass and to suppress the framework's resonant peak at the natural frequency of the test item mounted in the framework. For the laboratory evaluation, the test item hydraulic lines were connected to a 20 GPM hydraulic stand existing as part of the laboratory facility. The hydraulic fluid used with the test item for both the laboratory and wind tunnel evaluation was MIL-H-5606.

5.2 Specific Evaluation

5.2.1 Control and Instrumentation Operation

No difficulty was encountered in operating the test item in the laboratory with the interface unit. The trip levels for the rotation motion sensing circuitry were set at ± 0.375 inches at the control actuator output at a frequency of 20 Hz. This level was 75% of the motion limits in rotation. The bending trip level was set at ± 0.5 inches at 10 Hz at the accelerometer mounting point on the stabilator surface (35% Chord and Swept Back Station 66.37). This location was selected from mode shape data for the stabilator presented in McDonnell Aircraft Corporation report E801 titled "Model F-4J Airplane Slotted Leading Edge Stabilator Flutter Substantiation Report", dated 19 August 1966.

The 10 and 20 Hz frequencies used for establishing the safety shutdown trip levels correspond to the maximum gain frequencies for the accelerometer filter circuits (Ref. Figure 16).

Figure 18 shows the frequency response of the test item control actuator with the SAS section of the actuator engaged (without a damper module) and the half stabilator attached. The amplitude of the SAS actuator command is limited to ± 1.5 degrees of surface deflection by the normal stabilator control system design. Note that the control actuator did respond in the region of 10 to 20 Hz, although the amplitude was attenuated 15 to 24 Db from the amplitude at .1 Hz. This measured response indicated that excitation of the stabilator surface in the frequency region of interest was feasible using the SAS input. Since only frequency and damping of the rotational and bending modes were required, the amplitude of excitation needed to be only large enough to provide identification of the two parameters of interest. Subsequent testing with the analyzer indicated that the excitation level was adequate to allow the necessary parameter identification.

Operation of the safety actuator with the control electronics was satisfactory. Taking the safety actuator out of bypass did not block the commanded motion of the stabilator actuator, but did attenuate the motion and indicated an effective actuator stiffness change.

5.2.2 Resonant Frequency Response Measurements

As an initial approach to establishing the bending and rotational resonant frequency response characteristics, the Wavetec function generator was used as an input to the test item. The visible motion of the surface was observed as a sinusoidal input of varying frequency was applied to the SAS input. The bending frequency was quite obvious and occurred at 9.3 Hz. The rotational frequency was not as apparent in terms of observable amplitude but did appear at a nominal 20 Hz.

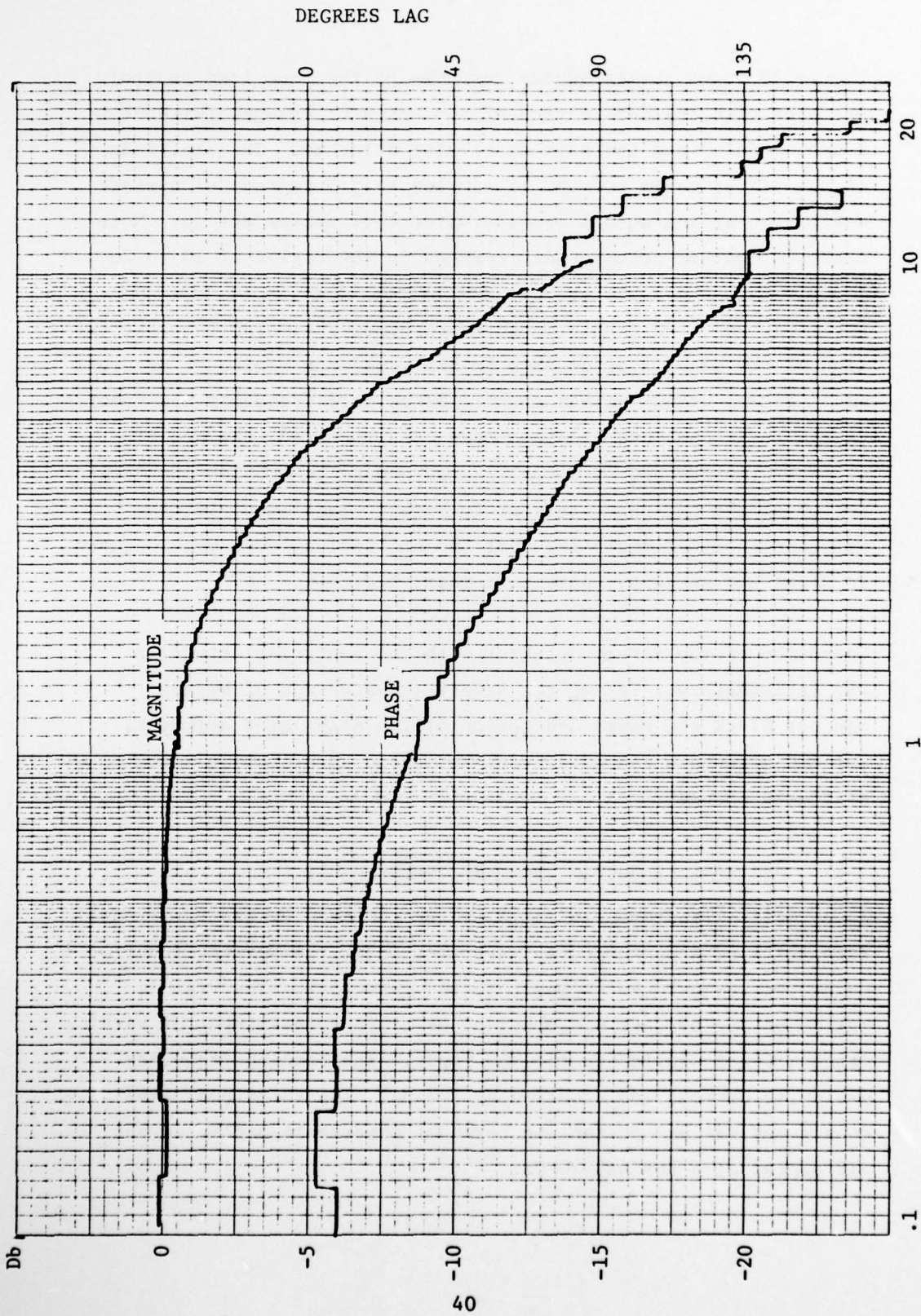


FIGURE 18 Frequency Response - Actuator Position Vs. SAS Command

The measured resonant frequencies compared favorably with the frequencies of 10.6 and 22.8 Hz measured by McDonnell Aircraft and listed in report E801. It was not expected that the bending mode frequency (at approximately 10 Hz) would change from a full stabilator to a half stabilator configuration. It was expected that the rotational resonant frequency would change. Since the stabilator rotational inertia was halved in going from a full to half stabilator configuration, the resonant frequency would normally increase (for the same actuator stiffness) by a factor of 1.414. However, since the stabilator actuator was operated with only one section pressurized and the modified actuator had a drive area of 57% that of a normal stabilator actuator, the actuator stiffness was theoretically reduced to 29% that of the normal stabilator actuator. The combination of lower rotational inertia and actuator stiffness should have produced a test item rotational resonant frequency of 58% the normal stabilator resonant frequency. However, since the measured resonant frequency was approximately the same as a full stabilator surface and normal actuator, the test item predicted flutter onset air speed should have been the same as for a full stabilator surface.

In using the HP 5420A analyzer for measuring the frequency of the rotational and bending modes for the stabilator, different inputs were applied to the SAS command input jacks. Initially a square wave input was used. For a frequency of .01 Hz, the displayed transfer function for the bending and rotational accelerations produced a smooth and unchanging curve after 20 averages. An input frequency of .1 Hz produced a much less smooth curve for the same number of averages. The random noise generator contained as part of the HP 5420A was also used as a test input. This input produced results equivalent to the .01 Hz square wave input in less measurement time and was selected for use for the balance of the wind tunnel and laboratory testing program.

Both the power spectral density (auto spectrum) and the peak hold spectrum (peak hold auto spectrum) methods were evaluated along with the transfer function technique for establishing the resonant frequencies and the shape of the resonant peaks for damping estimation. Figures 19 through 22 shows the transfer function results for the rotational accelerometer output/ SAS actuator output. Figure 19 shows the amplitude response with a distinct peak at 9.37 and 21.64 Hz (as indicated by the location of the vertical cursors). Figure 19 also includes the setup state for the analyzer for the transfer function measurement. Figure 20 shows the phase response curve for the same transfer function as shown in Figure 20. Notice the rapid change of phase angle at the 9.377 and 21.64 Hz frequencies.

One of the advantages of using the transfer function measurement with the HP 5420A analyzer is that the real and imaginary parts transfer function can be displayed separately. This proved very useful in identifying the actual resonant frequencies. Figure 21 shows a plot of the real components of the transfer function for the same response as shown on Figures 19 and 20. Note the sharp peaks at the 9.377 and 21.64 Hz frequencies. Figure 22 shows the imaginary part of the transfer function response. This figure shows the resonant peaks as large changes in the imaginary components. The response peak appearing at approximately 35 Hz in all the transfer function figures is the 2nd bending mode resonant frequency. McDonnell Aircraft report E801 lists the measured second bending frequency at 37.4 Hz. Note that the transfer function shows both the rotational and bending resonance characteristics. This is because the support frame used for the laboratory testing was not infinitely rigid and the bending resonance of the stabilator surface coupled through the frame motion to the rotational accelerometer. With the support used for the wind tunnel testing, the coupling was eliminated.

In using the signal analyzer for subcritical flight flutter testing, several options for display and excitation were available. For measurement and display, both transfer function and auto spectrum techniques were available. The auto spectrum technique also allowed using a peak hold option. For auto spectrum measurement, either wind tunnel turbulence or a forcing input (such as the stabilator actuator) could be used to excite the stabilator surface. Both a forcing function and the stabilator motion must be measured in order to generate a transfer function.

The auto spectrum and peak hold auto spectrum (termed power spectral density and peak hold spectrum respectively for a normalized spectrum) are techniques commonly used for subcritical flutter testing (Reference "Some Experience Using Subcritical Response Methods in Wind-Tunnel Flutter Model Studies" by Jerome T. Foughner, Jr., NASA Langley Research Center as published in NASA SP-415, October, 1975). Two additional techniques described in the referenced document are the co/quad and randomec methods, both of which require a particular unique analyzer for generation of the damping estimate. The randomec method uses wind tunnel turbulence excitation and the co/quad uses a sinusoidal forced excitation.

All the subcritical (below the actual flutter speed) response techniques are used to measure the frequency and damping in the critical vibration modes. By plotting and extrapolating the damping of the vibration modes of interest, the flutter point can be established.

The HP 5420A has an internal subroute which calculates the damping and frequency of resonance peaks. This subroutine works only for the transfer function mode of measurement and display. For the power spectral density, the damping is calculated by using the frequency bandwidth (at half power point) divided by the mode frequency.

SETUP STATE

MEASUREMENT : TRANSFER FUNCTION
AVERAGE : 20 , STABLE
SIGNAL : SINUSOIDAL
TRIGGER : FREE RUN , CHNL 1

CENT FREQ : 0.0 HZ
BANDWIDTH : 50.0000 HZ
TIME LENGTH : 5.12000 S
AF : 195.312 mHZ AT : 5.00000 mS

ADC CHNL	RANGE	AC/DC	DELAY	CAL (C1/C2)
2	10 V	DC	0.0 S	1.00000

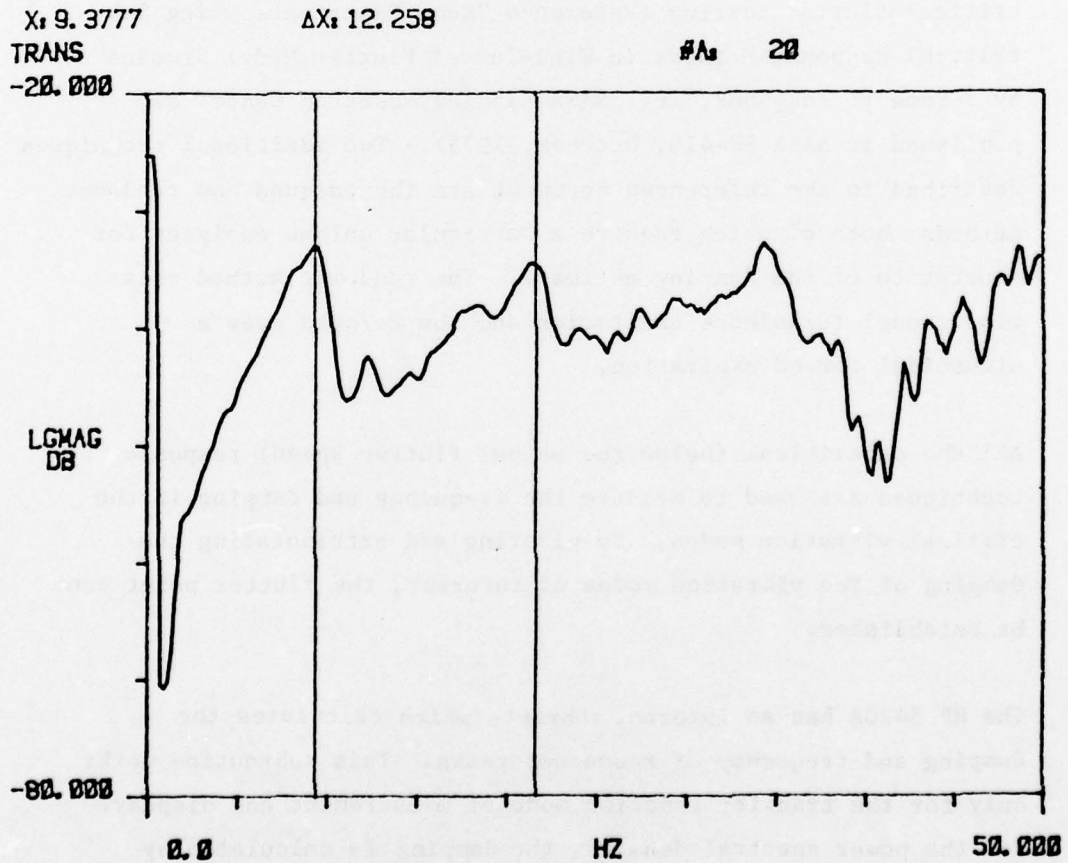


FIGURE 19 Rotational Accelerometer/SAS Output Response - Magnitude Curve

X: 9.3777

$\Delta X: 12.258$

#A: 20

TRANS

180.00

PHASE

-180.00

0.0

HZ

50.000

FIGURE 20 Rotational Accelerometer/SAS Output Response - Phase Curve

X: 9.6527
TRANS

$\Delta X: 12.258$

#A: 20

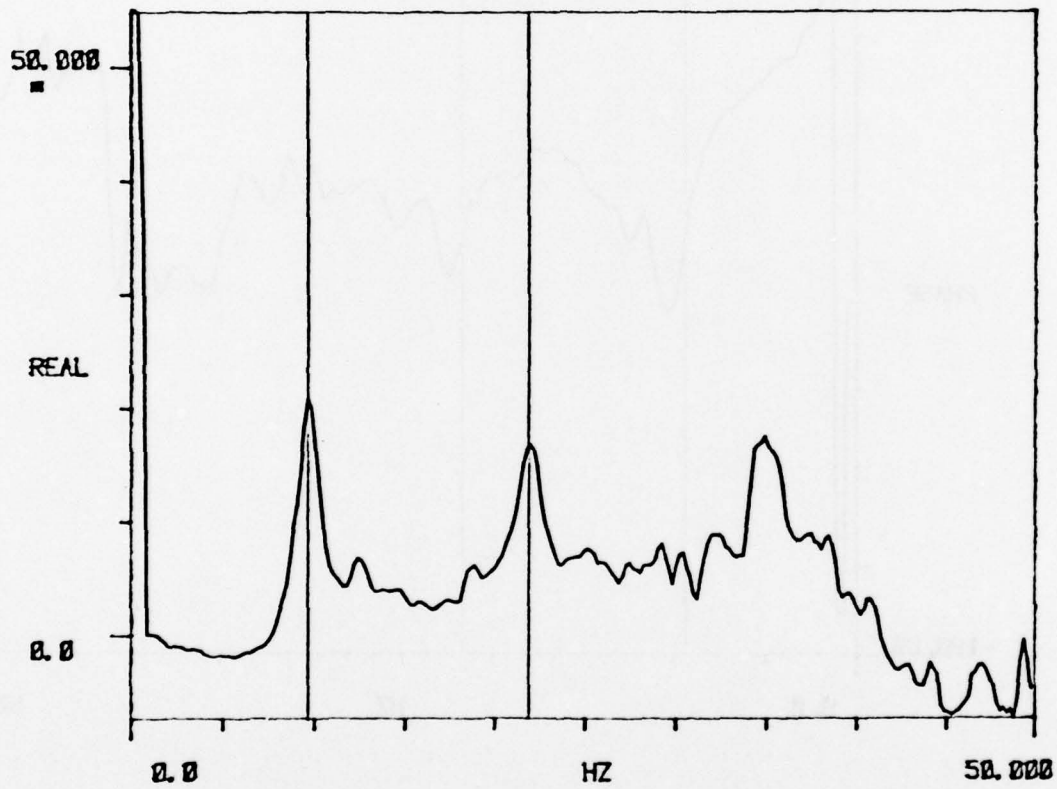


FIGURE 21 - Rotational Accelerometer/SAS Output Response - Real Part Curve

X: 9.6527

$\Delta X: 12.258$

#A: 20

TRANS

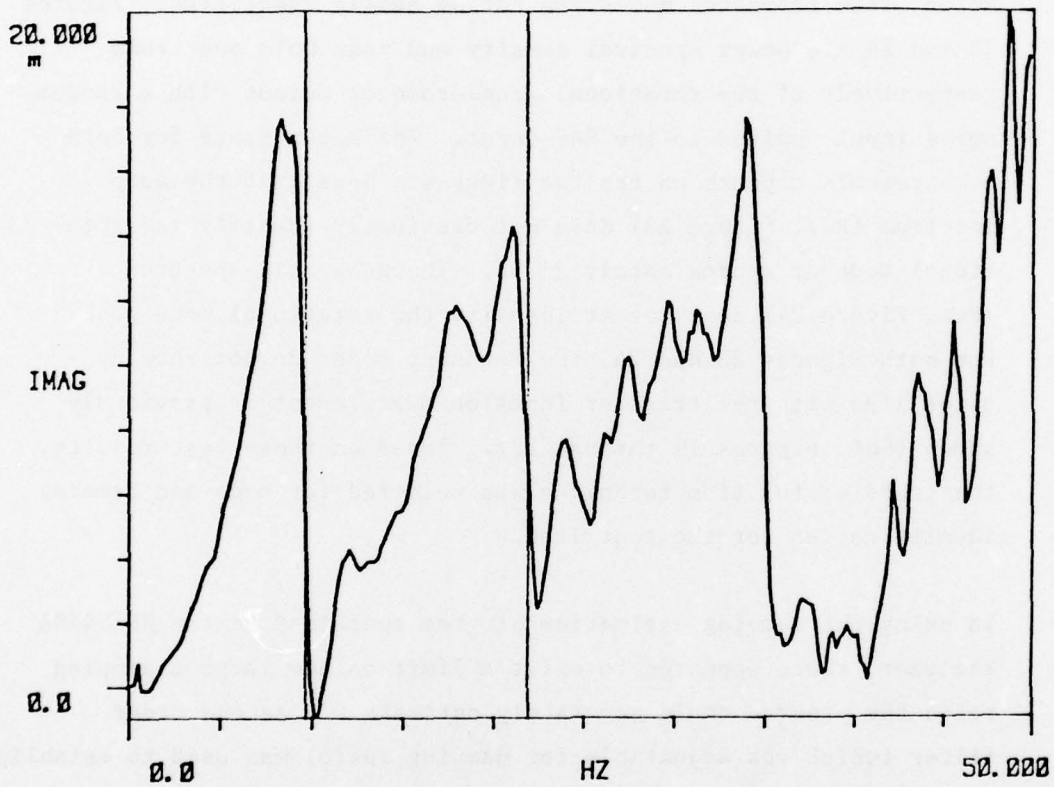


FIGURE 22 Rotational Accelerometer/SAS Output Response - Imaginary Part Curve

Note that in using the transfer function, the presentation of the response in complex form (magnitude + phase angle and/or real and imaginary components) provides a useful method of establishing the true resonance peaks. A true resonance peak exhibits both amplitude peaking and a significant phase angle change. Since the power spectral density measurements present only amplitude information, true resonance modes are not as easily identified. Figures 23 and 24 are power spectral density and peak hold spectrums respectively of the rotational accelerometer output with a random noise input applied to the SAS input. The setup state for both measurements appears on the two figures. Note that the auto spectrum (Ref. Figure 23) does not distinctly identify the rotational mode at approximately 21 Hz. The peak hold spectrum (Ref. Figure 24) does better identify the rotational mode peak. For both Figures 23 and 24, the resonant modes do not show up as well as with the transfer function measurement as previously shown (Ref. Figures 19 through 22). Based on these test results, the transfer function technique was selected for mode and damping identification for the test item.

In using the damping estimation program contained in the HP 5420A analyzer, there appeared to exist a limit on how large a damping ratio the program could accurately estimate. A second order filter (which was adjustable for damping ratio) was used to establish the accuracy limit. For damping ratios above .5, the program did not produce accurate estimates of the damping ratio. For damping ratios between .01 and .5 the damping ratio appeared to be accurate enough to use for the flutter testing.

X: 9.6527
A SPEC 1
-20.000

$\Delta X: 12.258$

#A: 50

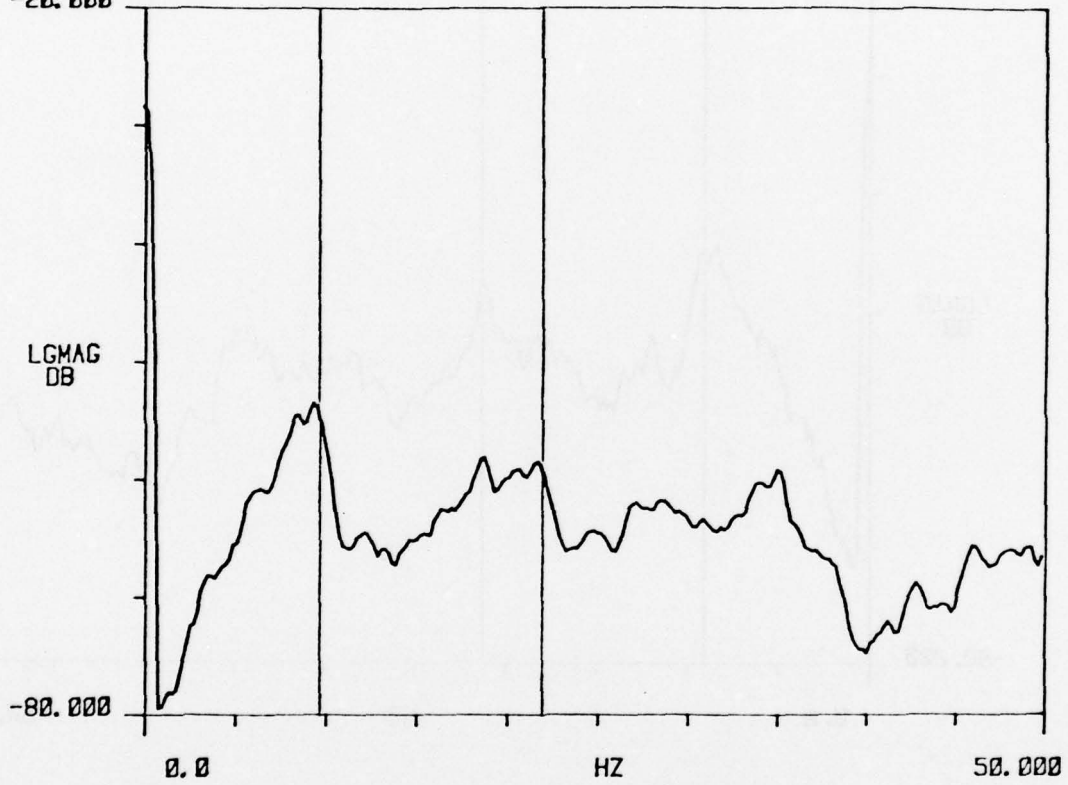


FIGURE 23 Rotational Accelerometer Response - Power Spectral Density

X: 9.2449
A SPEC 1
-20.000

$\Delta X: 12.258$

#A: 50

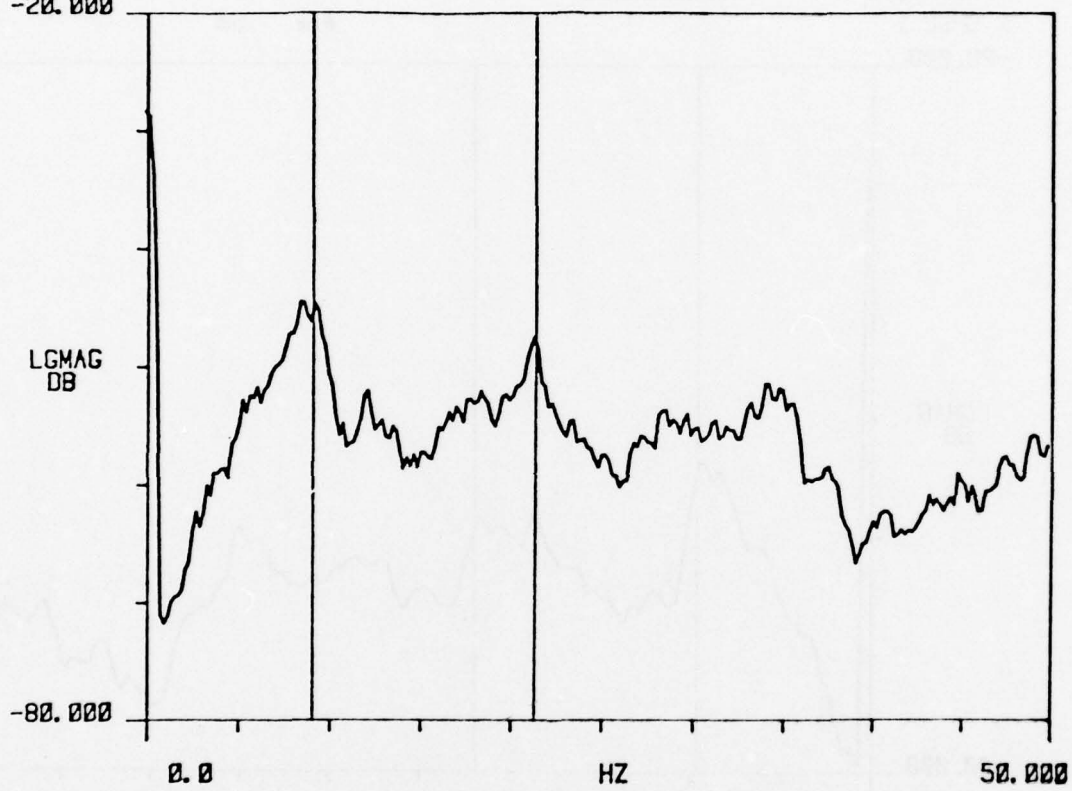


FIGURE 24 Rotational Accelerometer Response - Peak Hold Spectrum

During the laboratory evaluation, the effect of engaging and disengaging the damping module while exciting the surface with the SAS system was monitored. During this testing, the damping module did not have a measureable effect on the apparent damping of the rotational mode of the test item. The apparent reason for this characteristic was that the excitation level available from the SAS system was not sufficiently large enough (even at resonance) to create dynamic pressures sufficient to overcome the threshold pressure of the damping module. The measured differential pressure at 20 Hz during a frequency sweep (where the input amplitude was adjusted to a level just below that which would cause velocity saturation of the actuator output motion) was ± 17 psi across the actuator drive area. This was below the 40 psi differential pressure across the damping spool (Reference Figure 6) required to overcome the hysteresis of the damping spool. Since in the wind tunnel the air stream would create larger differential pressures and cause the damping module to operate, this laboratory test result was not considered to indicate any problem. For the wind tunnel tests, the differential pressure across the actuator drive area was monitored and the level did exceed the threshold of the damper module.

6. WIND TUNNEL EVALUATION

6.1 General

The test item was evaluated in the 16T wind tunnel at Arnold Engineering Development Center, Tennessee, during November 1978 as Project No. P41T-23. The test item was installed in a test cart which was moved into the test section for actual wind tunnel testing. The test item was installed in the side wall of the test section and attached to a sidewall balance and reflective plane designed and used for a prior test program. The balance

provided a rigid and massive mounting point for the stabilator and the control actuator assembly. The reflective plane allowed using a half stabilator surface instead of a full stabilator (which would not physically fit into the test section). Three nights of wind tunnel testing were conducted on the test item performance. All testing was conducted with subsonic operating conditions for the tunnel. For test operation, the Mach number was held constant at selected values and the dynamic pressure increased to change the test conditions. At each test condition, the damping and frequency of both bending and rotational resonance were measured and recorded. During the last night of testing, the damper module was replaced with two different shunt restrictions across the stabilator actuator drive area and the test item evaluated with some of the specific test conditions previously used with the damper module operating.

During testing, two minor problems occurred with the test item. One of the accelerometers used for measuring the bending motion failed. During the second night of testing, a panel which moved with the stabilator surface and used to cover the fuselage opening tore loose. Because a backup accelerometer had been installed initially, no correction for the failed accelerometer was required. The panel was replaced with a rigid sheet of aluminum that fastened to the fairing of the test item. Neither problem affected the satisfactory completion of the wind tunnel evaluation.

6.2 Test Section Installation

Figure 25 shows the stabilator as installed in the sidewall balance of the 16T test section. Note the two bending motion accelerometers installed on the stabilator surface. Between the surface and the reflection plane is the fairing constructed as part of the test item. The movable panel which was replaced during the actual wind tunnel testing is also shown on this figure.

Figure 26 shows a front view of the test item and reflection plane as installed in the test section. The two actuators shown in this figure and attached to the reflection plane are steering actuators for the leading edge of the reflection plane. This figure shows the test item stabilator actuator location in the installation.

Figure 27 shows the safety actuator and stabilator control actuator as viewed from below. The two rotational motion accelerometers are shown in this figure.

Before the test cart was moved to the wind tunnel for the actual wind tunnel testing, preliminary functional testing on the test item was conducted. This included testing of the safety circuitry and instrumentation. Figure 28 is a response amplitude plot for the rotational accelerometer output and SAS input. Note that the bending motion of the stabilator does not appear in the response plot. Figure 29 is an amplitude response plot for the bending accelerometer output and SAS input. Note that the rotational resonance does not appear in the bending motion response. The bending and torsional resonance motions of the test item were decoupled (this was not the case with the laboratory testing) with the rigid and massive mounting structure of the test section.

Note that the rotational resonance peak occurs at 17.3 Hz and the bending resonance peak occurs at 9.8 Hz. The bending

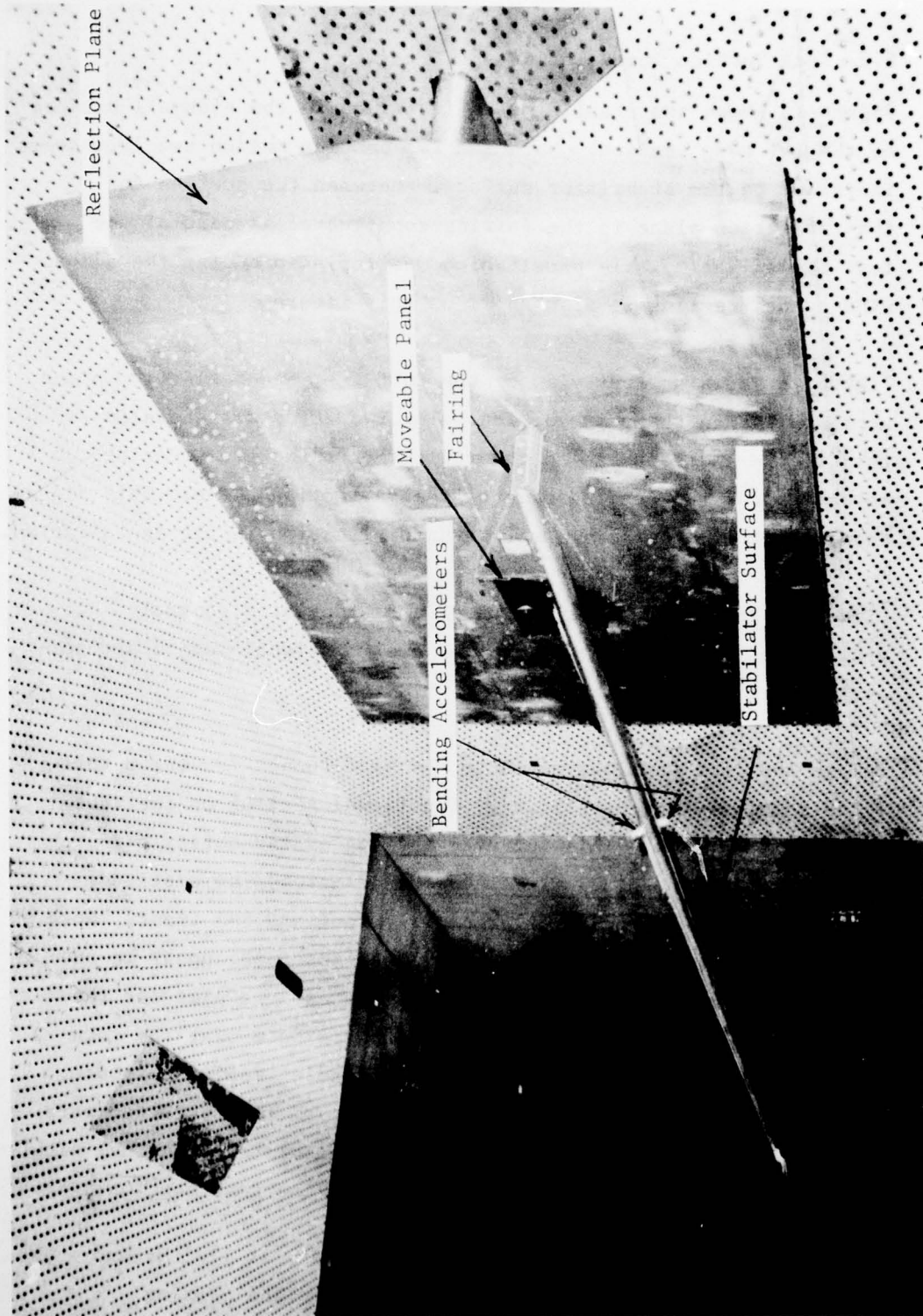


FIGURE 25 Test Section Installation - Oblique View

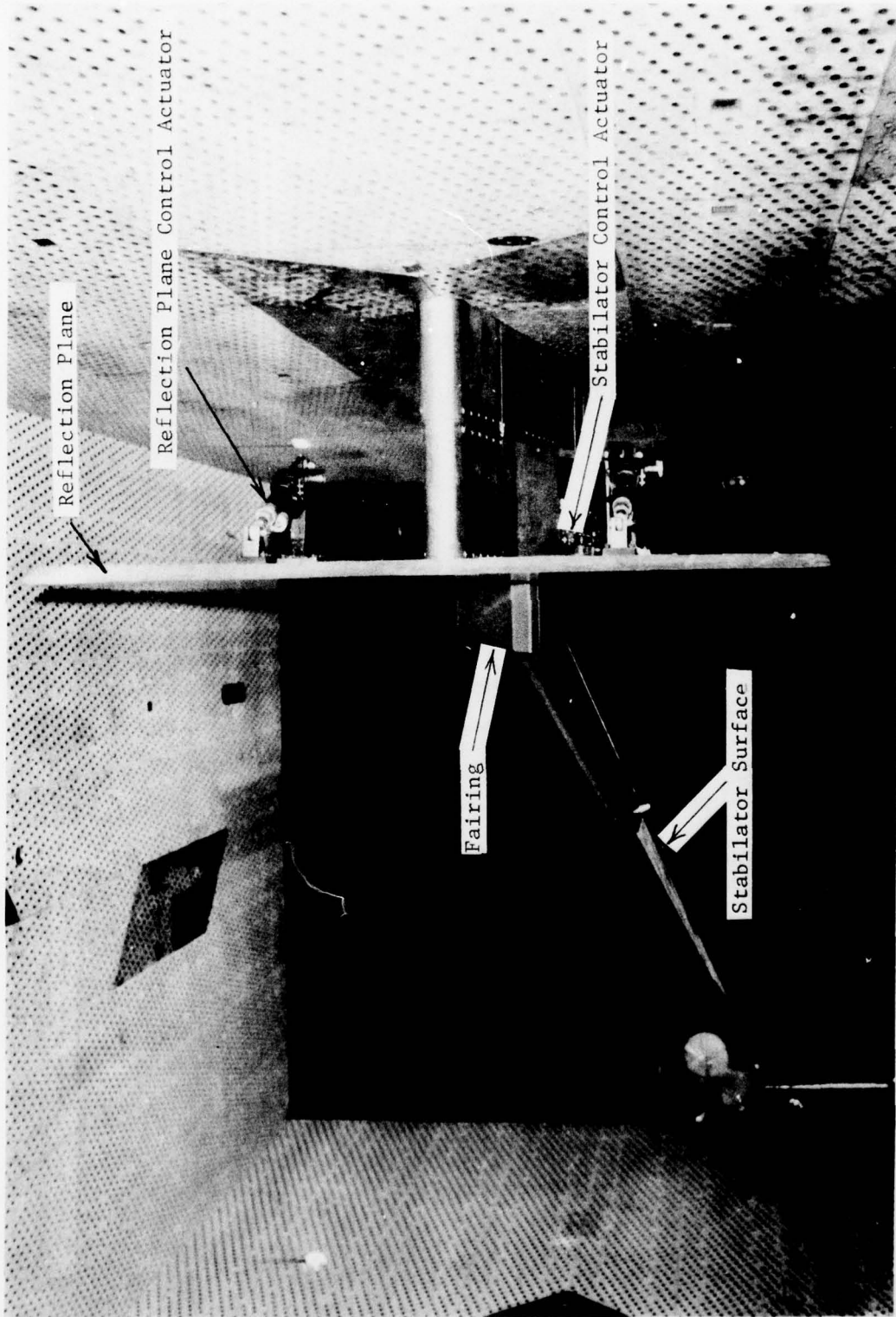


FIGURE 26 Test Section Installation - Front View

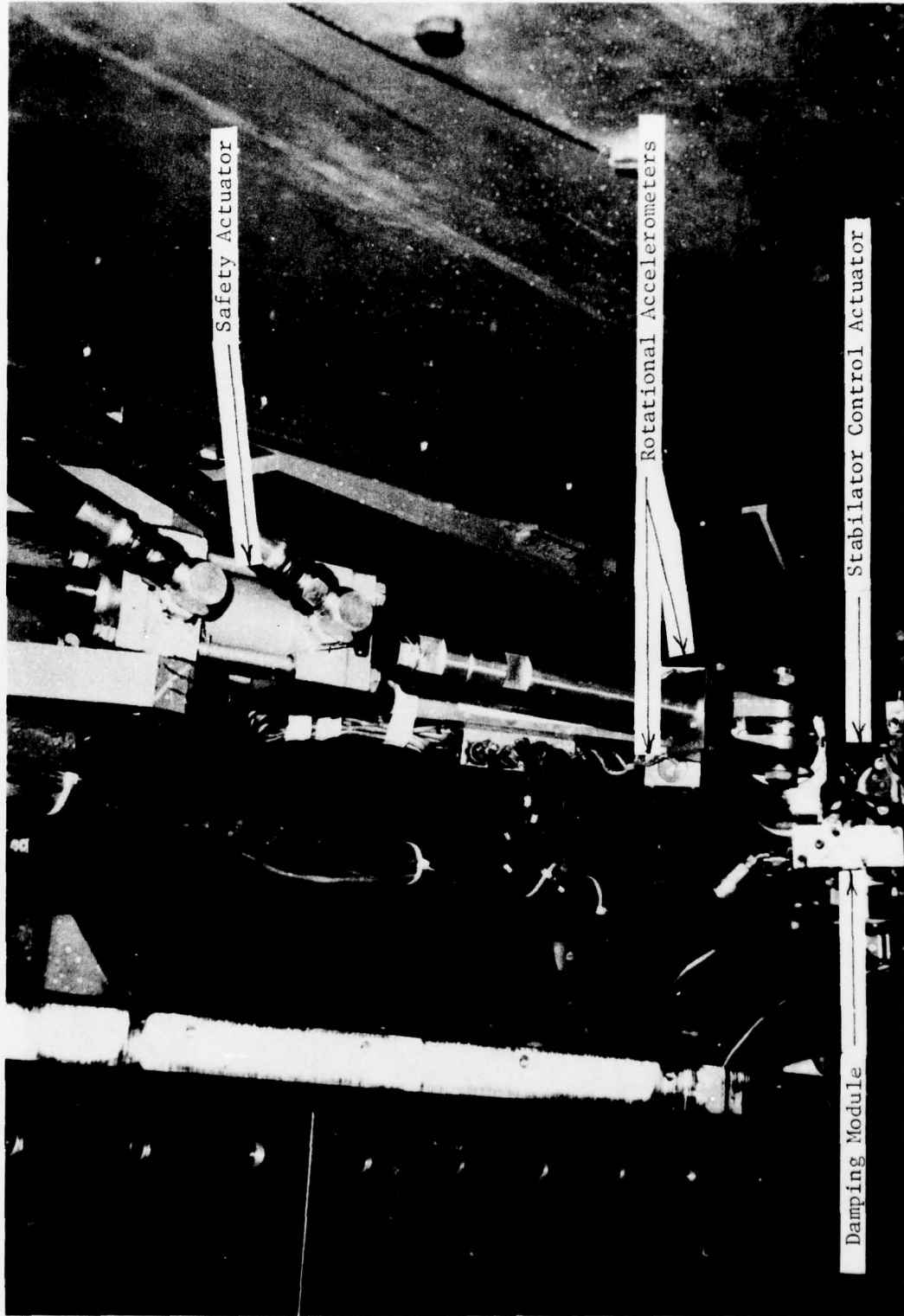


FIGURE 27 Test Section Installation - Bottom View

X: 17.344
TRANS
-10.000

R#: 7
Y: -18.702

#A: 40

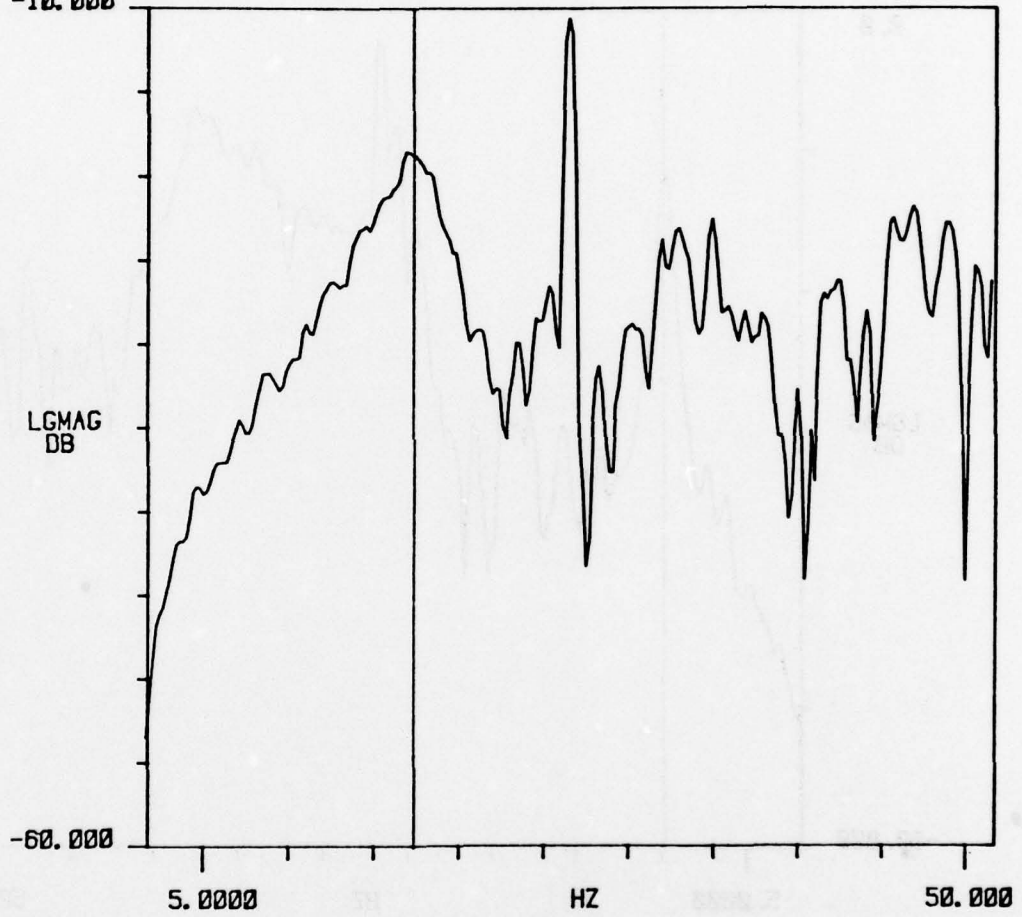


FIGURE 28 Test Section Testing - Rotational
Accelerometer/SAS Input Response

X: 9.8041
TRANS

Y: -11.685
R#: 11

#A: 40

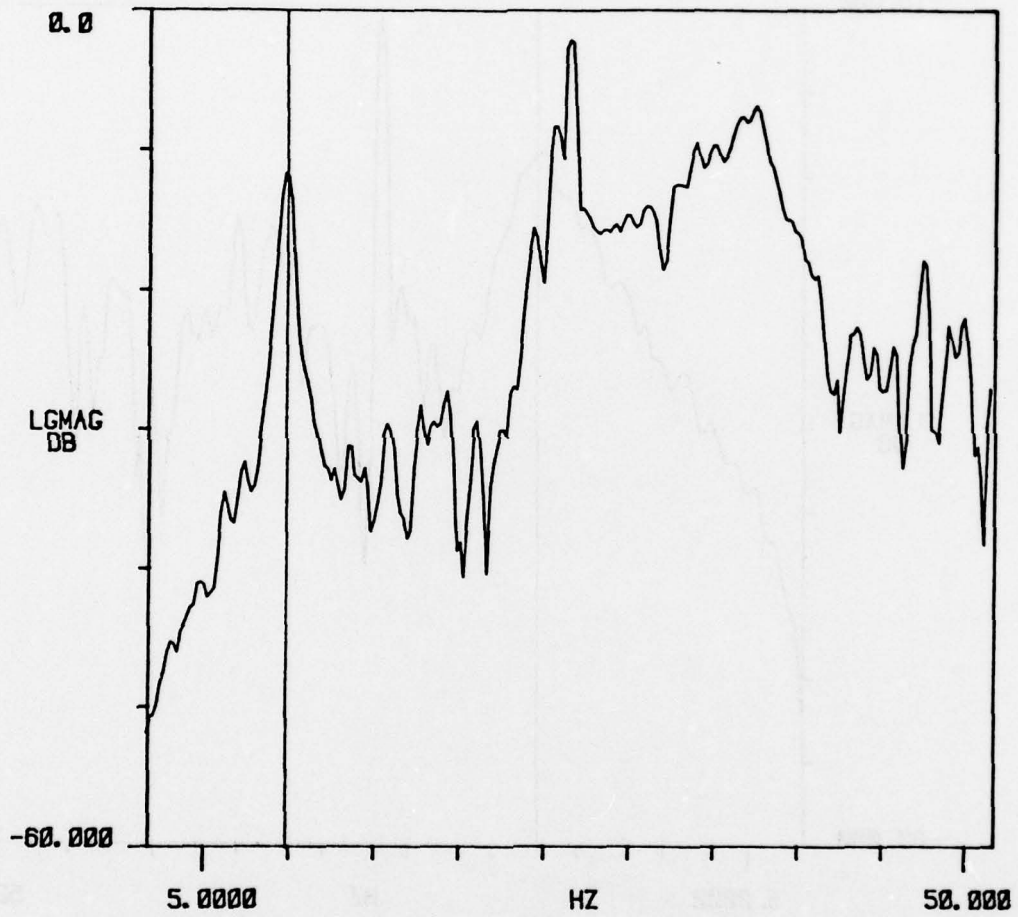


FIGURE 29 Test Section Testing - Bending
Accelerometer/SAS Input Response

resonance frequency agrees with that previously measured in the laboratory testing of the test item at WPAFB. The rotational resonance frequency is somewhat lower (17.3 Hz vs 21 Hz). The test data shown on Figures 28 and 29 were taken with 2000 PSI hydraulic pressure applied to the test item (since this was the maximum supply pressure available for the preliminary test checkout).

The amplitude peak between 25 and 30 Hz on both Figures 28 and 29 appeared to be associated with the setup state specifications for the analyzer. In order to exclude measuring the steady state output of the accelerometers, the center frequency of the bandwidth for the measurements of Figures 28 and 29 was specified to be 26.5625 Hz and the bandwidth 50 Hz. The 26.5625 Hz is exactly the frequency of the peak between 25 and 30 Hz on Figures 28 and 29. Figure 30 shows the setup state of the response measurements of Figures 28 and 29. This setup state was used for most of the response measurements taken during the wind tunnel testing. The peak at 26.562 appeared in all test results using the setup state of Figure 30. Since this response peak (apparent) was separated from the two resonance frequencies of interest and was a high "Q" peak, it created no problems in analyzing the test results.

Although it was felt that the apparent response peak at the bandwidth center frequency was not necessarily an inherent characteristic of the analyzer, the characteristic was not investigated further since it did not interfere with the analysis of the resonant modes of the test item.

6.3 Wind Tunnel Test Installation

For the testing of the flutter suppression mechanization in the wind tunnel, the control and instrumentation equipment was installed

in a wind tunnel control room adjacent to the test cart containing the stabilator surface. Figure 31 is a photograph of the control and instrumentation setup used for the wind tunnel testing. The function generator shown in the figure was used for excitation of the stabilator surface during preliminary checkout without the wind tunnel operating. The oscilloscope to the left of the function generator was used to monitor the stabilator actuator position and the input to the SAS input to the actuator. The response analyzer was used both for the excitation input and the response analysis of the motion stabilator.

The instrumentation tape recorder was used to record on magnetic tape the analog signals of rotational and bending accelerometer outputs, SAS actuator position and the differential pressure transducer output. Recordings of these signals throughout the wind tunnel testing were made in order to allow later analysis of the response data as required. The instrumentation recorder incorporated a voice channel which was used to identify the different test conditions for the recorded data. The instrumentation chart recorder used was an electrostatic recorder with 8 channels of recording provided. This recorder was used to record a short section of output data of the test item instrumentation at each test condition for immediate visual examination. The printer-plotter was connected to the response analyzer and was used to record response data on paper as required during the testing. The response analyzer also allowed recording on magnetic cassette tape in vector form the response data acquired at each test condition. Two oscilloscopes were used to visually monitor the output of the differential pressure transducers and the accelerometers during the wind tunnel testing.

SETUP STATE

MEASUREMENT : TRANSFER FUNCTION
AVERAGE : 20 . STABLE
SIGNAL : SINUSOIDAL
TRIGGER : FREE RUN . CHNL 1

CENT FREQ : 26.5625 HZ
BANDWIDTH : 50.0000 HZ
TIME LENGTH : 5.12000 S
 ΔF : 195.312 mHZ ΔT : 10.0000 mS

ADC CHNL	RANGE	AC/DC	DELAY	CAL (C1/C2)
* 1	10 V	DC	0.0 S	1.00000
* 2	10 V	DC	0.0 S	1.00000

FIGURE 30 Response Analyzer-Setup Tests - Flutter Tests

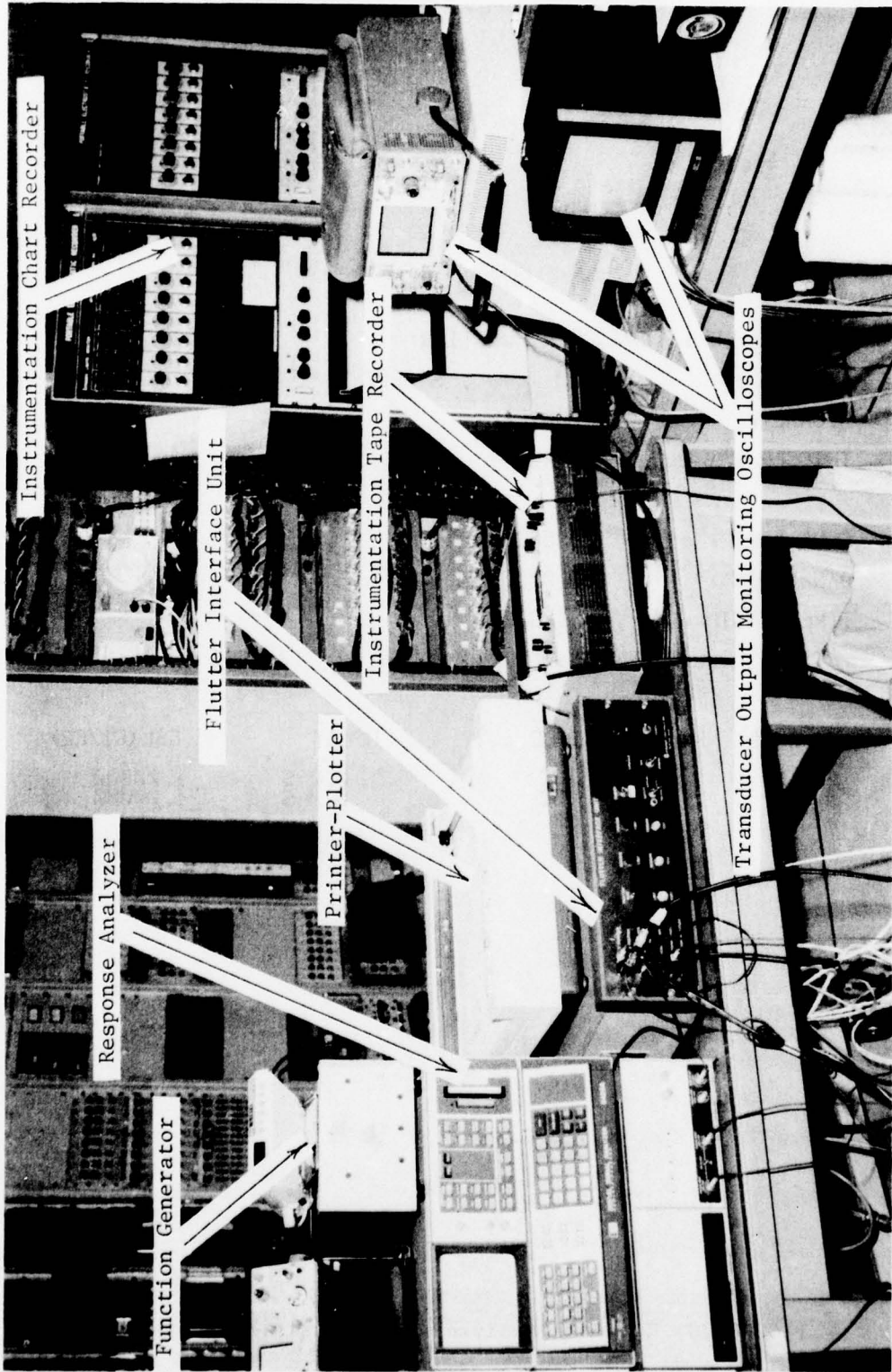


FIGURE 31 Wind Tunnel Testing Control & Measurement Setup

In addition to the instrumentation shown in Figure 31, movie cameras were installed in the tunnel sidewalls of the test section in order to photograph the stabilator motion at each test condition. Approximately 10 seconds of motion at each test condition was recorded. To allow continuous visual monitoring of the stabilator surface during the wind tunnel testing, closed circuit television was installed so that the stabilator surface could be observed throughout the testing. This closed circuit television was used to detect a sheet metal fairing panel failure during the test sequence.

6.4 Test Procedure

The general procedure used to evaluate the test item was to establish different dynamic pressure conditions at selected Mach numbers for the tunnel operating conditions and evaluate the resonant mode frequency and damping for the rotation and bending motions of the stabilator surface. Three different Mach number test conditions were used (Mach .6, Mach .8 and Mach .95). The majority of testing was conducted at Mach .95, since this test condition created the greatest observed activity of the differential loading pressure on the stabilator actuator drive area (and the greatest observed motion of the stabilator surface when excited by the input from the response analyzer). At each Mach number, the dynamic pressure was increased from 200 lb/sq ft to higher dynamic pressures in increments of 50 or 100 lb/sq ft. The maximum pressure used was 650 lb/sq ft, which at the Mach .95 test condition, approached the normal power limit for the tunnel operation.

At each test condition, the analyzer was used to obtain a response plot for the rotation and bending modes, with and without the damper module operational. In order to predict the potential onset of classical flutter, plots of the damping and the frequency for each of the modes was plotted as a function of the dynamic pressure for each Mach number.

In addition to plotting the bending and rotation frequencies as a function of the dynamic pressure, the ratio of the difference between the bending and rotation fundamental frequencies were calculated and plotted versus dynamic pressure to aid in predicting the potential onset of classical flutter. (A similar technique was used by McDonnell Aircraft in report E801 for predicting the flutter point). Since the two fundamental modes of rotation and bending coalesce at the flutter frequency, plotting the frequency shift with increasing air speed (or dynamic pressure) allows estimating the flutter onset point.

In order to obtain response plots from which the damping and resonant frequencies could be measured, it was necessary to allow the response analyzer to average the sampled data. A minimum of 20 sets of data was averaged for each response measurement. For some plots, it was necessary to increase the averages to greater than 100 in order to obtain a response plot which was unchanging with each new set of data averaged in. The response analyzer allowed establishing the number of averages for a satisfactory plot, since as each set of data was averaged in the change of the response plot due to that set of data could be observed. When the response plot no longer changed with the addition of new data, the averaging process was terminated and the measurement of the damping and resonant frequency made. It was generally necessary to increase the number of averages above 20 at the higher dynamic pressure conditions due to the increased noise on the accelerometer output signals.

In making the damping and resonant frequency estimates from the measured response, two techniques were used. One technique used the internal program provided in the HP 5420A. The second technique used the cursors to measure the half power points in order to calculate the damping for the resonant peaks. Because the

response plots exhibited deviations from the classical smooth peaking (even after 100 or more averages), the use of the internal program for damping estimation gave results that were sensitive to the position of the cursors used to define the resonant peak being measured. Therefore, the damping and resonant frequency estimation for five different cursor locations on each peak was recorded and the mean values and standard deviations calculated. The half power points were also used to calculate an estimated damping for the same resonant peak. The analyzer allowed this to be conveniently accomplished using the vertical cursors to measure the frequency and the horizontal cursors to establish the half power amplitude points.

Although the initial testing was at Mach .6 and .8, the tests conducted at Mach .95 were the most extensive of the test series. In addition to operating the control actuator with the damping module engaged and disengaged, additional Mach .95 testing with two different damping tubes installed across the control actuator was conducted. The dynamic pressure used for the tests was limited to 650 lb/sq ft. This corresponds to a knots equivalent air speed of 438 at sea level on a standard day. Based on Figure 6 of report E801 by McDonnell Aircraft and a fundamental bending frequency of 9.8 Hz with a fundamental rotation frequency of 17.34 Hz, flutter would not be expected until an equivalent sea level air speed of 530 knots equivalent air speed. The tunnel test conditions were therefore adequate to investigate the approach to a flutter condition, but not to reach the air speed at which report E801 predicted flutter would occur. The flutter point test condition would have exceeded the 200 megawatt power capability of the wind tunnel. Not being able to reach the predicted flutter air speed did not limit the investigation, since sub-critical testing was the investigation objective.

6.5 Test Results

6.5.1 Mach .6 Test Condition Results

Table 1 lists the results of analyzing the bending mode response plots for the frequency of peaking and damping of the first bending mode of the surface at Mach .6. The damping and frequency of peaking both with and without the damper on is listed. Since the damper was not designed to affect the bending mode of the surface motion, the effect of the damper operation on this mode was not expected to be significant. Note that the table lists both the results of the HP 5420A program and the bandwidth calculated damping for the bending motion.

Figure 32 shows a response plot for the bending motion acceleration at a dynamic pressure of 300 lb/sq ft with the damper off. Note that the response plot shows the vertical and horizontal cursors used for measuring the frequency and amplitude points for the half power points. The "X" value at the top of the plot is the frequency of the left vertical cursor. The " Δ X" value is the frequency spread between the vertical cursors. The "Y" value listed at the top of the response plot is the value of the bottom horizontal cursor and the " Δ Y" value is the amplitude spread between the horizontal cursors in Db. Note that the results of the internal calculation program for indicating the frequency peak and the damping is printed above the response plot.

Figure 33 is an expanded response plot of the peak shown in Figure 32. Note that the curve is not smooth and requires judgment in locating the cursors used for the HP 5420A internal program and the calculation of the damping using the frequency bandwidth for the half power points. This type of curve was typical for most of the test data obtained during the wind tunnel testing. Note also that for Figure 33, the number of averages taken was 60. The trend during the wind tunnel testing was to require

an increasing number of averages to obtain a "stable" response plot (with new data averaged in) as the Mach number and "q" increased in value.

As shown on Table 1, the damping values for the HP 5420A program and the bandwidth calculation do not closely agree. This is due to the response peaks defining the bending resonance not being a perfectly smooth curve. Note that the damping calculated by the HP 5420A program for the 250 lb/sq ft "q" condition is indicated as negative, an obvious error due to the irregularity of the particular peak on which the program was used. Part of the difficulty in obtaining satisfactory peak analysis for the bending mode was associated with the relative output level of the accelerometer outputs at the resonance peaks. The amplitude of the peaks for the first bending mode was only slightly above the background noise level. The damping results indicated on Table 1 do not indicate a particular trend or difference between the operation with and without the damper on. This was expected based on the motion mode that the damper was designed to affect.

The peak frequency measurements show some disagreement between the HP 5420A program estimate and the bandwidth measurements. This disagreement is also because of the irregularities in the curves defining the amplitude peaks. The frequency of the bending resonance peak did not appear to increase (at least within the accuracy of the measurement techniques) over the "q" range at this Mach number. This indicated that the flutter point at which the bending and rotational resonance frequencies coalesce was not being rapidly approached.

TABLE 1

Mach .6 Wind Tunnel Test Results

Bending Mode

Test Condition		Resonant Frequency & Damping Estimation					
"q" (lb/sq ft)	Damper Mode	HP5420A Program				Bandwidth Calculation	
		Mean Freq. Peak (Hz)	Std Dev	Mean Damping (% Critical)	Std Dev	Peak Freq. (Hz)	Damping (% Critical)
200	on	10.85	0.10	-0.72	0.53	10.70	3.15
	off	10.21	0.03	.29	0.22	10.20	4.94
250	on	11.18	0.02	4.32	2.07	11.00	6.86
	off	10.57	0.12	-1.14	0.39	10.50	3.58
300	on	11.02	0.12	-1.17	1.02	10.94	3.94
	off	11.53	0.08	2.39	0.14	10.65	5.32
350	on	10.75	0.08	1.55	0.75	10.70	4.16
	off	11.09	0.01	-1.07	0.67	10.70	9.70
400	on	10.60	0.06	2.19	0.44	10.60	4.60
	off	10.89	0.06	3.66	0.23	11.05	4.02
450	on	10.42	0.18	1.32	0.65	10.40	6.70
	off	10.45	0.01	0.98	0.51	10.50	4.15
500	on	10.86	0.16	-6.52	1.91	10.90	6.34
	off	11.51	0.14	-1.89	0.21	11.70	5.59

TRACE A	TRANS	PEAK VALUE	11.4218 E+8
UNITS X-HZ	Y-LGMAG DB	XDAMPING	2.21882 E+8
SIG TYPE 1			
#AVERAGES	68		
START HZ	1.75781 E+8		
DELTA HZ	195.312 E-3		

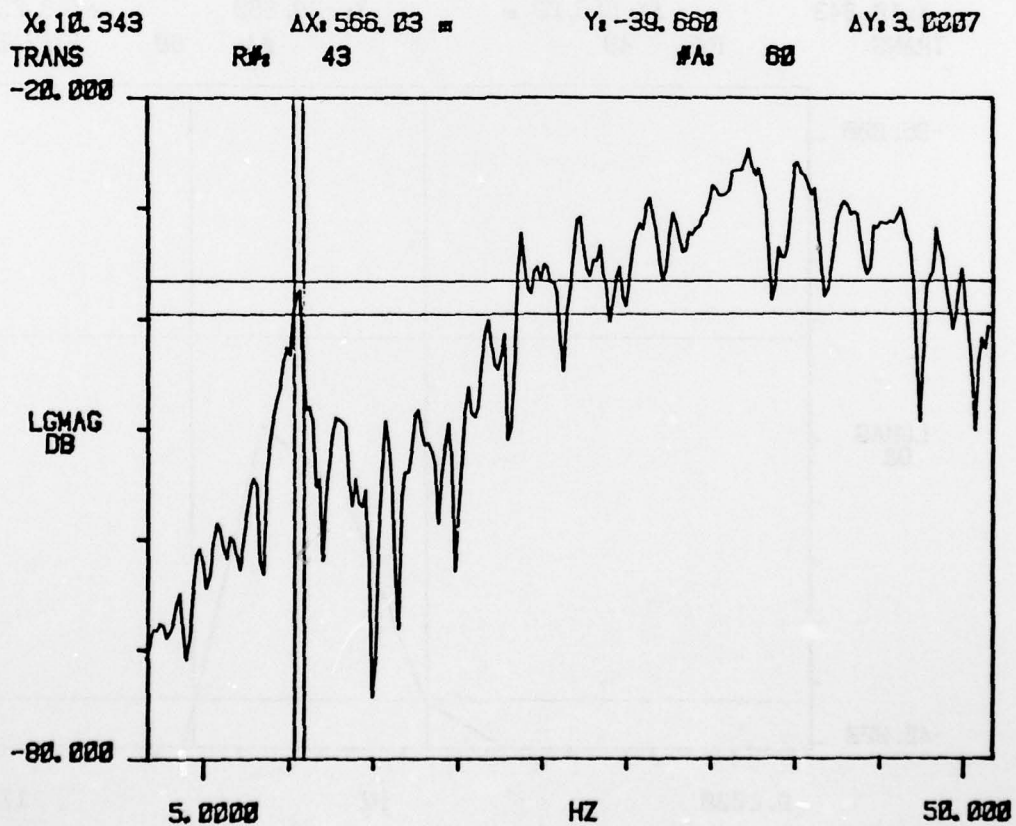


FIGURE 32 Bending Acceleration Amplitude Response -
Mach .6 and $q = 300$ lb/sq ft

X: 10.343 ΔX: 566.03 Y: -39.660 ΔY: 3.0007
 TRANS RA: 43 #A: 60 EXPAND

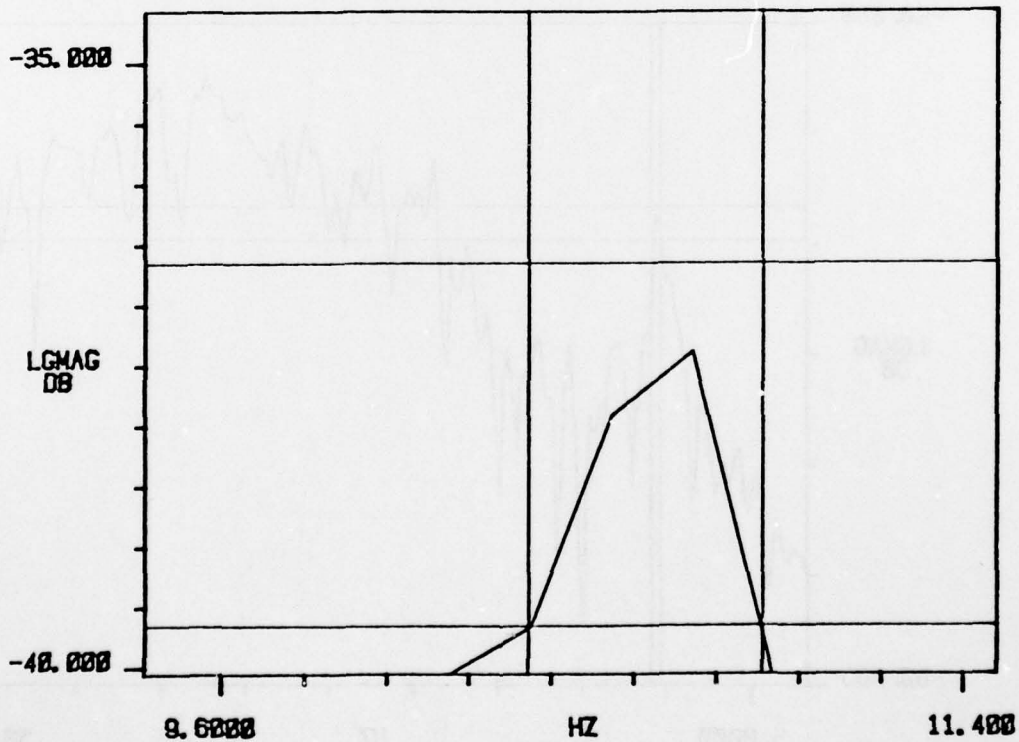


FIGURE 33 Expanded Acceleration Amplitude Response -
 First Bending Peak - Mach .6 and $q = 300$ lb/sq ft

Table 2 lists the results of analyzing the rotation mode response plots for the frequency of peaking and the damping of the first rotation mode of the surface at Mach .6. The damping and frequency of peaking both with and without the damper on is listed. The table lists both the results of the HP 5420A program and the bandwidth calculated damping for the rotation motion.

Figure 34 shows a response plot for the rotation motion acceleration response at a dynamic pressure of 350 lb/sq ft with the damper on. Figure 35 is an expanded section of Figure 34 and illustrates the irregularity characteristics of the response curve. Figure 36 is a response plot for the rotation motion for the rotation motion acceleration response at a dynamic pressure of 350 lb/sq ft with the damper off. Figure 37 is an expanded response plot for the acceleration response of Figure 36. As shown on Table 2, the damping with the damper on and off does not change significantly. Although some change was indicated with the change of damper operational mode, the amount and relative increase (or decrease) was not consistent at the different "q" conditions. However, the significant results were that the damper operation had very little effect upon the apparent damping of the rotational motion. This is inconsistent with the design theory. The damper should have provided a damping ratio of from .7 to 1 (or 70 to 100% of critical damping) when it was engaged.

Figure 38 shows the amplitude response at Mach .6 at a "q" of 500 lb/sq ft. For this figure the damper was turned off. Figure 39 shows the amplitude response at the same test condition with the damper turned on. The increase in dynamic pressure over that of Figures 34 and 35 (which creates a larger amplitude response than the lower "q" condition) did not change the damping characteristic change between the damper operating and not operating. Note on Figure 38 the irregular characteristic of the amplitude peak. As shown on this figure, 200 averages were used in obtaining the response plot. Even 200 averages did not produce a smooth curve for the peak.

TABLE 2

Mach .6 Wind Tunnel Test Results

Rotation Mode

Test Condition		Resonant Frequency & Damping Estimation					
"q" (lb/sq ft)	Damper Mode	HP5420A Program				Bandwidth Calculation	
		Mean Freq. Peak (Hz)	Std Dev	Mean Damping (% Critical)	Std Dev	Peak Freq. (Hz)	Damping (% Critical)
200	on	18.29	.09	3.62	.06	18.60	10.00
	off	18.2	.11	6.22	.87	17.92	8.30
250	on	19.18	.11	8.58	1.12	18.5	8.66
	off	19.47	0.46	8.25	0.76	18.5	8.01
300	on	19.01	0.27	8.88	2.83	18.50	11.39
	off	18.34	0.03	1.48	1.00	18.30	8.21
350	on	18.06	0.16	4.19	1.72	18.20	9.81
	off	19.02	0.33	18.17	4.13	18.10	5.67
400	on	18.00	0.07	9.30	0.94	18.80	15.00
	off	17.86	0.22	7.85	0.73	18.20	9.06
450	on	18.08	0.12	10.41	0.50	17.80	13.44
	off	18.41	0.33	8.49	0.00	18.60	16.55
500	on	18.18	0.17	6.26	0.22	18.40	13.71
	off	19.64	0.22	8.53	1.26	18.30	16.81

TRACE A	TRANS	PEAK VALUE	17.9145 E+0
UNITS X-HZ	Y-LGMAG DB	XDAMPING	3.60752 E+0
SIG TYPE 1			
#AVERAGES	19		
START HZ	1.75781 E+0		
DELTA HZ	195.312 E-3		

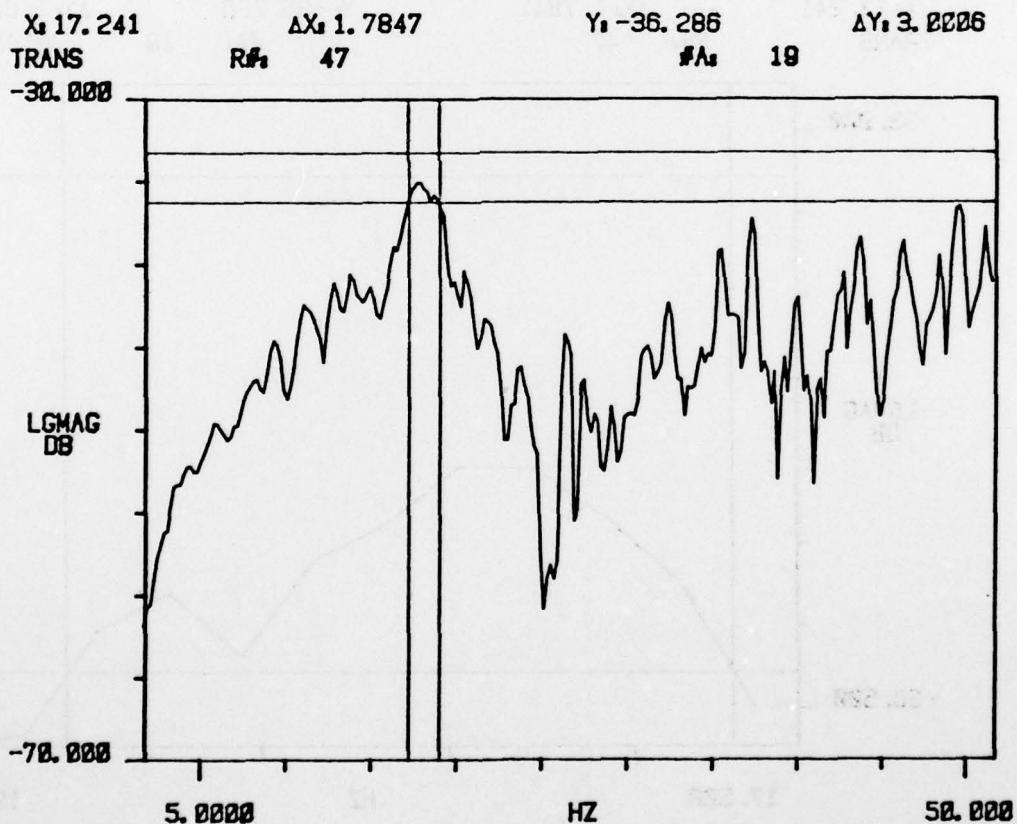


FIGURE 34 Rotational Acceleration Amplitude Response -
 Mach .6 and $q = 350$ lb/sq ft with Damper On

X: 17.241 ΔX: 1.7847 Y: -36.286 ΔY: 3.0036
 TRANS R#: 47 #A: 18 EXPAND

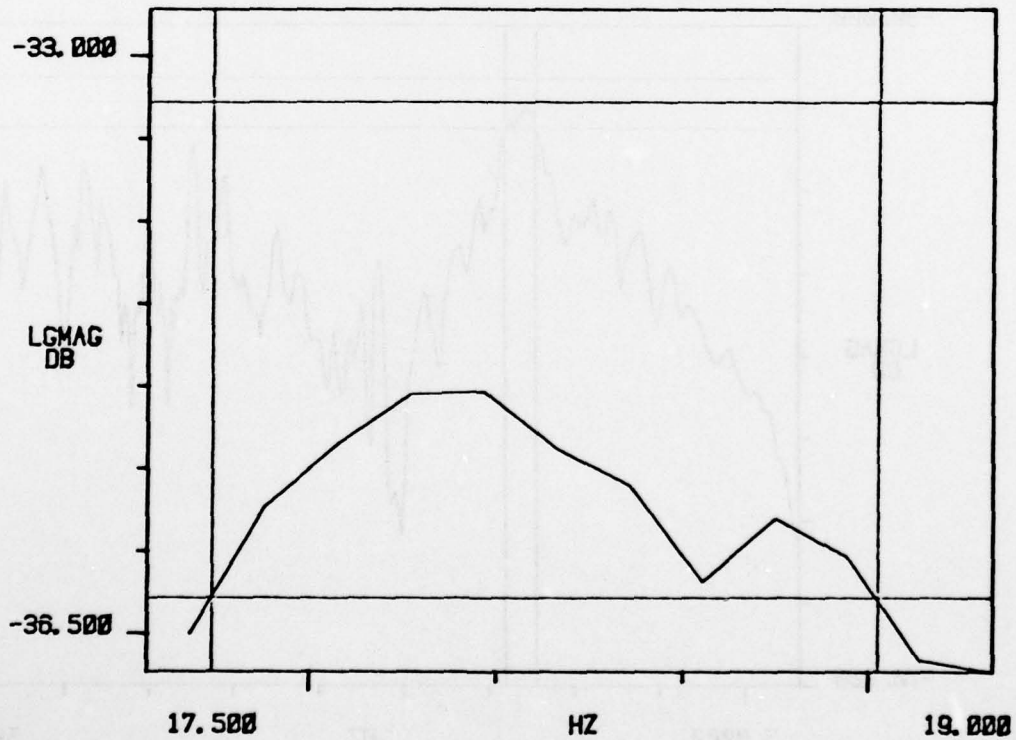


FIGURE 35 Expanded Acceleration Amplitude Response - First Rotation
 Peak - Mach .6 and $q = 350$ lb/sq ft With Damper On

TRACE A	TRANS	PEAK VALUE	18.2322 E+0
UNITS X-HZ	Y-LGMAG DB	XDAMPING	20.2557 E+0
SIG TYPE 1			
#AVERAGES	68		
START HZ	1.75781 E+0		
DELTA HZ	195.312 E-3		

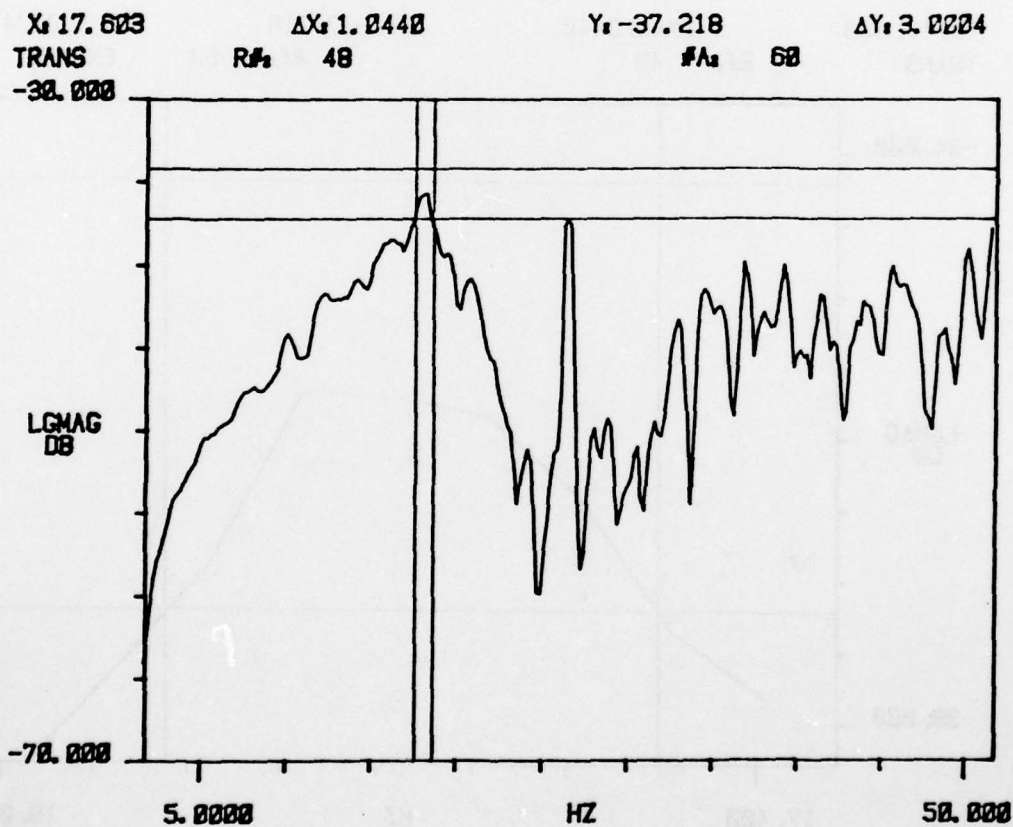


FIGURE 36 Rotational Acceleration Amplitude Response -
 Mach .6 and $q = 350$ lb/sq ft with Damper Off

X_1 17.623 ΔX_1 1.0440 Y_1 -37.218 ΔY_1 3.0034
 TRANS $R\#_1$ 48 $\#A_1$ 60 EXPAND

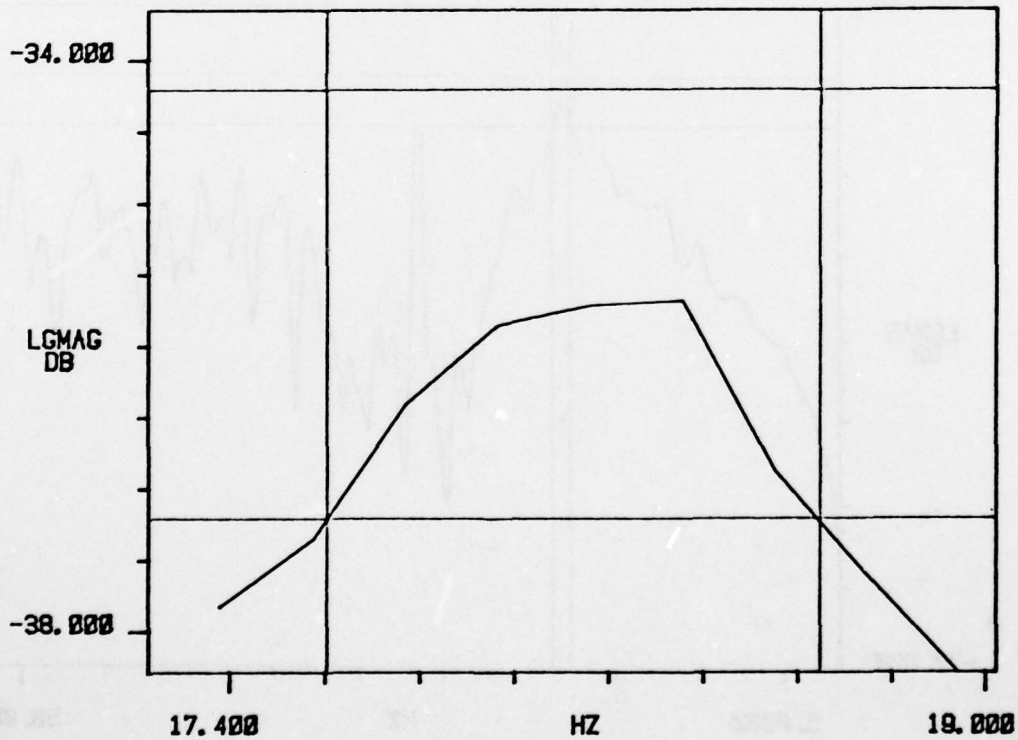


FIGURE 37 Expanded Acceleration Amplitude Response - First Rotation
 Peak - Mach .6 and $q = 350$ lb/sq ft With Damper Off

TRACE A	TRANS	PEAK VALUE	18.8942 E+0
UNITS X-HZ	Y-LGMAG DB	XDAMPING	8.74789 E+0
SIG TYPE 1			
#AVERAGES	200		
START HZ	1.75781 E+0		
DELTA HZ	195.312 E-3		

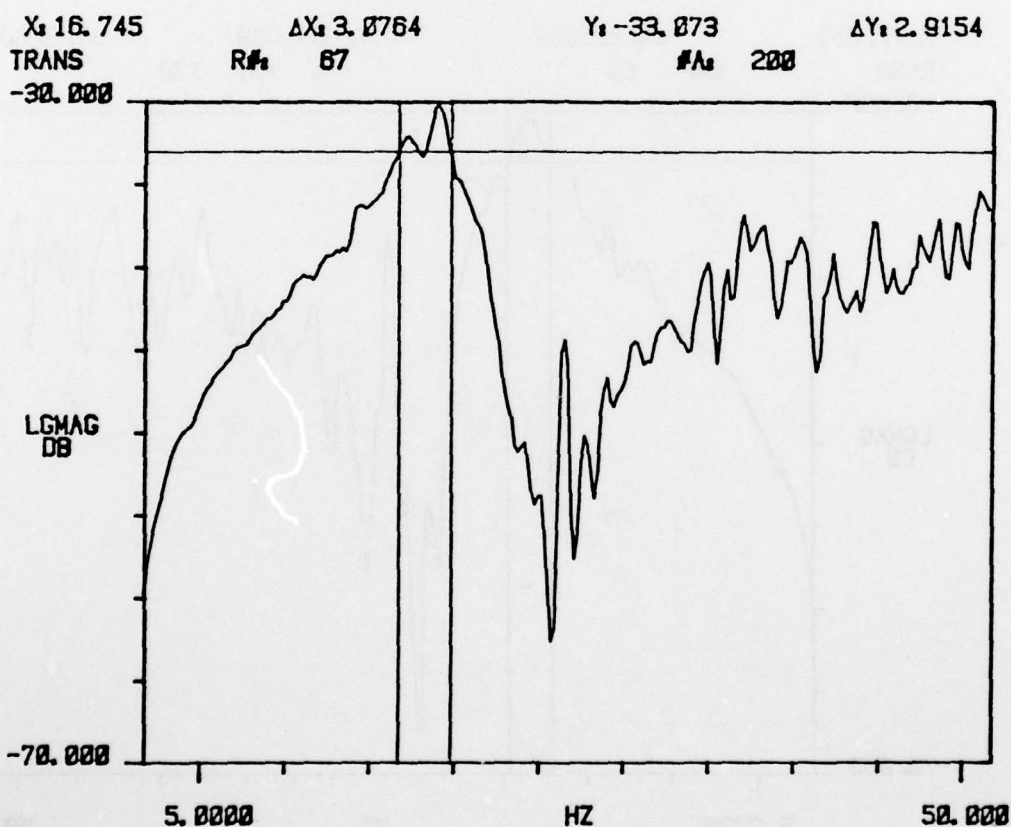


FIGURE 38 Rotational Acceleration Amplitude Response -
 Mach .6 and $q = 500$ lb/sq ft with Damper Off

TRACE A	TRANS	PEAK VALUE	18.7008 E+0
UNITS X-HZ	Y-LGMAG DB	XDAMPING	5.22089 E+0
SIG TYPE 1			
#AVERAGES	100		
START HZ	1.75701 E+0		
DELTA HZ	195.312 E-3		

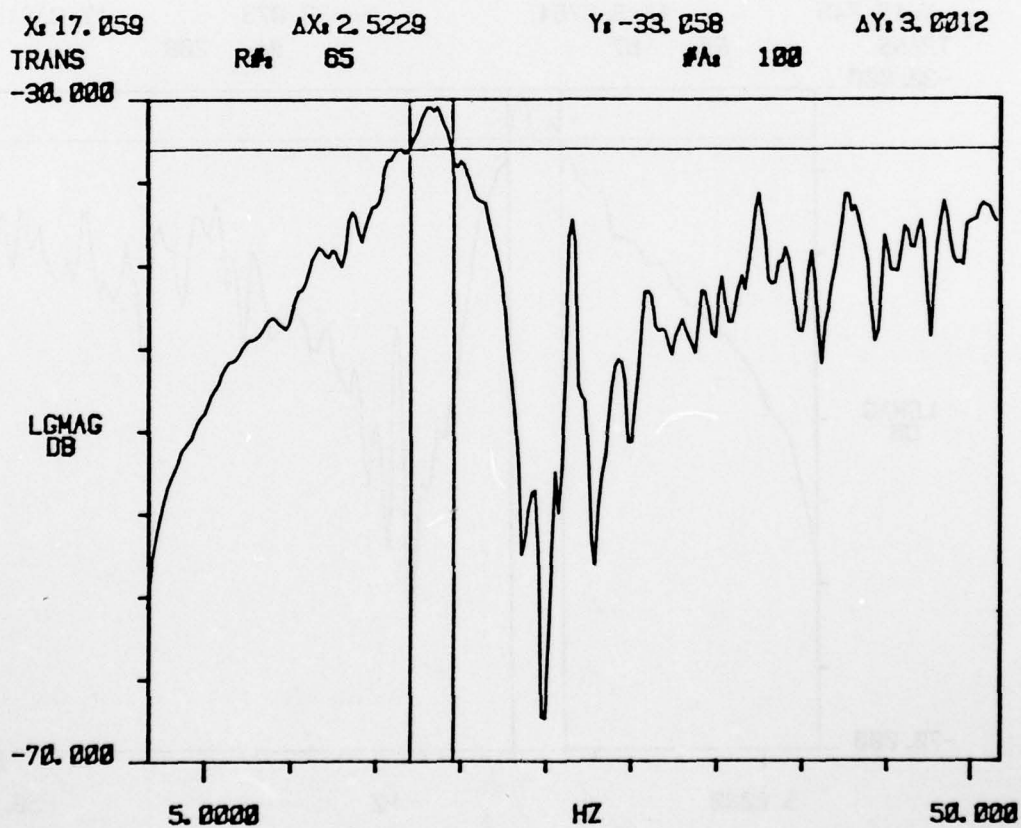


FIGURE 39 Rotational Acceleration Amplitude Response -
Mach .6 and q = 500 lb/sq ft with Damper On

6.5.2 Mach .8 Test Condition Results

Table 3 lists the results of analyzing the bending mode response plots for the frequency of peaking and the damping of the first bending mode of the surface at Mach .8. The damping and frequency of peaking both with and without the damper on is listed. As with the previous tables, the results of the HP 5420A program and the bandwidth calculated damping are presented for the bending motion.

Note that on Table 3 two different test measurements at a "q" of 500 are given. The second set of data was obtained 24 hours later than the first set and was a check test measurement. Figure 40 shows the bending accelerometer response at Mach .8 and a "q" of 500 lb/sq ft with the damper on. Figure 41 shows the bending accelerometer response at Mach .8 and a "q" of 500 lb/sq ft with the damper turned off. The results of Table 3 show no significant trends. The variation in damping and resonance frequencies are more consistent than the Mach .6 results. There is some minor increase in damping between the damper on and damper off test conditions at all "q" conditions. The frequency of the bending resonance peak as estimated by the HP 5420A and by the bandwidth measurement process showed fairly good agreement for most test conditions. The general trend of the frequency of the bending peak with increasing "q" was a slight increase in the frequency from 10.3 to 11.3 Hz for a "q" change from 200 to 500 lb/sq ft. Negative damping values are listed from three of the HP 5420A program estimation results since the program calculated a negative damping value for the "q" of 200 and one "q" of 300 test condition. These negative damping results are associated with the particular irregularities in the response peaks to which the program applied.

TABLE 3

Mach .8 Wind Tunnel Test Results

Bending Mode

Test Condition		Resonant Frequency & Damping Estimation					
"q" (lb/sq ft)	Damper Mode	HP5420A Program				Bandwidth Calculation	
		Mean Freq. Peak (Hz)	Std Dev	Mean Damping (% Critical)	Std Dev	Peak Freq. (Hz)	Damping (% Critical)
200	on	10.25	0.03	-5.42	1.57	10.30	4.64
	off	10.40	0.12	-1.41	1.22	10.30	4.13
300	on	10.65	0.03	3.01	0.62	10.65	4.18
	off	10.71	N.A.	N.A.	N.A.	N.A.	N.A.
400	on	10.99	0.25	4.31	1.92	11.43	8.71
	off	11.03	0.03	3.01	0.33	11.20	6.64
500	on	10.61	0.06	4.05	0.38	10.80	5.98
	off	10.88	0.06	3.31	0.87	10.90	4.63
500	on	10.80	0.03	5.18	0.60	11.30	9.35
	off	11.38	0.03	3.97	0.37	10.80	7.69

TRACE A	TRANS	PEAK VALUE	10.8493 E+0
UNITS X-HZ	Y-LGMAG DB	XDAMPING	3.69618 E+0
SIG TYPE 1			
#AVERAGES	60		
START HZ	1.75781 E+0		
DELTA HZ	195.312 E-3		

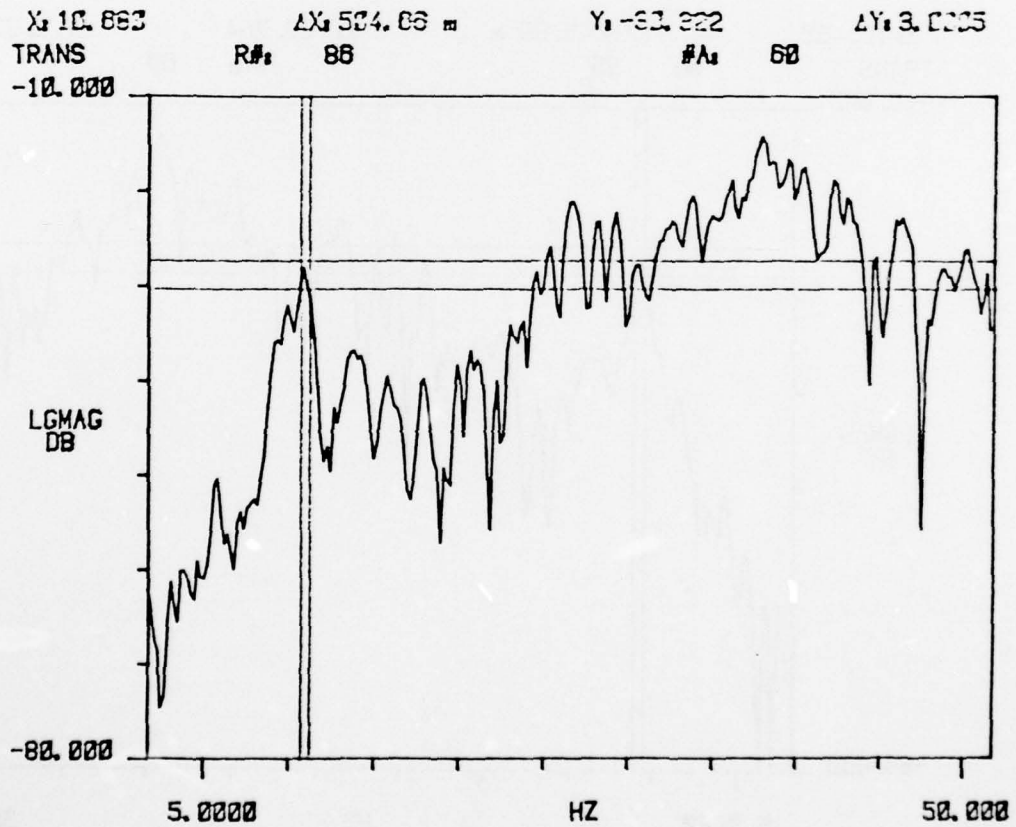


FIGURE 40 Bending Acceleration Amplitude Response -
 Mach .8 and $q = 500$ lb/sq ft with the Damper Off

AD-A080 133

DYNAMIC CONTROLS INC DAYTON OHIO

F/6 1/3

RESEARCH AND DEVELOPMENT OF CONTROL ACTUATION SYSTEMS FOR AIRCR--ETC(U)

AUG 79 G D JENNEY

F33615-77-C-3077

UNCLASSIFIED

AFFDL-TR-79-3117-VOL-1

NL

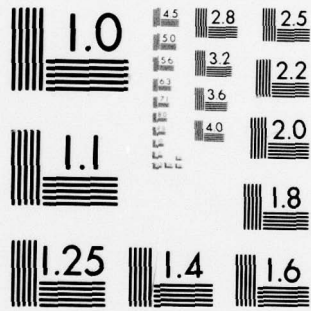
2 of 3

AD

A080133

1





MICROCOPY RESOLUTION TEST CHART
 NATIONAL BUREAU OF STANDARDS-1963-A

TRACE A	TRANS	PEAK VALUE	10.6512 E+0
UNITS X-HZ	Y-LGMAG DB	XDAMPING	4.34945 E+0
SIG TYPE 1			
#AVERAGES	60		
START HZ	1.75781 E+0		
DELTA HZ	195.312 E-3		

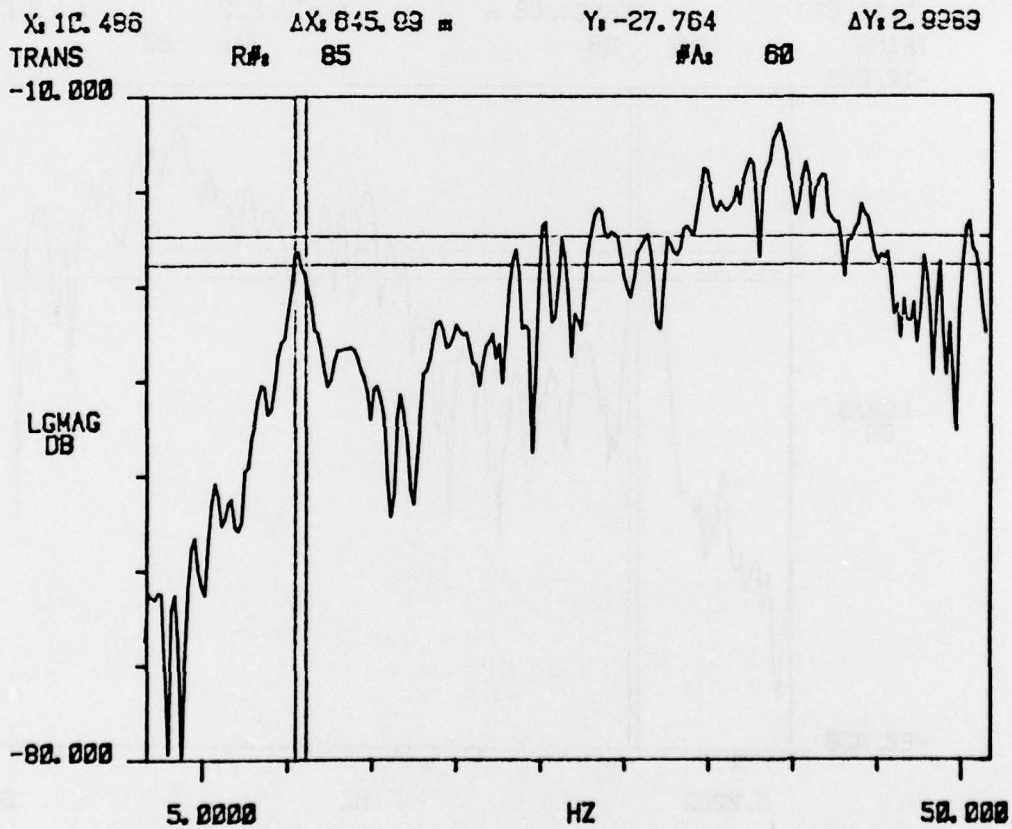


FIGURE 41 Bending Acceleration Amplitude Response -
 Mach .8 and $q = 500$ lb/sq ft with the Damper On

Table 4 lists the first rotational mode peak frequencies and damping for the wind tunnel test conditions of Mach .8 and the "q" varied in steps of 100 from 200 lb/sq ft to 500 lb/sq ft. The HP 5420A program for damping and peak frequency and the bandwidth calculated results are listed for both the damper turned on and off. As with the results listed on Table 3, two separate 500 lb/sq ft test condition measurements are listed.

Figure 42 is a response plot for the rotational accelerometer with the damper turned off and a "q" of 500 lb/sq ft. Figure 43 is an expanded plot of the rotational peak shown on Figure 42. Figure 44 is a response plot for the rotational accelerometer with the damper turned on at the "q" of 500 lb/sq ft test condition. Figure 45 is an expanded plot of the rotational peak shown on Figure 44. On both the expanded plots of Figures 43 and 45 the curve irregularity is apparent, even though the "un-expanded" curve appears reasonably smooth.

The particular results of the data analysis do not indicate trends different from that obtained from the Mach .6 test data. The HP 5420A program results do not closely agree with the bandwidth calculations. This is again due to the irregularities associated with the curves defining the rotational mode resonance peaks. However, the results of no significant change in the rotational mode damping with the damper turned on and off is evident as a general result. Little change in the peak frequencies of the rotational resonance occur with increasing dynamic pressure, indicating that the flutter onset point is not being rapidly approached.

TABLE 4

Mach .8 Wind Tunnel Test Results

Rotation Mode

Test Condition		Resonant Frequency & Damping Estimation					
"q" (lb/sq ft)	Damper Mode	HP5420A Program				Bandwidth Calculation	
		Mean Freq. Peak (Hz)	Std Dev	Mean Damping (% Critical)	Std Dev	Peak Freq. (Hz)	Damping (% Critical)
200	on	17.99	0.31	5.64	1.12	18.3	12.10
	off	17.33	0.18	9.66	1.01	17.0	14.14
300	on	17.53	0.12	2.60	0.38	18.0	19.10
	off	18.52	0.23	2.92	1.01	17.9	6.85
400	on	18.13	0.03	4.38	0.51	18.3	8.15
	off	18.57	0.08	4.17	1.35	18.6	4.13
500	on	18.68	0.31	1.78	1.64	18.3	5.88
	off	18.33	0.02	6.53	1.22	18.6	11.10
500	on	18.18	0.07	4.86	0.50	18.2	5.79
	off	17.97	0.07	6.11	0.50	18.1	10.71

TRACE A	TRANS	PEAK VALUE	18.1358 E+8
UNITS X-HZ	Y-LGMAG DB	XDAMPING	8.94021 E+8
SIG TYPE 1			
#AVERAGES	68		
START HZ	0.0 E+8		
DELTA HZ	195.312 E-3		

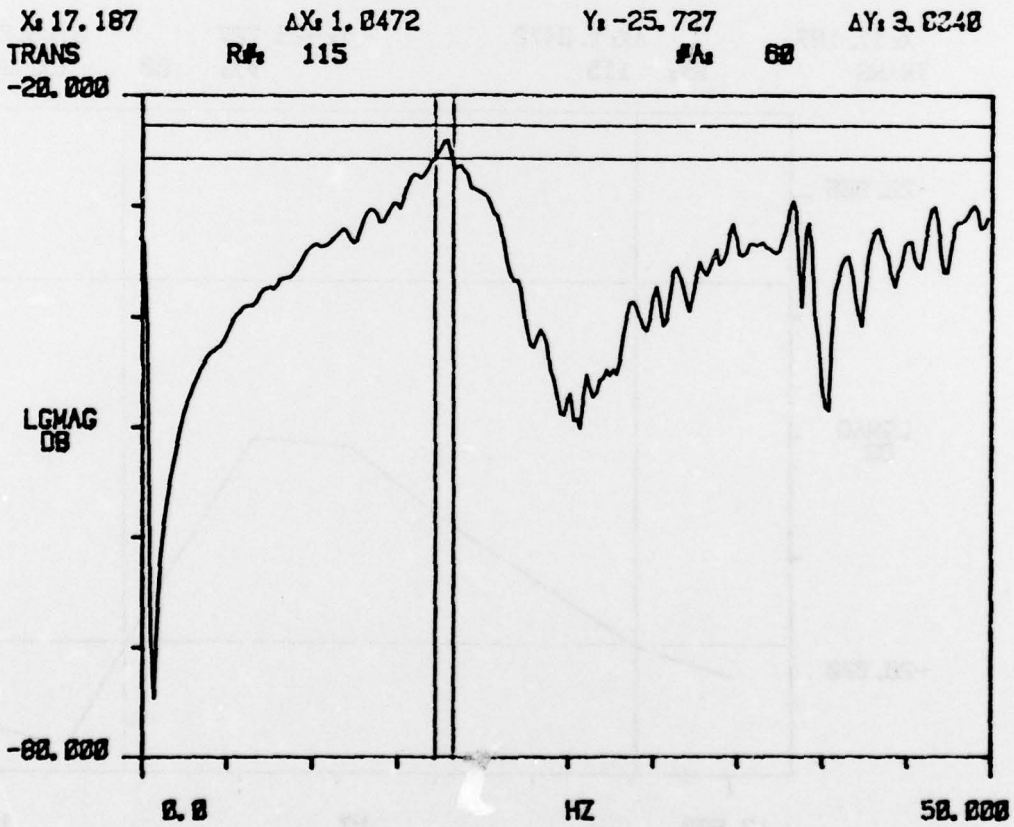


FIGURE 42 Rotational Acceleration Amplitude Response -
 Mach .8 and $q = 500$ lb/sq ft with Damper Off

X_c 17.187 ΔX_c 1.0472 Y_c -25.727 ΔY_c 3.0248
 TRANS RA 115 #A 68 EXPAND

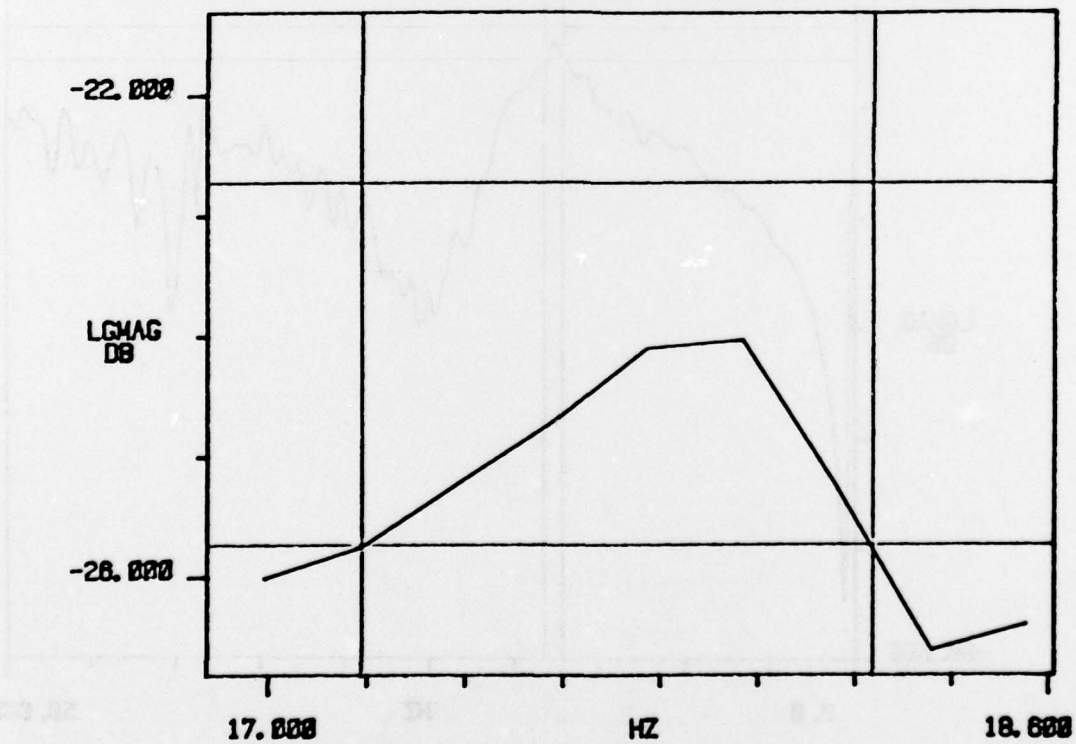


FIGURE 43 Expanded Acceleration Amplitude Response - First Rotation
 Peak - Mach .8 and $q = 500$ lb/sq ft with Damper Off

TRACE A	TRANS	PEAK VALUE	18.2746 E+0
UNITS X-HZ	Y-LGMAG DB	XDAMPING	4.86806 E+0
SIG TYPE 1			
#AVERAGES	60		
START HZ	0.0 E+0		
DELTA HZ	195.312 E-3		

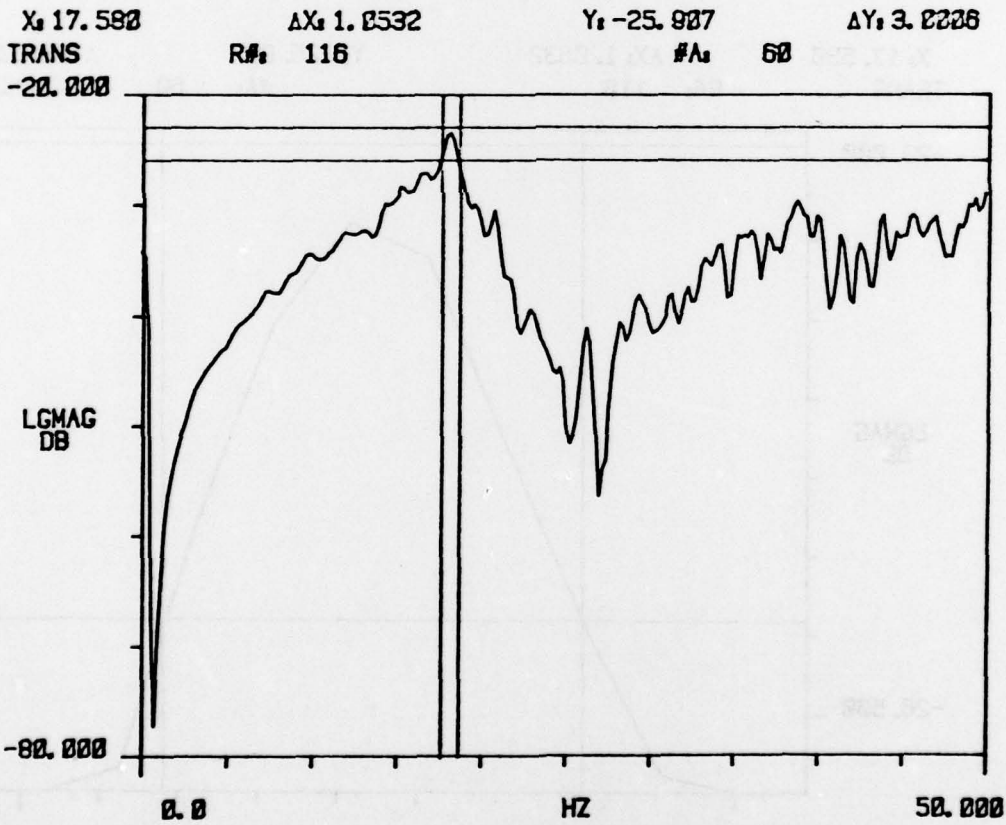


FIGURE 44 Rotational Acceleration Amplitude Response -
Mach .8 and q = 500 lb/sq ft with Damper On

X₁ 17.580
TRANS

ΔX₁ 1.8532
R#₁ 116

Y₁ -25.927
#A₁ 60

ΔY₁ 3.8208
EXPAND

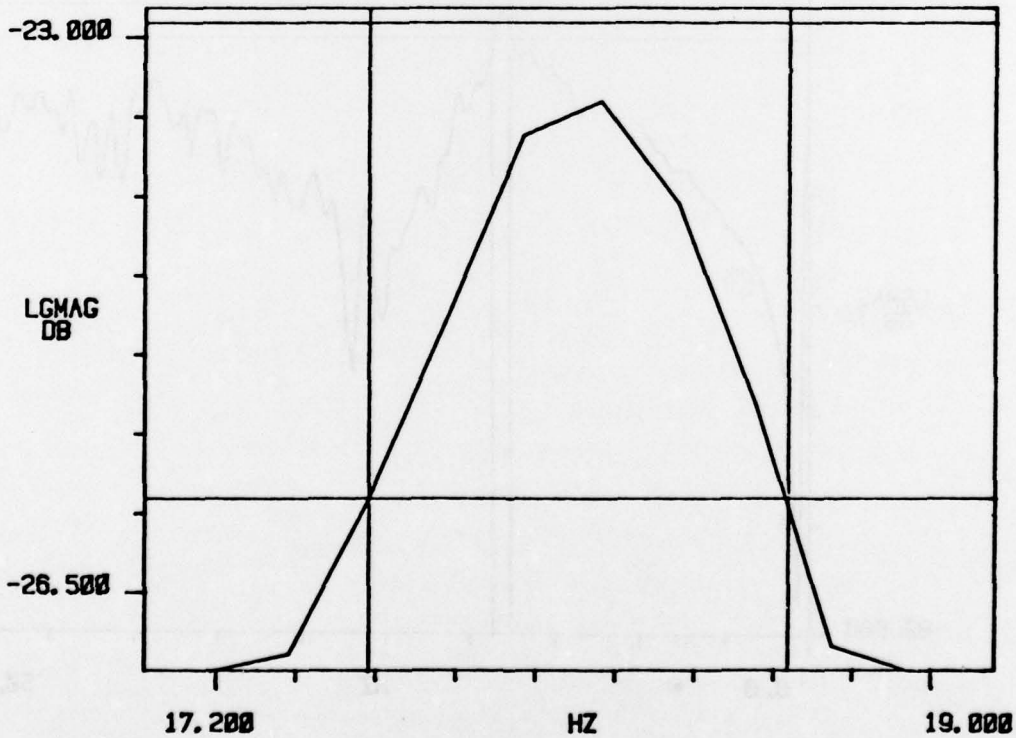


FIGURE 45 Expanded Acceleration Amplitude Response - First Rotation
Peak - Mach .8 and q = 500 lb/sq ft With Damper On

6.5.3 Mach 0.95 Test Condition Results

Table 5 lists the results of analyzing the bending mode response plots for the frequency of peaking and damping of the first bending mode of the surface at Mach .95. The damping and the frequency of peaking both with and without the damper on is listed. As with the previous tables, the results of the HP 5420A program and the bandwidth calculated damping are presented for the bending motion. The range of "q" variation was from 200 to 650 lb/sq ft (which was the highest "q" test condition used during the wind tunnel testing).

As shown on Table 5, the calculated results from both the HP 5420A program and the bandwidth procedure were more consistent than the previous Mach .6 and .8 test conditions. The frequencies for the resonance peak of the first bending mode exhibited good correlation between the two calculation methods (with the exception of one point at a "q" of 200 lb/sq ft). The first bending mode peak frequency increased slightly with increasing "q" as was expected from the general flutter characteristic for the surface. Except for the calculated result for the damping at the one 200 lb/sq ft "q" test condition, the damping for the first bending mode was within the range of .02 to .08% of critical. This is in the range expected from McDonnell Aircraft's report E801. Little change in the damping was apparent with changing the operational mode of the damper from on to off. This is consistent with the fact that the damper was designed to be effective only on the rotational mode of the surface. The improved correlation between the calculation methods and the reduced variation in the calculated results (compared to Mach .6 and .8 test condition results) is directly attributable to the improvement in the measured response curve irregularities. Figure 46 shows the response curve obtained at a "q" of 500 lb/sq ft with the damper on. Figure 47 is an expanded response curve of the first bending mode peak shown on Figure 46.

TABLE 5

Mach 0.95 Wind Tunnel Test Results

Bending Mode

Test Condition		Resonant Frequency & Damping Estimation					
"q" (lb/sq ft)	Damper Mode	HP5420A Program				Bandwidth Calculation	
		Mean Freq. Peak (Hz)	Std Dev	Mean Damping (% Critical)	Std Dev	Peak Freq. (Hz)	Damping (% Critical)
200	on	10.10	.13	10.28	.31	11.10	4.23
	off	10.74	.20	3.19	.36	10.50	4.98
300	on	11.22	.22	4.73	1.27	11.20	6.89
	off	10.75	0.06	2.10	0.42	10.95	3.13
400	on	11.02	0.03	4.10	0.56	11.00	3.03
	off	10.86	0.05	2.84	0.44	10.65	3.62
500	on	11.15	0.03	4.31	0.20	11.25	4.30
	off	11.08	0.08	5.47	0.74	11.15	4.23
550	on	11.64	0.01	3.67	0.26	11.70	5.08
	off	11.06	0.08	4.75	0.54	11.40	5.41
600	on	11.70	0.05	6.51	0.73	11.40	4.24
	off	11.41	0.16	4.28	0.87	11.65	4.50
650	on	11.82	0.08	5.33	0.60	12.00	6.98
	off	11.47	0.10	5.10	0.70	11.50	7.85

TRACE A	TRANS	PEAK VALUE	11.7171 E+0
UNITS X-HZ	Y-LGMAG DB	XDAMPING	8.84831 E+0
SIG TYPE 1			
#AVERAGES	40		
START HZ	1.75781 E+0		
DELTA HZ	195.312 E-3		

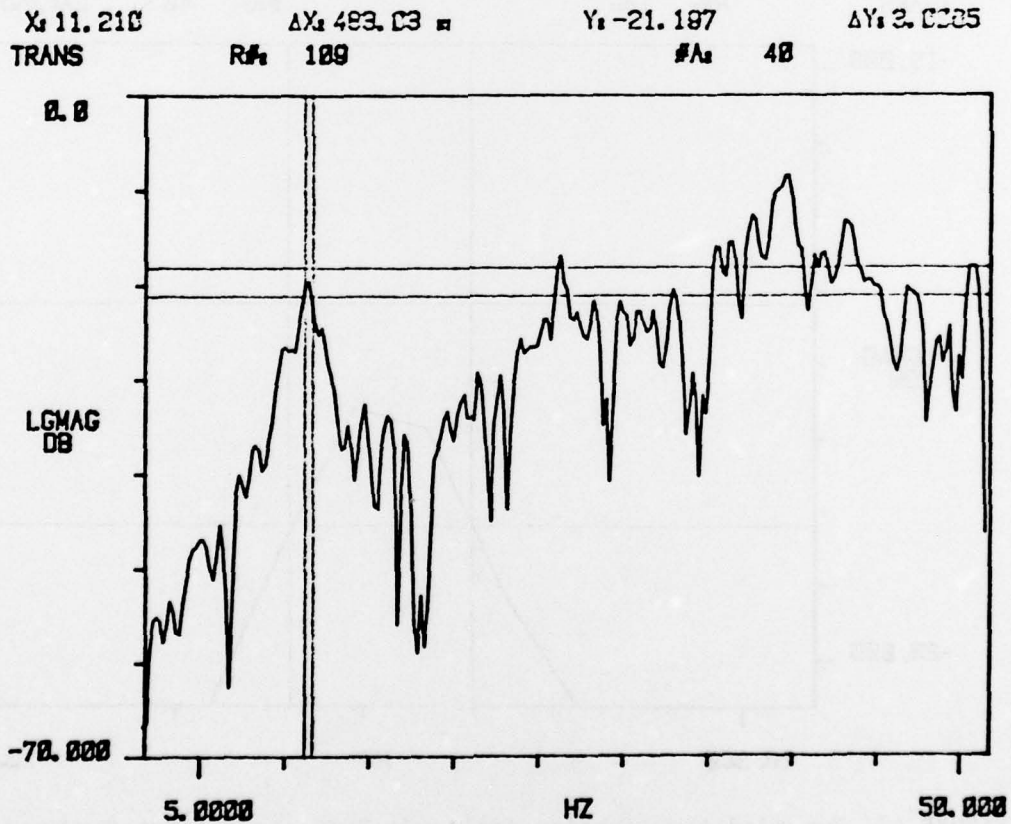


FIGURE 46 Bending Acceleration Amplitude Response -
 Mach 0.95 and $q = 500$ lb/sq ft with the Damper On

X: 11.210 ΔX: 452.23 m Y: -21.127 ΔY: 3.2325
 TRANS R#: 109 #A: 40 EXPAND

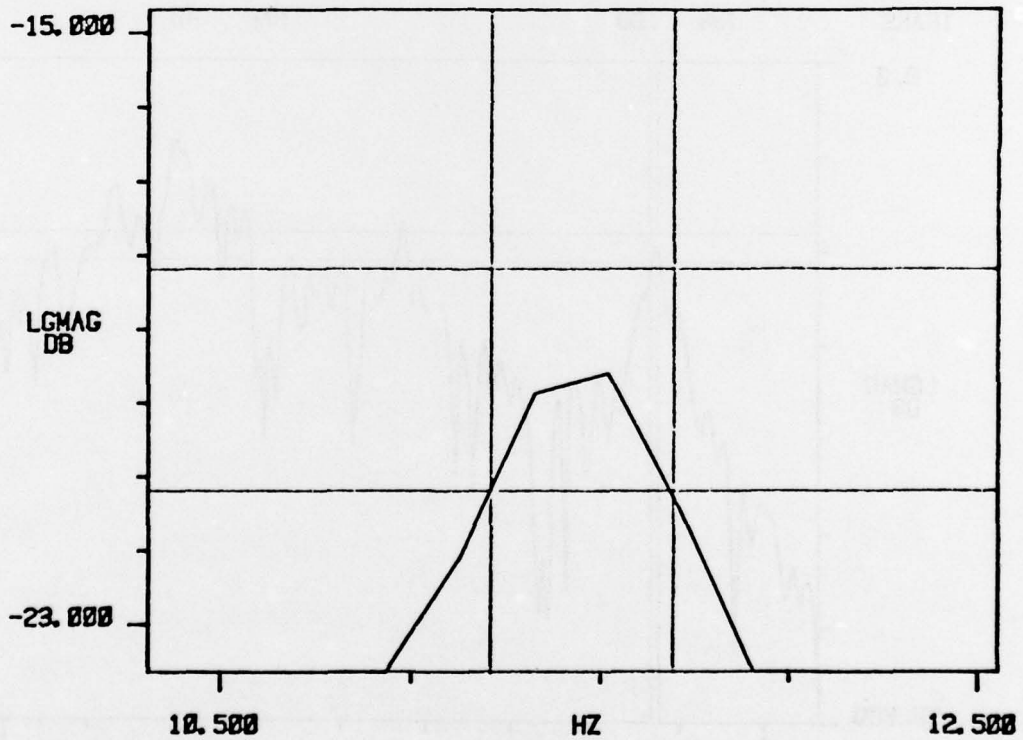


FIGURE 47 Expanded Acceleration Amplitude Response - First Bending
 Peak - Mach 0.95 and $q = 500 \text{ lb/sq ft}$ with Damper On

TABLE 6

Mach 0.95 Wind Tunnel Test Results

Rotation Mode

Test Condition		Resonant Frequency & Damping Estimation					
"q" (lb/sq ft)	Damper Mode	HP5420A Program				Bandwidth Calculation	
		Mean Freq. Peak (Hz)	Std Dev	Mean Damping (% Critical)	Std Dev	Peak Freq. (Hz)	Damping (% Critical)
200	on	18.08	0.37	8.63	1.81	18.30	9.76
	off	17.91	0.61	5.58	0.45	18.75	4.60
300	on	19.13	0.08	7.10	0.62	19.00	6.61
	off	18.28	0.03	5.45	0.46	18.50	3.35
400	on	18.24	0.04	4.93	0.44	18.50	5.34
	off	18.78	0.41	5.45	0.29	18.60	4.83
500	on	18.52	0.17	6.43	1.76	18.30	5.34
	off	18.10	0.02	5.48	1.29	18.40	7.46
550	on	18.90	0.17	6.85	0.57	18.70	5.71
	off	18.66	0.20	5.57	0.60	18.50	9.47
600	on	18.38	0.13	6.92	0.15	19.00	10.40
	off	18.30	0.13	7.08	0.47	18.50	4.91
650	on	19.21	0.32	5.00	0.61	18.70	11.14
	off	18.56	0.13	6.70	0.51	18.70	9.24

TRACE A	TRANS	PEAK VALUE	11.3884 E+0
UNITS X-HZ	Y-LGMAG DB	XDAMPING	3.85361 E+0
SIG TYPE 1			
#AVERAGES	40		
START HZ	1.75781 E+0		
DELTA HZ	195.312 E-3		

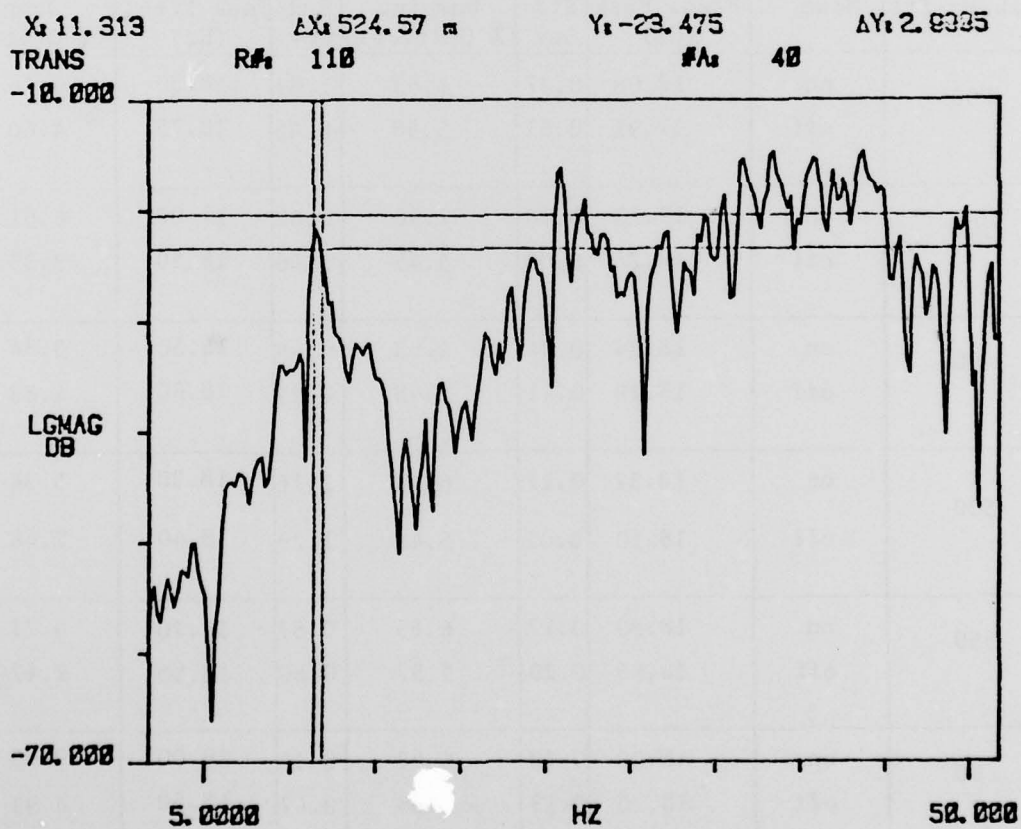


FIGURE 48 Bending Acceleration Amplitude Response -
 Mach 0.95 and $q = 500$ lb/sq ft with the Damper Off

X: 11.313 ΔX: 524.57 m Y: -23.475 ΔY: 2.6335
 TRANS R#: 118 #A: 48 EXPAND

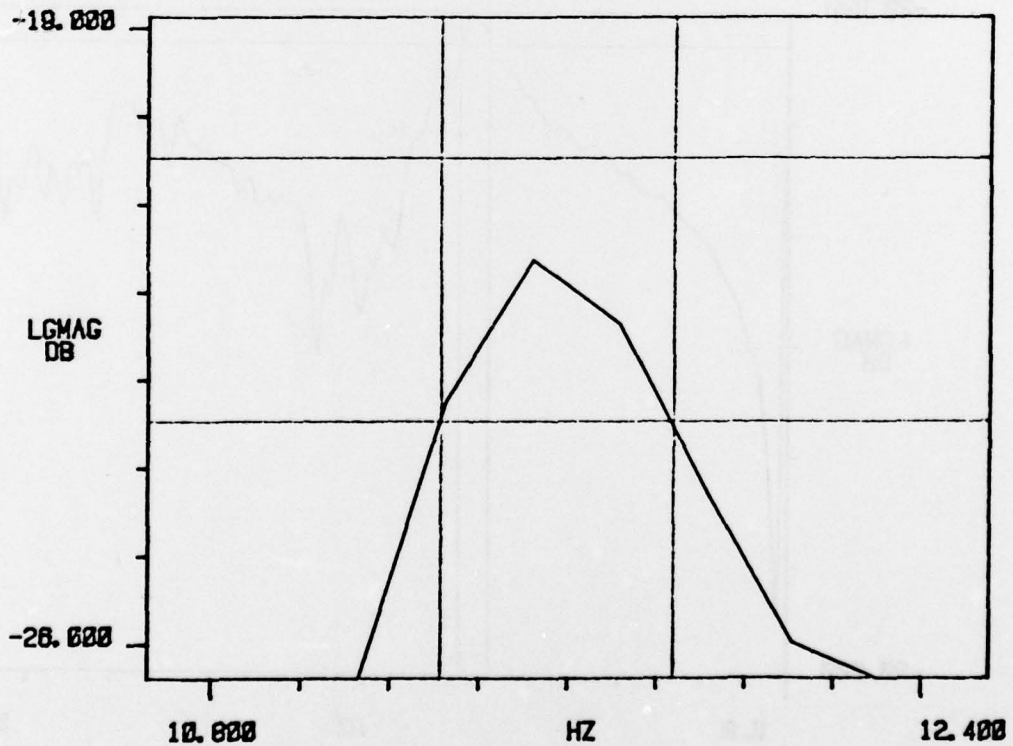


FIGURE 49 Expanded Acceleration Amplitude Response - First Bending Peak - Mach 0.95 and $q = 500$ lb/sq ft with Damper Off

TRACE A	TRANS	PEAK VALUE	18.8485 E+8
UNITS X-HZ	Y-LGMAG DB	XDAMPING	8.21127 E+8
SIG TYPE 1			
#AVERAGES	68		
START HZ	0.0 E+8		
DELTA HZ	195.312 E-3		

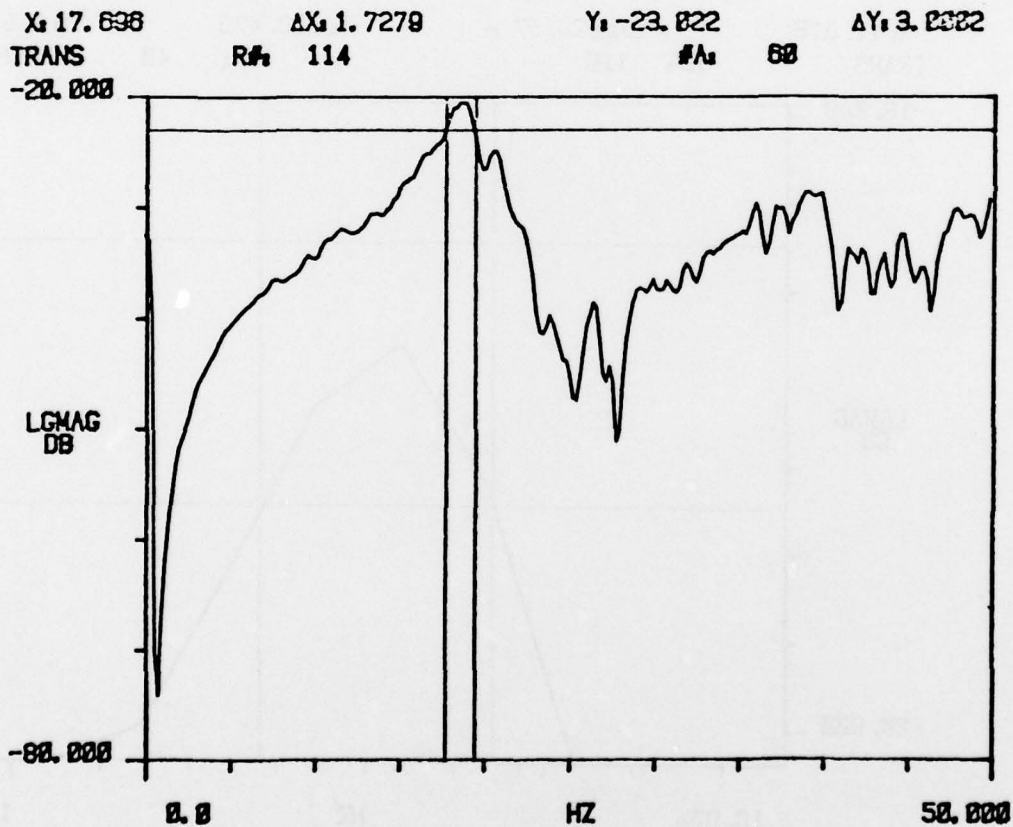


FIGURE 50 Rotational Acceleration Amplitude Response -
 Mach 0.95 and $q = 650$ lb/sq ft with Damper Off

X: 17.636 ΔX: 1.7278 Y: -23.322 ΔY: 3.6332
 TRANS R#: 114 #A: 68 EXPAND
 -20.000

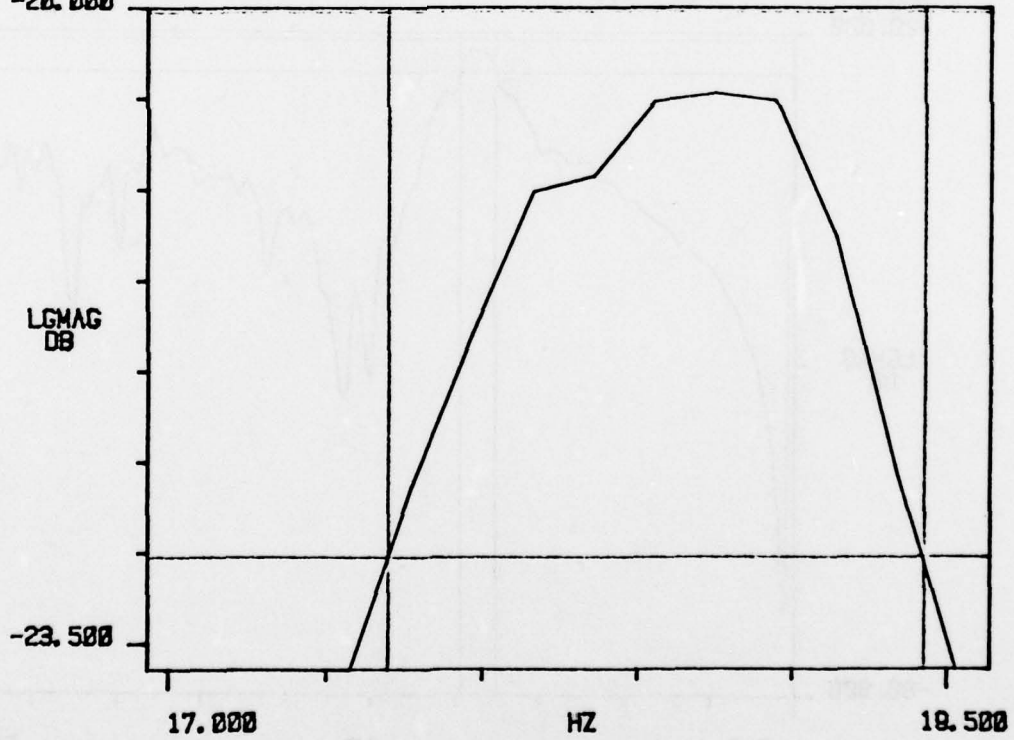


FIGURE 51 Expanded Acceleration Amplitude Response - First Rotation
 Peak - Mach 0.95 and $q = 650$ lb/sq ft with Damper Off

TRACE A	TRANS	PEAK VALUE	19.4835 E+0
UNITS X-HZ	Y-LGMAG DB	XDAMPING	4.97251 E+0
SIG TYPE 1			
#AVERAGES	60		
START HZ	16.9922 E+0		
DELTA HZ	195.312 E-3		

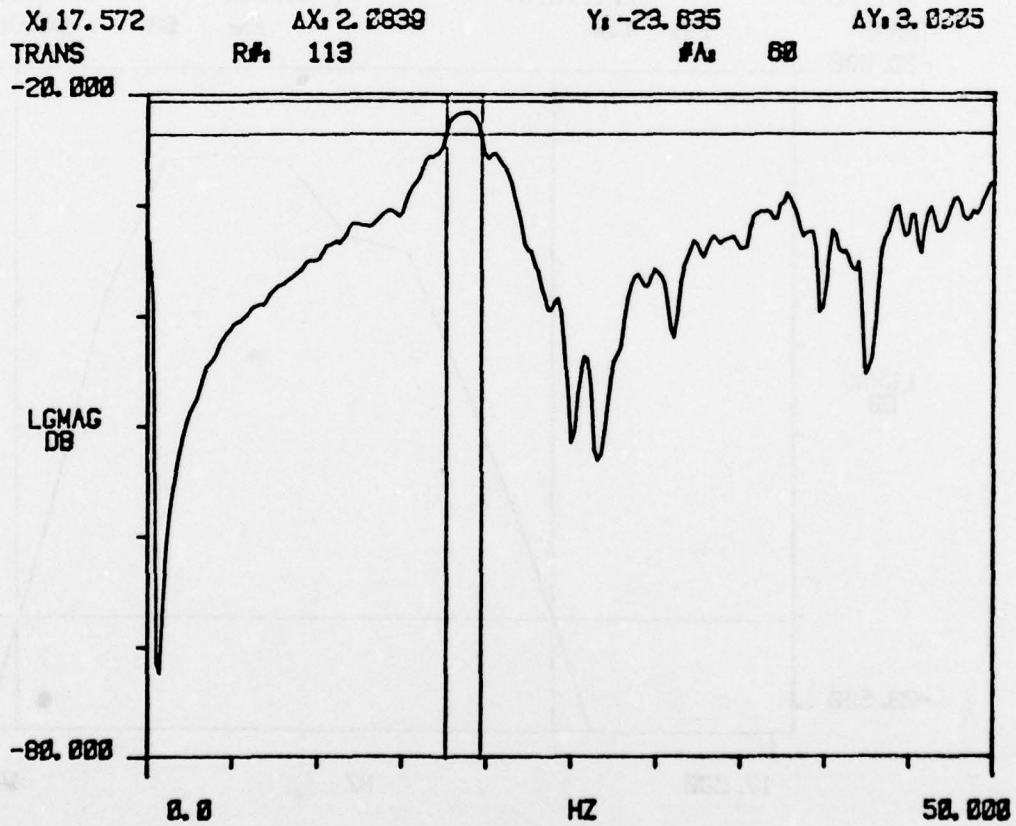


FIGURE 52 Rotational Acceleration Amplitude Response -
 Mach 0.95 and $q = 650$ lb/sq ft with Damper On

X_1 17.572 ΔX_1 2.0830 Y_1 -23.635 ΔY_1 3.0805
 TRANS R/A_1 113 #/A₁ 60 EXPAND

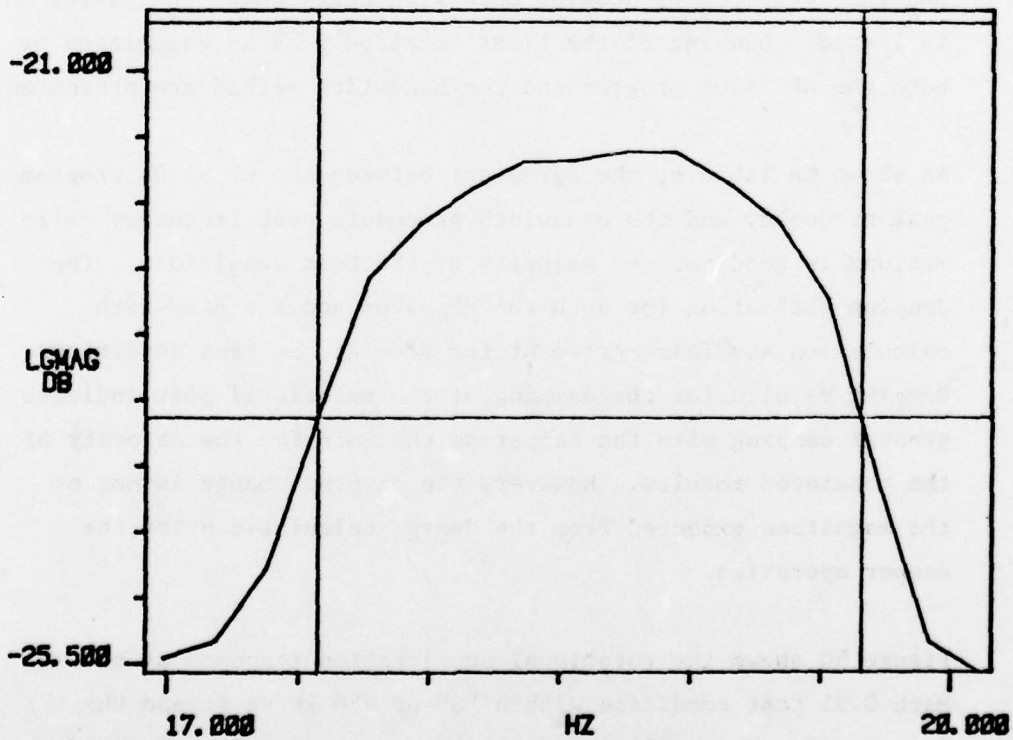


FIGURE 53 Expanded Acceleration Amplitude Response - First Rotation
 Peak - Mach 0.95 and $q = 650$ lb/sq ft with Damper On

Figure 48 shows the response curve obtained at a "q" of 500 lb/sq ft and Mach 0.95 test condition with the damper turned off. Figure 49 is an expanded response curve of the first bending mode peak shown on Figure 48. Note that although the response curves on the expanded response curves of Figures 47 and 49 are not perfectly smooth, the curves do not exhibit large irregularities or dips. The changes of slopes that do occur on the curves correspond to the analyzer's frequency delta of .195 Hz.

Table 6 lists the results of analyzing the rotational mode response plots for the frequency of peaking and damping of the first rotation mode of the surface at Mach 0.95. The damping and the frequency of peaking both with and without the damper on is listed. Damping of the first rotation peak as calculated by both the HP 5420A program and the bandwidth method are presented.

As shown on Table 6, the agreement between the HP 5420A program peak frequency and the bandwidth procedure peak frequency estimations is good for the majority of the test conditions. The damping estimation for both the HP 5420A and the bandwidth calculation has fair agreement for some of the test conditions. Damping results for the damping of the rotational peak indicate greater damping with the damper on than off for the majority of the tabulated results. However, the damping change is not of the magnitude expected from the design calculations for the damper operation.

Figure 50 shows the rotational acceleration response at the Mach 0.95 test condition with a "q" of 650 lb/sq ft and the damper off. Figure 51 is an expanded response plot of the first rotational response peak of Figure 50. Figure 52 shows the rotational acceleration response at the same test conditions as for Figure 51 with the Damper on. Figure 53 is an expanded

response plot of the first rotational response peak of Figure 52. The response plots for the two conditions of damper on and off show little change due to the damper operation.

Since the test results of the damper module operation did not show the expected damping of the first rotational resonance peak, additional testing was performed with the damper module operation replaced with damping (leakage) tubes placed across the drive area of the test actuator. The testing used two different damping tubes, one with a damping flow rate approximately equal to the design damping flow rate characteristic of the damper module and the other with a damping flow rate approximately 5 times the design damping flow characteristic of the damper module. The damping module was designed on a bandpass response basis and did not exhibit a leakage path across the actuator drive area at very low or high frequencies. The damping tubes used created a damping flow across the actuator drive area which was essentially independent of load pressure frequency (over the frequency range of interest).

6.5.4 Mach 0.95 Damping Tube Results

Table 7 shows the results of analyzing the bending acceleration response characteristics of the operation of the small and large damping tubes across the stabilator control actuator. The estimated frequency of peaking by the HP 5420A program agreed with the bandpass estimation method results quite closely. The damping estimation by the same two methods did not agree for many of the test conditions, due probably to the observed irregularities in the response peak curves. Figure 54 is the response plot measured for the Mach 0.95 test condition with a "q" of 550 lb/sq ft with the large damping tube. Figure 55 is an expanded plot of the first bending mode peak shown on Figure 54. Note that 160 averages were used in obtaining the plot. The irregularity of the peak as shown on both Figures 54 and 55 is typical of the response plots obtained for the bending accelerometer response

TABLE 7

Mach 0.95 Wind Tunnel Test Results

Bending Mode

Test Condition		Resonant Frequency & Damping Estimation			
"q" (lb/sq ft)	Damper Tube	HP5420A Program		Bandwidth Calculation	
		Freq. Peak (Hz)	Damping (% Critical)	Peak Freq. (Hz)	Damping (% Critical)
200	Small	10.27	2.13	10.30	5.84
	Large	10.65	3.72	10.40	2.55
300	Small	10.27	5.47	10.60	7.52
	Large	10.85	0.10	10.85	1.84
400	Small	10.58	6.33	10.80	5.07
	Large	11.02	4.18	10.80	5.07
500	Small	10.87	4.36	10.80	4.02
	Large	10.94	6.23	11.00	9.41
550	Small	11.20	5.46	11.35	9.36
	Large	11.14	4.70	11.00	6.51
600	Small	11.06	6.26	11.00	6.96
	Large	11.70	3.67	11.70	6.78
650	Small	11.50	4.34	11.70	10.85
	Large	11.32	3.77	11.10	8.67

TRACE A	TRANS	PEAK VALUE	11.0578 E+0
UNITS X-HZ	Y-LGMAG DB	XDAMPING	5.08745 E+0
SIG TYPE 1			
#AVERAGES	160		
START HZ	0.0 E+0		
DELTA HZ	125.000 E-3		

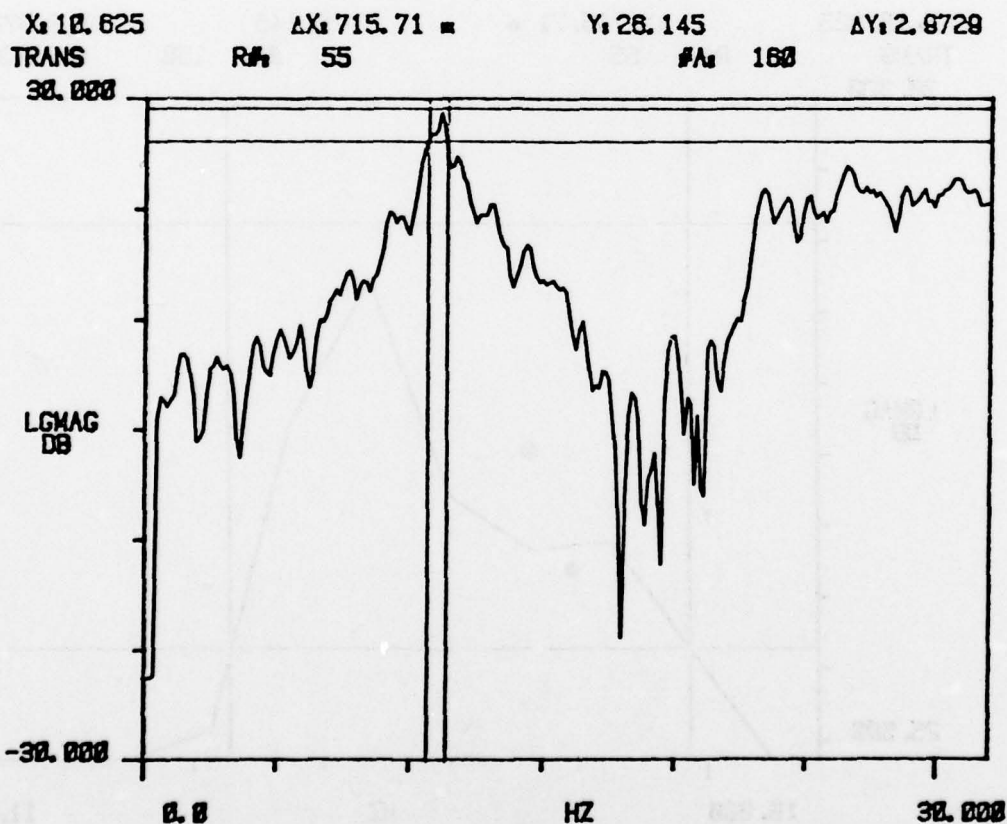


FIGURE 54 Bending Accelerometer Amplitude Response - Mach 0.95 and $q = 550$ lb/sq ft with Large Damping Tube

X: 10.625 ΔX: 715.71 Y: 28.145 ΔY: 2.8728
 TRANS Rf: 55 #A: 160 EXPAND
 30.000

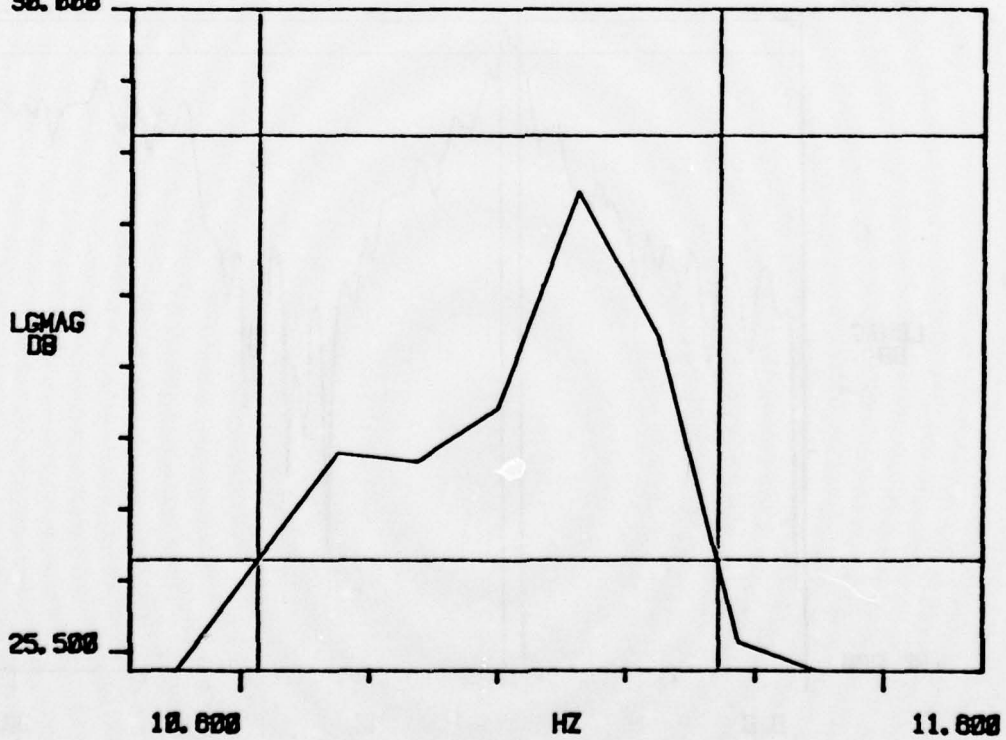


FIGURE 55 Expanded Acceleration Amplitude Response, Full Bending Peak -
 Mach 0.95 and $q = 550$ lb/sq ft with Large Damping Tube

measurements with the damping tubes. Figure 56 shows the response plot of the bending acceleration with the small damping tube at the Mach 0.95 test condition with a "q" of 550. Figure 57 shows the expanded response plot of the first bending peak as shown on Figure 56. Note that although 200 averages were used in obtaining the response data, the first bending peak shown on Figures 56 and 57 still exhibits an irregularity in the curve analyzed for the frequency peak and the damping. As expected from the design of the test item, the damping tubes did not affect the damping of the first bending resonance peak. The damping estimated for the resonance is similar to that previously estimated for the mode with the damper module used in its two operational modes.

Table 8 shows the results of analyzing the rotational acceleration response characteristics for the large and small tube restrictions across the stabilator control actuator. The damping indicated by the HP 5420A did not agree closely with that estimated using a bandpass calculation. The peak frequency indicated did agree with the bandpass estimated results for many of the test conditions. The damping with either damping tubes across the test actuator did not increase from that previously obtained with the damper module in operation.

Figure 58 shows the response for the rotational accelerometer at the Mach 0.95 test condition with a "q" of 550 lb/sq ft and the small damping tube installed across the test actuator. Figure 59 is an expanded plot of the first rotational peak shown in Figure 58. Note that although 200 data averages were used, the resonance peak shows significant irregularities. Figure 60 shows the response for the rotational accelerometer at Mach 0.95 test condition with a "q" of 550 lb/sq ft and the large damping tube installed across the test actuator. Figure 61 is an expanded plot of the first rotational peak shown in Figure 59.

TABLE 8

Mach 0.95 Wind Tunnel Test Results

Rotation Mode

Test Condition		Resonant Frequency & Damping Estimation			
"q" (lb/sq ft)	Damper Tube	HP5420A Program		Bandwidth Calculation	
		Freq. Peak (Hz)	Damping (% Critical)	Peak Freq. (Hz)	Damping (% Critical)
200	Small	17.88	9.27	18.00	13.38
	Large	17.89	4.23	17.80	11.23
300	Small	17.37	11.15	18.50	6.71
	Large	18.06	7.83	18.30	10.13
400	Small	18.07	6.97	18.40	9.34
	Large	18.40	4.77	18.40	9.69
500	Small	18.89	5.10	18.50	13.19
	Large	18.21	5.87	18.60	5.19
550	Small	18.34	5.37	18.00	11.11
	Large	18.44	6.21	18.40	9.16
600	Small	18.05	7.39	18.50	6.37
	Large	18.23	8.13	18.20	8.16
650	Small	16.65	-12.17	18.40	6.75
	Large	17.79	3.93	18.45	2.95

TRACE A	TRANS	PEAK VALUE	11.1981 E+0
UNITS X-HZ	Y-LGMAG DB	XDAMPING	5.48883 E+0
SIG TYPE 1			
#AVERAGES	200		
START HZ	0.0 E+0		
DELTA HZ	125.000 E-3		

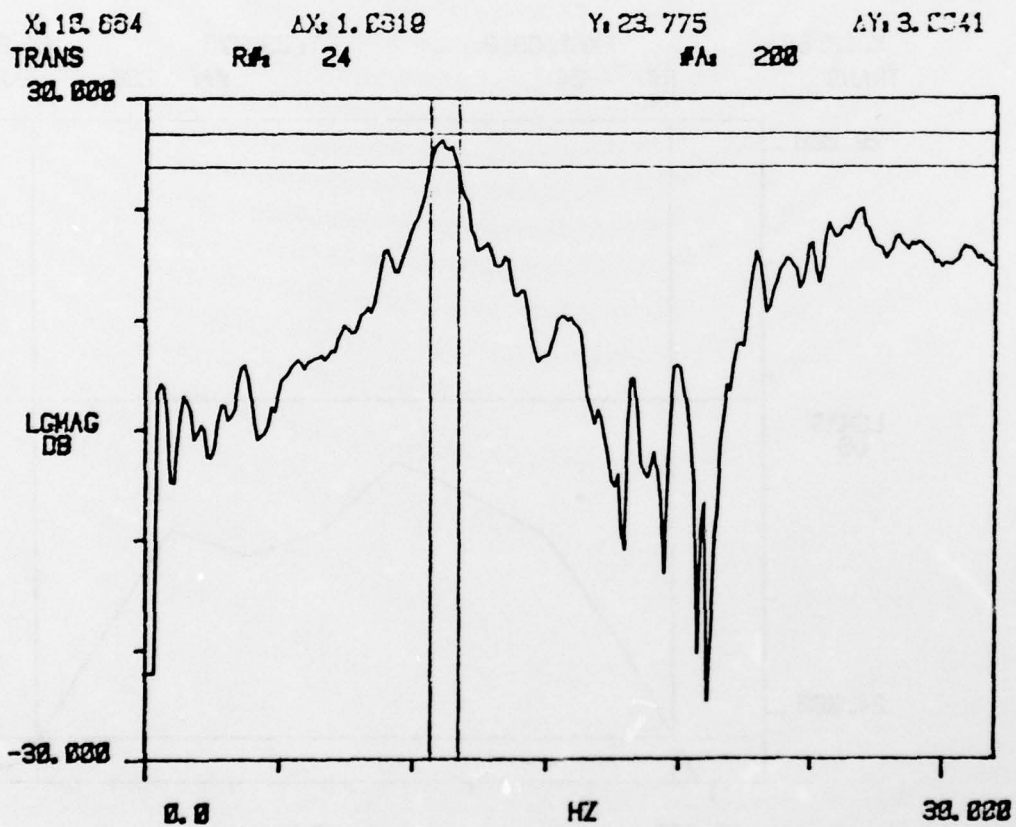


FIGURE 56 Bending Acceleration Amplitude Response - Mach 0.95 and $q = 550$ lb/sq ft with Small Damping Tube

X: 10.684
TRANS

ΔX : 1.0319
R/A: 24

Y: 23.775
#A: 200

ΔY : 3.0041
EXPAND

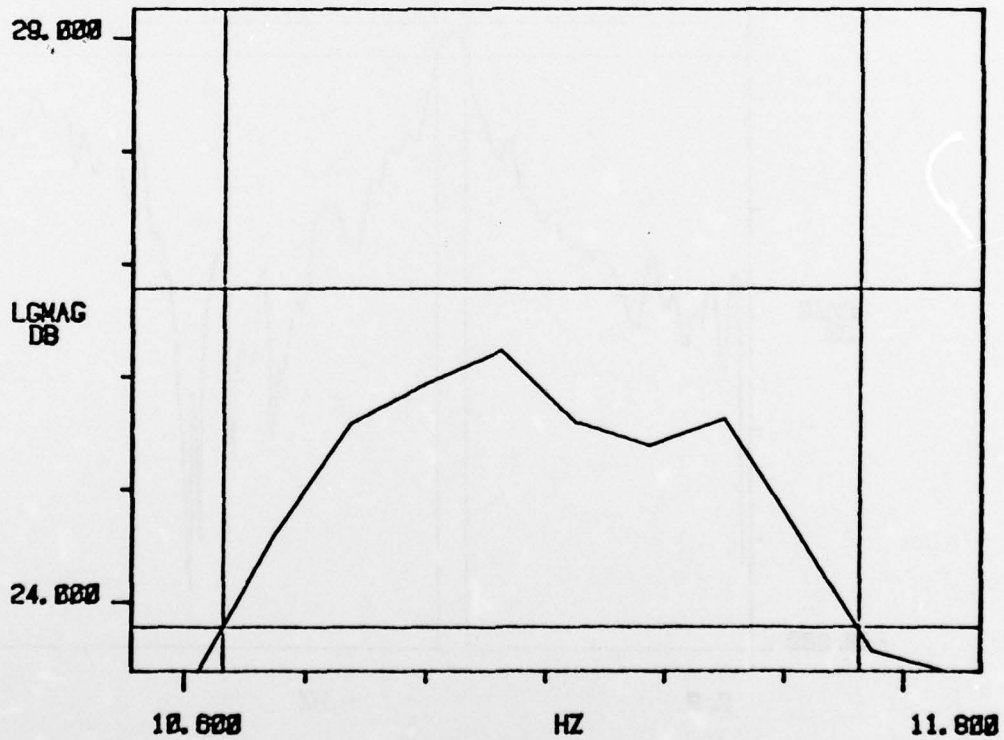


FIGURE 57 Expanded Acceleration Amplitude Response, Full Bending Peak - Mach 0.95 and $q = 550$ lb/sq ft with Small Damping Tube

TRACE A	TRANS	PEAK VALUE	18.3079 E+0
UNITS X-HZ	Y-LGMAG DB	XDAMPING	5.18631 E+0
SIG TYPE 1			
#AVERAGES	200		
START HZ	0.0 E+0		
DELTA HZ	125.000 E-3		

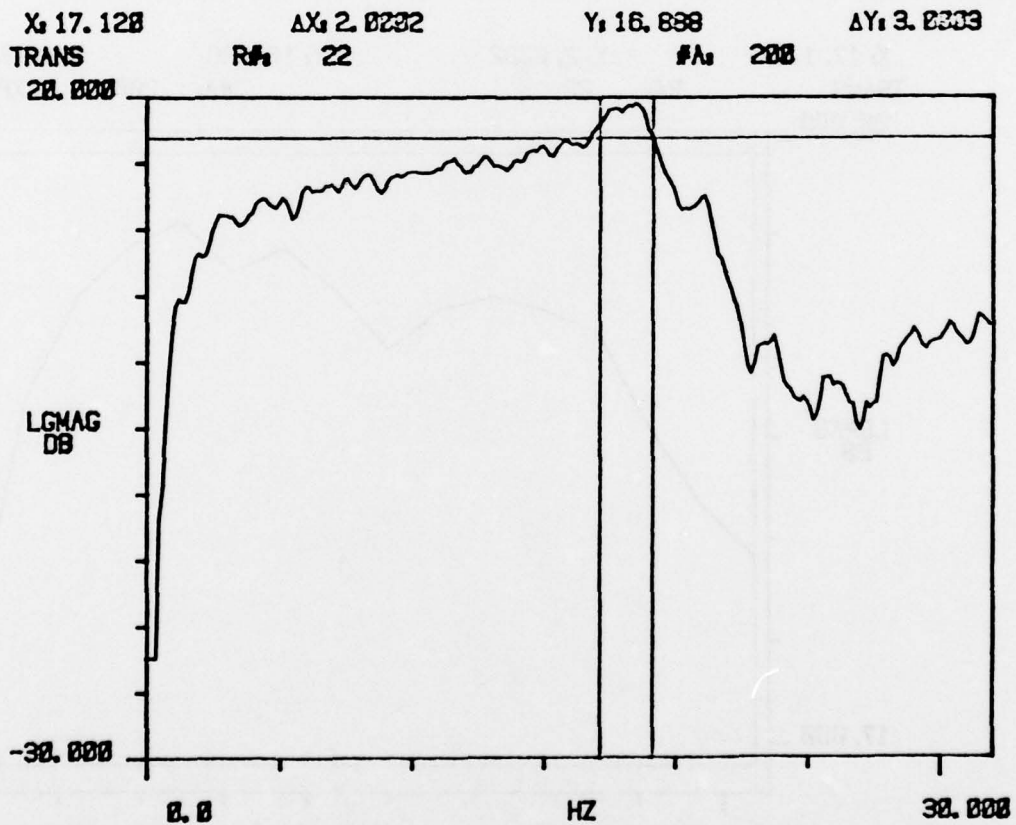


FIGURE 58 Rotational Accelerometer Amplitude Response - Mach 0.95 and $q = 550 \text{ lb/sq ft}$ with Small Damping Tube

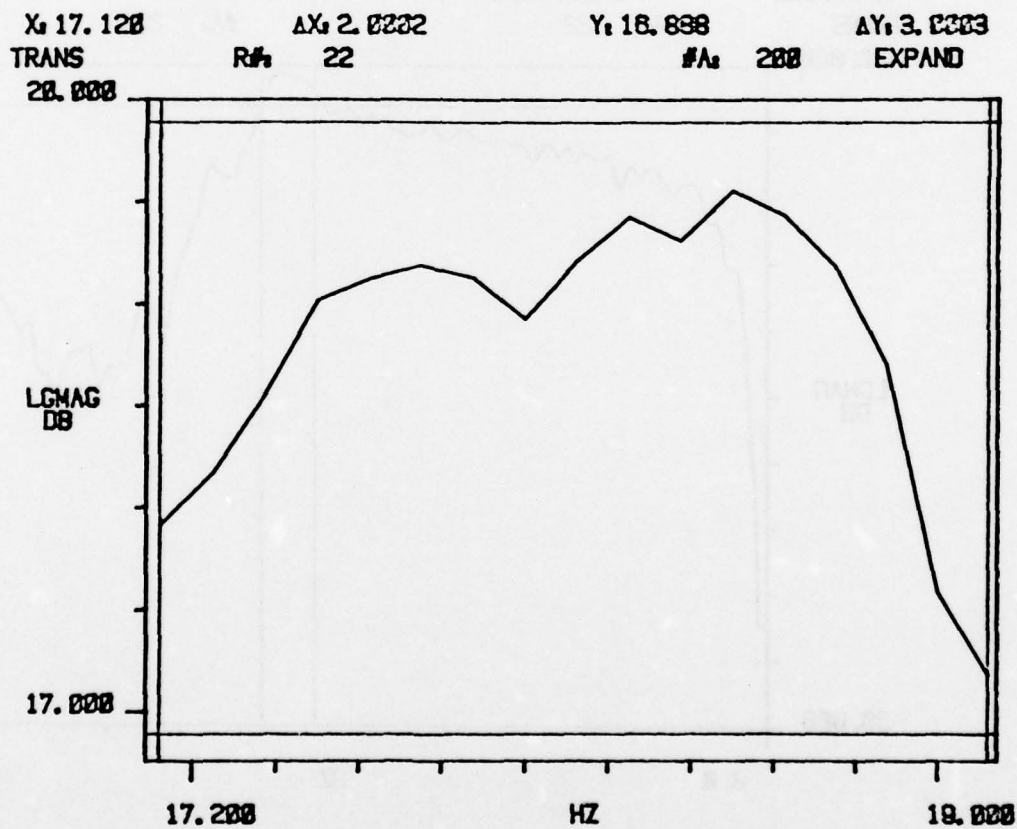


FIGURE 59 Expanded Acceleration Amplitude Response, Full Rotational Peak -
 Mach 0.95 and $q = 550$ lb/sq ft with Small Damping Tube

TRACE A	TRANS	PEAK VALUE	18.2438 E+0
UNITS X-HZ	Y-LGMAG DB	XDAMPING	5.74988 E+0
SIG TYPE 1			
#AVERAGES	68		
START HZ	0.0 E+0		
DELTA HZ	125.000 E-3		

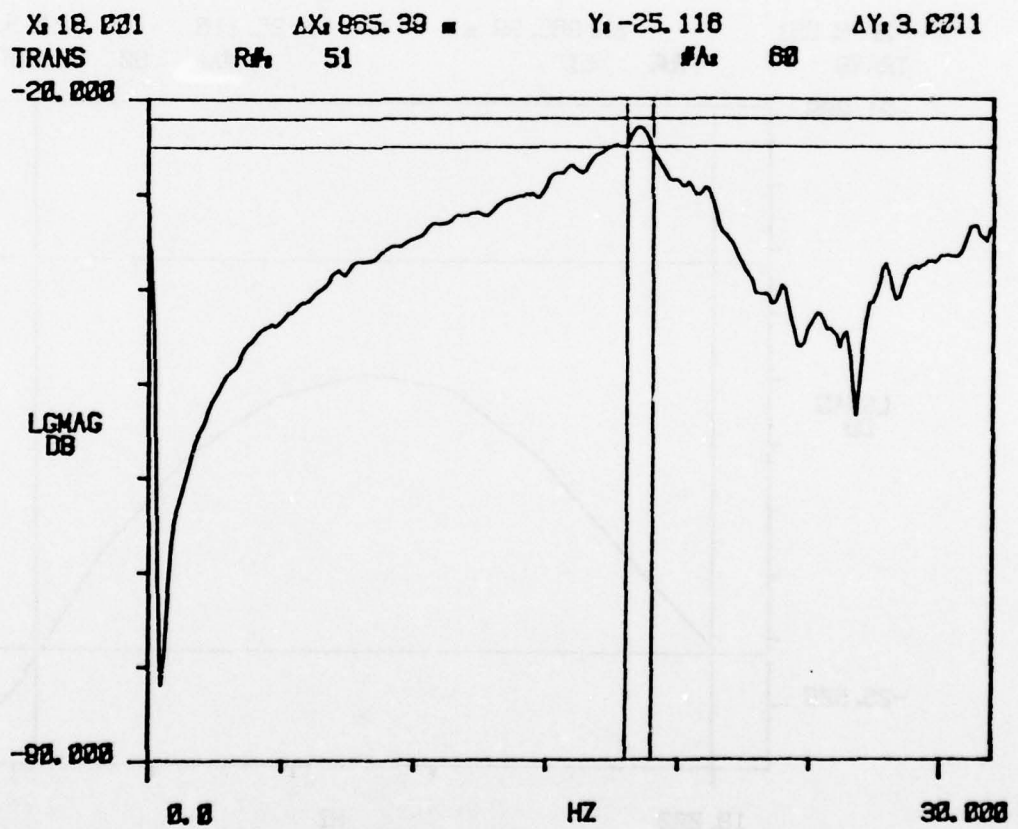


FIGURE 60 Rotational Acceleration Amplitude Response - Mach 0.95 and $q = 550$ lb/sq ft with Large Damping Tube

X: 18.031 ΔX: 965.39 Y: -25.116 ΔY: 3.0311
 TRANS R#: 51 #A: 68 EXPAND

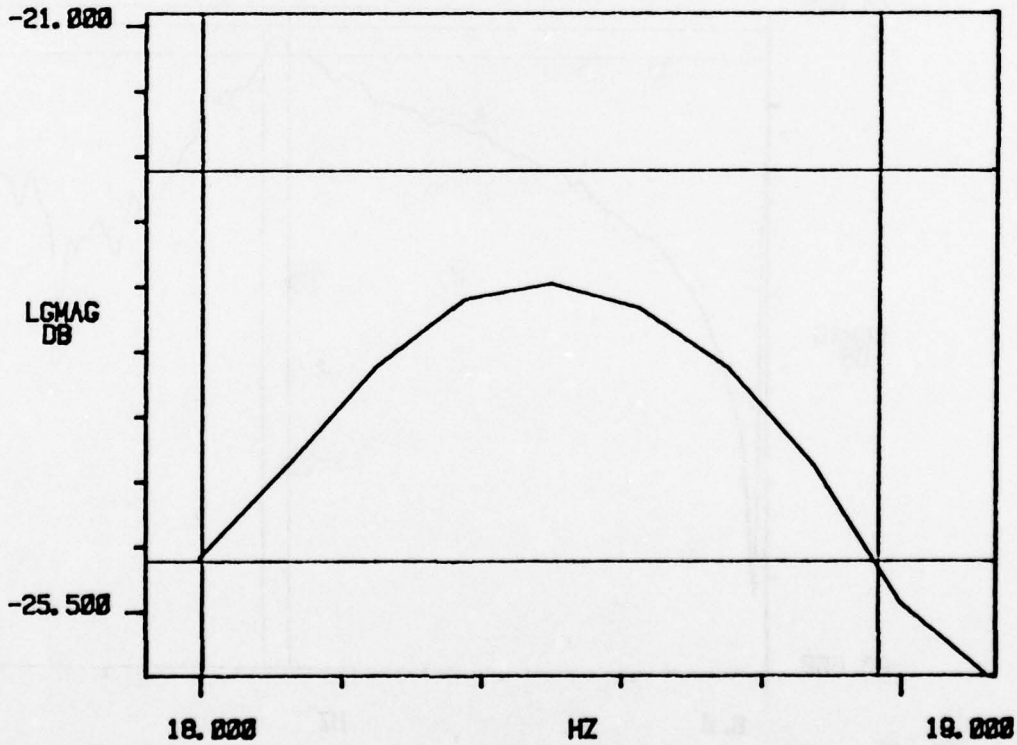


FIGURE 61 Expanded Acceleration Amplitude Response, Full Rotational Peak - Mach 0.95 and $q = 550$ lb/sq ft with Large Damping Tube

Note that the response measurements for the tests performed with the damping tubes that the bandwidth used for the analyzer measurements was reduced to 32 Hz (as compared to the 50 Hz bandwidth used with the previous wind tunnel tests). This was done in order to reduce the frequency delta used by the analyzer to produce the response plots (in an attempt to reduce the irregularities in the response peak curves). The effect on the curve irregularity (as demonstrated by Figures 58 and 59) was not significant.

7. CONCLUSIONS AND RECOMMENDATIONS

Based upon the laboratory testing, the damping module tested in the wind tunnel operated as designed in terms of the frequency response and damping flow gain characteristics. The laboratory testing did indicate that the threshold characteristics of the module were somewhat higher than desirable for optimum performance.

The analyzer allowed evaluating the response characteristics of the stabilator surface satisfactorily. The damping change expected from the design calculations was large enough that the inconsistencies in the damping estimation (based on the measured response curves using the HP 5420A and bandwidth estimates) did not impair the performance evaluation.

The results of the operational testing in the wind tunnel indicated that the operation of the damping module was not effective in damping the rotational mode of the stabilator surface. The result was not due to an incorrectly operating module, since using a leakage tube across the control actuator in place of the damper module gave essentially the same results in terms of the rotational mode damping. Since the rotational mode of the stabilator showed no change in damping, with the damper module operation, it is concluded that the flutter suppression technique would not be effective as tested. However, since the technique of using negative pressure feedback to damp mechanical resonances has been successfully applied elsewhere, (for example, the S-IC engine position control system), the test results present an anomaly. The test results are also inconsistent with the fact that the F-4 stabilator actuator is oversized (having a force capability of 36,000 lb compared to the maneuvering force requirement of 8,600 lb) in order to increase its stiffness and hence the rotational resonance frequency.

Therefore, there appears to be an anomaly which should be investigated somewhat further before the rotational resonance damping technique is labeled as being unsatisfactory for slab type surface flutter mode damping. In order for the technique to be theoretically applied, the surface must move as a rigid body in rotation and the control actuator must be the principle stiffness element for the rotational stiffness of the actuator and surface assembly. The F-4 stabilator, based upon other reports and testing, appears to meet this criteria. However, the indication from the wind tunnel tests performed on test item under this contract indicated that the rotational mode is decoupled from the control actuator at the first resonance peak. Therefore, it is recommended that further testing of the stabilator and actuator be conducted to establish the motional characteristics of the test item. This testing should be directed at verifying or disproving that the test item meets the actuator stiffness and rigid body criteria.

SECTION III

FLIGHTWORTHINESS TESTING DIRECT-DRIVE ACTUATOR

1. INTRODUCTION

The testing conducted under the contract effort was flight worthiness testing of hardware based on a direct drive Fly-By-Wire demonstration unit developed under Air Force Contract F33615-75-C-3068 and described in detail in AFFDL-TR-91. The following is a brief summary of the mechanization.

Figure 62 shows the direct drive control system in block diagram form. The control system is a fail-operate configuration where a first failure (hydraulic or electric) still allows the control system to operate with a satisfactory level of performance. The system is based on using two self-monitored control channels and a two section electrohydraulic control actuator. The control actuator uses two high force capability servovalve drivers directly connected to a tandem power spool. In the normal operating mode, both self-monitored control channels operate, commanding the two direct drive valve drivers. The valve drivers are a moving coil design. Either control channel with its moving coil driver has sufficient force capability to drive the tandem power spool to maximum stroke. The two self-monitored control channels are completely independent and are brought together only at the tandem power spool.

For the control system to meet the "fail-operate" criteria, hardover failures in either control channel must be prevented. Hardover failures in the command and feedback paths of each control channel are detected and removed. This is accomplished using monitor feedback and command elements and comparing the

outputs of the control channel with the monitor elements. For example, on Figure 62, command input 2 and feedback 2 are used as the monitor for command input 1 and feedback 1. The comparison is made after the summing junction at the control loop error point. Disagreement between the command and monitor portions of each control channel cause the command portion to be disconnected from control. The effect of hardover failures of the servo amplifiers driving the force motors are eliminated by using two amplifiers and two separate coils for the direct drive valve driver. The servo amplifiers are cross-strapped in their feedback paths so that failures of one amplifier-coil section are offset by the output of the other section.

In order for the system shown on Figure 62 to withstand single electrical or hydraulic failures, four independent electrical supplies and two hydraulic supplies are used.

In addition to the components shown on Figure 62 and for the purpose of preflight checkout and inflight display, a pilot's control system monitor module is required. During flight, notification of a channel failure for each of the self-monitoring control channels is displayed to the pilot. Upon disagreement between the monitor and the control portions of each control channel, a comparator both disconnects the control channel from the servovalve driving amplifiers and causes a failure warning light on the monitor to illuminate. Preflight checkout of the control system is provided by using the monitor module to inject test signals into the control channels to check the channel comparators and servoamplifier cross-strap connection. The servoamplifiers are connected to "LED" display lights to indicate current polarity and level so that a preflight inspection can verify correct operation.

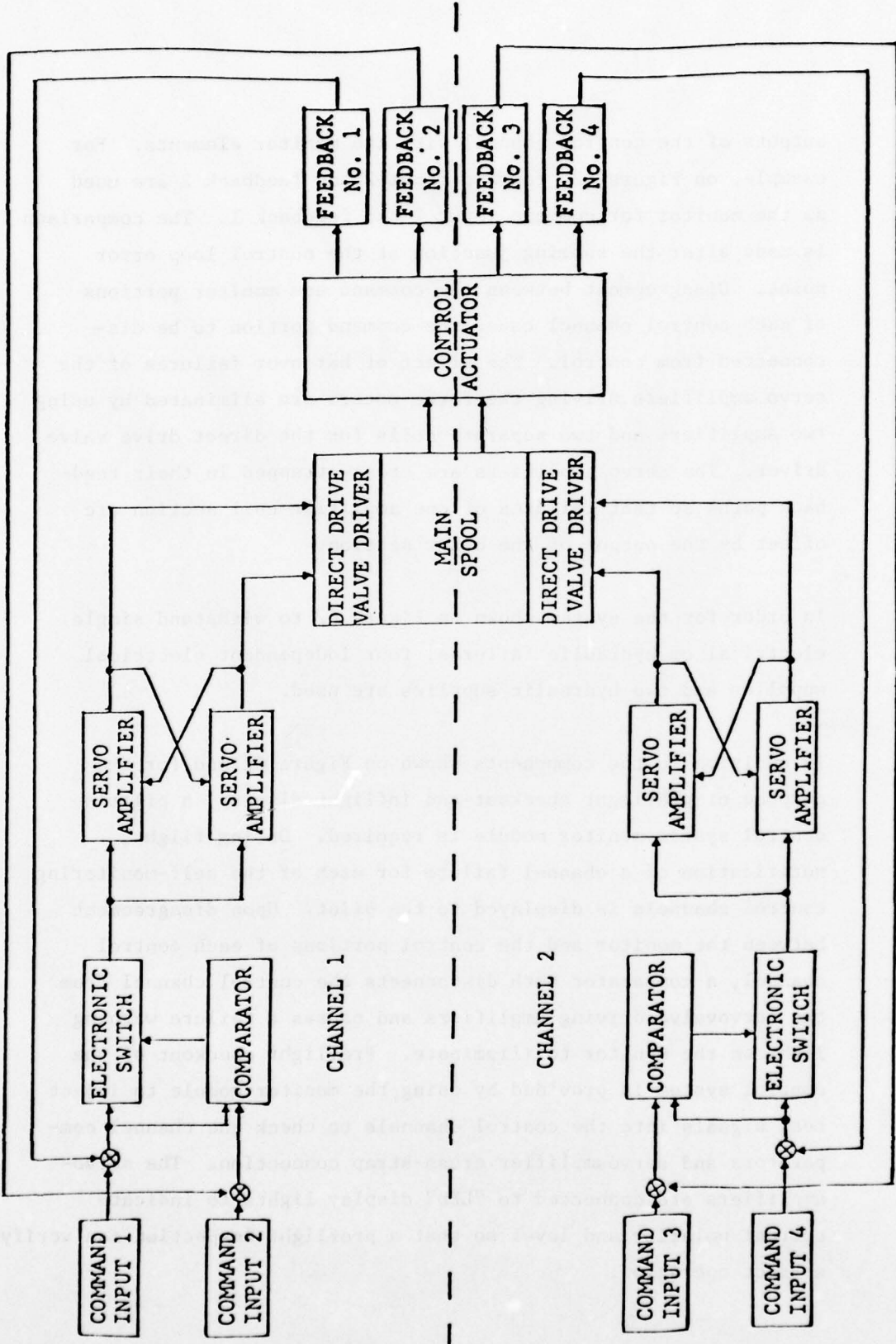


FIGURE 62 DIRECT DRIVE "FAIL-OPERATE" CONTROL SYSTEM

Figure 63 shows the direct drive aileron actuator fabricated for the F-4 flight test installation. Note that the direct drive valve is mounted to an adapter manifold between the valve and the normal F-4 aileron actuator. The actuator shown is designed for mounting in the left wing of an F-4 actuator. The manifold was incorporated to shift and rotate the direct drive valve on the control actuator in order to accommodate the particular aircraft installation. The actuator differs from the demonstration hardware in two additional areas. The electrical connections to the valve are routed internally through the adapter manifold from the connectors mounted on the electrical connection box. The manifold incorporates "plug in" connectors for the connections to the force motor coils. These connectors are mounted on the interface between the force motors and the manifold. The second change is in the feedback position transducer mounting. A support bearing and rod were added to the transducer assembly in order to eliminate a potential resonance problem with the support arm connecting the transducers to the actuator.

One internal difference between the flight actuator design and the demonstration unit is the diameter and stroke of the flow control spool. The diameter of the flight test actuator spool is .625 inches while the demonstration spool diameter was .500 inches. In addition, the stroke of the flight test actuator spool is \pm .025 inches while the demonstration spool stroke was .014 inches. The porting areas of the flight actuator valve were also made unequal, in order to match the slew rate characteristics of the normal F-4 aileron actuator with a manual input. The port widths of the flight actuator valve were shaped to create flow gain characteristics which gave one flow gain slope for small inputs and a second flow gain slope for large inputs. This again was done to match the flow gain characteristics of a normal F-4 aileron actuator control valve.

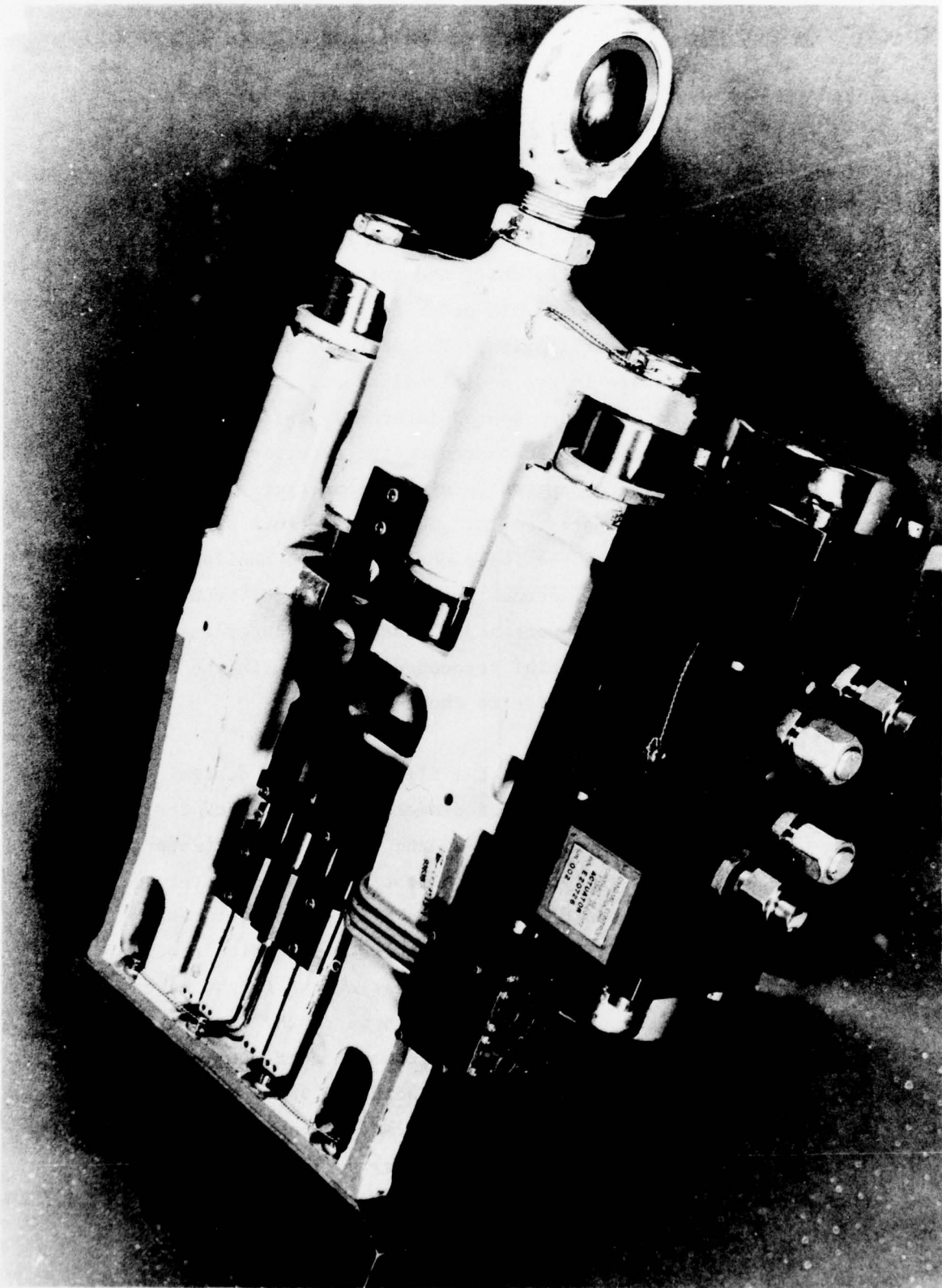


FIGURE 63 Direct Drive Aileron Flight Test Actuator

Figure 64 shows the electronic modules used for the flight test system. The electronic modules are essentially the same design as those used for the demonstration system with one exception. The exception is the display method for the servo amplifier drive currents for the force motors. The demonstration system used relays and electrical wires for driving the display lights on the pilot's monitor module. For the flight test system, the connection between the amplifiers and the pilot's system monitor was accomplished using fiber optic cables, transmitters and receivers. The fiber optic connection is the preferred method from a survivability aspect. "Off the shelf" fiber optic hardware was not available at the time the demonstration system was fabricated and at that time not used. Note that in addition to the electronic modules shown on Figure 64, four power supplies with an output voltage of ± 18 volts are required for the control system operation.

2. FLIGHTWORTHINESS TEST PROCEDURE

The flightworthiness testing of the flight hardware consisted of evaluating one set of hardware in accordance with the requirements of MIL-STD-810C and a test procedure document written by Dynamic Controls, Inc. and approved by the Air Force for qualifying the control system. The test procedure in general involved initial operational testing of the control system in order to establish acceptability of the nominal performance. The system was then subjected to high temperature, low temperature, temperature/altitude and vibration and shock environmental testing. The environmental test conditions were selected for the specific aircraft and equipment locations. Appendix A is the flightworthiness test procedure including the nominal performance testing required. Appendix B is the test report for the shock test. The remaining environmental test results are presented in AFAS/RWF Report No. 7804-79 and are not included in this technical report.

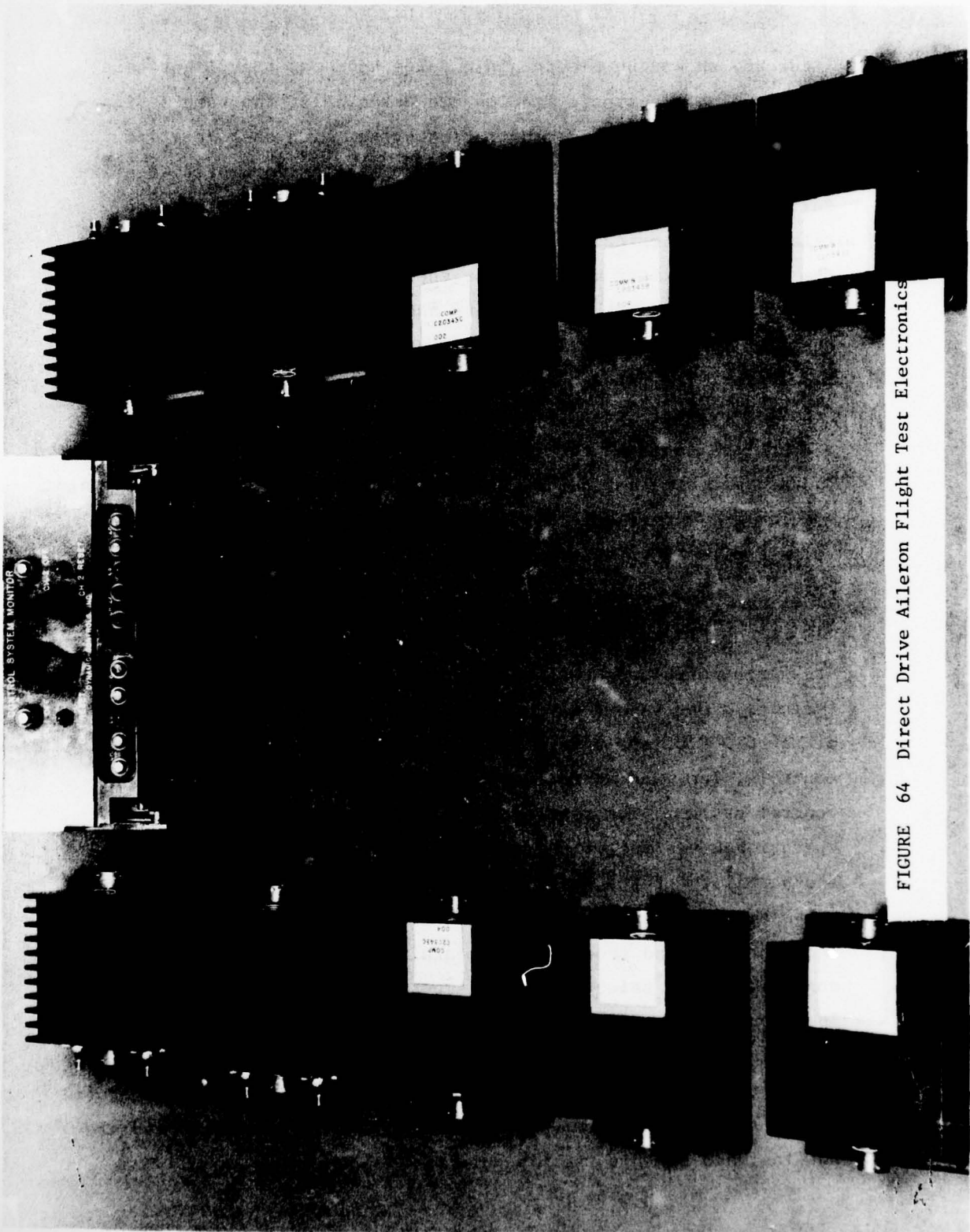


FIGURE 64 Direct Drive Aileron Flight Test Electronics

The environmental testing, with the exception of the shock tests, were conducted by the Air Force Avionics Laboratory, Dynamics and Environmental Evaluation Branch at Wright-Patterson AFB, Ohio. The shock testing was conducted by the Air Force Flight Dynamics Laboratory, Combined Environments Test Group, at Wright-Patterson AFB, Ohio. The "before" and "after" nominal performance testing was conducted by Dynamic Controls, Inc. personnel in the Actuation Laboratory, Bldg. 145, Wright-Patterson AFB, Ohio.

3. TEST RESULTS SUMMARY

The direct drive system which was subjected to the environmental testing completed the test sequence with two minor deficiencies revealed.

The first deficiency was the linearity deviation of the Bourne feedback potentiometers used for the actuator position feedback transducers. These were Bourne Model 184 plastic film potentiometers which were rated for the temperature environment specified for the control actuator operation (-65°F to 250°F). However, linearity deviations of the potentiometers during the high temperature testing created a nuisance disconnect problem. Therefore, for the flight test hardware, a Beckman potentiometer qualified for the temperature environment and manufactured under part number 1471-29 has been used in place of the Bourne potentiometers. These Beckman potentiometers use a Cermet element and have been environmentally tested and passed for the same operating conditions as those for the actuator position application with the control system.

The second deficiency was revealed after the shock testing. The flex pivots used in the suspension of the force motor coils failed under shock loading. A larger (and stronger) flex pivot was incorporated into the suspension in addition to the mechanical stroke stops for the power spool motion. The valve and force motor assembly was then retested for the shock loading and passed with no difficulty

4. CONCLUSIONS AND RECOMMENDATIONS

The direct drive mechanization as tested and modified to correct deficiencies revealed by the environmental testing is deemed to meet the flightworthy requirements for testing in an F-4 aircraft.

Since the system is apparently operationally suited for flight test evaluation, recommendations concerning the test system will depend on the flight test results. Changes in the detail design to lower the weight and reduce the vulnerability and size are not relevant until satisfactory flight test results on the general system have been obtained.

SECTION IV

ANGULAR RATE SENSING ACTUATOR EVALUATION

1. INTRODUCTION

The rate sensing actuator evaluated under the contract effort was supplied by Dynamic Controls, Inc., Dayton, Ohio, to the Air Force Flight Dynamics Laboratory. The actuator was designed to perform the stability augmentation function when inserted in an aircraft flight control system.

The purpose of a stability augmentation system used with an aircraft control system is to increase the damping of the short period mode of aircraft motion in a control axis. The increased damping is accomplished by sensing the angular rate of motion of the aircraft about an axis and using the sensed rate as a negative feedback loop in the control system for that axis. The angular rate feedback is applied over a limited frequency range which is centered on the natural frequency for the control axis motion. The most common stability augmentation design uses a rate gyro to sense angular rate, an electrohydraulic actuator to convert an electrical signal to mechanical motion, and a set of electronics to condition the rate gyro signal and control the electrohydraulic actuator.

The actuator evaluated is designed to replace the normal stability augmentation system, including the rate gyro and the associated control electronics for the system. The actuator evaluated requires only hydraulic power for the augmentation function. The mechanization consists of an inertial reference, an eddy-current coupler, and a hydraulic actuator controlled by a flapper-nozzle hydraulic control stage. The inertial reference incorporates permanent magnets mounted on a support disc which is pivoted with instrument bearings

at its geometric center. The magnets are the principal mass of the inertial reference. The eddy-current coupler consists of a conductive ring mounted so it passes through the air gap of the inertial reference magnets. The coupler is mounted on a torsion tube which restrains its rotation. The rate of angular displacement of the inertial reference relative to the coupler ring creates a torque on the ring which is used as an input to the hydraulic actuator. An input torque to the actuator causes a deflection of the flapper of the flapper-nozzle control stage which modulates flow to the actuator piston. Deflection of the flapper causes the actuator to move until feedback from the actuator piston creates an opposing torque on the flapper support rod sufficient to center the flapper between the nozzles.

The actuator submitted for evaluation was designed as an alternative to the fluidic mechanizations for stability augmentation which have been used on several helicopters on a prototype or development basis. The mechanization has the advantage of requiring less hydraulic power and having less temperature sensitivity than the fluidic mechanizations. The general requirements to which the actuator was designed are the following:

1. Bandpass corner frequencies:

Lower	.06 Hz
Upper	1.0 Hz

2. Minimum Phase angle at the lower break frequency $+30^{\circ}$

3. Maximum Phase angle at the upper break frequency -90°

- | | |
|----------------------------------|---|
| 4. Maximum rate input | 40°/sec |
| 5. Maximum variation of response | +20%
(-40° to 275°
fluid temperature) |

These performance parameters were selected as representative of a typical yaw axis stability augmentation system requirements, such as a Boeing 707 or a UH-1B helicopter. The exact bandpass required for an individual aircraft will vary slightly, principally in the upper break frequency selection. The lower break frequency is determined by a general requirement for non-interference with pilot inputs at frequencies below .1 Hz. The stroke of the actuator output was designed to be $\pm .400$ inches. The actuator drive area was established at $.675 \text{ in}^2$. The designed nominal gain of the mechanization was established at .01 inches/(degree/sec).

The .01 inches/(degree/sec) at the bandpass center frequency coincides with a UH-1B yaw axis fluidic augmentation system gain at 60°F fluid temperature.

The operating supply pressure for the evaluation actuator is 3000 psi. The hydraulic fluid used with the mechanization is MIL-H-5606.

The rate sensing actuator assembly as tested weighed 14.2 lbs filled with hydraulic oil. The sensor portion of the actuator weighed 4.1 lbs. The overall dimensions for the mechanization are 9.45 inches wide, 11.45 inches long and 5.85 inches high. Figures 65, 66 and 67 show the three views of the mechanization evaluated.

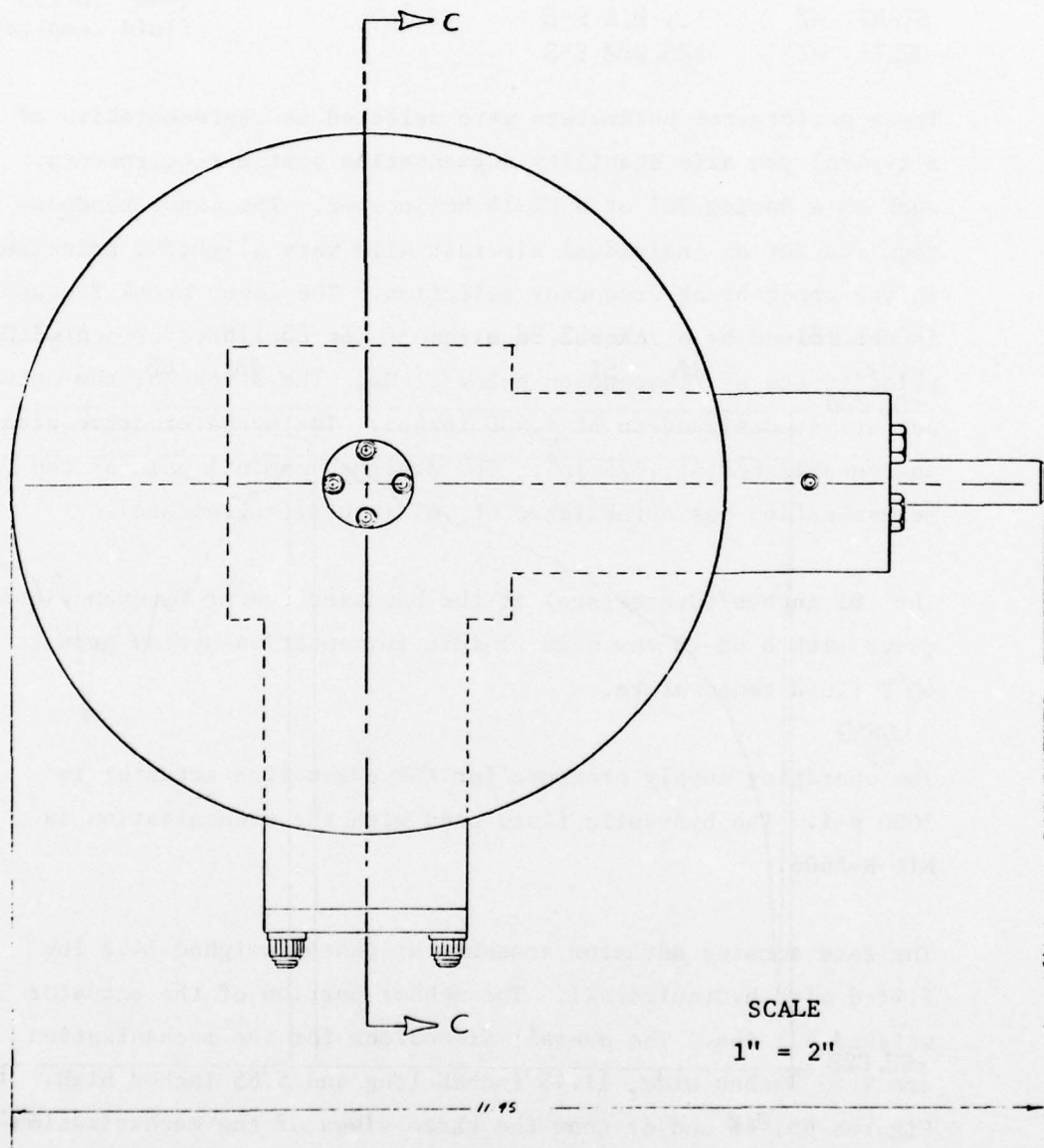
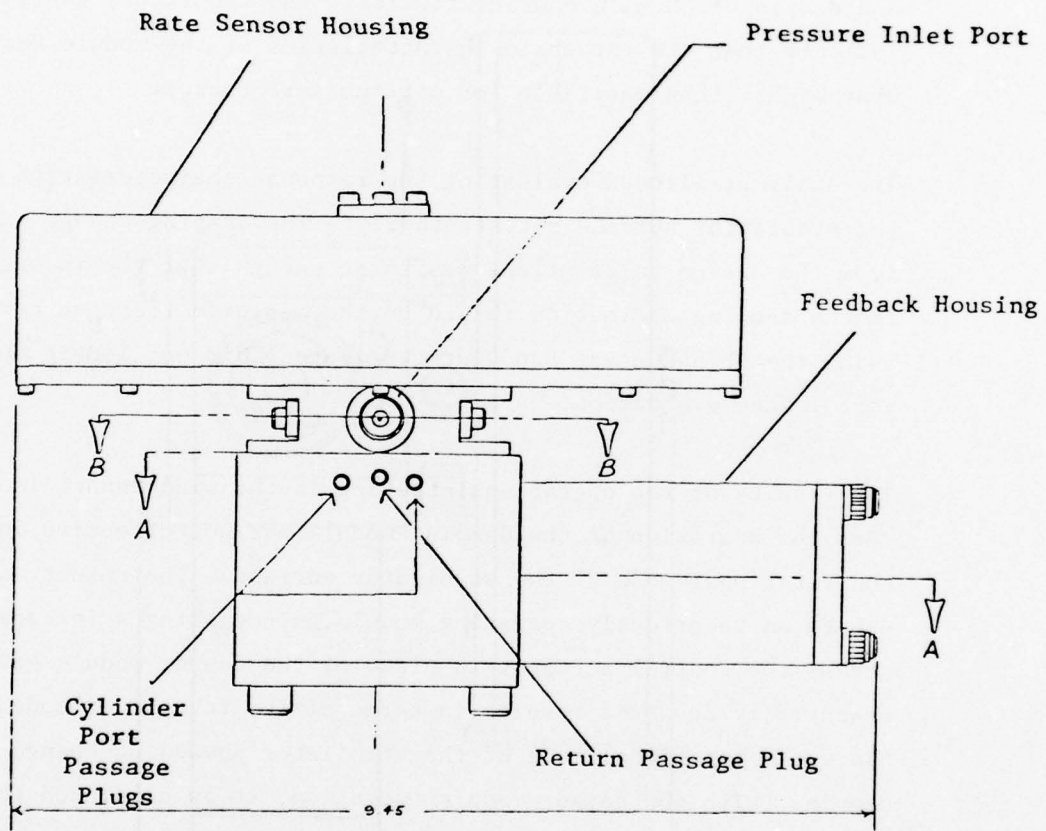


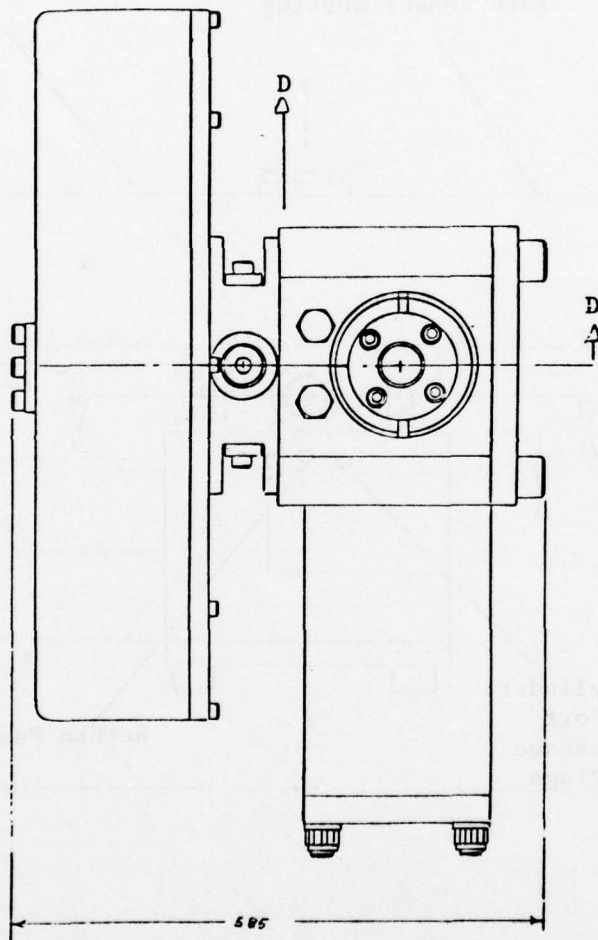
FIGURE 65

Rate Sensing Actuator Top View



SCALE
1" = 2"

FIGURE 66
Rate Sensing Actuator Rear View



SCALE

1" = 2"

FIGURE 67

Rate Sensor Actuator Front View

Figures 68 and 69 are sectioned assembly drawings of the internal construction of the augmentation mechanization. Note that as shown in Figure 66, a cartridge actuator assembly is used for the mechanization with laminar pressure drop piston rod seals incorporated into the cartridge.

2. EVALUATION TESTS

2.1 General

The object of the evaluation tests performed on the rate sensing actuator was to measure the performance characteristics of the mechanization for comparison with the predicted performance for the mechanization.

The tests performed were primarily frequency response, gain and threshold tests. Hydraulic power consumption was also measured. Included were low temperature operational tests with a fluid temperature of -40°F . The unit was operated with MIL-H-5606 hydraulic oil.

The majority of the performance tests were performed using an oscillating rate table constructed for the test series. An eight channel Brush recorder was used to record both the rate table motion and the actuator output motion. Frequency response data was reduced from the chart recorder records. The following subsections present the particular tests conducted and the results with a comparison to the design values.

2.2 Specific

2.2.1 Rate Coupler Torque and Linearity

As a test for the rate coupling torque from the eddy current rate coupler, the magnet assembly and coupling ring for the rate sensor were mounted in a lathe. The coupler ring was driven by the head stock of the lathe. The magnet assembly was mounted to allow the assembly to rotate on its support bearings and was engaged with the coupler ring. A force gauge and wire loop were used to restrain

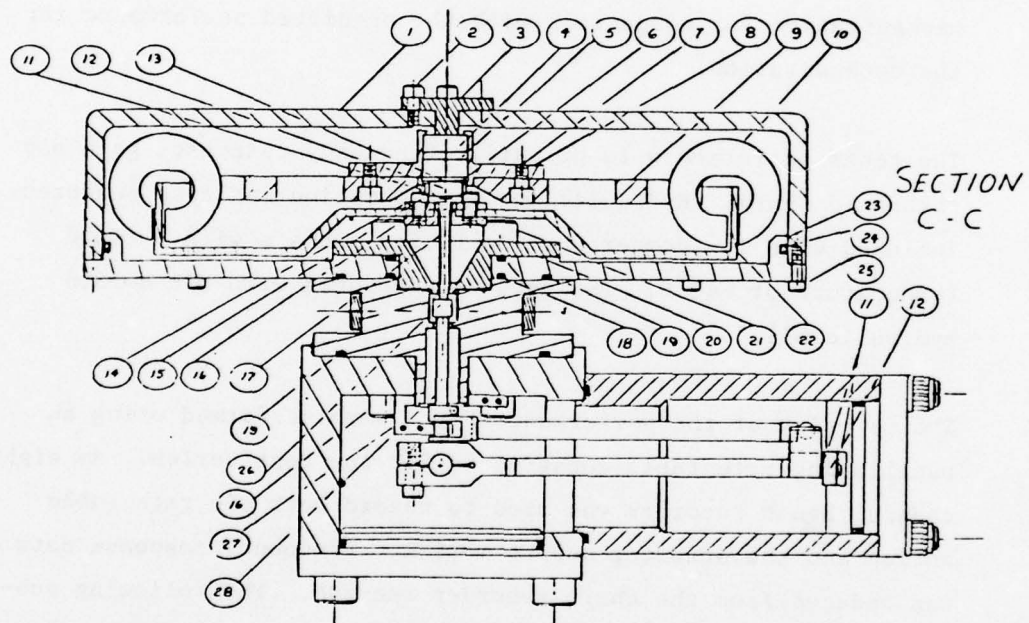


FIGURE 68
Section C Rate Sensing Actuator

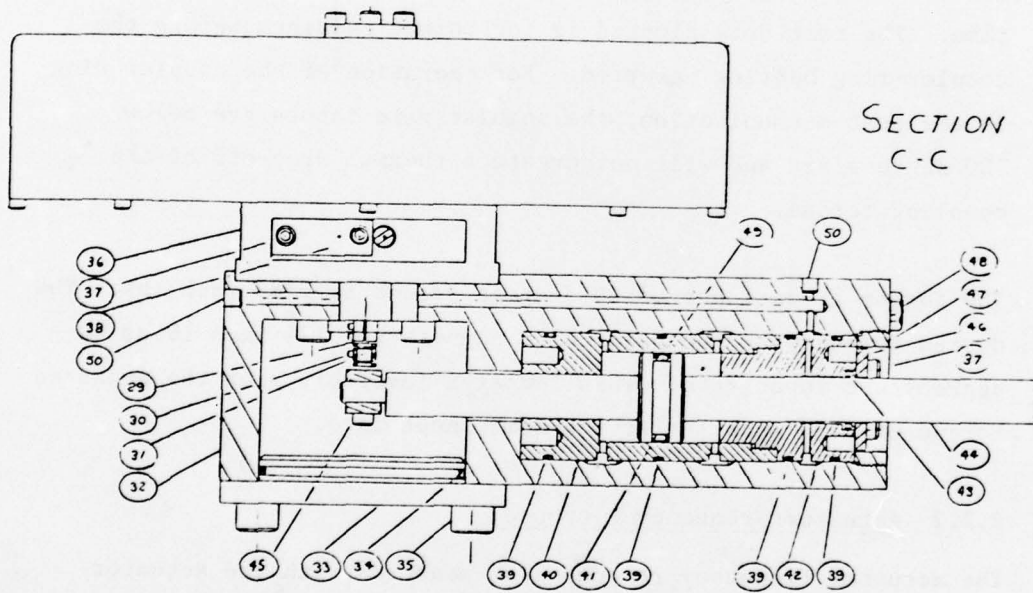


FIGURE 69
Section D Rate Sensing Actuator

the magnet ring from rotating with the coupling ring as the coupling ring was driven by the headstock. The lathe was operated at its five slowest available speeds (60, 120, 240, 315 and 480 RPM). Calibration of the force gauge was checked by using test weights and a precision balance and the recorded test readings for the coupler corrected for the force gauge error. Figure 70 is a plot of the test results. The coupler torque is quite linear with angular input rate. During the testing, a heating effect of the coupler ring was observed at the higher RPM conditions. At a given test point, this caused the output torque to drop off with time. The test data plotted is for torque readings before the coupler ring heating occurred. For operation of the coupler ring in the test mechanization, the angular rate inputs are below 100 degrees/sec and will not create a thermal drop-off of the coupling torque.

The torque at an input of 40 degrees/second is .189 inch lbs. The design torque with the particular magnets is .174 inch lb at 40 degrees/sec input rate. This compares favorably with the measured torque of .189 inch lbs at the same input rate.

2.2.2 Actuator Frequency Response

The actuator frequency response was measured with the actuator mounted on the rate table with the magnet assembly removed from its housing. The coupling ring was driven with a torque input by attaching a small arm to the edge of the coupling ring. The arm was then engaged with a small cantilever gram scale which was attached to the stationary frame of the rate table. The rate table was driven to apply a peak input torque of .1 in lb to the coupling ring. This input torque was large enough to be above the actuator threshold and less than the level which would cause flow saturation of the control stage. Figure 71 shows a sketch

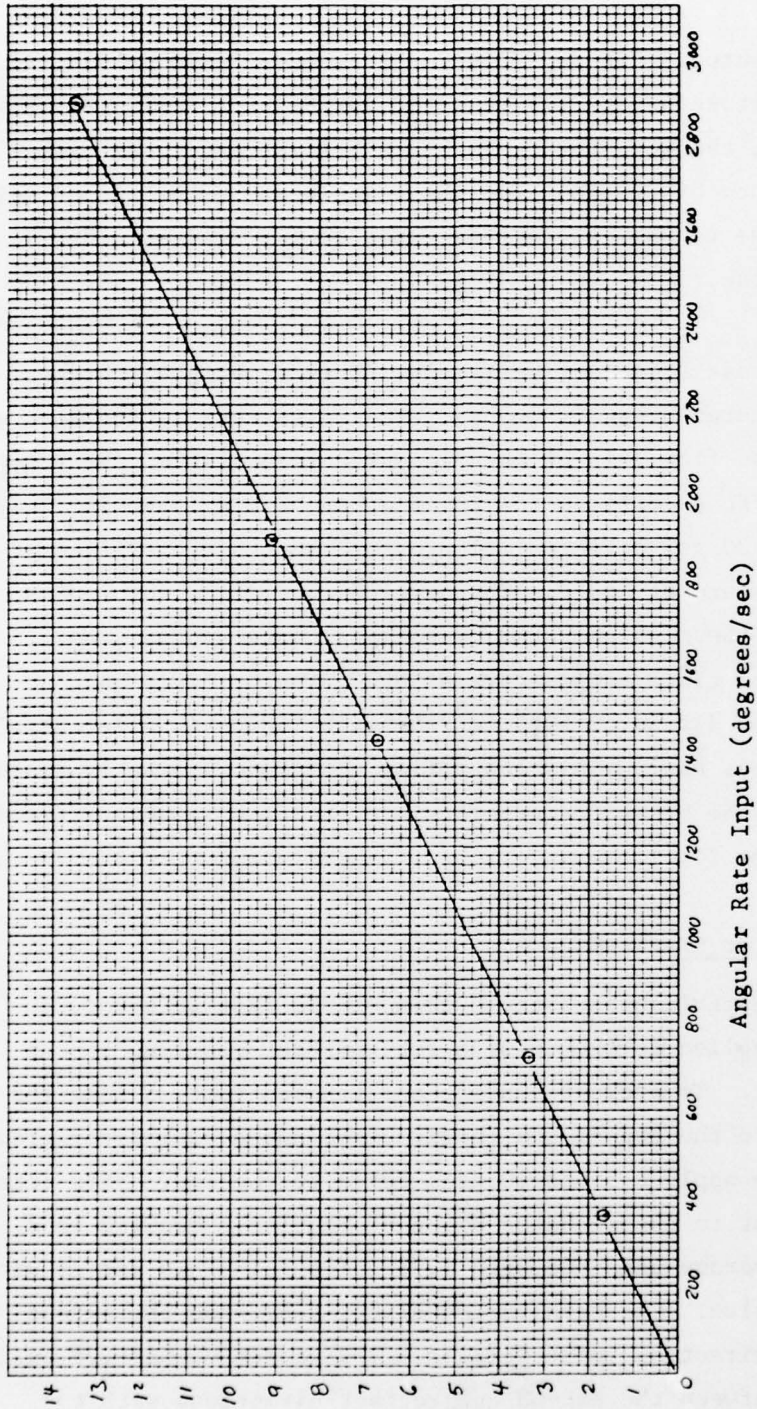


FIGURE 70
Eddy Current Coupler Torque Characteristics

T_c
(in lb)

of the test setup. Figure 72 is the frequency response plotted from the chart recorder data recorded during this test. As shown on Figure 72, the actuator response is a first order lag with a -3 db break frequency of .09 Hz. The phase angle at .09 Hz is -54 degrees which is close to the -45 degrees expected for a first order lag system response.

The design break frequency was .1 Hz. This is slightly higher than the measured break frequency. The difference is due to the lower measured flow gain of the flapper-nozzle stage. The rated flow for the feed orifices for the flapper-nozzle stage is .097 in³/sec at 1500 psi differential pressure across the orifice at a fluid temperature of 100°F. The orifices were flow checked as installed in the test actuator by using a beaker and a stop watch. At the fluid temperature of 80°F, the orifices had an average measured flow of 1084 in³/sec with 1500 psi differential pressure across them. This lower flow corresponds exactly to the reduction in the break frequency (since the flow gain is determined by the leakage flow).

2.2.3 Actuator Static Gain

In order to establish the static gain of the test actuator, a torque was applied to the torsion tube without the coupler cup mounted to it. To prevent bending the torsion tube, a long rod was clamped to the top of the torsion tube and a cantilever gram scale used to apply a 5 and 10 gram force to the rod. This created a torque input to the actuator without creating a bending load. The static average gain measured 1.31 in/in lb. This agrees with the design value. The gain varied slightly between the extend and retract direction input torques. The variation was .05 in/in lb difference between the extend and retract directions with the average being 1.31 in/in lb.

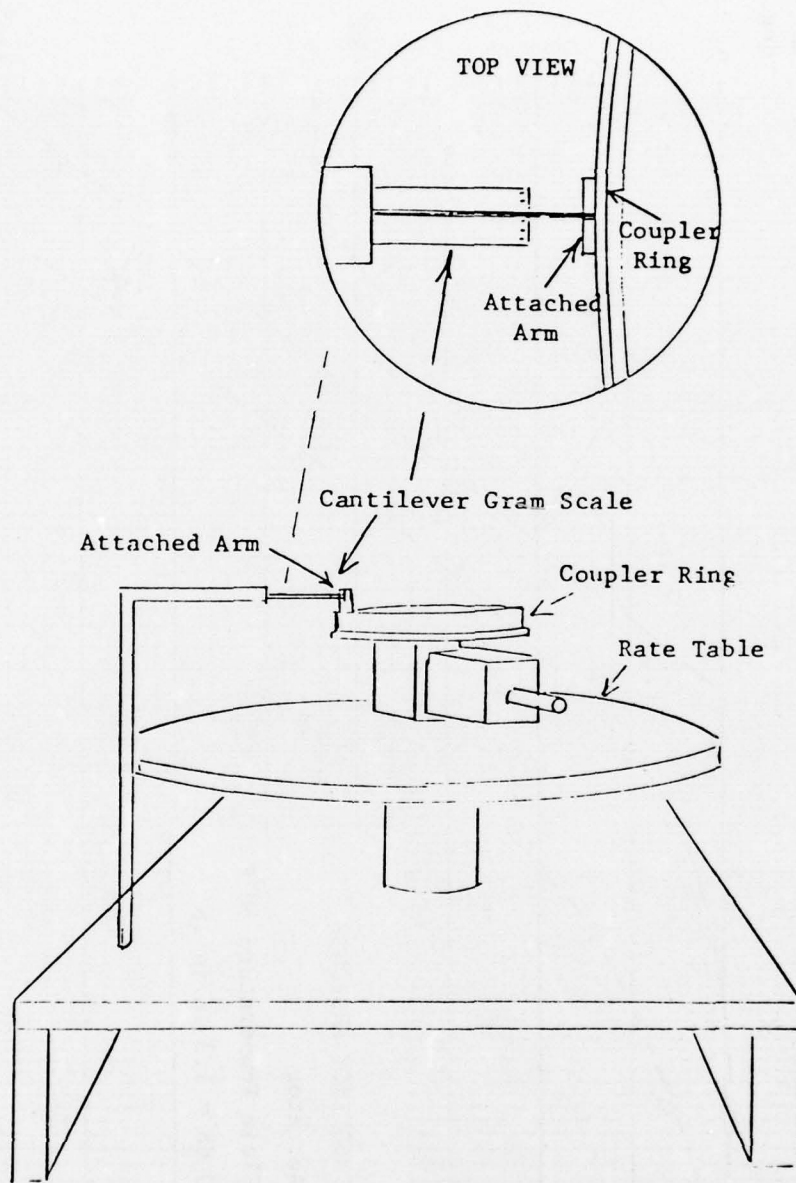


FIGURE 71
Actuator Response Test Setup

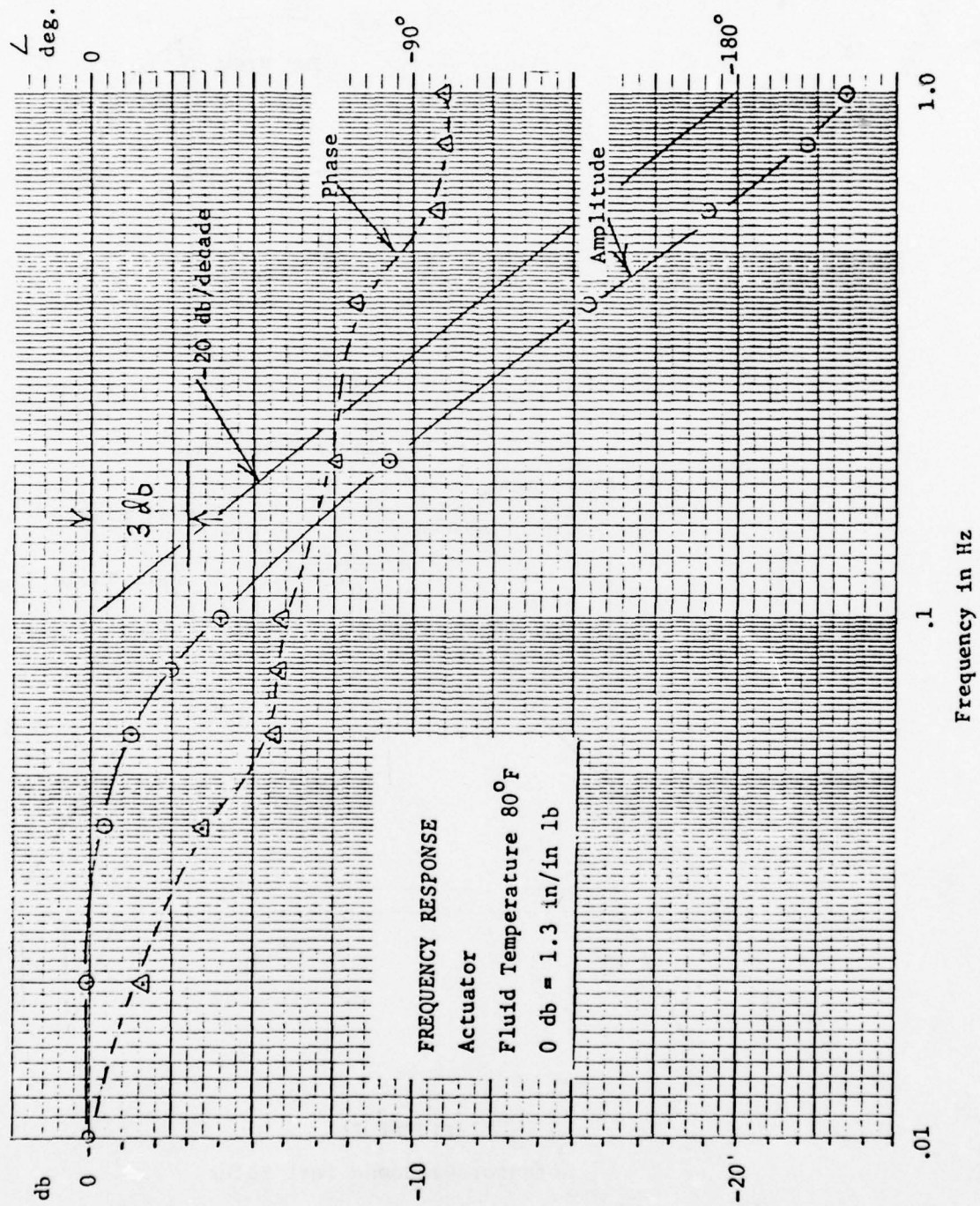


FIGURE 72
Actuator Frequency Response

2.2.4 Threshold Measurements

In order to measure the threshold of the mechanization, a sinusoidal input of gradually increasing amplitude was applied to the rate table while recording the output of the rate sensing actuator. The input level in degrees/sec at frequencies of .5 and 1 Hz which caused a measurable output from the rate sensing actuator was defined as the threshold at that test condition. This threshold was also measured at -22°F .

Figure 73 shows the rate-sensing actuator as mounted on the rate table. The pressure gauges attached to the end of the actuator are connected to the cylinder ports. A scale marked off in degrees is attached to the edge of the rate table and a pointer installed to provide visual reference for the table motion. As shown in Figure 73, the top of the cover for the inertial sensor has two access holes installed in it. This allows applying an input torque to the coupler ring for actuator response measurements. A position potentiometer is mounted next to the actuator and has one end attached to the actuator output rod. This is an infinite resolution film potentiometer with a rated linearity of .25% full scale.

Table 9 is a listing of the measured threshold at a particular test condition or with a particular configuration.

TABLE 9
Measured Threshold

Frequency (Hz)	Threshold (deg/sec)	Test Condition
.5	.071	80 ^o F fluid temp. magnet suspension
1.0	.0628	80 ^o F fluid temp. magnet suspension

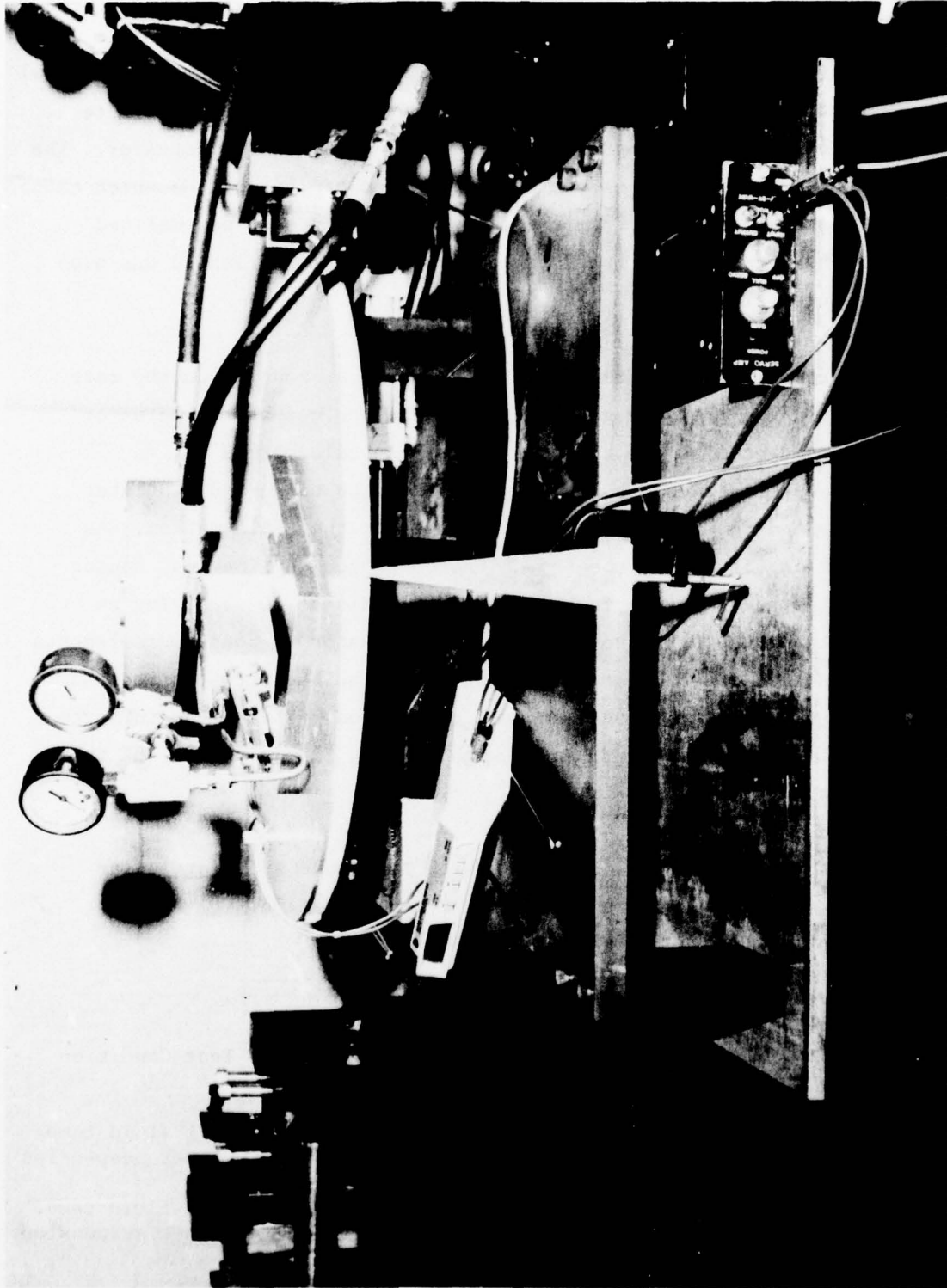


FIGURE 73 Rate Sensing Actuator on Test Rate Table

TABLE 9 (cont'd)

Frequency	Threshold	Test Condition
1.0	.14	80°F fluid temp. without magnetic suspension
1.0	1.32	-22°F fluid temp. magnetic suspension

Figure 74 shows an example record taken while making a threshold measurement. As shown on the figure, the input motion of the rate table is gradually increased and the output motion of the rate sensing actuator recorded. The rate table motion is measured with a rotary potentiometer mounted beneath the table and used as a position feedback transducer for the table. The point at which the actuator starts to respond to the input motion is the threshold point.

Notice that the threshold increased for the low temperature operation. This is believed to be due to the combination of increased actuator seal friction at low temperatures and a reduction of the pressure gain of the flapper-nozzle stage as the leakage flow drops off with temperature.

The effect of the addition of the magnetic suspension is also apparent from Table 9. The magnetic suspension used with the inertial sensor was a holding magnet installed in the cover of the inertial sensor so that it offset the force on the rotating magnet assembly due to gravity. At the same test condition of 1 Hz, the threshold reduced from .14 deg/sec to .062 deg/sec with the addition of the magnetic suspension. This was unexpected, since the design starting torque for the bearings used for the inertial reference was specified low enough that the bearing torque

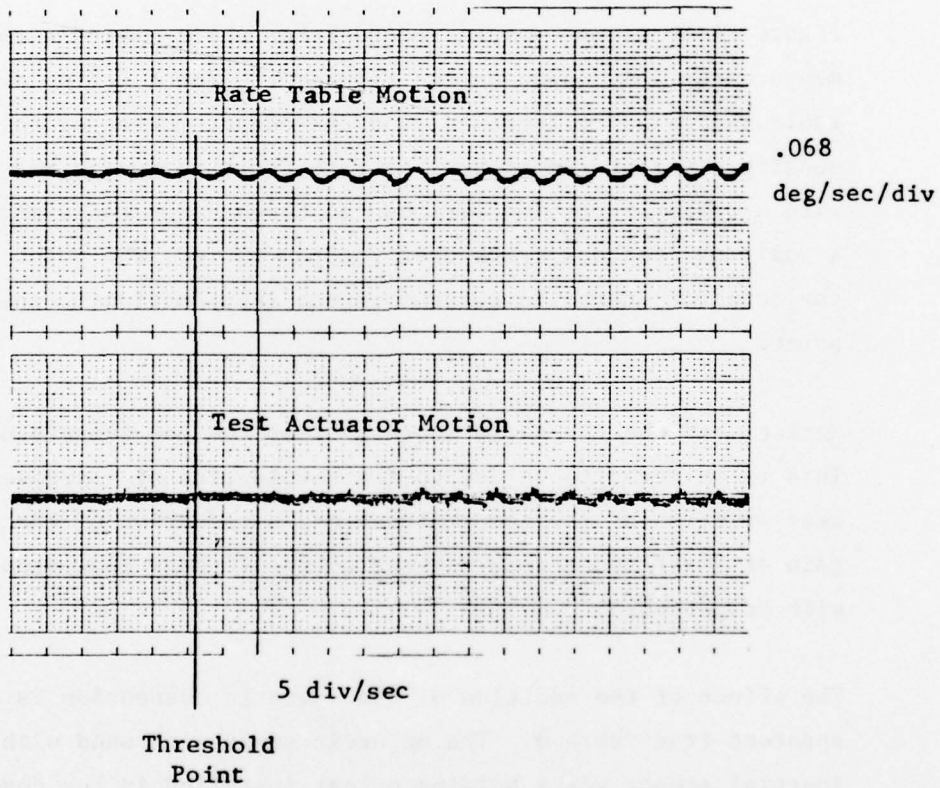


FIGURE 74
Threshold Data Strip

should not have shown up in the threshold. The conclusion is therefore that the bearings used were out of tolerance with respect to their rated starting torque.

2.2.5 Actuator Seal Friction

The static friction force to move the actuator when pressurized was tested. The actuator cylinder ports were connected together with a shorting tube. A force gauge was used to measure the starting force on the actuator with normal system pressure of 3000 psi applied. The starting force measured 16 lbs in both directions with the actuator starting at mid stroke. The test was repeated with the actuator depressurized. The starting force reduced by 1 lb. This indicates that the cartridge and laminar seal configuration is successful in maintaining a low breakout force for the augmentation actuator.

2.2.6 Bandpass Response

To establish the bandpass frequency response for the rate sensing actuator, the actuator response for rate table input motions was recorded on the chart recorder for frequencies from .05 to 10 Hz. Figure 75 is an example record taken at .3 Hz. The input amplitude at each frequency was adjusted to provide an undistorted actuator output waveform. This amplitude insured that the response of the actuator was measured at a point where the non-linearities of threshold and saturation would not influence the response measurement. Figure 76 is the frequency response plot of the bandpass. The -3 db break frequencies occur at .1 Hz and 1 Hz. The phase angle at .1 Hz is + 23 degrees. The phase angle at 1 Hz is -56 degrees. The + 28 degree phase angle at .1 Hz is 2 degrees below the anticipated minimum phase angle. The difference is a result of the 55 degree phase lag (instead of 45 degree)

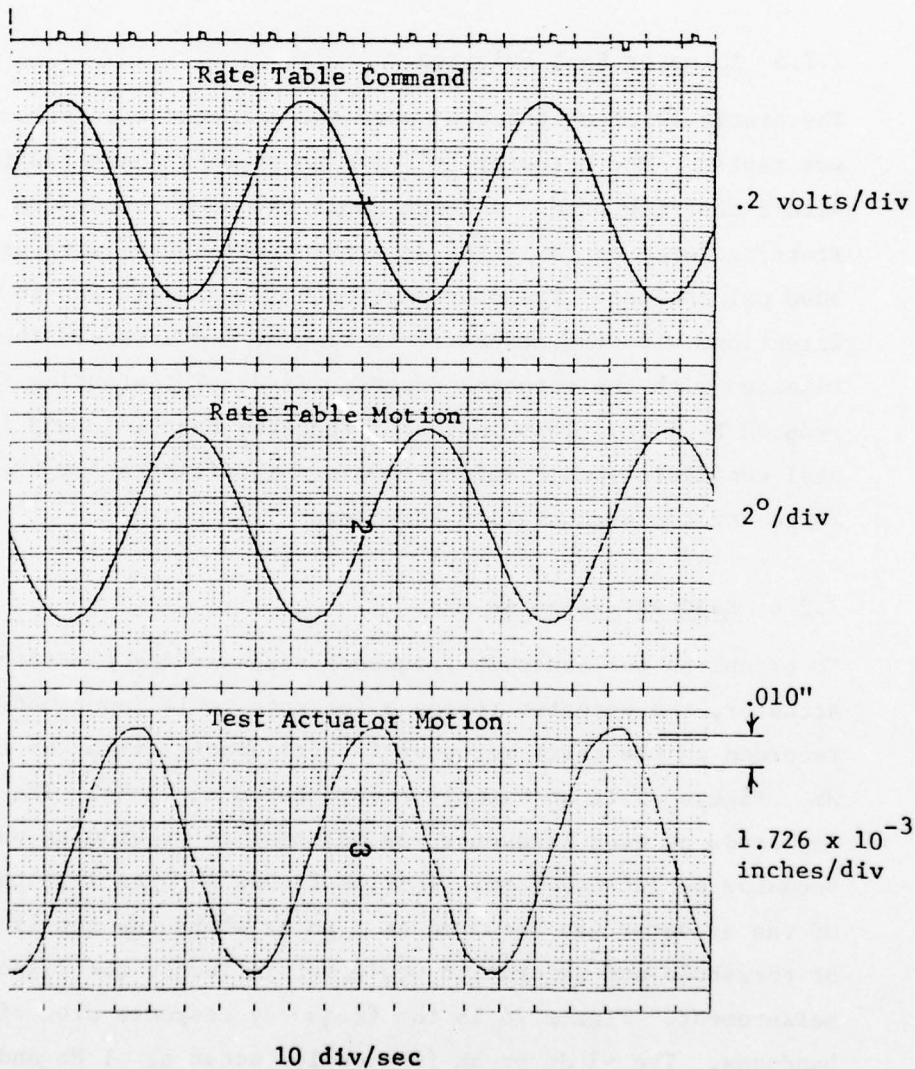


FIGURE 75

.3 Hz Frequency Response Data Strip

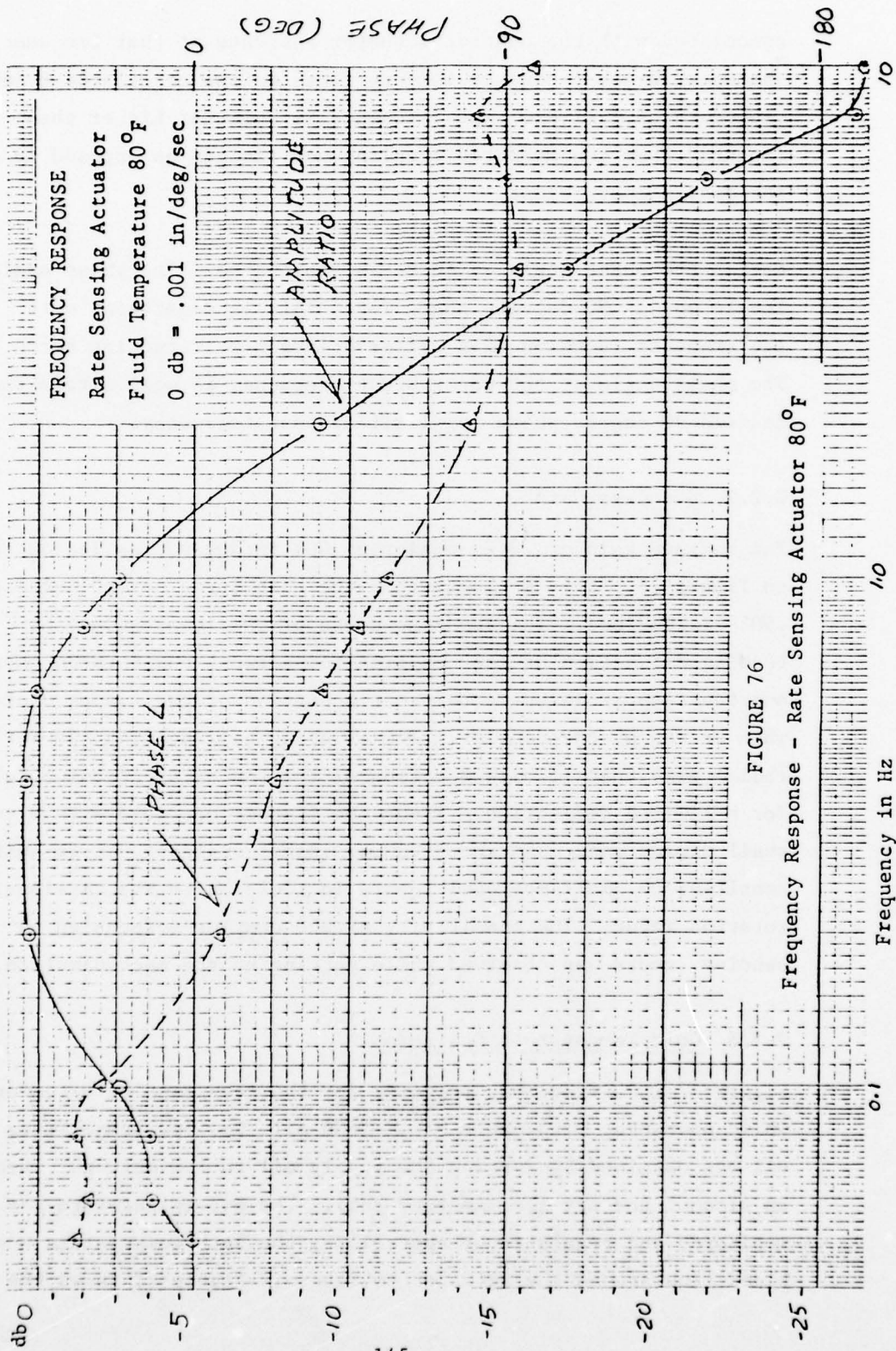


FIGURE 76
 Frequency Response - Rate Sensing Actuator 80°F

associated with the control actuator response at that frequency. The upper break frequency is very close to the calculated break frequency of 1.21 Hz. The frequency is somewhat higher than expected from the measured coupling coefficient as opposed to the design coefficient.

Notice the phase angle as 10 Hz is approached. The phase angle levels out at 90 degrees phase lag. This is consistent with the transfer function of a differentiation over two lag terms. The phase angle at the upper break frequency is well within the desired 90 degree phase lag limit at that frequency.

2.2.7 Bandpass Gain

The maximum gain at .3 Hz measured .001 in/deg/sec as indicated on Figure 76. This is lower than the calculated design value of .0057 in/deg/sec. The apparent cause of the lower gain is a bending deflection of the coupling rod between the torsion tube and the flapper which cancels out a portion of the flapper rotation when driven by the coupler. The existing ball bearing has sufficient radial play that it allows motion of the top of the torsion tube for a limited deflection. Since the flapper operates with a very small dimensional clearance (.00047 inches or less), it is quite sensitive to small motional inputs in addition to the torsional rotation input. The sensitivity of the coupler suspension to bending inputs was observed while setting up the mechanization.

2.2.8 Cold Temperature Operation

Figure 77 is a frequency response for the rate sensing actuator while operating with -40°F MIL-H-5606 oil. The low temperature oil was obtained by running the supply oil to the actuator through an alcohol and dry ice immersed coil. The oil temperature was monitored and regulated by controlling the bath temperature and bleed flow around the actuator to return. Figure 78 shows the cold

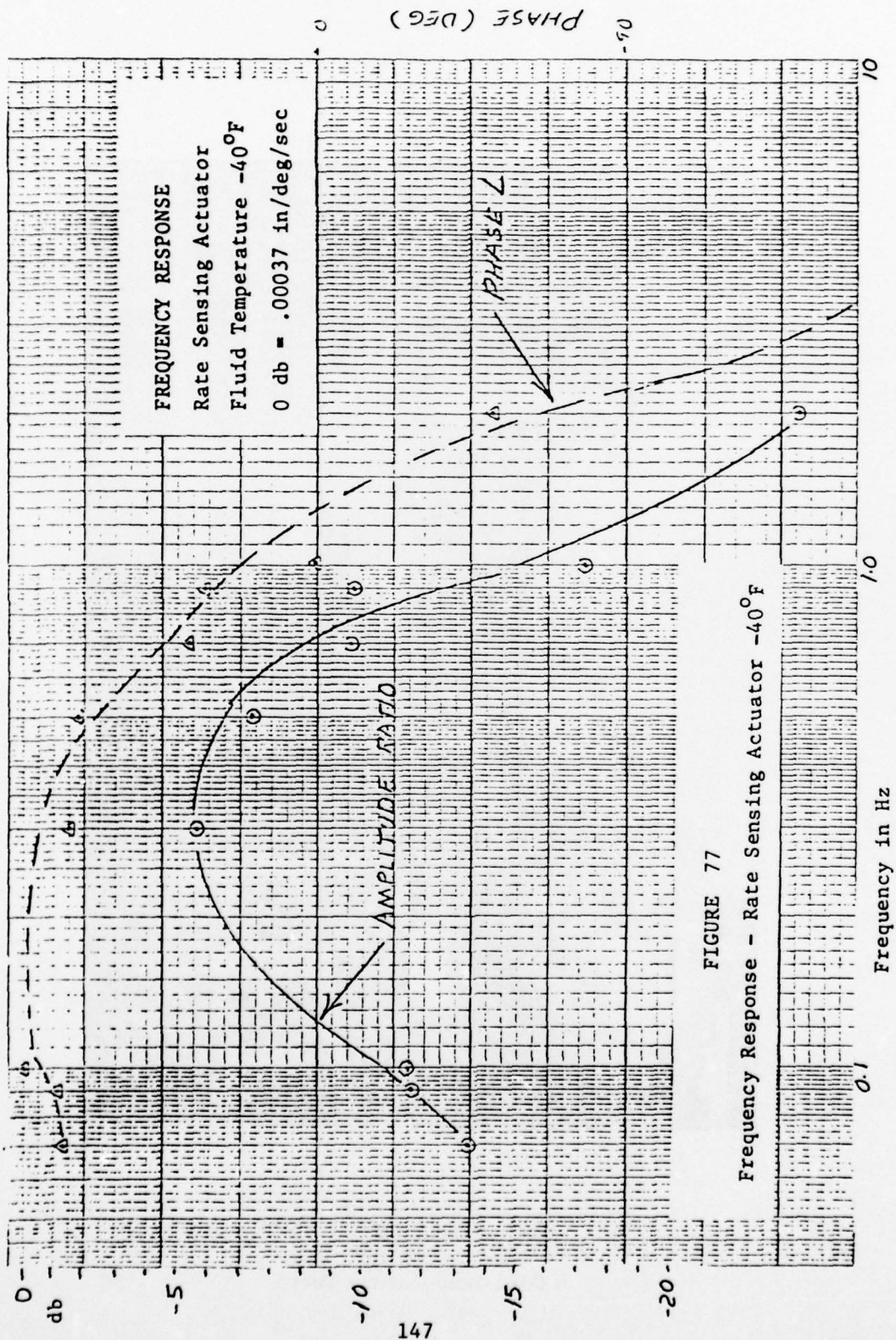


FIGURE 77
Frequency Response - Rate Sensing Actuator -40°F

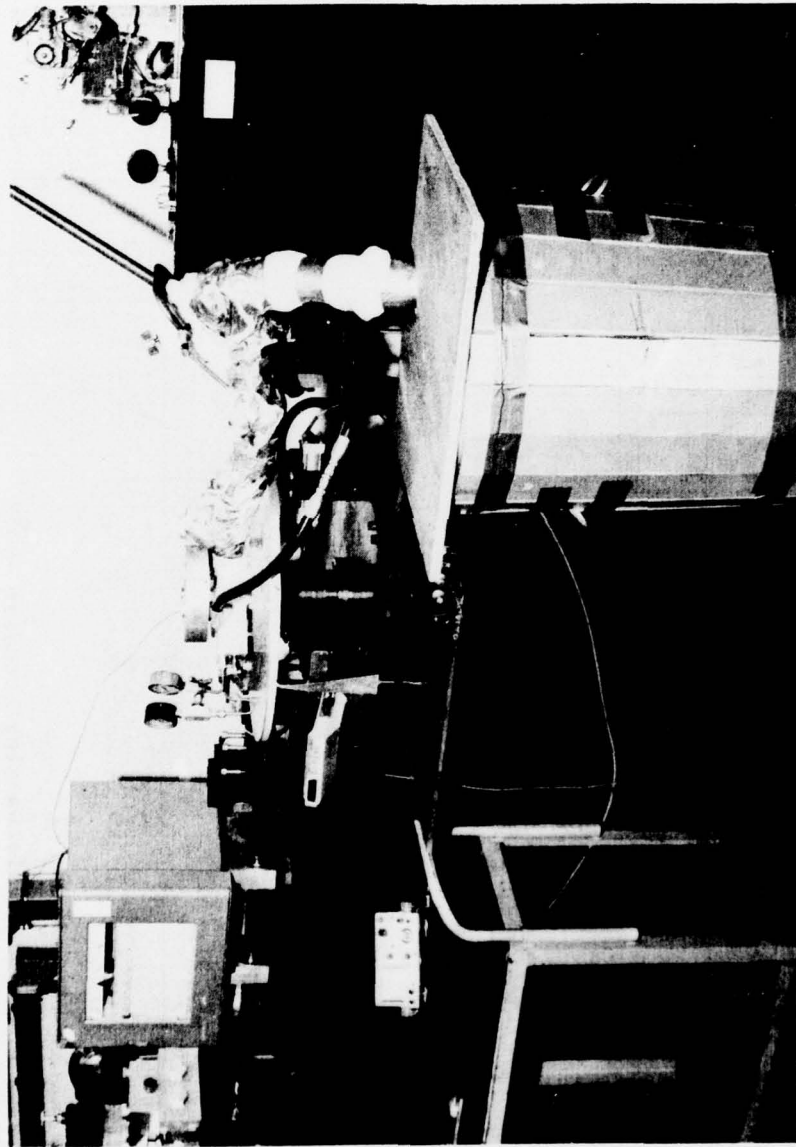


FIGURE 78

Cold Temperature Test

temperature test apparatus. The insulated can in the foreground contains alcohol and dry ice. A coil connected to the hydraulic supply is immersed in the alcohol. The temperature of the inlet oil to the test actuator is instrumented and recorded using the Brown recorder at the left of the rate table.

The response shown on Figure 77 is attenuated from that of the 80°F fluid temperature operation. During the low temperature testing, cylinder port pressure gauges were monitored. At -40°F, the cylinder port pressures dropped to 900 psi (compared to the normal 1500 psi), indicating the viscosity sensitivity of the upstream orifices.

Figure 79 is a frequency response data strip at .5 Hz taken during operation at -40°F fluid temperature.

2.2.9 Dynamic Range

Figures 80, 81 and 82 are data strips of the actuator response with a gradually increasing amplitude at frequencies of .1 Hz, .3 Hz and 1 Hz. Both the threshold characteristics and waveform with increasing amplitude and gain linearity are represented on these figures.

3. CONCLUSIONS AND RECOMMENDATIONS

The rate sensing actuator operated as predicted by the design with one exception.

The frequency response of the actuator and the bandpass response of the mechanization agreed with the design calculations. The threshold values were higher than expected based on the manufacturer's starting torque ratings for the bearings used to support the inertial reference. However, the thresholds measured under .1 deg/sec

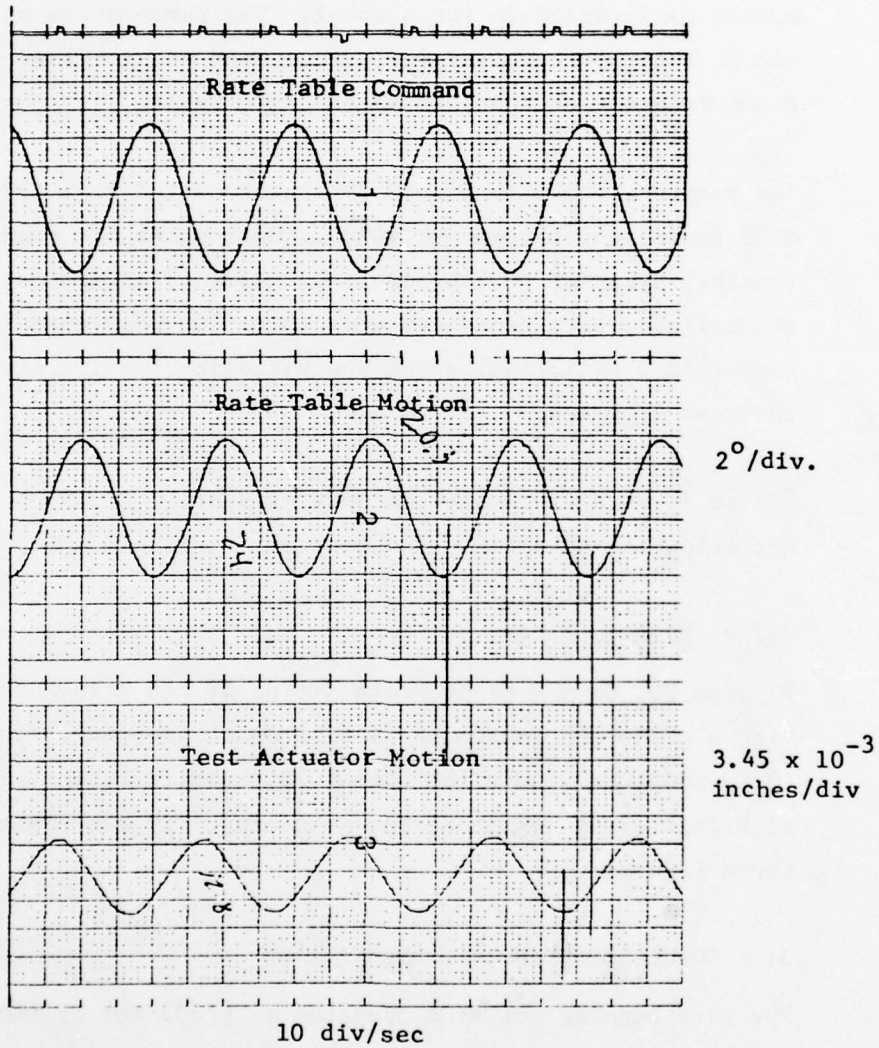


FIGURE 79
 Frequency Response Data Strip -40°F



FIGURE 80
 .1 Hz Amplitude Response Data Strip

ISH ACCUCHART

Gould Inc., Instrument Systems Divi

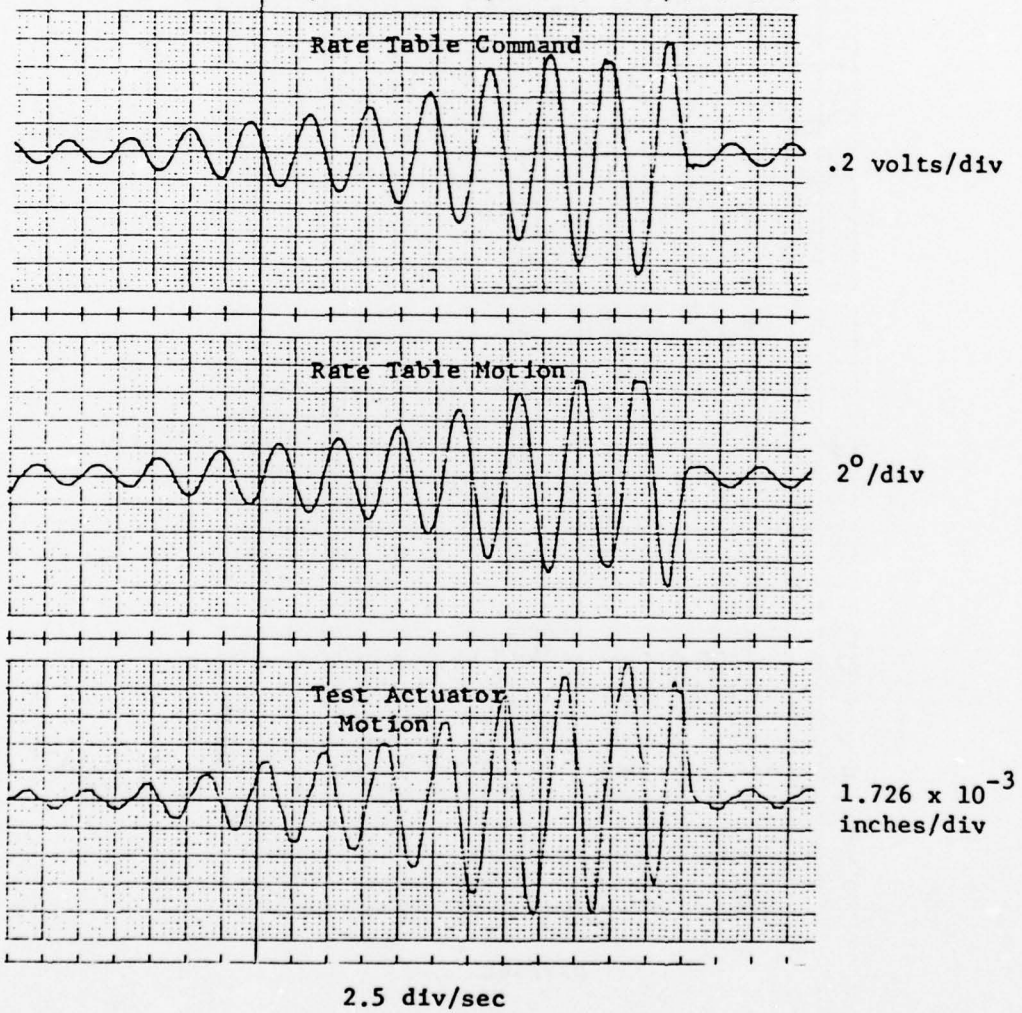


FIGURE 81

.3 Hz Amplitude Response Data Strip

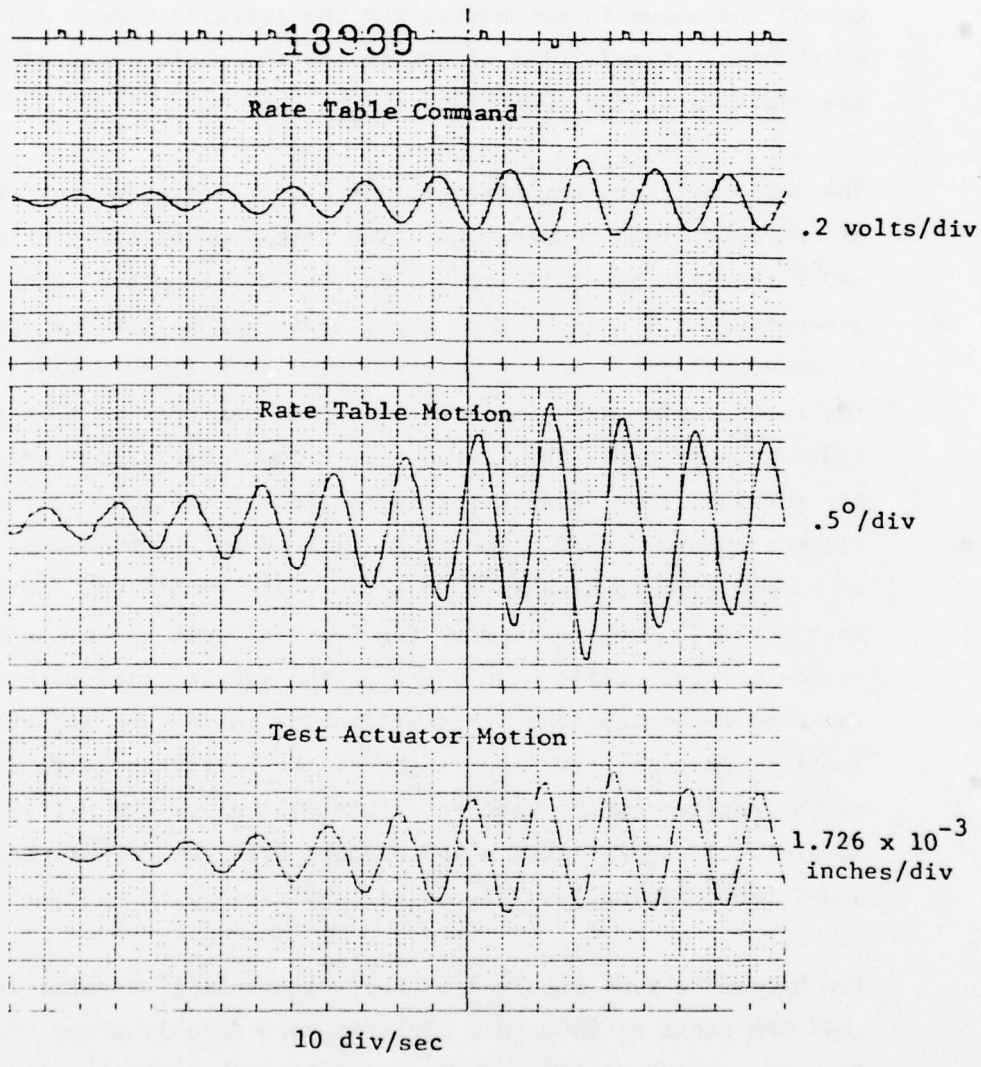


FIGURE 82

1 Hz Amplitude Response Data Strip

over the bandpass of the mechanization. This is well under the .5 deg/sec design threshold limit for the mechanization. The use of the magnetic suspension for the inertial sensor appeared worthwhile. A reduction of 50% in the threshold resulted from the addition of the suspension to the unit.

The response characteristics at -40°F were degraded from those of the 80°F fluid temperature. The rate-sensing actuator's -40°F response generally resembled the 80°F response and was attenuated by 8.5 db. Since the fluidic mechanizations (developed by Honeywell Inc.) do not operate below 40°F fluid temperature, the rate-sensing actuator performed comparatively well at the -40°F fluid temperature. The key to better low temperature performance for the rate sensing actuator lies with the orifices of the nozzle-flapper control stage. The feed orifices and nozzles would have to be modified to make them less viscosity sensitive. An approach that could be used to improve the feed orifices is to use a series of sharp edged orifices in place of the single orifices used in the test mechanization. This will allow making the individual orifices large so that the length of the orifice hole to diameter of the orifice can be reduced. This will allow the orifices to more closely approximate a sharp edged orifice, rather than a short tube, giving less viscosity sensitivity.

The hydraulic flow required by the rate-sensing actuator is .044 GPM total at 3000 psi. This is considerably lower than the flow required by similar functioning fluidic mechanizations.

The rate sensing actuator does require a minor improvement in the bearing support for the coupling rod. This can be accomplished by replacing the upper ball bearing support for the torsion tube with a flex pivot similar to that used on the lower portion of

the coupling rod. This will eliminate the torsion rod bending which results in a lower system gain at center frequency of the bandpass than that predicted by calculation. It is recommended that this modification be made and then further testing to evaluate the performance again be conducted.

In general, it is concluded that the mechanization demonstrated the design approach validity and the unit worked as predicted by the design calculations. The mechanization appears to have performance characteristics that are desirable enough that further development is recommended.

APPENDIX A

TEST PROCEDURE

Flight Worthiness Tests

Direct Drive FBW

21 October 1977

Contract F33615-77-C-3077

Dynamic Controls, Inc.

Dayton, Ohio

1.0 PURPOSE

The purpose of this specification is to provide a procedure for the testing to establish flight worthiness for the direct drive FBW control system developed by Dynamic Controls, Inc. for the Air Force under contracts No. F33615-75-C-3068 and F33615-77-C-3077.

2.0 TEST SEQUENCE

The test sequence, applicable sections of this specification, and the reference documents are as follows:

Test	Section	Reference
1. Performance	4.1	
2. Low Temperature	4.2	MIL-STD-810C, Method 502, Section 3.1, Procedure I
3. Operational	4.3	
4. High Temperature	4.4	MIL-STD-810C, Method 501, Section 3.2, Procedure II
5. Operational	4.3	
6. Temperature-Altitude	4.5	MIL-STD-810C, Method 504, Section 3.1, Procedure I, Steps 2, 7 and 11.
7. Operational	4.3	
8. Life Cycle	4.6	MIL-V-27162, Section 3.5.2.7
9. Operational	4.3	
10. Shock	4.7	MIL-STD-810C, Method 516, Section 3.3
11. Operational	4.3	
12. Vibration	4.8	MIL-STD-810C, Method 514, Procedure I Curve C
13. Performance	4.1	

3.0 TEST INFORMATION AND TOLERANCES

3.1 Information

Unless otherwise specified, the following will apply:

Hydraulic Fluid - MIL-H-5606
Hydraulic Inlet Pressure - 3000 ± 150 PSIG
Hydraulic Outlet Pressure - 0 to 150 PSIG
Hydraulic Flow Rate - 0 to 20 GPM
Electrical Power - ± 15 VDC @ 2 Amps/Supply (4 Req'd)

Ambient Test Conditions shall be as follows:

Temperature - 60 - 95° F
Relative Humidity - 50 - 90%
Barometric Pressure - 28.5 to 30.5 " Hg.

3.2 Test Tolerances

Temperature	$\pm 2^{\circ}\text{F}$
Pressure	$\pm 5\%$ of value
Amplitude	$\pm 10\%$ of value
Frequency	$\pm 2\%$ for frequencies above 20 Hz $\pm 1/2$ Hz for frequencies below 20 Hz
Acceleration	$\pm 10\%$ of value
Voltage	$\pm 1\%$ of value
Current	$\pm 1\%$ of value

4.0 TEST PROCEDURES

4.1 Performance Test Setup

The test setup for making the performance measurements is shown on Figure 1.

4.1.1 Static Threshold

Apply a 0.01 Hz triangular wave form input to the direct drive system. Increase the amplitude of the input until a measureable output change occurs. Record both the input and the output.

Repeat with Channel 1 failed electrically and Channel 2 operating.

Repeat with Channel 2 failed electrically and Channel 1 operating.

The maximum allowable static threshold shall be as follows:

With both channels operating - 1.25% of the maximum input command

With one channel operating - 2.75% of the maximum input command

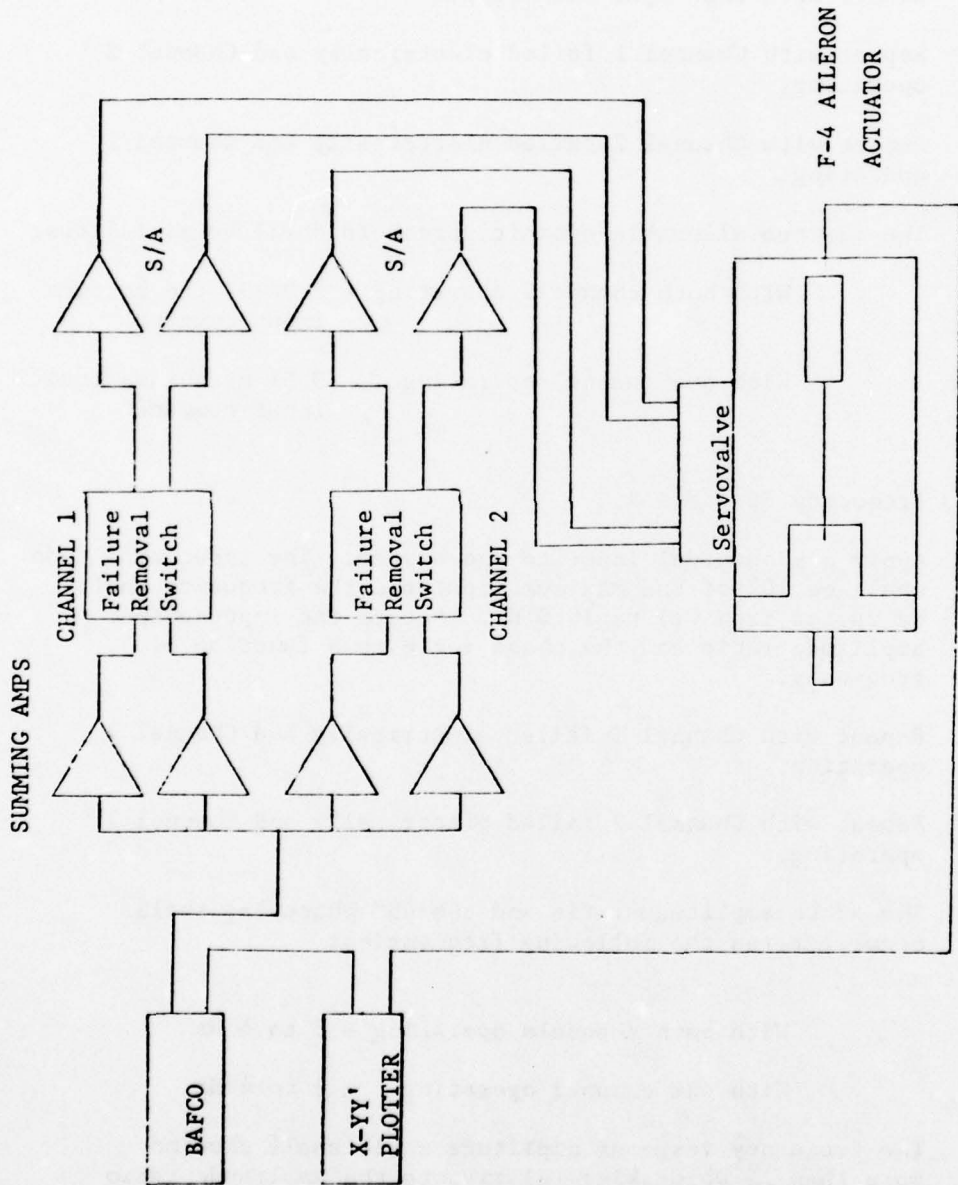


FIGURE A-1 DIRECT DRIVE PERFORMANCE TEST SETUP

4.1.2 Dynamic Threshold

Apply a sinusoidal input of 2.5 Hz to the system. Increase the amplitude until a measurable output change occurs. Record both the input and output.

Repeat with Channel 1 failed electrically and Channel 2 operating.

Repeat with Channel 2 failed electrically and Channel 1 operating.

The maximum allowable dynamic threshold shall be as follows:

With both channels operating - 2.0% of the maximum input command

With one channel operating - 3.5% of the maximum input command

4.1.3 Frequency Response

Apply a sinusoidal input to the system. The input amplitude shall be 10% of the maximum input and the frequency shall be varied from 0.1 to 10.0 Hz. Record the input-output amplitude ratio and the phase angle as a function of frequency.

Repeat with Channel 1 failed electrically and Channel 2 operating.

Repeat with Channel 2 failed electrically and Channel 1 operating.

The -3 Db amplitude ratio and the 45° phase lag shall occur between the following frequencies:

With both channels operating - 6 to 8 Hz

With one channel operating - 3 to 4 Hz

The frequency response amplitude ratio shall show no more than .5 Db peaking relative to the amplitude ratio at .1 Hz.

4.1.4 Linearity

Apply a 0.01 Hz triangular waveform input to the system. The amplitude of the input shall be 105% of the input to achieve full stroke of the actuator. Record the input and output.

Repeat with Channel 1 failed electrically and Channel 2 operating.

Repeat with channel 2 failed electrically and Channel 1 operating.

The maximum allowable linearity error shall be as follows:

With both channels operating - 1.0%

With one channel operating - 1.0%

4.1.5 Hysteresis

Apply a 0.01 Hz triangular waveform input to the system. The amplitude shall be 10% of the full stroke input. Record the output vs the input.

Repeat with Channel 1 failed electrically and Channel 2 operating.

Repeat with Channel 2 failed electrically and Channel 1 operating.

The maximum allowable hysteresis shall be as follows:

With both channels operating - 1.5% of maximum input

With one channel operating - 1.5% of maximum input

4.1.6 Saturation Velocity

Apply a 0.01 Hz square wave to the system input. The amplitude shall be 110% of the input to achieve full stroke of the actuator. Record the actuator output position vs time.

Repeat with Channel 1 failed electrically and Channel 2 operating.

Repeat with Channel 2 failed electrically and Channel 1 operating.

The maximum allowable time for extend and retract rates shall be as follows:

With both channels operating - Extend - .75 sec.
Retract - 1 sec.

With one channel operating - Extend - .75 sec.
Retract - 1 sec.

4.1.7 Transient Response

Apply a 0.01 Hz square wave to the system input. The input amplitude shall be 10% of the input to achieve full stroke. Record the actuator output vs time.

Repeat with Channel 1 failed electrically and Channel 2 operating.

Repeat with Channel 2 failed electrically and Channel 1 operating.

The maximum allowable time required to achieve 63% of the final value shall be as follows:

With both channels operating - .1 sec.

With one channel operating - .2 sec.

4.1.8 Detection Level

Apply a gradually increasing voltage to the input of one channel (either the command or monitor input) to cause the failure logic to trip. Record the input level causing failure detection. Repeat with a voltage of the opposite polarity.

Repeat for the input to the second channel.

The absolute value of the positive and negative voltages causing failure detection shall agree with each other within 10%. The voltages causing failure detection shall agree between channels within 10%.

The amplitude recorded initially shall be used as a baseline value. Subsequent test data shall agree within \pm 20%.

4.1.9 Preflight Checkout Operation

Perform the preflight checkout sequence as follows:

1. Use the failure inject switch to inject a failure into a control channel. The failure switch should be held in the inject position and the channel's current indicating lights observed.
2. Operate the reset switch to reset the failure detection circuit.
3. With hydraulic power off, operate the control channel with an input and observe the current indicating lights.
4. Repeat for the second control channel

For correct operation, the following should be observed:

1. Operation of the failure inject switch should immediately cause the amber failure indicating light to illuminate and remain on. With the failure inject switch held in the "on" position, the current indicating lights for the channel should indicate opposite current direction.
2. Operation of the failure reset switch should cause the amber failure indicating light for the channel to go out.
3. With a control input applied to the control channel and with hydraulic power off, the current indicating lights should illuminate in pairs, indicating the same current direction. The input level for illumination shall be approximately the same for each indicating light.

4.2 LOW TEMPERATURE TESTING

Figure 2 shows the temperature-time relationship for the low temperature testing.

Install the valve/actuator package in the test chamber. Lower the temperature

to -65°F (-54°C) and maintain the temperature for 24 hours. At the end of 24 hours, raise the chamber temperature to -40°F (-40°C) and maintain for 4 hours. At the end of this period, subject the package to the operational test (ref. 4.3) while leaving the test chamber at the -40° temperature. During the low temperature testing and the operational test, record the following:

1. Time
2. Temperature
3. Relevant Operational Data

4.3 OPERATIONAL TEST

With the control actuator at mid position, apply an input step of 25% of the input level for maximum stroke. Repeat with a step of the same amplitude and opposite polarity. Record the position vs time for the actuator motion.

The response times to reach 63% of the final value for each test condition shall not exceed the following:

Extend Motion - .20 sec.

Retract Motion - .20 sec.

The time response shall exhibit no ringing and less than 10% overshoot.

4.4 HIGH TEMPERATURE

Figure 3 shows the temperature-time relationship for the high temperature testing.

Install the valve/actuator package in the test chamber. Increase the chamber temperature to 120°F (49°C) and maintain for 6 hours.

Increase the chamber temperature to 160°F (71°C) within a one hour period and maintain this temperature for 4 hours.

Decrease the chamber temperature to 120°F (49°C) within a one hour period.

Repeat the preceding three step cycle two additional times for a total of three 12 hour cycles.

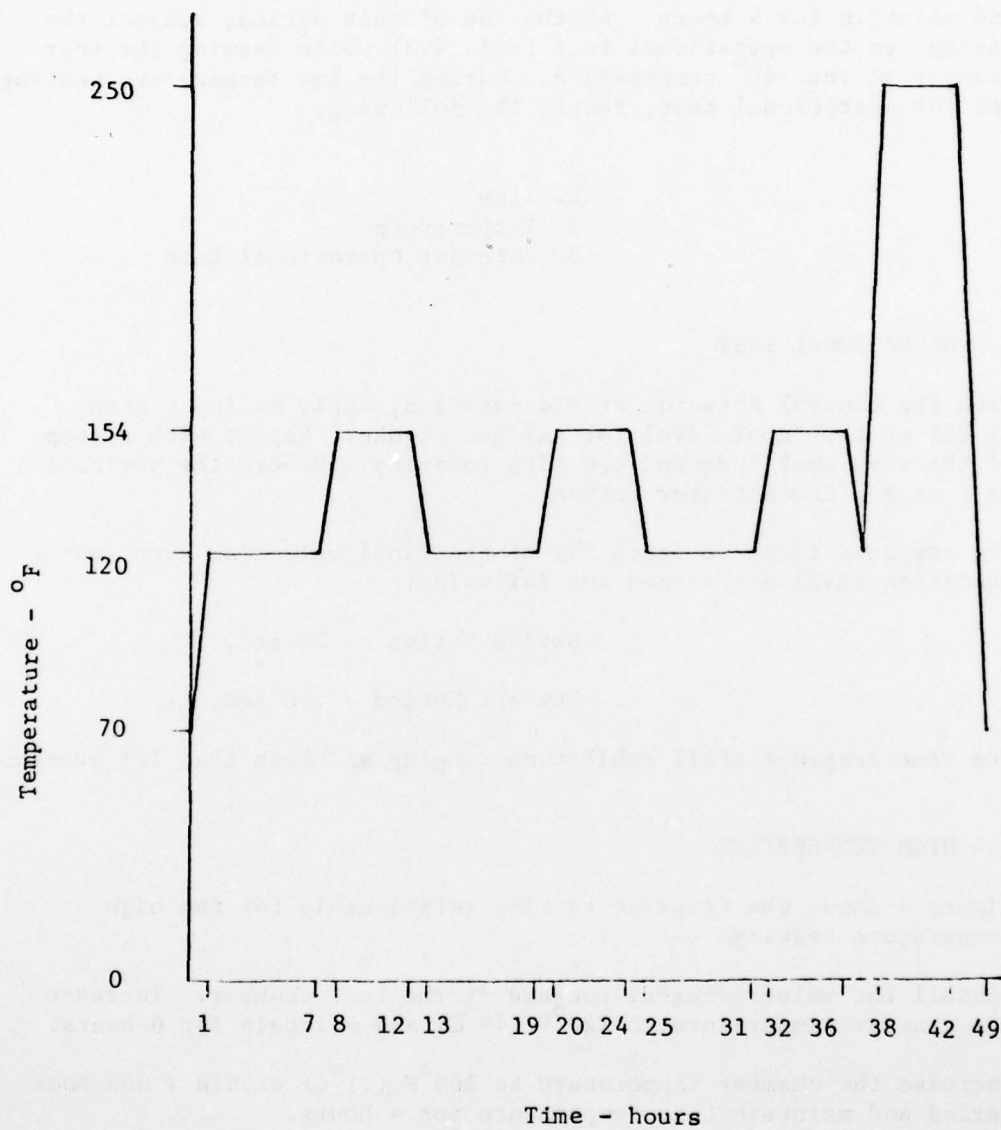


FIGURE A-3 High Temperature Test

At the conclusion of the temperature cycles, increase the chamber temperature to 250°F (121°C). Maintain this temperature for a four hour period. After the end of four hours, subject the test package to the operational test of 4.3.

Return the package (non-operating) to ambient conditions and allow a stabilization period of 4 hours. At the conclusion of this period, subject the system to the operational test of 4.3.

During the testing, record:

1. Time
2. Temperature
3. Relevant Operational Data

4.5 TEMPERATURE-ALTITUDE TEST

4.5.1 General

Place the electronic modules in the test chamber and make all connections to the actuator package. Instrument one command amplifier and one servoamplifier module per figures 4 and 5 respectively. Record the following for the three test procedures:

1. Temperatures (module and chamber)
2. Altitude
3. Input to Modules
4. Actuator Position

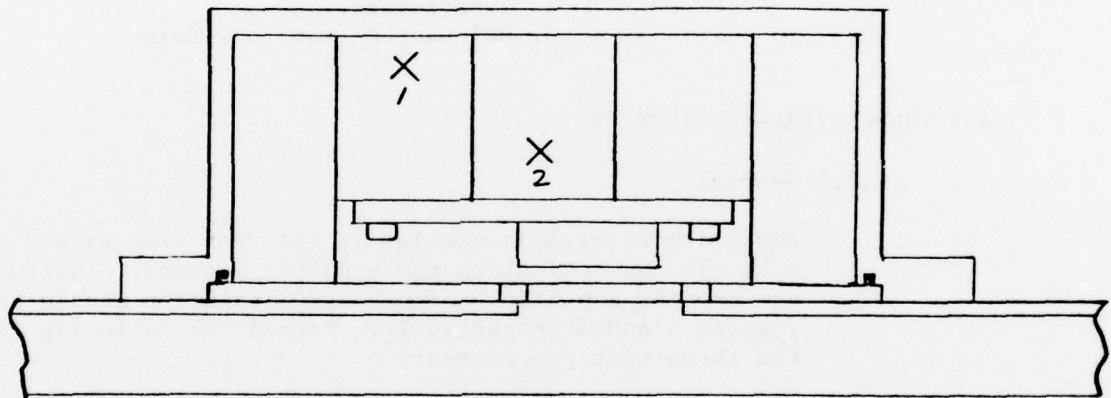
In the following tests, the rate of temperature and pressure change shall not exceed 1.8°F (1°C) and 0.5 in. Hg. per second.

4.5.2 Test I

With the electronic modules non-operating, adjust the chamber conditions to the following:

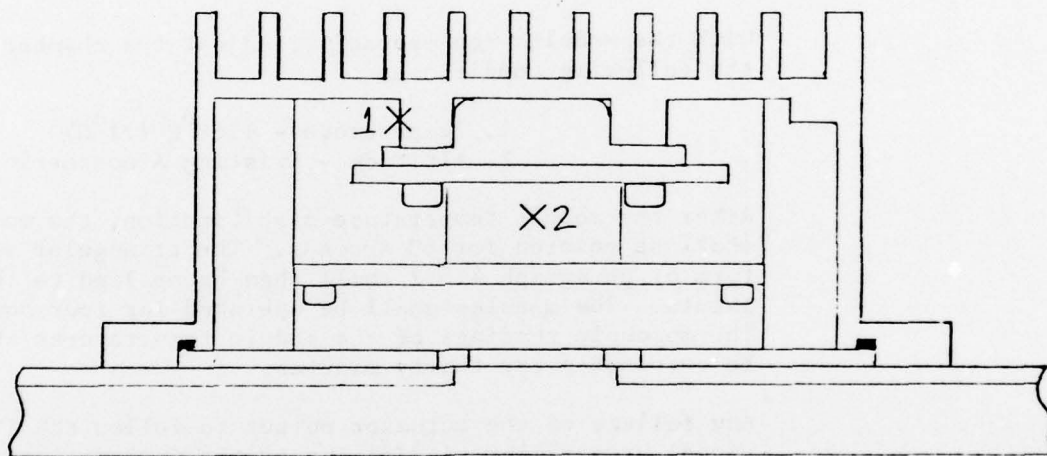
1. Temperature - -65°F (-54°C)
2. Altitude - Existing Atmospheric

After module temperature stabilization (a change of less than 2°C per hour of the module temperature), the modules shall be powered for 60 seconds. A triangular waveform of 100% of full input signal at .01 Hz shall be



1. MODULE WALL TEMPERATURE
2. AMBIENT TEMPERATURE

FIGURE A-4 Command Amplifier Thermocouple Location



- 1 HEAT SINK TEMPERATURE
- 2 AMBIENT TEMPERATURE

FIGURE A-5 Thermocouple Locations for Power Amp Module

applied to the system as an input for a total of 10 Hz. The modules shall then be turned off and restabilized at -65°F . The preceding shall be repeated two more times for a total of three cycles.

Any failure of the actuator output to follow the input or a failure indication by the failure logic shall be cause for rejection.

4.5.3 Test II

With the modules non-operating, adjust the chamber to the following conditions:

1. Temperature - $+160^{\circ}\text{F}$ (71°C)
2. Altitude - Existing Atmospheric

After the module temperature stabilization, the modules shall be powered for 60 seconds. The triangular waveform of paragraph 4.5.2 shall then be applied to the inputs. The modules shall be operated for four hours. Thermocouple readings of the module temperatures shall be recorded every thirty minutes.

Any failure of the actuator output to follow the input signal or a failure indication by the failure logic shall be cause for rejection.

4.5.4 Test III

With the modules non-operating, adjust the chamber to the following conditions:

1. Temperature - 50°F (10°C)
2. Altitude - 70,000 ft. above sea level

After module temperature stabilization, the modules shall be powered for 60 seconds. The triangular waveform of 4.5.2 shall then be applied to the system inputs. The modules shall be operated continuously for four hours. Thermocouple readings of the modules shall be recorded every thirty minutes.

Any failure of the actuator output to follow the input signal or a failure indication by the failure logic shall be cause for rejection.

4.6 LIFE CYCLE TESTS

The direct drive system shall be subjected to a 200 hour life cycle test. The test will be performed by operating the system with the following inputs (which make up a single 5 hour test sequence):

Input Amplitude (% of rated max input)	Frequency (Hz)	Duration (hours)	Cycles (no.)
100	.01	1	36
50	.1	1	360
10	1	2	7,200
5	10	1	36,000

The total test shall consist of repeating the 5 hour test sequence with a one hour interval of no operation between the 5 hour sequences. The total cycles logged during the 200 hours of operation shall be a minimum of 1,743,000.

4.7 SHOCK

Figure 6 shows the shock pulse amplitude vs time profile to be used for the shock testing.

Mount the test specimen to the shock machine and subject it to a saw tooth shock pulse of 20 ± 3 g's for a $11 \pm .75$ millisecond time duration. Three shocks shall be applied along mutually perpendicular axes of the test specimen for a total of 18 shocks.

The specimens shall not be operating during the test. The test shall be conducted at ambient temperature. At the end of the shock test, the system shall be subjected to the operational test of 4.3.

For each specimen tested, the following data shall be recorded:

1. Temperature
2. Shock pulse profile
3. Relevant operational data

Where identical components are used in the direct drive system, only one representative component will be tested.

4.6 LIFE CYCLE TESTS

The direct drive system shall be subjected to a 200 hour life cycle test. The test will be performed by operating the system with the following inputs (which make up a single 5 hour test sequence):

Input Amplitude (% of rated max input)	Frequency (Hz)	Duration (hours)	Cycles (no.)
100	.01	1	36
50	.1	1	360
10	1	2	7,200
5	10	1	36,000

The total test shall consist of repeating the 5 hour test sequence with a one hour interval of no operation between the 5 hour sequences. The total cycles logged during the 200 hours of operation shall be a minimum of 1,743,000.

4.7 SHOCK

Figure 6 shows the shock pulse amplitude vs time profile to be used for the shock testing.

Mount the test specimen to the shock machine and subject it to a saw tooth shock pulse of 20 ± 3 g's for a $11 \pm .75$ millisecond time duration. Three shocks shall be applied along mutually perpendicular axes of the test specimen for a total of 18 shocks.

The specimens shall not be operating during the test. The test shall be conducted at ambient temperature. At the end of the shock test, the system shall be subjected to the operational test of 4.3.

For each specimen tested, the following data shall be recorded:

1. Temperature
2. Shock pulse profile
3. Relevant operational data

Where identical components are used in the direct drive system, only one representative component will be tested.

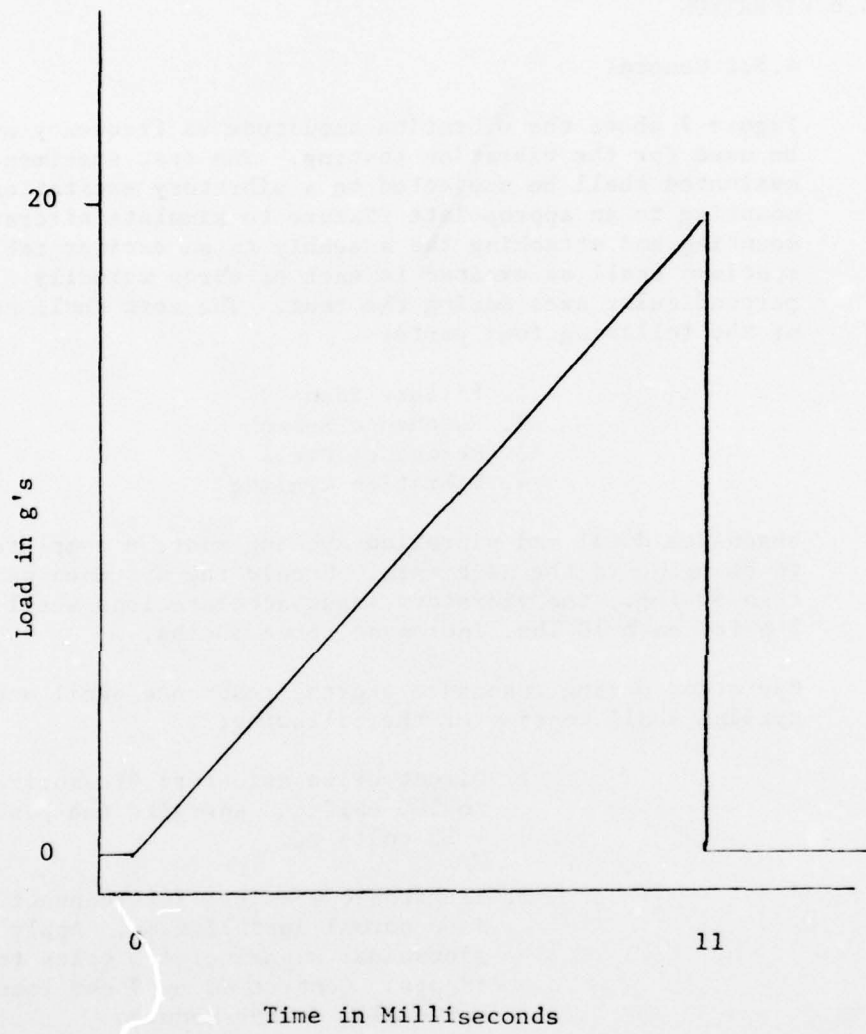


FIGURE A-6 Terminal Peak Sawtooth Shock Pulse

4.8 VIBRATION

4.8.1 General

Figure 7 shows the vibration amplitude vs frequency sweep to be used for the vibration testing. The test specimen to be evaluated shall be subjected to a vibratory excitation by mounting to an appropriate fixture to simulate aircraft mounting and attaching the assembly to an exciter table. The specimen shall be excited in each of three mutually perpendicular axes during the test. The test shall consist of the following four parts:

1. Fixture Scan
2. Resonance Search
3. Resonance Dwell
4. Vibration Cycling

Resonance dwell and vibration cycling must be completed prior to changing to the next axis. Should the specimen weigh more than 50 lbs., the vibratory input accelerations shall be reduced 1 g for each 10 lbs. increment above 50 lbs.

Operation during resonance search, resonance dwell and vibration cycling shall consist of the following:

1. Direct drive actuator: Pressurize all ports to 500 PSIG and energize the position with + 15 volts DC.
2. Electronic modules: Interconnect modules as in a normal installation. Apply a 2.5 Hz sinusoidal signal of + 5 volts to all system inputs. Connect dummy 8 ohm loads to the servovalve driver modules.

For each specimen the following test of 4.8.2, 4.8.3 and 4.8.4 shall be used.

4.8.2 Fixture Scan

Mount the fixture to the exciter table. Mount the drive accelerometer directly adjacent to a test specimen mounting point. Instrument a representative sample number of the remaining specimen mounting points to determine the response

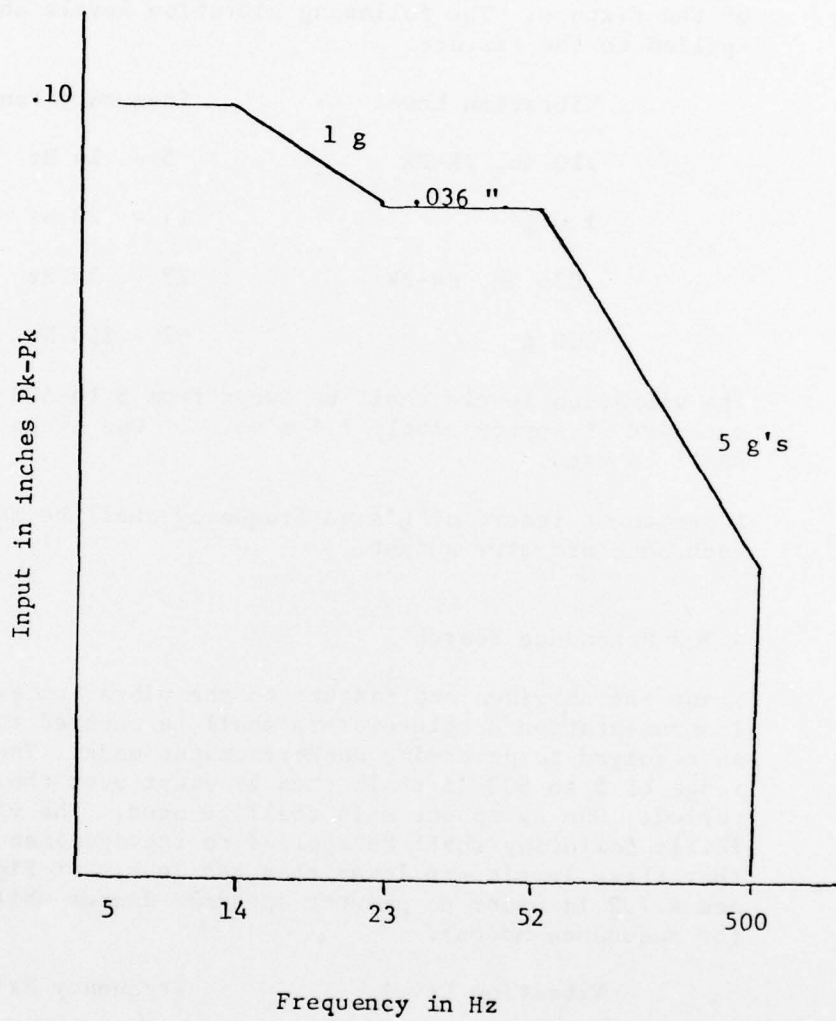


FIGURE A-7 VIBRATION TEST CURVE

of the fixture. The following vibration levels shall be applied to the fixture.

Vibration Level	Frequency Range
.10 in. Pk-Pk	5 - 14 Hz
1.0 g	14 - 23 Hz
.036 in. Pk-Pk	23 - 52 Hz
5.0 g	52 - 500 Hz

The vibration levels shall be swept from 5 to 500 Hz over a period of approximately 7.5 minutes. One sweep per axis shall be used.

A permanent record of g's vs frequency shall be made for each accelerometer output.

4.8.3 Resonance Search

Mount the specimen and fixture to the vibration exciter table. Instrumentation accelerometers shall be mounted to the specimen as required to determine each resonance mode. The frequency range of 5 to 500 Hz shall then be swept over the 7.5 minute period. One sweep per axis shall be used. The vibration levels following shall be applied to the specimen (note that these levels are lower than the levels of Figure 7 and 4.7.2 in order to prevent specimen damage while searching for resonance modes).

Vibration Level	Frequency Range
.02 in. Pk-Pk	5 - 14 Hz
.2 g	14 - 23 Hz
.0072 in Pk-Pk	23 - 52 Hz
1.0 g	52 - 500 Hz

A hand held accelerometer probe and/or a stroke light may be used as aids in determining resonance modes.

A permanent record of g's vs frequency shall be plotted for each accelerometer. The test specimens shall be non-operating during the resonance search.

4.8.4 Resonance Dwell

From the data taken during the resonance scan, determine the frequencies at which resonance occurs in each axis. The specimen shall then be vibrated along each axis at the most severe resonant frequencies according to the following:

No. of Resonances	Total Time at Resonances per axis
0	0
1	½ hr.
2	1 hr.
3	1½ hrs.
4	2 hrs.

Where more than one resonance occurs, the time spent at each resonance is ½ hr. with the input vibration amplitude determined by Figure 7.

If more than four significant resonances have been found for any one axis, the four most severe resonances must be chosen for the test. In the event of a change in resonant frequency during the dwell period, the frequency shall be adjusted to maintain the resonant condition.

At the completion of each resonance dwell, the unit shall be subjected to a visual examination. During the testing, the following information shall be recorded:

1. Input amplitude
2. Frequency
3. Time at each resonance
4. Any evidence of failure

4.8.4 Vibration Cycling

Upon completion of the resonance dwell in each axis, the unit shall be subjected to vibration cycling. This shall be performed as follows:

AD-A080 133

DYNAMIC CONTROLS INC DAYTON OHIO
RESEARCH AND DEVELOPMENT OF CONTROL ACTUATION SYSTEMS FOR AIRCR--ETC(U)
AUG 79 G D JENNEY

F/6 1/3

F33615-77-C-3077

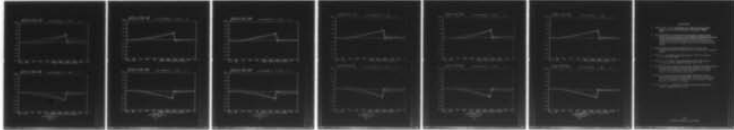
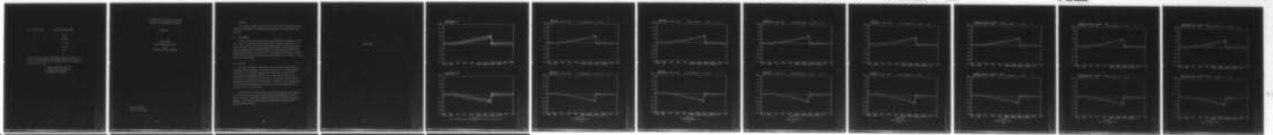
UNCLASSIFIED

AFFDL-TR-79-3117-VOL-1

NL

3 of 3

AD
A080133

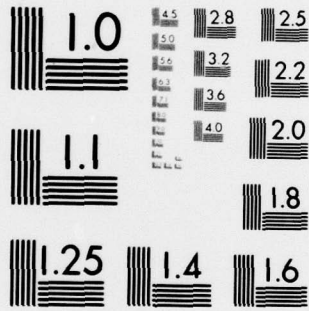


END

DATE
FILMED

3 - 80

DDC



MICROCOPY RESOLUTION TEST CHART
NATIONAL BUREAU OF STANDARDS-1963-A

No. of Resonances	Cycling Time per Axis
0	3 hrs.
1	2½ hrs.
2	2 hrs.
3	1½ hrs.
4	1 hr.

The sweep rate for the cycling time shall be 5 - 500 - 5 Hz over a 15 minute period. The input vibration amplitude to the specimen shall be as shown on Figure 7. During the cycling test, record:

1. Input vibration amplitude
2. Input vibration frequency
3. Cycling time elapsed
4. Evidence of failure

AIR FORCE FLIGHT DYNAMICS LABORATORY
COMBINED ENVIRONMENTS TEST GROUP

APPENDIX B

TEST REPORT
MIL-STD-810C SHOCK TEST
FOR
DIRECT DRIVE FBW ACTUATOR

Project 24030212
Date: 9 April 1979

I. PURPOSE

The purpose of this report is to document shock test data that was obtained for support of flightworthiness tests for a Direct Drive FBW Actuator.

II. BACKGROUND

A Direct Drive FBW Actuator has been developed by Dynamics Control, Inc., under contract to the Air Force Flight Dynamics Laboratory. In order to assure that the unit be qualified flight worthy in accordance with selected portions of MIL-STD-810C, the Combined Environments Test Group (AFFDL/FEE) was contacted by the Air Force Flight Dynamics Laboratory's Control Systems Development Branch (AFFDL/FGL) to conduct the shock portion of the testing.

III. RESULTS

The test specimens involved were a control valve and a number of electronic control modules. Each unit was tested on a Ling 330 shaker controlled by a Hewlett-Packard digital controller to shock pulse identified in MIL-STD-810C of 20 ± 3 g's amplitude for an $11 \pm .75$ millisecond time duration. Three shocks were applied along mutually perpendicular axes of the test specimens. Appendix A is a presentation of test reference and tolerance plots followed by actual test data compared to the test reference.

Testing of the control valve had to be done again since a failure of the valve was discovered by FGL personnel upon examination after initial testing. The second series of tests on the valve resulted in no failures, and all electronic control modules passed testing on the initial series of tests.

TEST DATA

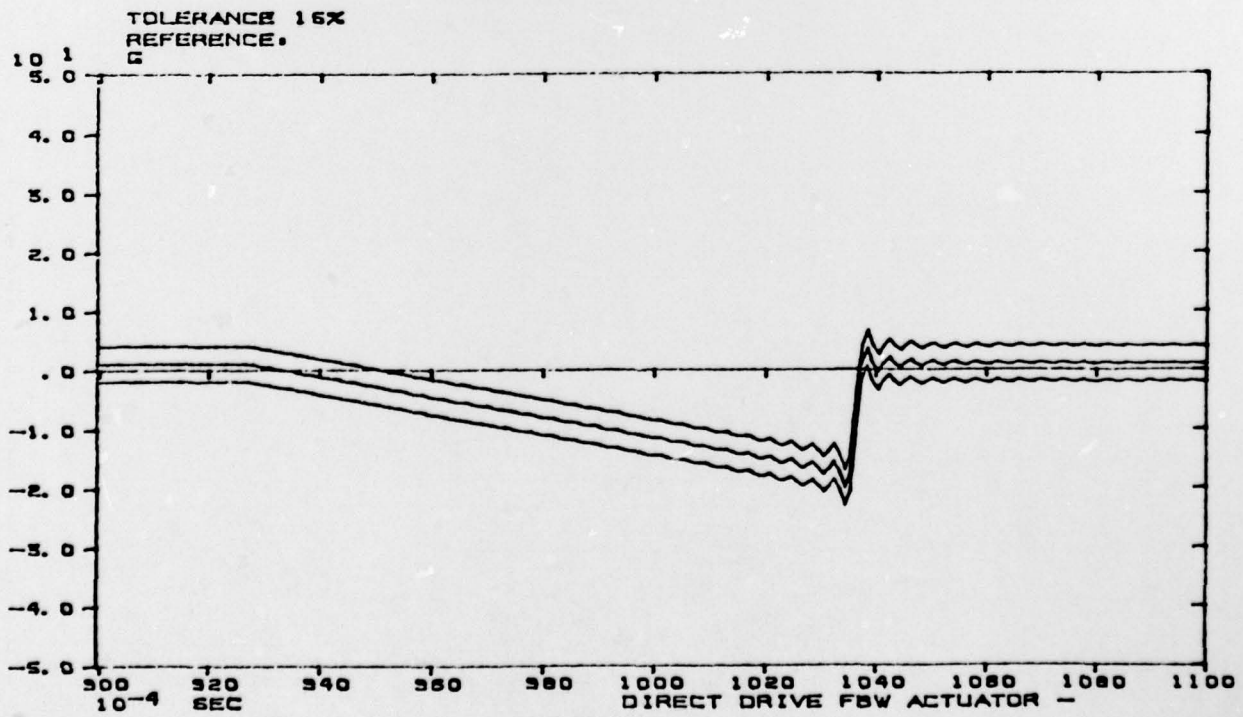
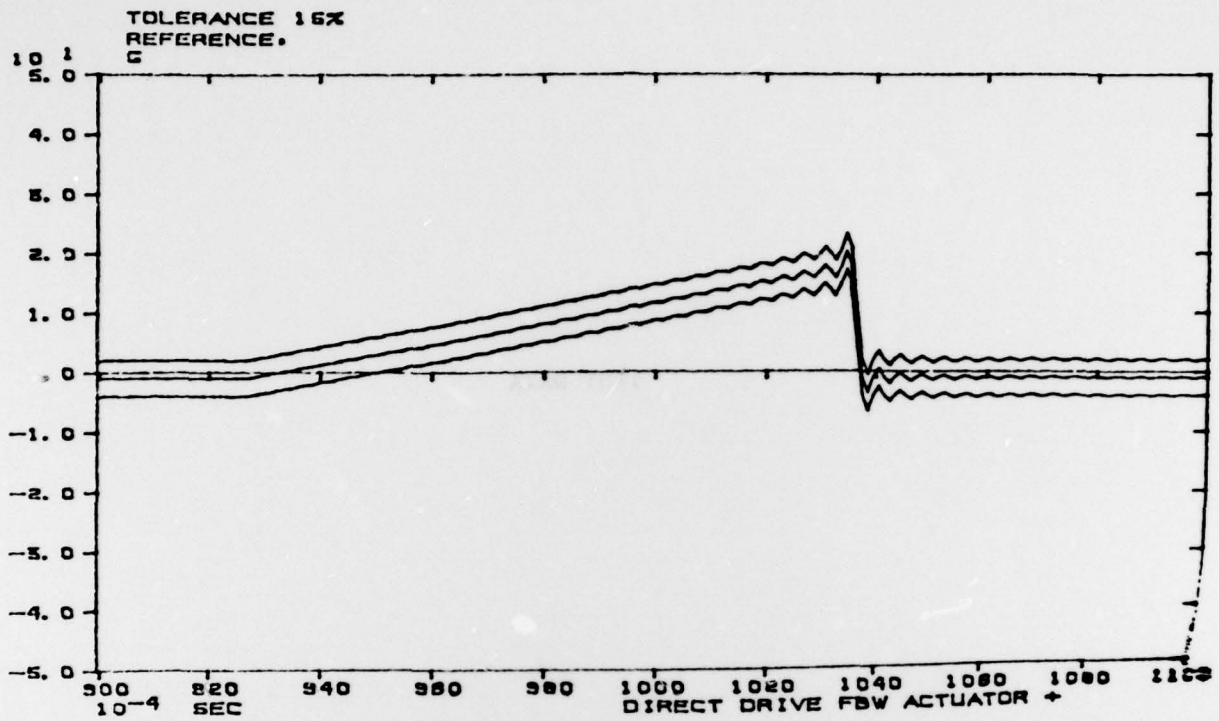


FIGURE B-1
Positive and Negative Shock Pulse References and Tolerances
182

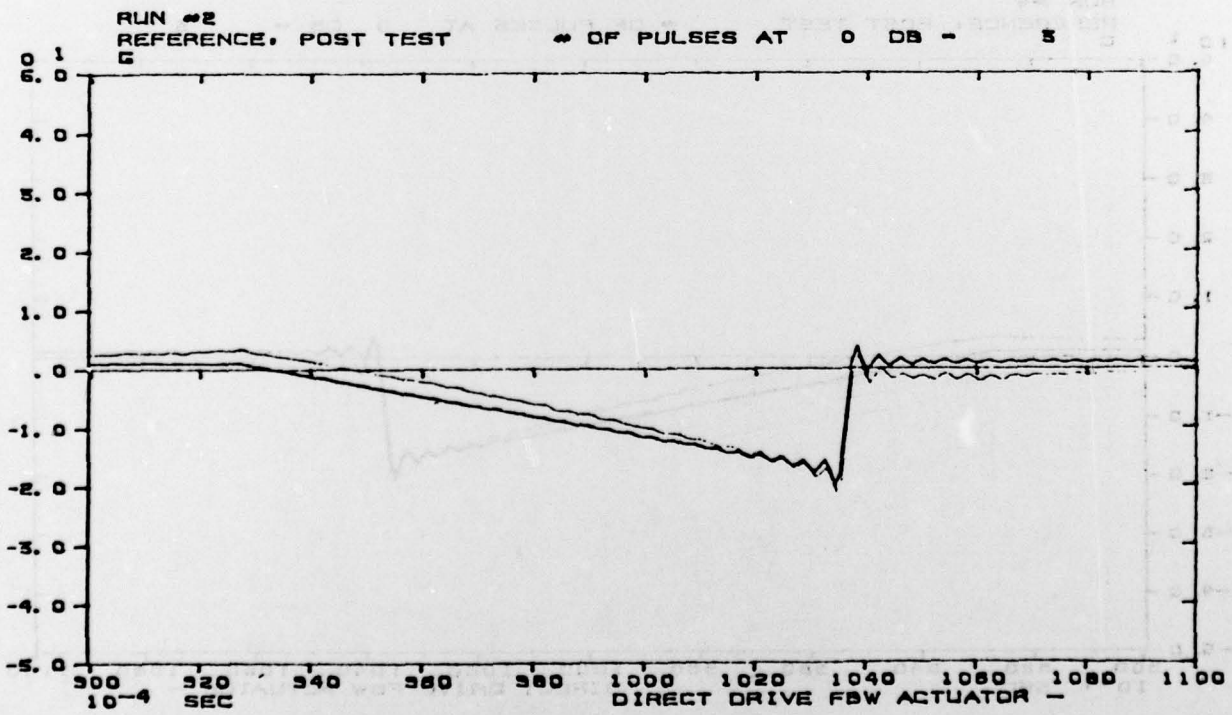
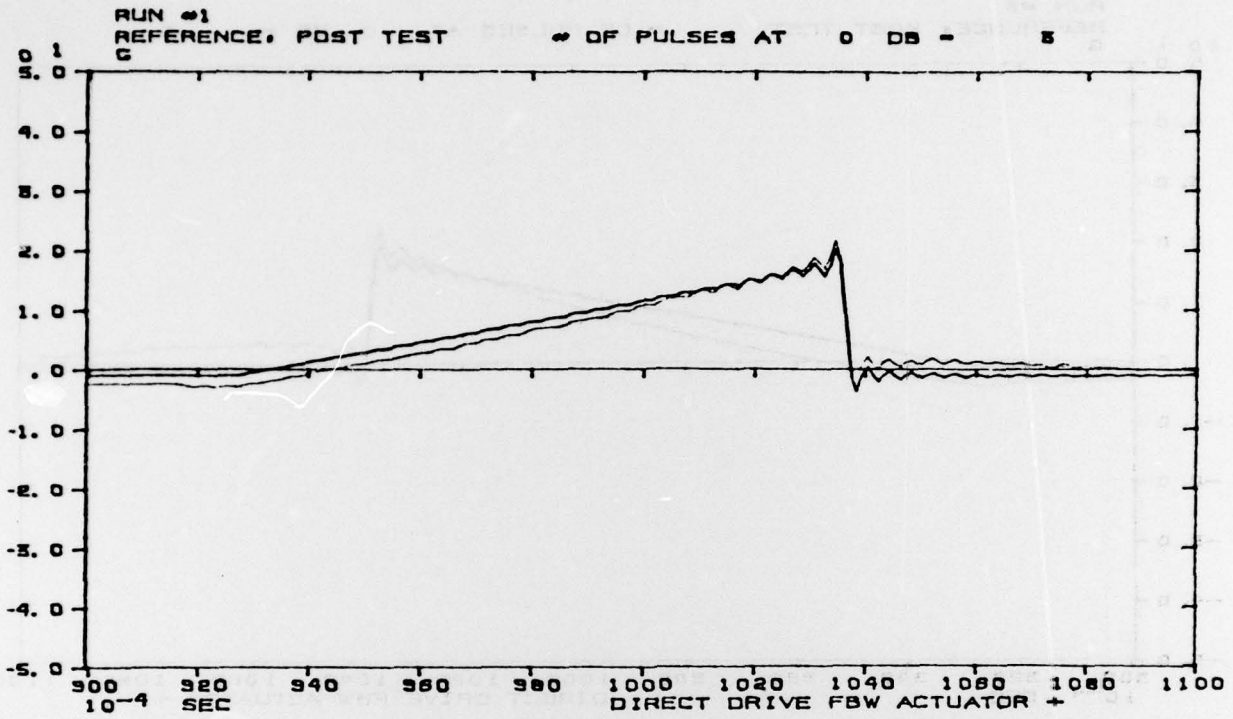


FIGURE B-2
 Electronic Module - A
 183

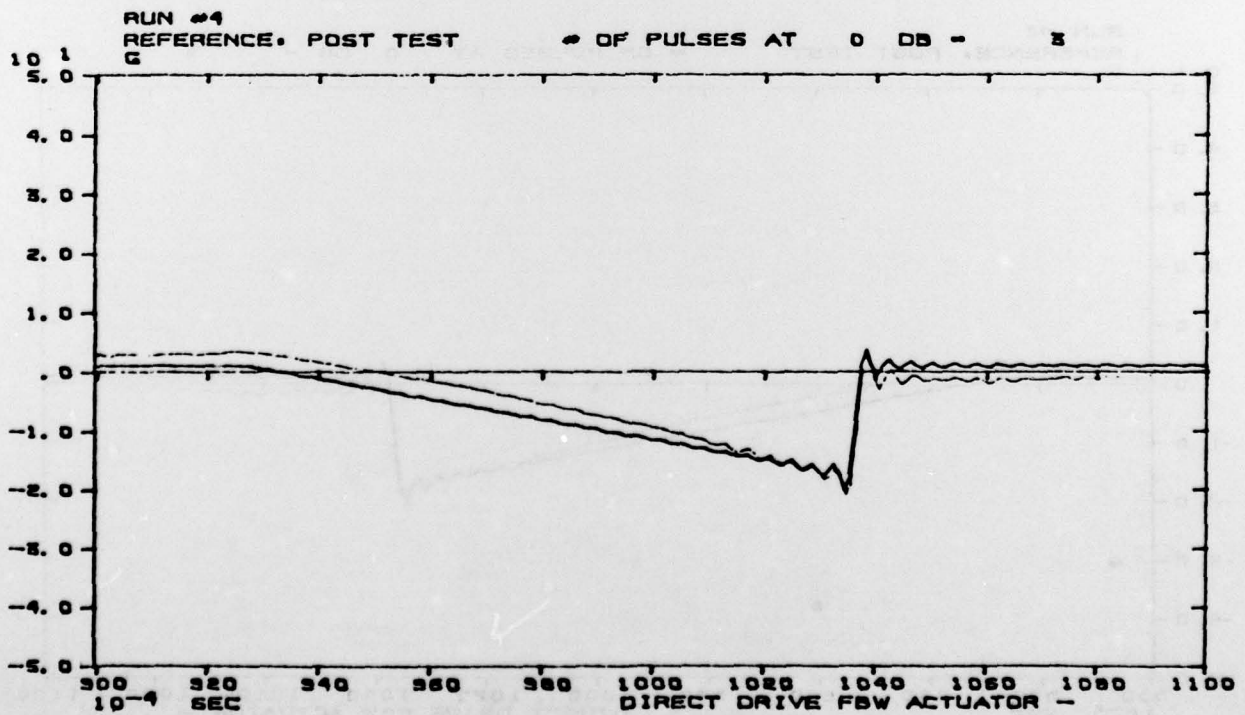
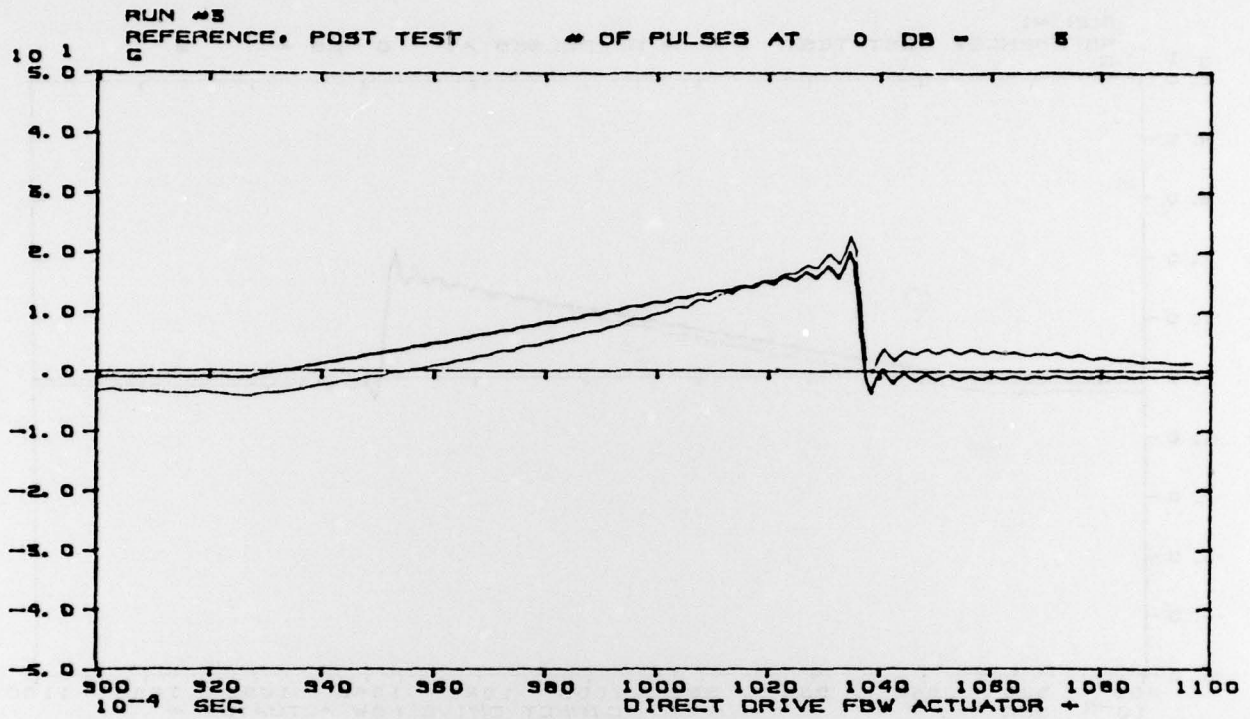


FIGURE B-3
 Electronic Module - B

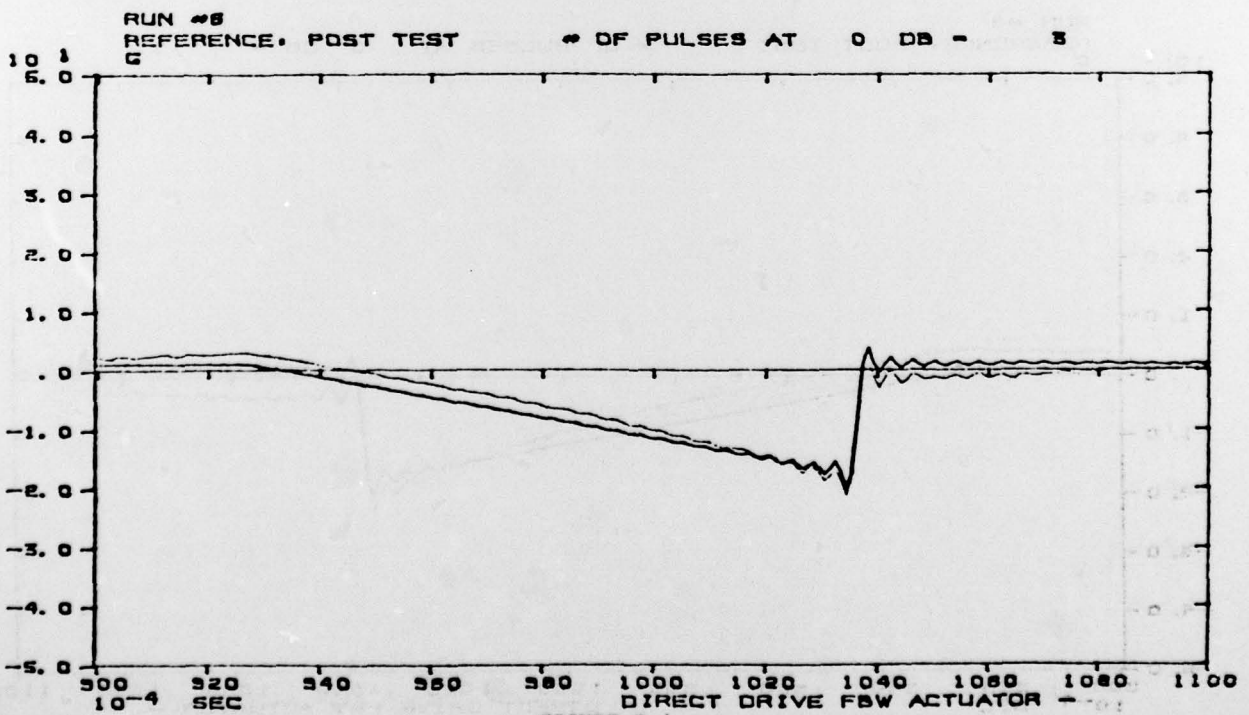
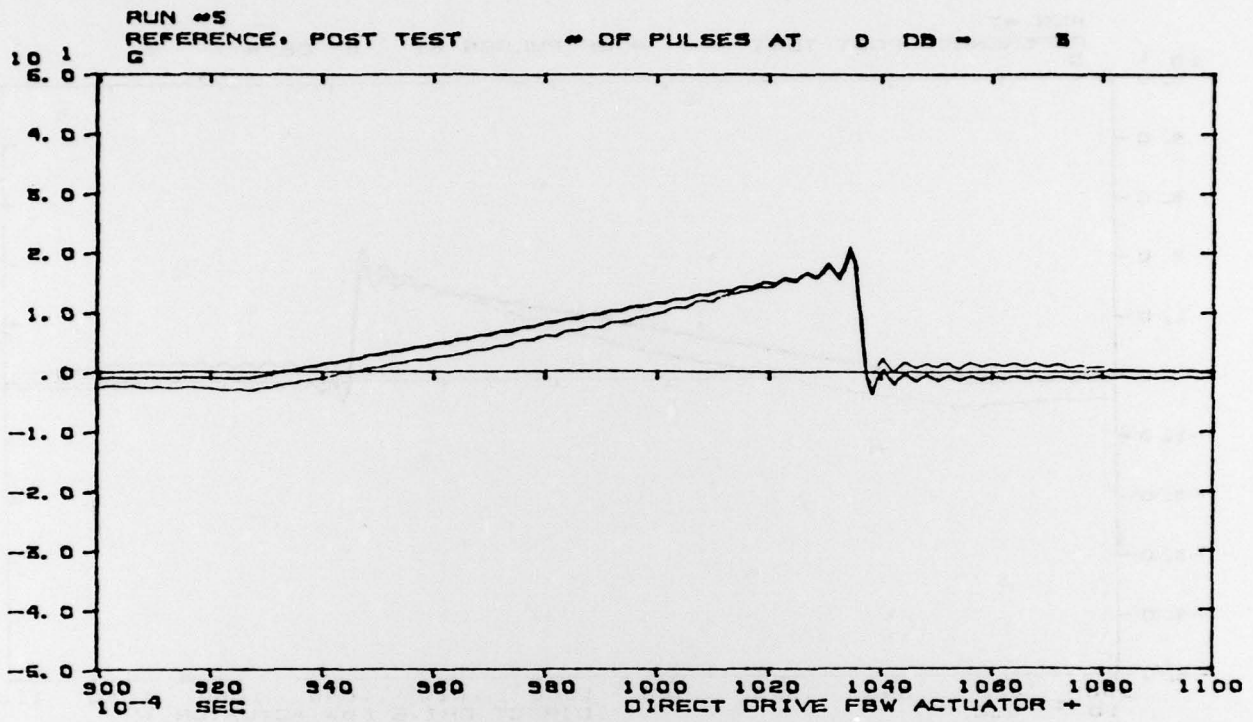


FIGURE B-4

Electronic Module - C

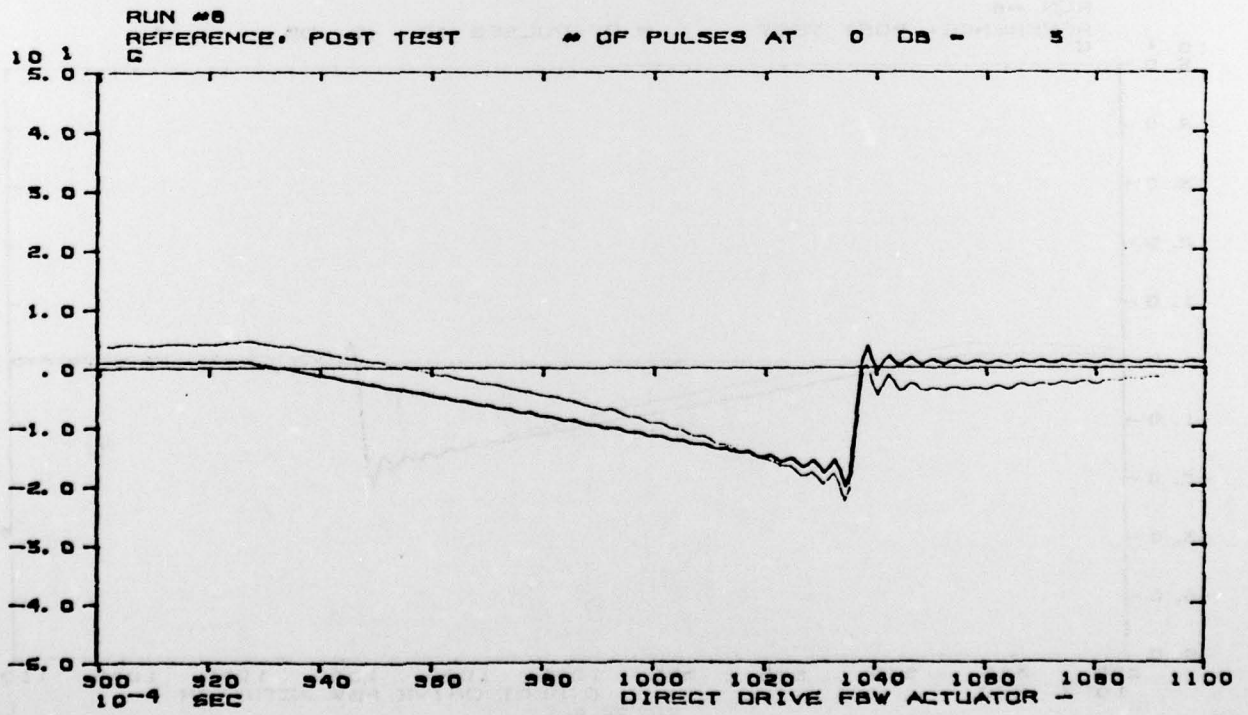
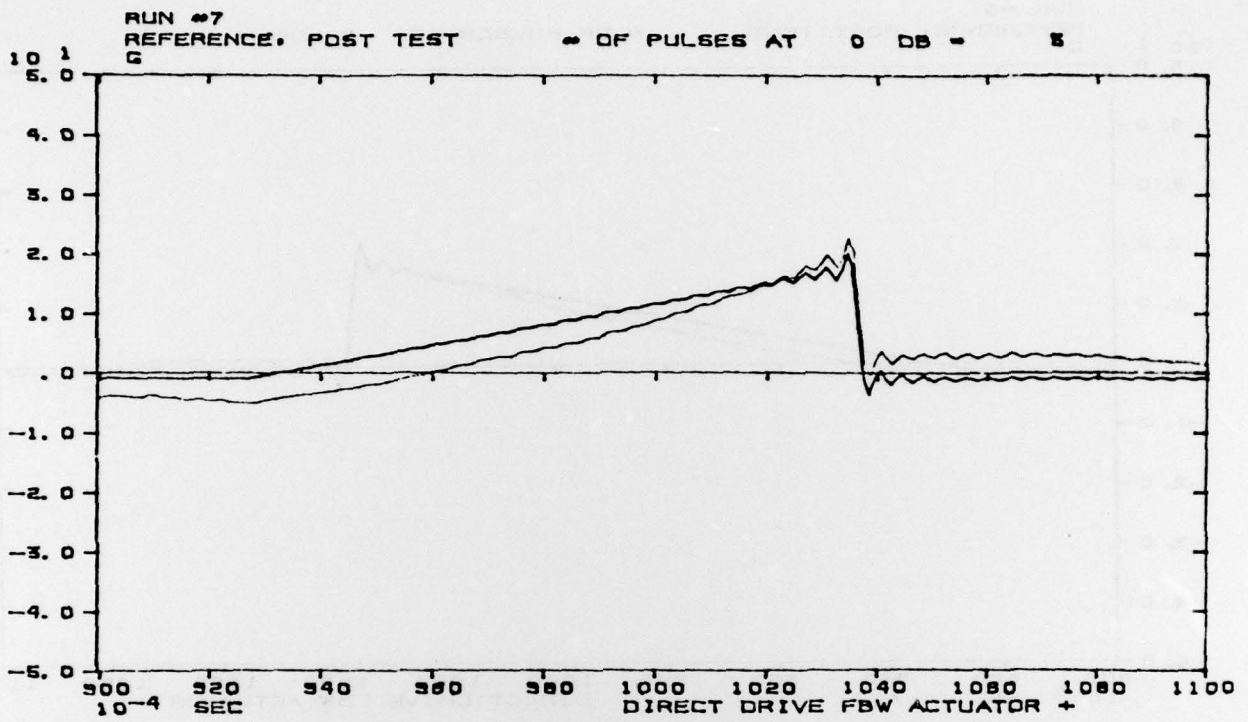


FIGURE B-5
 Electronic Module - D

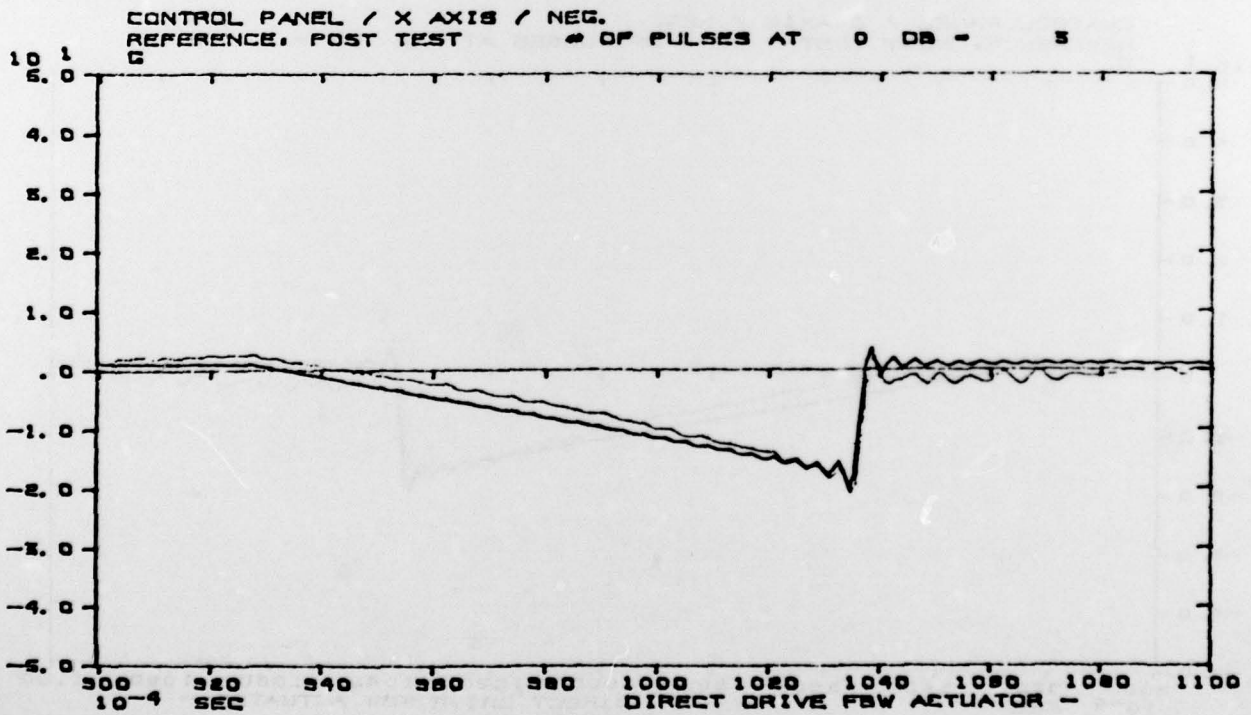
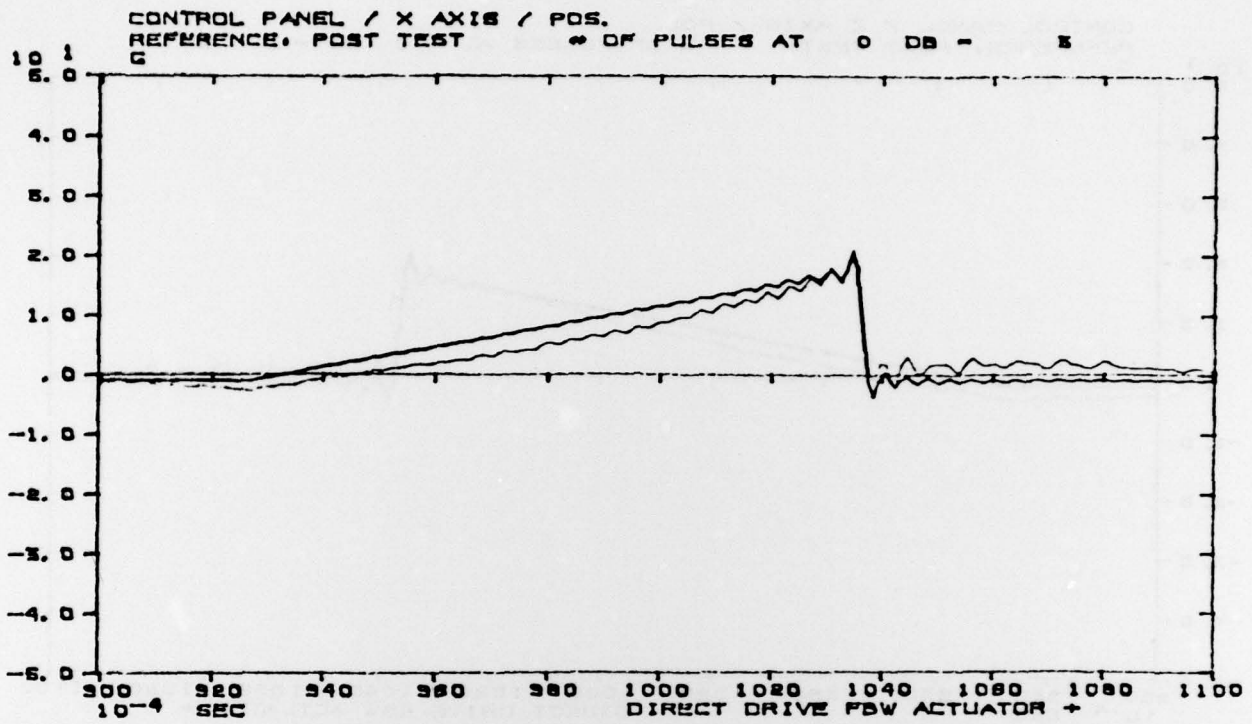


FIGURE B-6
 Control Panel X Axis

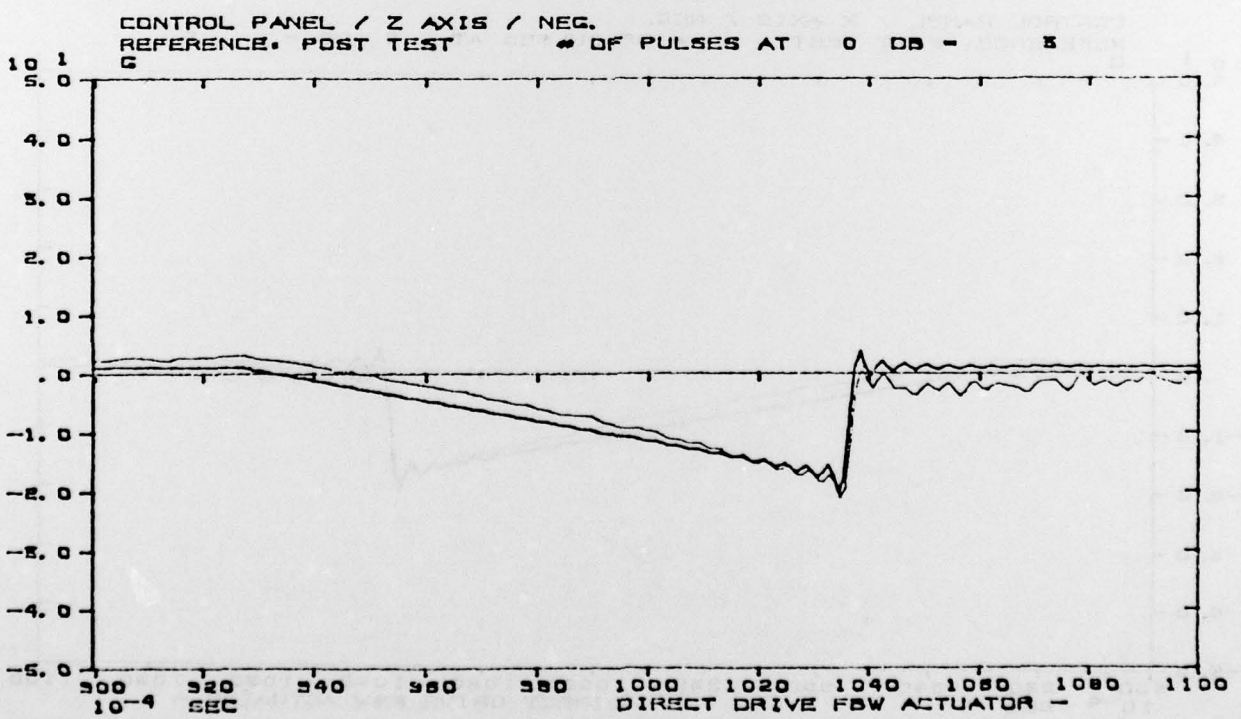
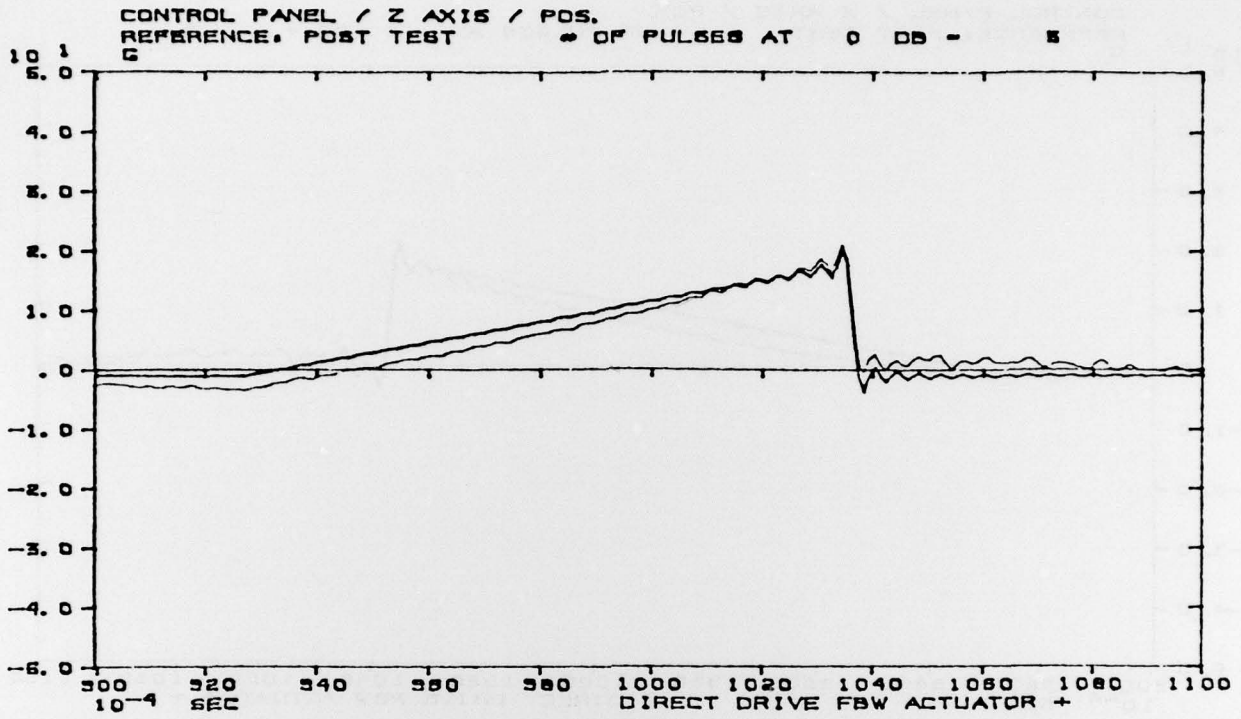


FIGURE B-7
 Control Panel Z Axis
 188

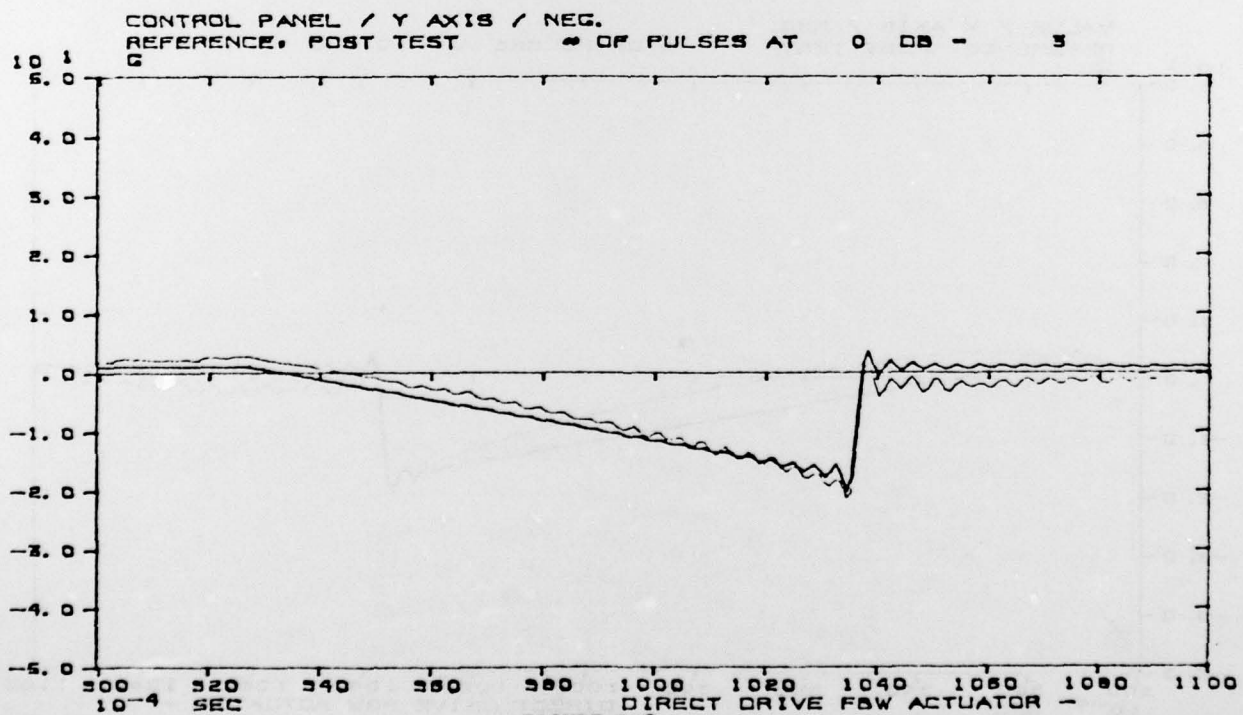
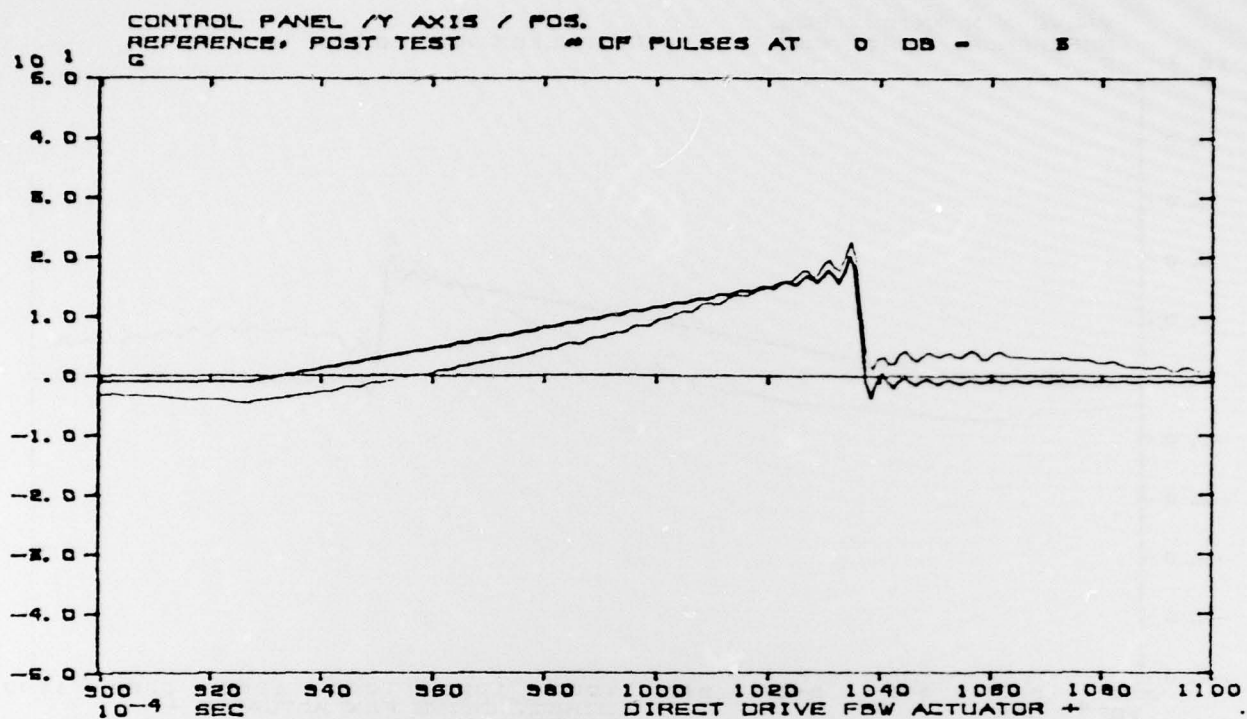


FIGURE B-8

Control Panel Y Axis

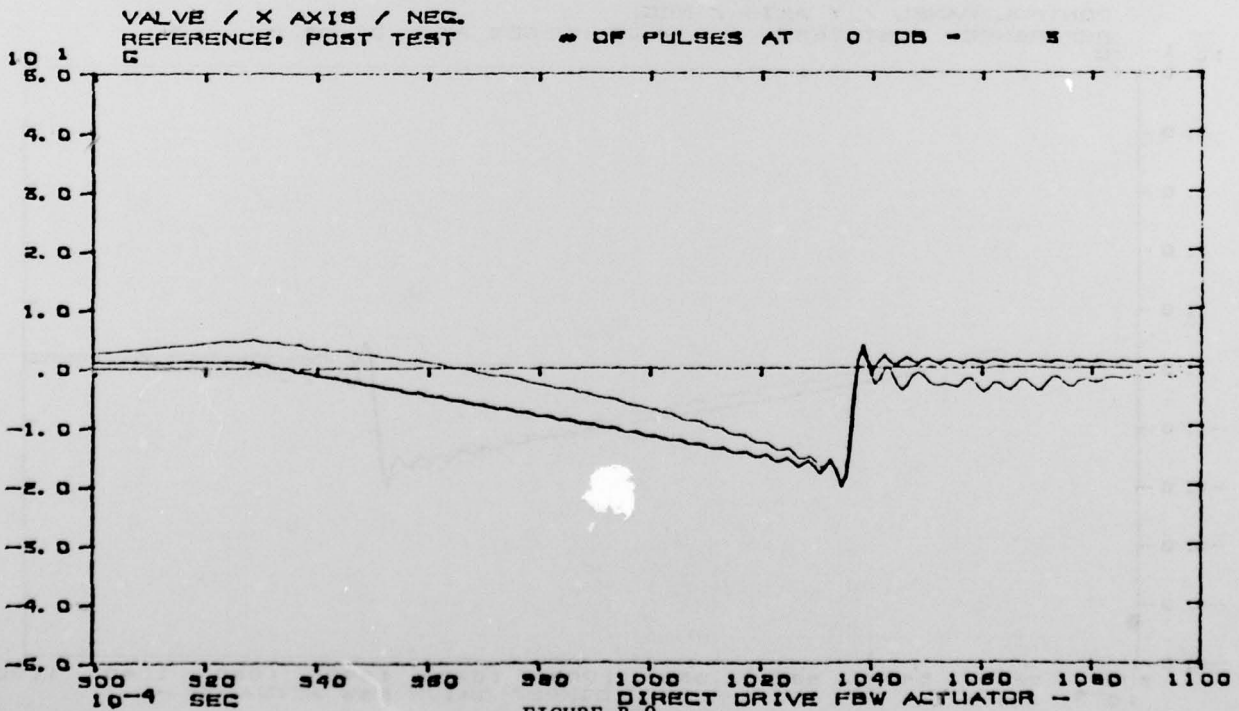
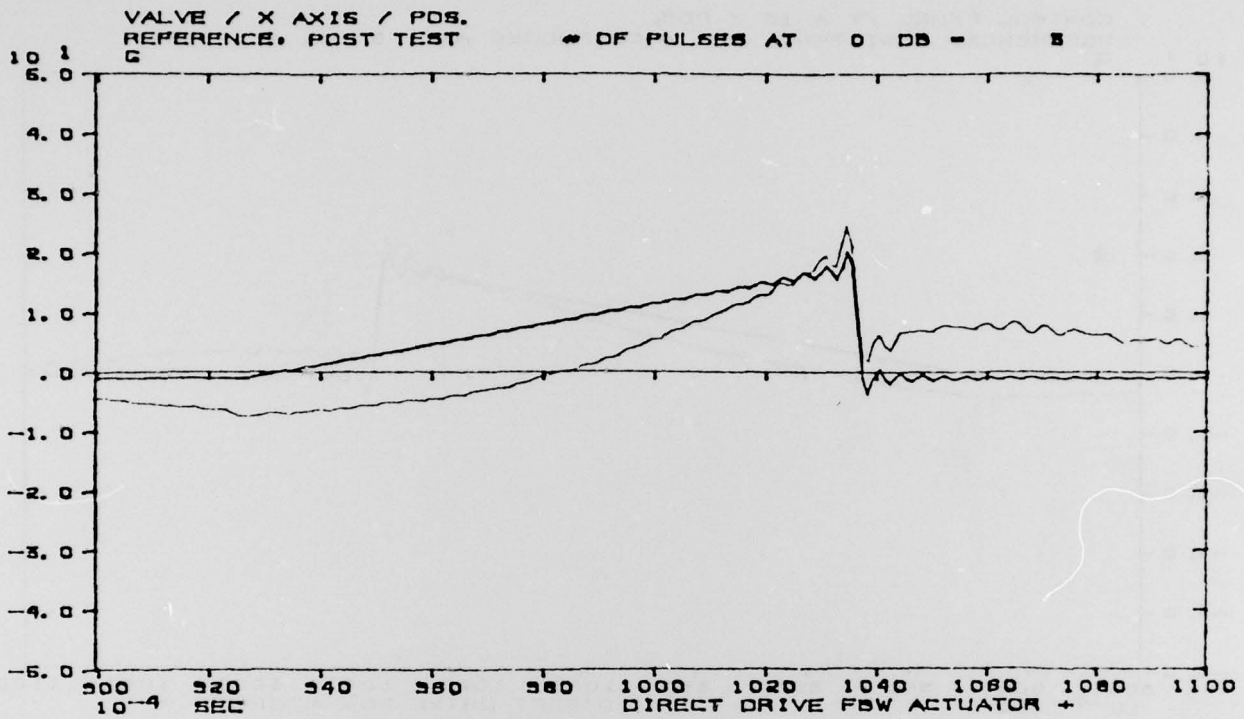


FIGURE B-9
 Control Valve X Axis
 First Test
 190

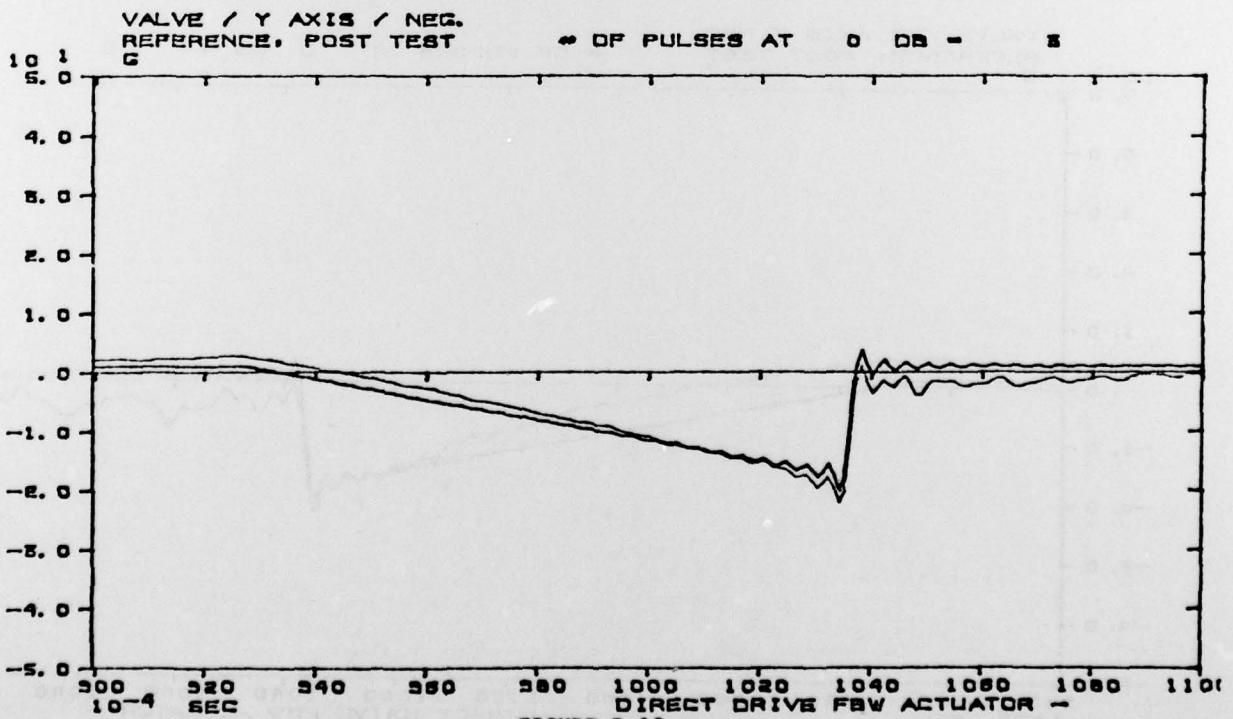
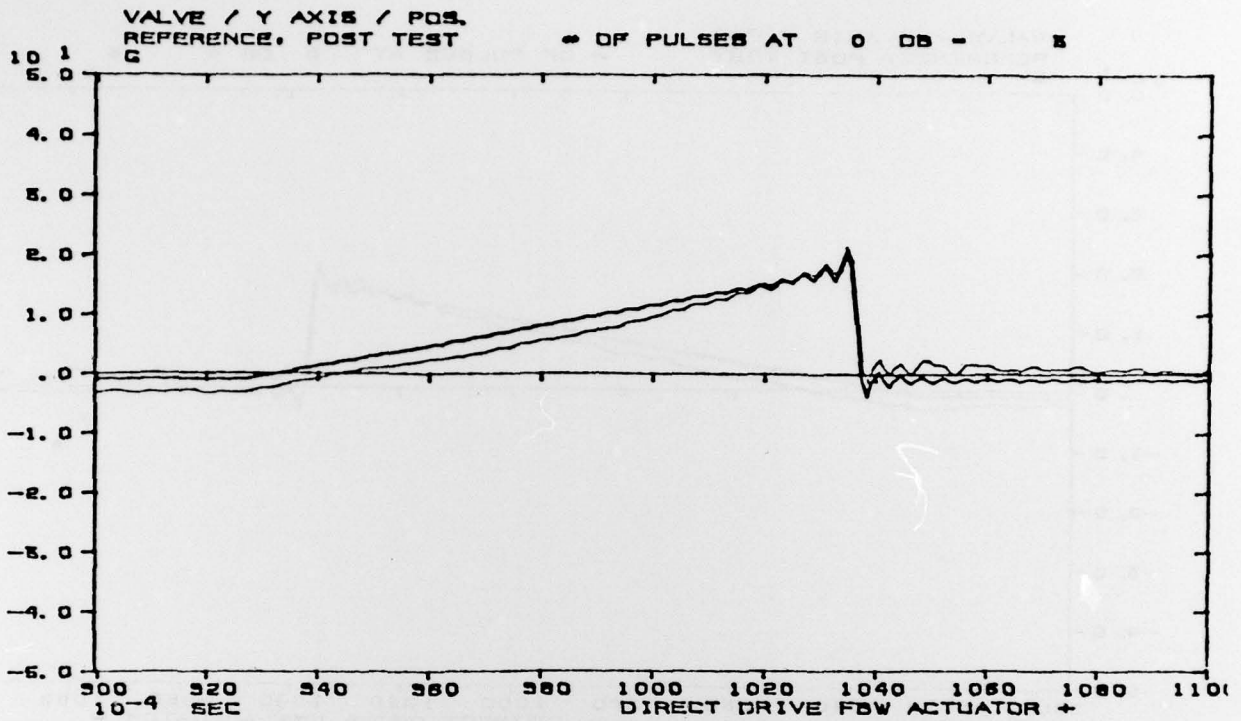


FIGURE B-10
Control Valve Y Axis
First Test

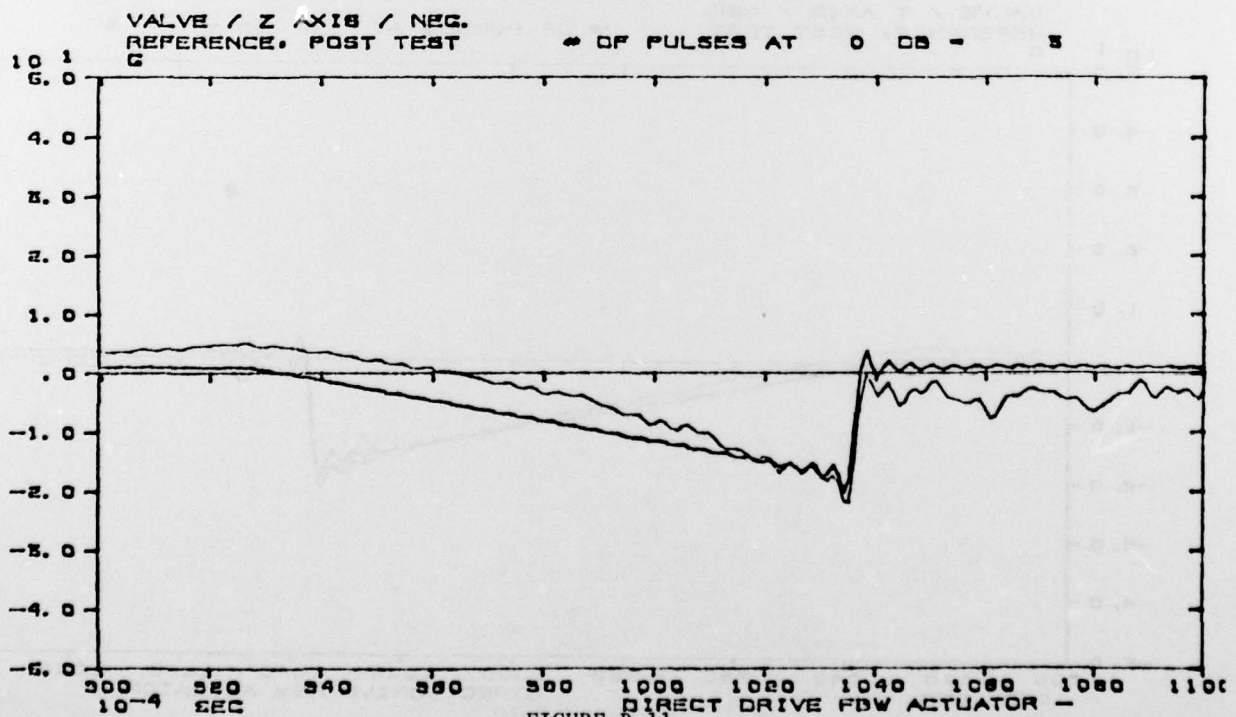
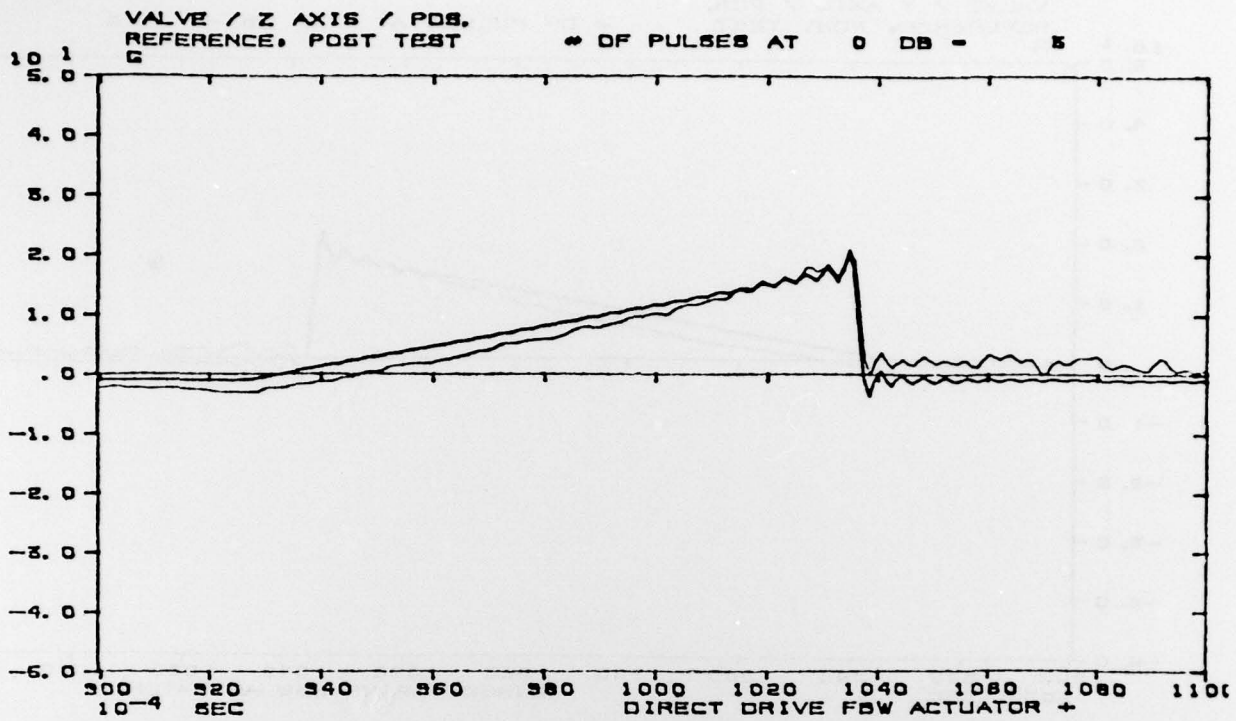


FIGURE B-11
Control Valve Z Axis
First Test

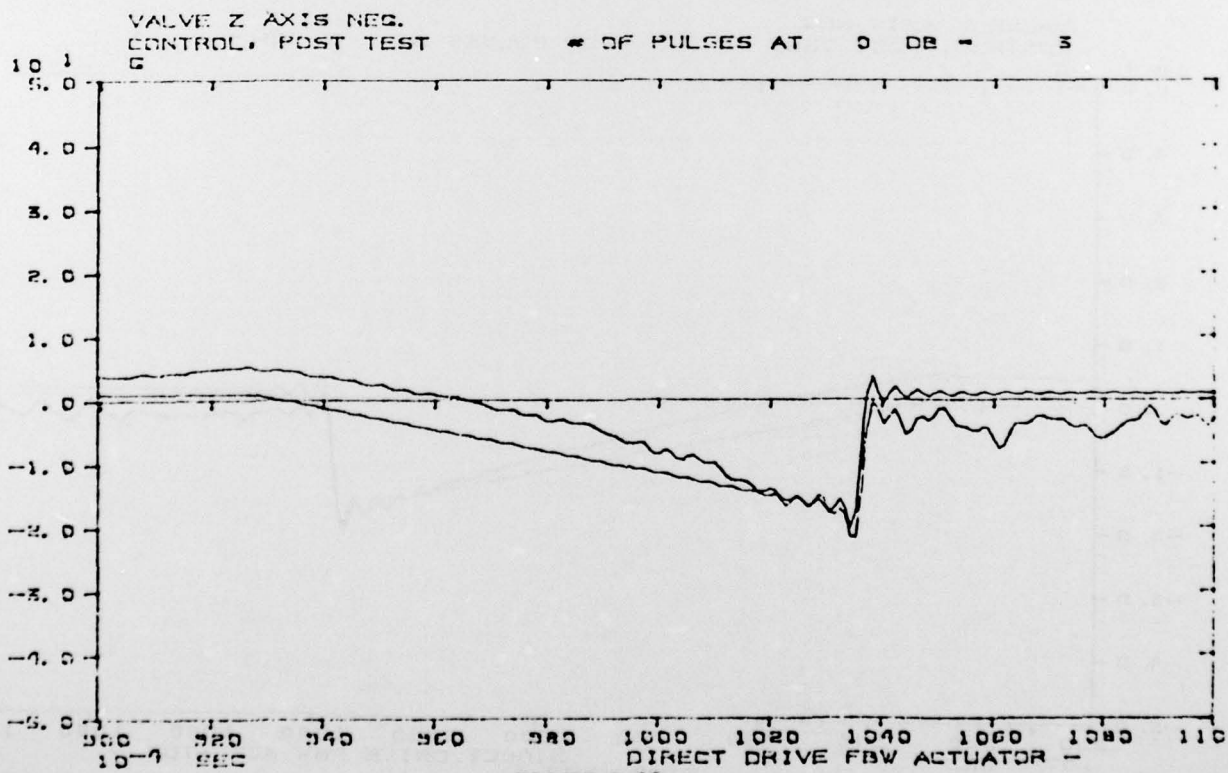
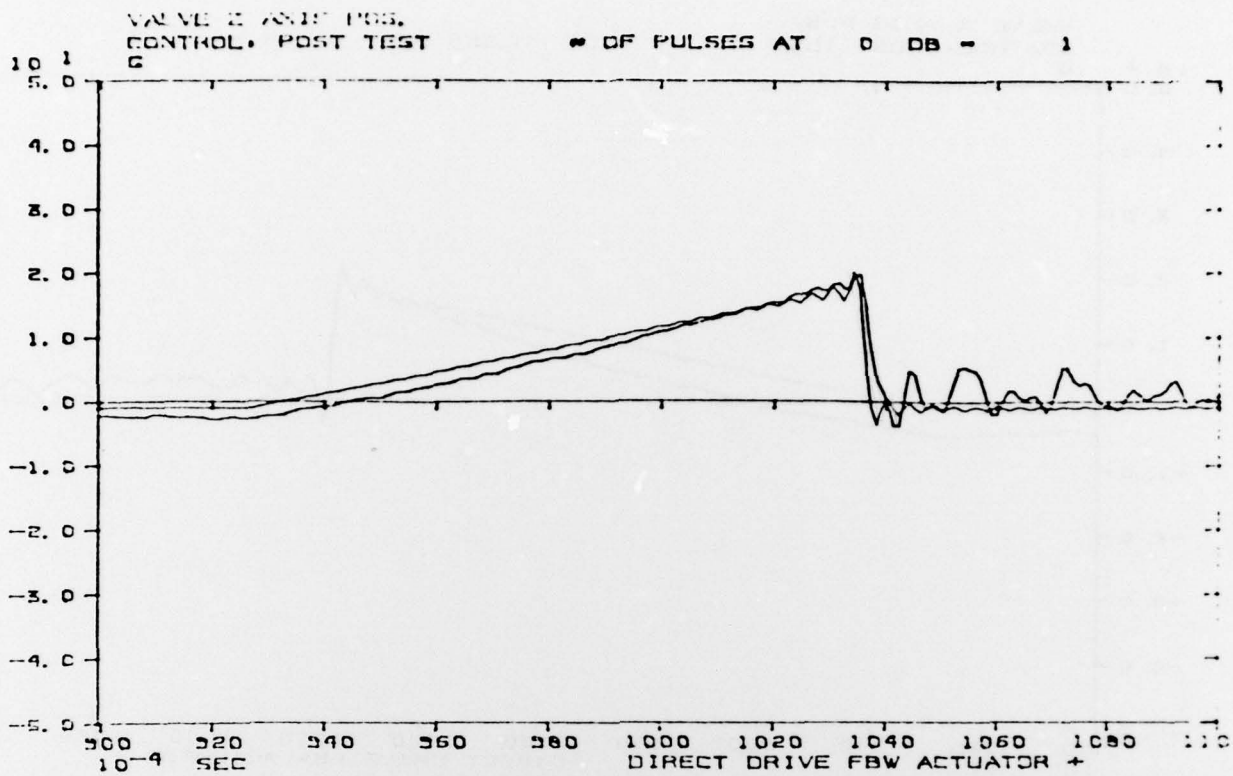


FIGURE B-12
Control Valve Z Axis
Second Test

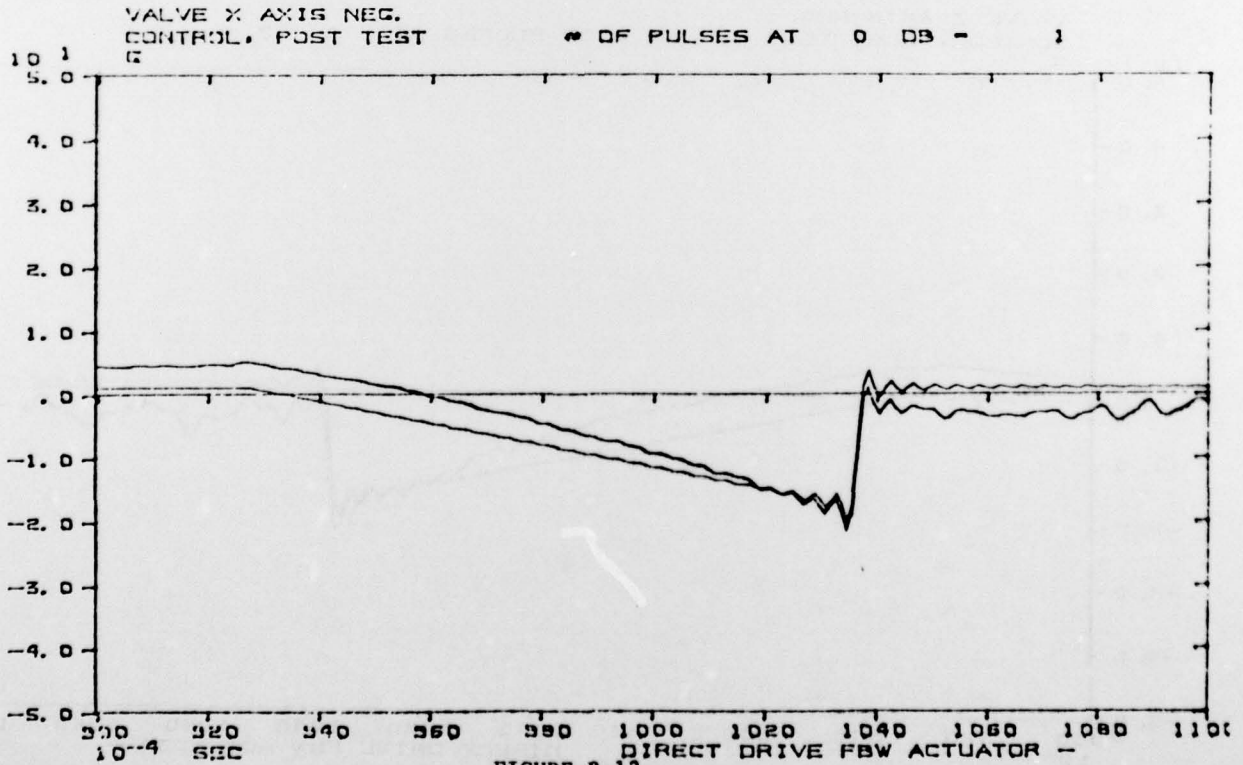
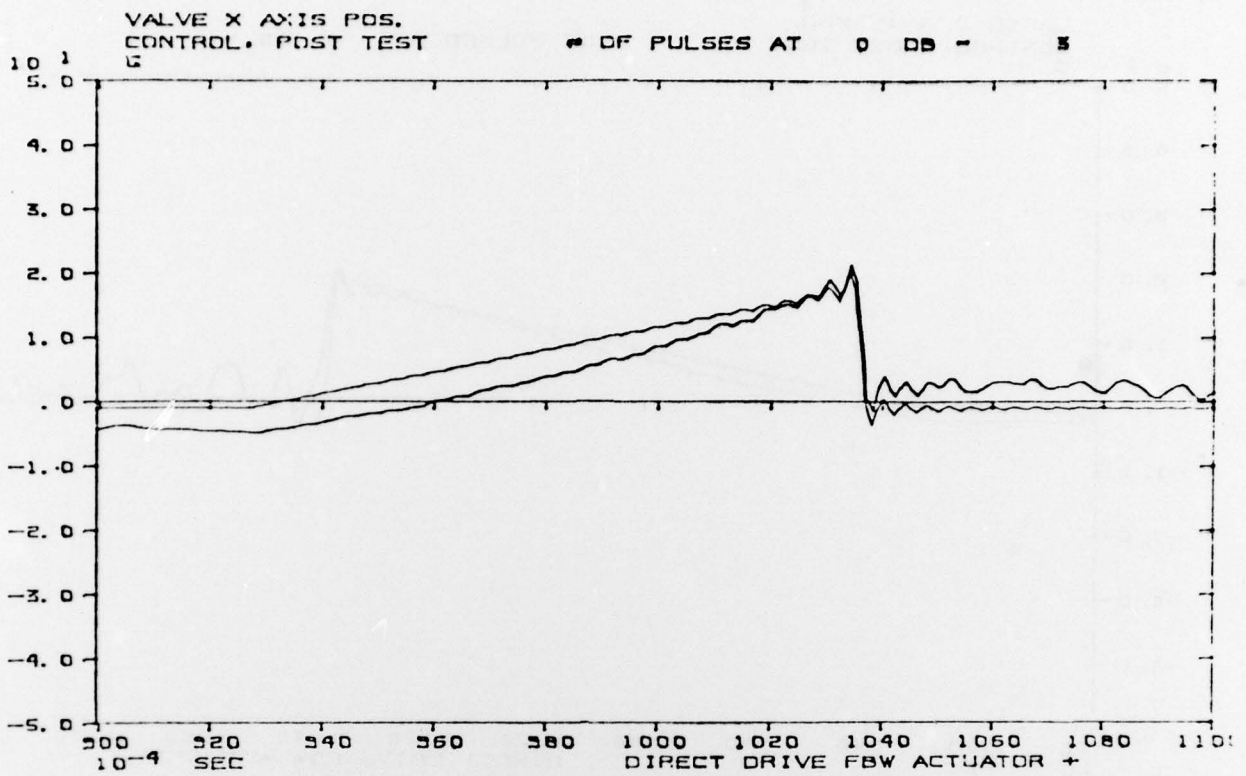


FIGURE B-13
Control Valve X Axis
Second Test

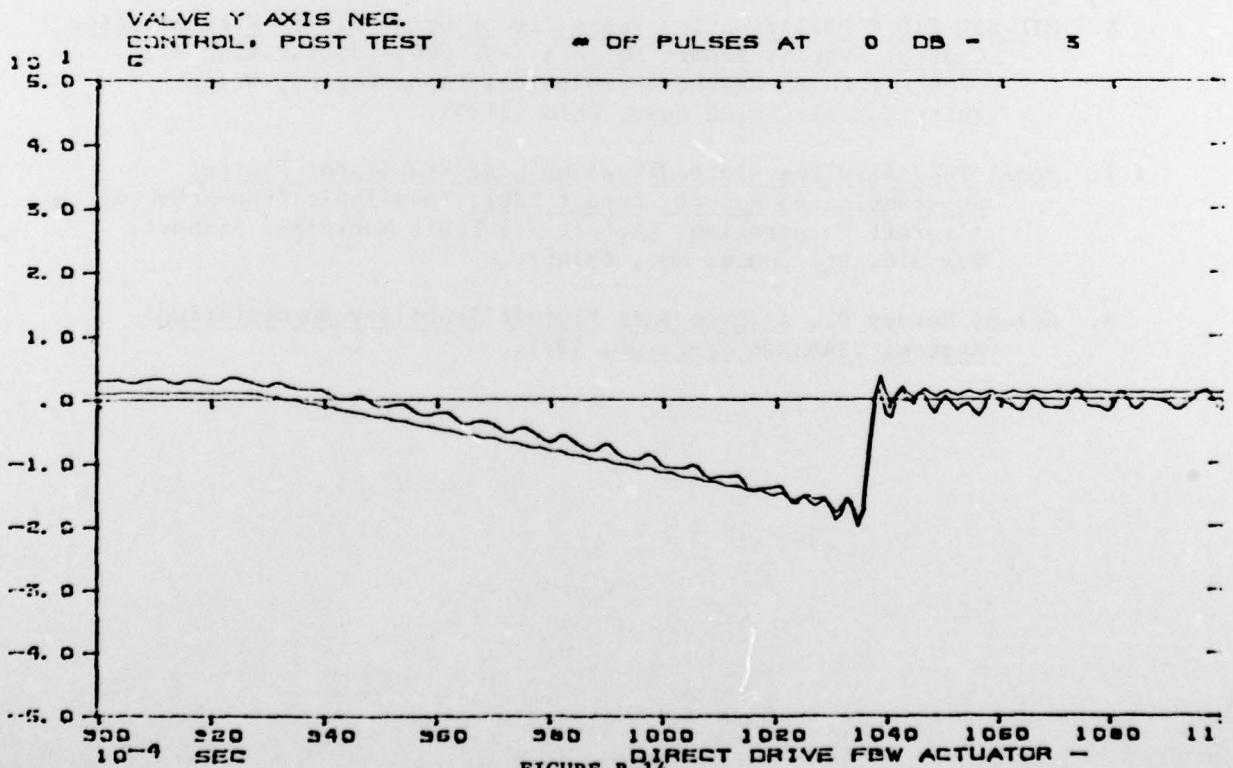
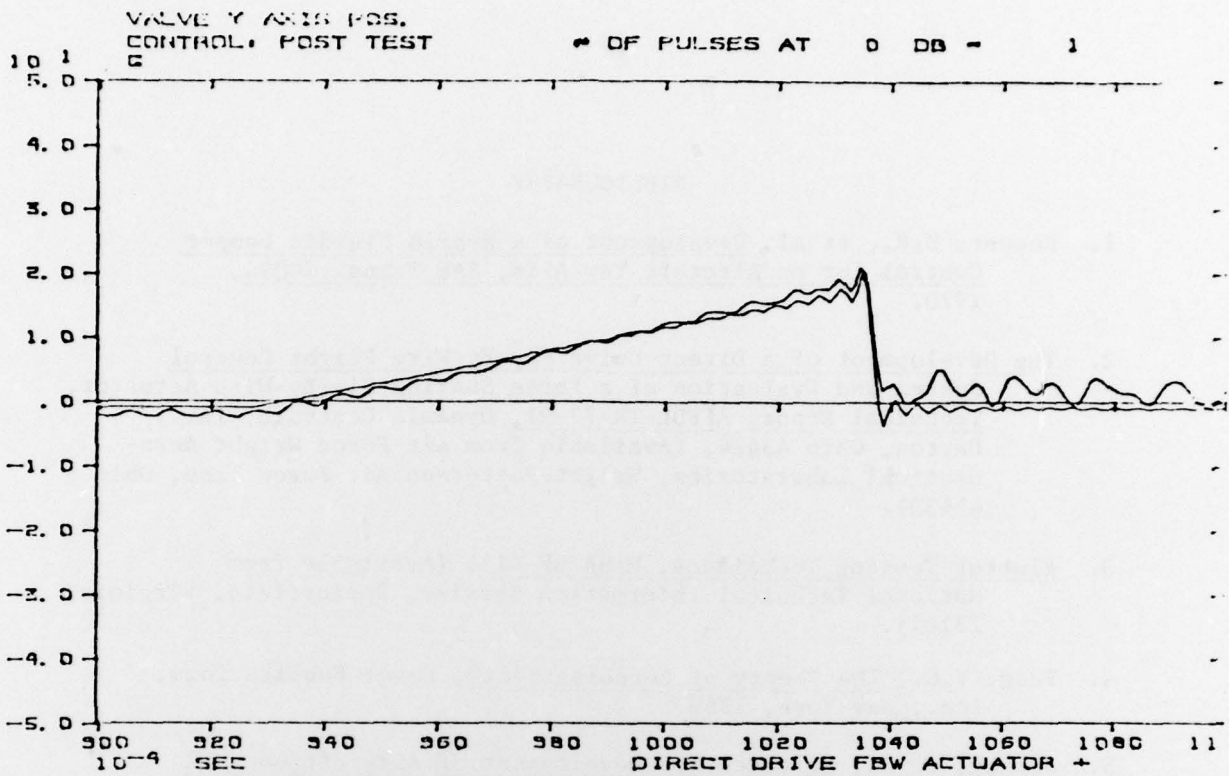


FIGURE B-14
Control Valve Y Axis
Second Test

BIBLIOGRAPHY

1. Cooper, D.R., et al, Development of a Hybrid Fluidic Damper Control for an Aircraft Yaw Axis, SAE Trans. 70094, 1970.
2. The Development of a Direct Drive Fly-By-Wire Flight Control System and Evaluation of a Force Sharing Fly-By-Wire Actuator, Technical Report AFFDL-TR-77-91, Dynamic Controls, Inc., Dayton, Ohio 45424, (Available from Air Force Wright Aeronautical Laboratories, Wright-Patterson Air Force Base, Ohio 45433).
3. Flutter Testing Techniques, NASA SP-415, (Available from National Technical Information Service, Springfield, Virginia, 22161).
4. Fung, Y.C., The Theory of Aeroelasticity, Dover Publications, Inc., New York, 1969.
5. Jenney, G. J., Research and Development of Aircraft Control Actuation Systems, AFFDL-TR-75-29, March, 1975.
6. MIL STD 810 C Qualification Tests Direct Drive Fly-By-Wire Actuator Control System, Report No. AFA /RWF 7804-79, (Available from Air Force Wright Aeronautical Laboratories, Wright-Patterson Air Force Base, Ohio 45433).
7. Model F-4J Airplane Slotted Leading Edge Stabilator Flutter Substantiation Report, Report E801, (Available from McDonnell Aircraft Corporation, Lambert-St. Louis Municipal Airport, Box 516, St. Louis, Mo., 63166).
8. Ogren, Harvey D., A Three-Axis Fluidic Stability Augmentation System, USAAMRDL TR-71-30, 1971.